Investigating the role of IRF8 in Atherosclerosis and Ageing

This thesis is submitted for the degree of Doctor of Philosophy, University College London

Rikah Louie

February 2020

Declaration

I, Rikah Louie confirm that the work presented in this thesis is my own. Where information has been derived from other sources, I confirm that Dr Matthew Gage designed the mouse breeding strategy, generated and initially maintained both WT^{LdlrKO} and M-$IRF8KO^{LdlrKO}$ mouse colonies and performed the pilot experiments of which this thesis was based upon. I also confirm that Prof Ines Pineda-Torra performed the initial bioinformatic RNA-sequencing analysis using the Partek software.

Dedication

I dedicate this thesis to my parents and my Nani, for it is only due to their unwavering support that this has been possible.

ਨਾਨੀ, ਇਹ ਪੀਐਚਡੀ ਤੁਹਾਡੇ ਲਈ ਸਮਰਪਿਤ ਹੈ. ਤੁਹਾਡੀ ਅਟੱਲ ਸਹਾਇਤਾ ਤੋਂ ਬਿਨਾਂ ਇਹ ਸੰਭਵ ਨਹੀਂ ਹੁੰਦਾ

Abstract

Atherosclerosis is the leading pathology underlying cardiovascular disease, with increasing prevalence amongst the aged population. This inflammatory, lipid-mediated disorder is caused by the accumulation of lipid-laden macrophages in the arterial vessels. Thus, reducing blood flow and ultimately leading to vessel occlusion. IRF8 is a haematopoietic transcription factor that is crucial for the development of myeloid cells and known to mediate their inflammatory responses.

This thesis investigates the role of myeloid-IRF8 in atherosclerosis development and the mechanism underlying IRF8s involvement. This thesis also investigates transcriptional differences in myeloid-IRF8 expression amongst the healthy young and aged population to determine the potential of using IRF8 as a biomarker of ageing. Upon generating a novel myeloid-IRF8 deficient mouse model (M-IRF8KO^{LdlrKO}), mice were challenged with a high fat western diet. Quantification of atherosclerotic lesions within the aortic root demonstrated M-IRF8KO^{LdlrKO} mice developed significantly less plaque in comparison to WT^{LdlrKO} controls. Thus, demonstrating myeloid-IRF8 reduction retards atherosclerosis development. Mechanistic studies, using RNA-sequencing, highlighted significant IRF8 regulation of genes involved in inflammation, chemotaxis and lipid metabolism. Therefore, contributing to IRF8-mediated differences in macrophage foam cell formation, cholesterol ester content and macrophage migration. This thesis also identifies IRF8-mediated differences in macrophage IFNβ signalling in atherosclerosis. This has enhanced our understanding of the role of IFNβ in atherosclerosis and how targeting IRF8 may alter macrophage response to IFNβ in atherosclerosis.

Taken together, this thesis has identified a novel role for myeloid-IRF8 reduction in atherosclerosis and enhanced our understanding of differences in the transcriptional regulation of IRF8 and its target genes in response to IFNβ and in myeloid cells from the healthy aged population.

Impact statement

The research performed within this thesis has benefits both within and outside of academia. The work presented has increased our knowledge of the role of macrophage IRF8 in Atherosclerosis; the leading cause of Cardiovascular-related deaths worldwide. From an academic point of view, this research has significantly enhanced our scientific understanding of the regulation that the transcription factor; IRF8, elicits on macrophage function within atherosclerosis. The expertise of this research has highlighted different methodologies that can be used in identifying how critical processes leading up to the development of Atherosclerosis are impacted by IRF8 under different inflammation-inducing conditions. Furthermore, this expertise is applicable to multiple therapy areas, where the role of a gene in different processes is under question.

Collectively, the novel findings of this research have proved pivotal in gaining additional funding, from UCB pharma, to further investigate the role of IRF8 in human subjects at risk of cardiovascular disease. Following on from this, this work is actively being used in the application of grant funding to further our scientific understanding of the role of macrophage-IRF8 in other therapy areas and the functional implications this can have when translated.

This research demonstrates IRF8-regulated signalling pathways may serve as a potential therapeutic target for the prevention of atherosclerosis development. With recent advances in gene therapy technologies and their success in clinical trials across a range of disease areas, the findings of this thesis can contribute to the development of gene therapies focused towards Atherosclerosis, positively impacting many people's lives both nationally and internationally.

Acknowledgements

I would like to convey my sincerest gratitude and appreciation for the support and knowledge provided by my supervisor Prof Ines Pineda-Torra. Your guidance and given opportunities have allowed me to grow as a scientist and an individual, where I have come to realise my true strengths and capabilities. Whilst these opportunities have taught me to view the world through slightly less 'rose-tinted' glasses, I will remain forever grateful for the life-long skills and mental strength they have instilled in me. I would like to express my appreciation to Dr Matthew Gage. Thank you for training me as a young budding scientist and providing both academic and emotional support over the years. I would also like to say a HUGE thanks to Prof Derek Gilroy. Thank you so much for being such a wonderful mentor, friend and an absolute inspiration to be around. Thank you for believing in me and providing me with opportunities that have elevated my career, both inside and outside of academia! I feel truly honoured to have worked alongside you and had the experience of learning from the very best!

A special thanks to both the IPT and Gilroy group for you have all been amazing friends and an absolute laugh to be around. I'm so lucky to have shared my PhD experience with such an amazing group of people who have been both my pillar of strength and shoulder to cry on, thank you all! A massive thanks to my best friend and partner in crime (literally) Amit Patel! Words can't describe how genuinely grateful I am to have met you, I don't know where I would be without you! All the jokes, mischievous antics, shenanigans, drunken nights at Simmons have made these the best 3 years yet!

Most importantly, I want to say a massive thank you to my family who have been such an incredible support system. I am deeply grateful for my parent's patience (especially my mum) and their love and belief in me. A special thank you to my mum and grandmother who have kept me sane, boosted my morale during the tough times and always had faith in me. My parents, brother, sister and grandmother have always been my biggest strength and always will be.

Table of contents

List of Figures

List of Tables

Abbreviations

25HC – 25 Hydroxycholesterol

27HC – 27 Hydroxycholesterol

ACAT – Acetyl-CoA Acetyltransferase 1

AIM2 – Absent in melanoma 2

AP-1 – Activating protein-1

BMDM – Bone marrow derived macrophages

CCR2 – C-C chemokine receptor 2

CDC – Conventional dendritic cell

CDP – Common dendritic progenitor

cGMP – Cyclic guanosine monophosphate

GMP – Granulocyte-myeloid progenitor

CHOP – C/EBP-homologous protein

Cmklr1 – Chemokine like receptor 1

CML – Chronic myeloid leukaemia

CMoP – Common myeloid progenitor

Cxcl10 – Chemokine interferon-γ inducible protein 10

DBD – DNA binding domain

DMEM – Dulbecco's Modified Eagle Medium

EDTA – Ethylenediaminetetraacetic acid

EICE – Ets-interferon consensus elements

eNOS – Endothelial nitric oxide synthase

ER – Endoplasmic reticulum

ES – Embryonic stem cells

Fcer1g – Fc Fragment Of IgE Receptor Ig

Gas – Gamma activated sequence

GM-CSF – Granulocyte-macrophage colony stimulating factor

GMP – Granulocyte-myeloid progenitor

H&E – Haematoxylin and Eosin

HSC – Haematopoietic stem cells

IAD – Interferon association domain

IFN - Interferon

IFNγ – Interferon gamma

IFNβ – Interferon beta

IRFs – Interferon regulatory factors

ISG – Interferon stimulated gene

LDL – Low density lipoprotein

LMPP - Lymphoid-primed multipotent progenitors

LOX - Lipoxygenases

LXR – Liver X receptor

Lyz2 – Lysozyme 2

MCP-1 – Monocyte chemoattractant protein-1

MCSF – Macrophage colony stimulating factor

MDP – Myeloid-dendritic progenitor

MERTK – Mer tyrosine kinase

MPO - Myeloperoxidase

NAFLD – Non-alcoholic fatty liver disease

NO – Nitric oxide

oxLDL – Oxidised LDL

PPARγ - Peroxisome proliferator-activated receptor γ

PBS – Phosphate buffered saline

pDC – Plasmacytoid dendritic cell

RNA – Ribonucleic acid

RNA-seq – RNA sequencing

SMC – Smooth muscle cell

SRB1 – Scavenger receptor B1

TLR4 – Toll like receptor 4

TNFα – Tumour necrosis factor alpha

UPR – Unfolded protein response

VSMC – Vascular smooth muscle cells

Chapter 1. Introduction

1.1 Atherosclerosis

Atherosclerosis is a chronic inflammatory, lipid-mediated disorder and the underlying cause of myocardial infarction and stroke [1]. It is one of the leading causes of Cardiovascular-related deaths worldwide, accounting for 1 in every 4 cardiovascular-related mortalities [2]. Atherosclerosis is a progressive disorder that begins during the first 20 years of life and develops slowly over time [3]. This chronic disease is initiated by an increase in circulating low density lipoprotein (LDL) that passively diffuses across the arterial sub endothelium, in regions of arterial branching and disturbed blood flow [4]. The arterial endothelium functions as a permeable barrier between the blood and tissues where it acts as a transducer of mechanical stimuli [5].

1.1.2 Lesion initiation

Endothelial cells form the inner lining of blood vessels, where they regulate the transport of nutrients to the underlying tissue and coordinate the formation of new blood vessels [6], [7]. Endothelial cells are therefore, highly plastic allowing them to switch from a resting quiescent state to a highly proliferative migratory state [8]. Shear stress is a force that laminar blood flow exerts on endothelial cells and can influence the phenotype, function and quiescent endothelial cell state [9], [10]. Differences in shear stress caused by perturbed blood flow, at regions of arterial branching, can activate endothelial signalling pathways, including NF-κB that promotes thrombosis and inflammation [9]. This results in a compromised dysfunctional endothelium that can contribute to atherosclerotic lesion initiation

and development. Disturbed blood flow contributes to the altered cuboid morphology of endothelial cells, reducing cell uniformity (**Fig 1.1 A-iii**). These regions classically demonstrate a reduction in vaso-protective nitric oxide (NO), formed by endothelial nitric oxide synthase (eNOS). Within arteries, eNOS is the most common NOS isoform known to constitutively produce low levels of vascular NO. This contributes to the dilation of blood vessels, by stimulating soluble guanylyl cyclase and increasing the expression of cyclic guanosine monophosphate (cGMP) in smooth muscle cells [11]. Vascular NO additionally inhibits platelet aggregation and adhesion by interfering with the ability of leukocyte cell surface adhesion molecules, I-CAM and V-CAM, from forming an adhesive bond with the endothelial cell surface [12]. Therefore, reductions in eNOS contribute to a compromised endothelial cell barrier [13], resulting in the increased accumulation and retention of athero-genic LDL particles within the arterial sub-endothelium.

In contrast, athero-resistant regions are exposed to laminar sheer stress, resulting in the activation of pathways that maintain endothelial integrity. These regions often display an increase in the expression of transcription factors; KLF2 and KLF4 which are activated by the MEK5/ERK5/MEF2 signalling pathway [14], [15]. This promotes eNOS induced NO, enhancing endothelial cell survival and proliferation therefore maintaining an effective barrier against LDL uptake. Collectively, this contributes to the overall site-specific development of atherosclerotic plaques.

1.1.3 Inflammation and foam cell formation

Within the atherogenic arterial regions, the inflammatory environment of the sub endothelium renders the LDL particles prone to oxidation by circulating myeloperoxidase (MPO) [16], lipoxygenases (LOX) [17], iNOS [18] and NADPH oxidases [19]. Therefore, resulting in the formation of oxidized LDL (oxLDL). Activated endothelial cells promotes NF-κB signalling, which enhances the expression of selectins (E-selectin, P-selectin) and adhesion markers (ICAM-1, VCAM-1) [9], [20]. This promotes monocyte rolling, adhesion and transmigration into the arterial intima (**Fig 1.1 B-3**). The hyperlipidaemic environment, associated with atherosclerosis development, promotes the frequency of pro-inflammatory monocytes within the circulation, specifically Ly-6C^{hi} monocytes in mouse models [21], [22]. This is due to the expansion of the bone marrow derived common monocyte progenitor population and increased mobilisation of monocytes from the bone marrow by the C-C chemokine receptor type 2 (CCR2) [23]. Ly6-C^{hi} monocytes have also been shown to bind P-selectin and E-selectin more readily than resident Ly-6C^{lo} monocytes, suggesting preferential entry of pro-inflammatory monocytes into the arterial intima [24]. Within the intima, monocytes are exposed to a variety of growth factors; M-CSF, GM-CSF and stimuli; interferon-gamma (IFN-γ), toll-like receptor 4 (TLR4), tumour necrosis factor alpha (TNFα), stimulating their differentiation into different macrophage subsets [25]–[27] (**Fig 1.1 B-5**), which are addressed in section 1.1.6. Macrophages internalize oxLDL, via cell surface scavenger receptors including; CD36 and scavenger receptor B1 (SR-B1) [28] (**Fig 1.1 B-6**). The oxLDL is degraded by macrophage lysosomes to form free cholesterol. The free cholesterol is trafficked to the endoplasmic reticulum where it is esterified by Acyl-

coenzyme A: cholesterol acyltransferase (ACAT) enzymes to form cholesterol esters [29], [30]. The cholesterol esters are then stored in lipid droplets resulting in foam cell formation [30]. Collective accumulation of foam cells contributes to fatty streak formation which is a characteristic of one of the early stages of atherosclerotic plaque formation [31] (**Fig 1.1 A-ii**).

1.1.4 Progression to fibrous plaques

Foam cell deposits within the arterial sub endothelium promotes resident vascular smooth muscle cell (VSMC) proliferation, migration and apoptosis, upon secretion of extracellular vesicles that contain proteins, lipids and nucleic acids that regulates the VSMC actin-cytoskeleton pathway [32] (**Fig 1.1 B-7**). Furthermore, macrophages and T-cells contribute to VSMC proliferation and migration via enhanced production of homocysteine and angiotensin II [33], [34]. Elevated homocysteine promotes endothelial cell dysfunction, VSMC proliferation and intimal thickening via stimulation of MAPK-induced c-Fos and c-Myb [35]. Alongside VSMC proliferation, binding of CD40L to its receptor CD40 is also crucial in atherosclerotic plaque formation [36]. This ligand-receptor interaction promotes macrophage and T-cell induction of IFNγ, enhancing inflammation. This interaction has been proven highly important in the development of atherosclerosis as inhibition of CD40L lessens plaque inflammation whilst promoting plaque stability by enhancing fibrosis [36]. VSMCs and macrophage foam cells produce a complex matrix of collagen, elastin and proteoglycans forming a fibrous cap surrounding the core of the foam cell lesion, which can later affect lesion stability [31]. As the lesions advance, increased macrophage-induced TGF-β signalling promotes collagen formation, contributing

to atherosclerotic plaque and fibrous cap development [37]. The fibrous cap forms a barrier to prevent the plaque from rupturing.

1.1.5 Advanced lesions and thrombosis

The development of vulnerable plaques and resultant cardiovascular events depends upon the composition and stability of atherosclerotic plaques. As the extracellular lipid core increases, extracellular cholesterol forms in lipid droplets. However, excess free cholesterol, due to reductions in ACAT1, can saturate the endoplasmic reticulum (ER) membrane, evoking an ER stress response [38], [39]. As the cholesterol content of the ER membrane is relatively low [40], excessive cholesterol loading activates the ER unfolded protein response (UPR) [41]. The UPR functions to reduce ER stress upon promoting the transcription of genes known to re-esterify excess free cholesterol [42] or induce cell death upon activation of the transcription factor C/EBP-homologous protein (CHOP) [43]. Activation of CHOP promotes apoptosis of cholesterol-laden macrophages by repressing the expression of cell-survival protein, Bcl-2 [44]. Concomitantly, the apoptotic cells are removed from the intima via the binding of macrophage cell-surface receptors to apoptotic cell recognition motifs where they are removed in a process known as efferocytosis. The kinase, c-Mer tyrosine kinase (MerTK) is a macrophage receptor known to promote the effective clearance of apoptotic cells within plaques [45]. However, the enhanced free cholesterol within cholesterol-laden macrophage foam cells and pro-inflammatory environment of the plaque, promotes proteolytic cleavage of MerTK, reducing its expression and ability to remove apoptotic macrophage foam cells from the plaque environment [45]. Inefficient removal of apoptotic foam cells

results in the release of macrophage lipid content and tissue factor, contributing to necrotic core formation [45], [46] (**Fig 1.1 B-8**). Apoptotic foam cells promote the expression of proteases that degrade the extracellular matrix, thinning the fibrous cap thereby affecting plaque stability.

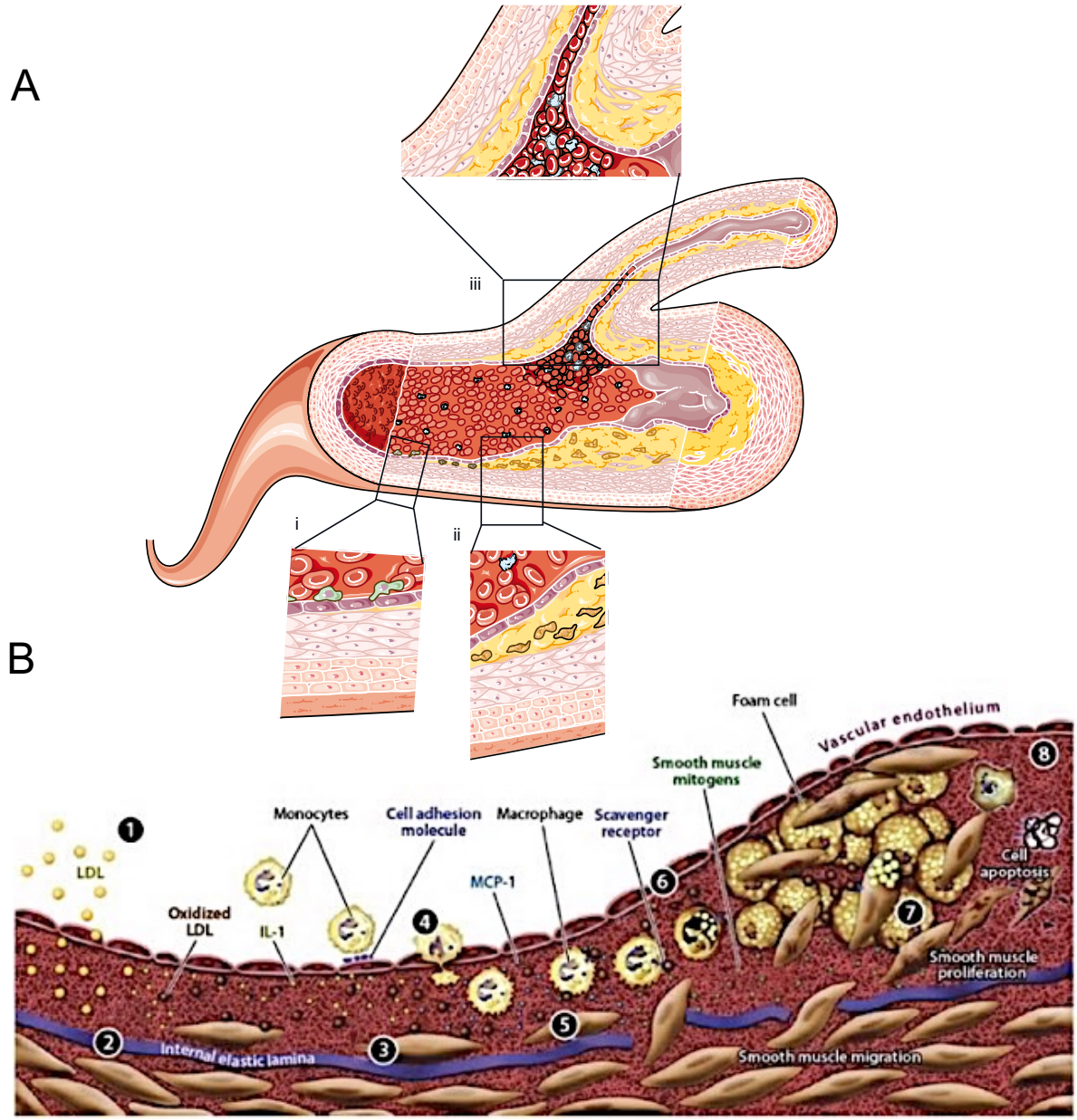

Fig 1.1 Atherosclerosis progression.
(A). Overview of atherosclerotic plaque development along the arterial lining and arterial branch points. (i) Arterial lining free of atherosclerotic plaque. (ii) Moderate stage plaque with accumulation of foam cells protruding into the arterial intima (6,7, and 8). (iii) Increased development of atherosclerotic plaque at arterial branch point, due to altered endothelial cell morphology, in comparison to adjacent linear arterial sub endothelium. Images adapted from [47] and servier medical art (https://smart.servier.com). (B) The 8 stages of development of an atherosclerotic plaque. (1 and 2) LDL moves into the sub endothelium and is oxidized by macrophages and smooth muscle cells. (3 and 4) Monocytes transmigrate across the arterial endothelium. (5) Monocytes differentiate into macrophages which engulf oxLDL to form (6) foam cells. Foam cells enhance the release of growth factors and cytokines that attracts additional monocytes and promotes (7) resident vascular smooth muscle cell proliferation. (8) Defective clearance of apoptotic foam cells contributes to necrotic core formation and development of advanced atherosclerotic plaque.

1.1.6 Macrophages in Atherosclerosis

In atherosclerosis, the innate immune cells, macrophages, have a central role in the growth, progression and stability of arterial plaques. The proinflammatory environment of the plaque can compromise macrophage function and promote disease progression [48]. During the early stages of atherosclerotic plaque development, monocytes are recruited to the sub endothelium where they differentiate into macrophages with the aim of clearing accumulated modified lipoproteins [49]. Although initially beneficial, increased accumulation of lipoproteins within the sub endothelium reduces the ability of macrophages to effectively clear all lipoproteins, resulting in the development of macrophage lipid-engorged foam cells [50]. Foam cell formation is a hallmark feature in the onset of atherosclerotic plaque formation. The diminished migratory capacity of macrophage foam cells causes them to accumulate within the arterial sub endothelium (**Fig 1.1 A-ii**), where they secrete chemo attractants (Mcp-1) [51], [52] and pro-inflammatory cytokines (reactive oxygen species, IL-6, TNF-α) promoting monocyte transmigration and the modification of circulating lipoproteins [53], [54].

Increased accumulation of modified LDL is known to promote glycolysis, oxidative damage and inflammation via the activation of the TLR4-TLR6 cascade [55]. The increased macrophage uptake of oxLDL, via scavenger receptors; SR-A, SR-B1, Cxcl16 and CD36, promotes lysosomal destabilisation, impairing cholesterol and fatty acid metabolism whilst activating the pro-inflammatory NLRP3 inflammasome [39], [53], [55], [56]. The engagement of macrophage scavenger receptors with oxLDL can also contribute to plaque macrophage

proliferation [57]. Considering monocyte recruitment has been shown to predominate early stage atherosclerotic plaque development [58], studies by Robbins et al., 2013 demonstrate macrophage proliferation largely contributes to the advancement of atherosclerotic plaques. Interestingly, they had shown macrophage proliferation contributes to 30% of early stage plaques and approximately 87% of advanced stage plaques [57]. The accumulation of proliferating macrophages and subsequent cholesterol loading contributes to the retention of plaque macrophages in the arterial wall. Increased macrophage cholesterol loading has been shown to promote the expression of neuroimmune guidance cues, including netrin-1 and semaphorin-3ε, both known to promote macrophage retention [59], [60]. Furthermore, an increase in inflammatory macrophage CD11d signalling has also been shown to contribute to plaque macrophage retention, where a reduction in plaque macrophage content and lipid deposition was identified in mice lacking CD11d [61]. Additionally, increased vascular endothelial cell expression of junctional adhesion molecule C (JAM-C), also contributes to macrophage retention upon blocking the reverse transmigration of macrophages within the atheroma [62]. Collectively, this contributes to reduced macrophage egress and increased atherosclerotic plaque development.

Increases in the accumulation of aortic macrophages and lipid content, leads to the resultant increase in macrophage cholesterol uptake. Under homeostatic conditions modified lipoproteins taken up by plaque macrophages are transported to the late endolysomal compartments where they are hydrolysed to form free cholesterol [30]. This free cholesterol is either trafficked for cellular

export or delivered to the endoplasmic reticulum where it is re-esterified by ACAT enzymes to form cholesterol esters [30]. Cholesterol esters are stored as lipid droplets within the macrophage where they contribute to foam cell formation and are pivotal in the initiation of atherosclerotic plaque development [63], [64]. During the initial stages of plaque development, macrophages efflux cholesterol via the ABC cholesterol transporters; Abca1 and Abcg1 [65], [66]. These cholesterol transporters are regulated by the nuclear liver-x-receptor (LXR) which is activated by cholesterol metabolites; 27-hydroxycholesterol and 25-hydroxycholesterol [67]–[69]. In order for macrophages to effectively efflux cholesterol, via Abca1, a constant supply of ATP must be provided from mitochondria to enable Abca1-mediated cholesterol transport [65], [70]. This is due to the ability of ATP to fuel Abca1 activity in mediating transmembrane LDL transport to ApoA1, for it to be further metabolised in the liver. However, dysregulated macrophage mitochondrial function compromises the ability of macrophages to effectively efflux cholesterol via Abac1, contributing to foam cell formation and defective reverse cholesterol transport [71].

Defects in the esterification of free cholesterol and cholesterol efflux can lead to macrophage death within the atherosclerotic plaque [72]. Advanced atherosclerotic plaques display enhanced ER stress which further contributes to macrophage apoptosis [73]. However, decreasing ER stress has been shown to reduce atherosclerotic plaque development, highlighting the importance of macrophage ER stress in the progression of atherosclerosis [74]. Altered macrophage phenotype and function remains pivotal to plaque progression, specifically as the combination of defective cholesterol efflux, enhanced cell

death and defective efferocytosis of apoptotic macrophages results in secondary necrosis [75]. The concomitant release of cellular lipids into the plaque contributes to the formation of a lipid rich acellular necrotic core that is amongst the defining features of vulnerable advanced atherosclerotic plaques [31].

Macrophages have therefore, been identified as a crucial immune cell in the development and progression of atherosclerosis. However, their function and phenotype can vary depending upon the local tissue environment [76], genetic and epigenetic factors [77]. For this reason, several studies have been performed investigating plaque macrophage phenotype and function in human carotid plaques and mouse aortic plaques [78]–[81]. Studies by Cochain and colleagues reveal three distinct macrophage subsets from atherosclerosis prone-$LDLR^{KO}$ mice [78]. They uncovered a resident like macrophage subset that harbour a similar transcriptional profile to healthy aortic macrophages, an inflammatory subset that were highly enriched for Il-1β and trem2hi macrophages that harboured a transcriptional profile enriched in lipid metabolic and catabolic processes. Collectively this study [78] highlights how distinct aortic macrophage subsets, characterised on their different gene expression profiles, may contribute to the altered macrophage phenotype and function associated with atherosclerosis.

To better understand the characteristics of lipid-laden foamy macrophages that are formed during the initiation of atherosclerosis development, Kim et al.,2018, compared the transcriptional profile of foamy aortic macrophages to non-foamy aortic macrophages from western diet-fed $LDLR^{KO}$ mice [79]. Using

RNA sequencing analysis on the CD45+ leukocyte aortic macrophage population, Kim and colleagues reveal the intimal non-foamy macrophages where enriched in pro-inflammatory genes, including IL-6 and IL-1β, in comparison to foamy aortic macrophages. Furthermore, they demonstrated foamy macrophage accumulation positively correlated with atherosclerosis severity, thereby demonstrating foamy intimal macrophages are less likely to drive lesional inflammation [79].

In humans, Lin et al., 2019 reveal a novel transcriptomic signature in macrophages from the carotid plaques of symptomatic patients, whom previously suffered a stroke, and asymptomatic patients whom have not suffered any cardiovascular event [82]. Similarly to Cochain and colleagues, Lin et al.,2019 also identify clusters of macrophages that display distinct transcriptomic differences. Macrophages from asymptomatic plaques displayed an increase in pro-inflammatory, IL-1 and IL-6 signalling, lipid uptake and metabolism, via enriched Apoc1 and Apoe and cholesterol transportation via Npc2 [82]. Whereas macrophages from symptomatic plaques displayed increased enrichment of genes involved in RXR/PPARα signalling, known to promote the polarization of macrophages to an alternative M2 phenotype and genes enriched in iron metabolism and iron storage [82]. This is characteristic of intraplaque haemorrhaging [83] and has been previously associated with atherosclerotic plaque progression and instability [31].

Collectively these data demonstrate the importance of macrophage function across all stages of atherosclerotic plaque development. Although macrophages

are crucial for maintaining optimal cholesterol metabolism and homeostasis, mitochondrial maintenance and effective clearance of apoptotic cells, the mechanism underlying their functional role in atherosclerosis is not well understood. Many studies have uncovered transcriptional differences amongst aortic and plaque macrophages from western diet fed mice [78], [79] alongside macrophages from human carotid plaques [84]. However, the regulation of these transcriptional differences by specific transcription factors is still poorly understood.

1.2 Interferon Regulatory Factors

Interferon regulatory factors (IRFs) consist of a family of 9 IRFs that have been identified in the mammalian and murine species. All 9 IRFs have been characterised according to their multi domain structure. They share a common N-terminal helix-turn-helix DNA binding domain (DBD) that binds to a core IRF motif; GAAA. They also possess a peptide linker and a less well conserved C-terminal interferon association domain (IAD) [85] to which they form unique protein-protein interactions (**Fig 1.2**), lending to the IRFs ability to function as transcriptional activators or repressors [86]. The carboxy terminal therefore confers specificity to each individual IRF. Based on the structure of the DNA binding domain, each IRF can be sub-grouped into subfamilies of IRFs that bind to similar transcription factor partners and thus to similar response element sequences (**Fig 1.2**) [87]. An additional subset of IRF proteins (IRF4,5,7) also contain an auto-inhibitory domain. This regulates their activity based on conformational changes that are either dependant or independent on their phosphorylation [88]–[90]. IRFs are able to activate and expand immune responses specifically via the IFN and TLR signalling cascades, where they form

binding partners with transcription factors that enable activation of a select subset of genes [91]–[94].

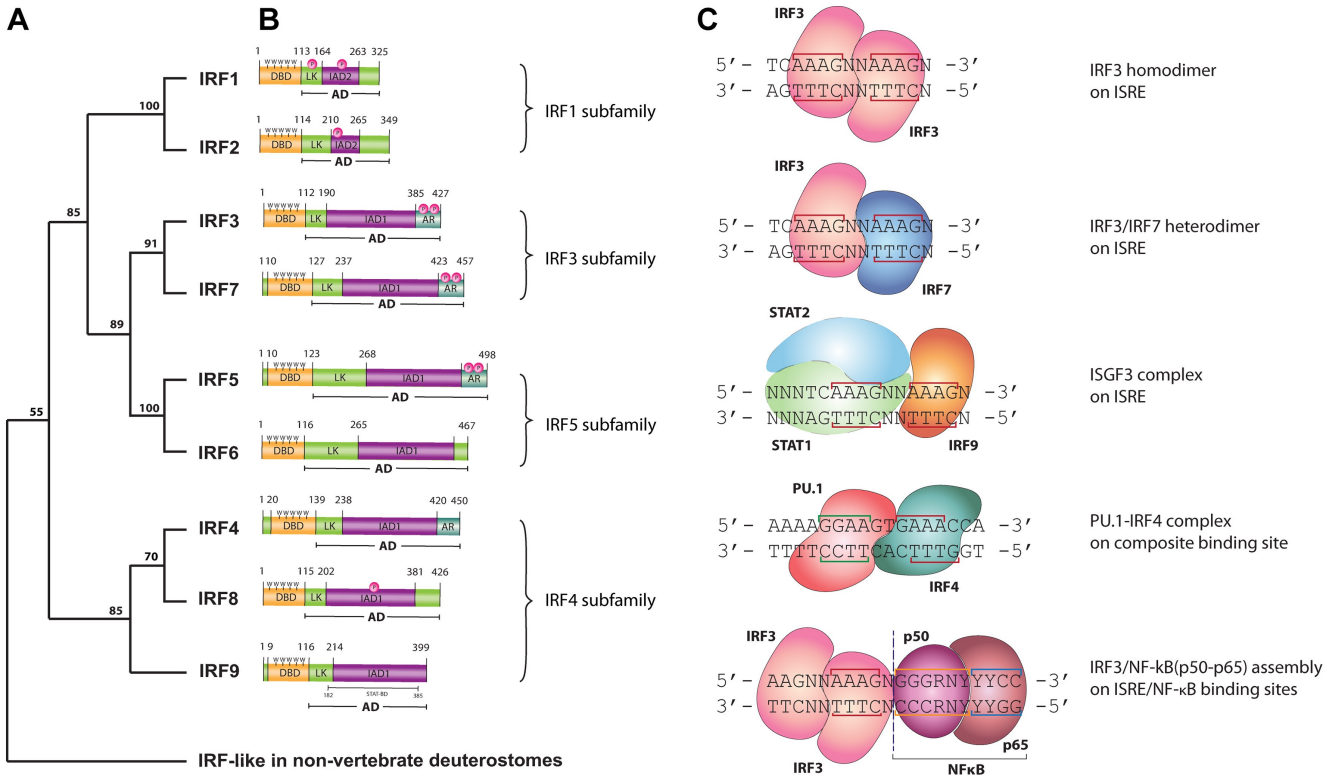

Figure 1.2 Structure of IRFs, their binding site sequences and their phylogenetic tree. (A) Phylogenetic tree of all IRFs as identified from the NCBI BLAST server. (B) Structure of the IRF proteins and their functional domains (DBD = DNA binding domain, LK = linker region, IAD = Interferon association domain, AR = autoinhibitory region, AD = activation domain). (C) Binding site sequences formed from different IRF binding partners. Image from [95]

IRF1 is ubiquitously expressed and has been implicated in the development of many diseases. Upon exposure to tuberculosis, mice that lack IRF1 displayed a reduction in iNOS expression and increased CD4/CD8+ T-cell ratio [96]. Reduced IRF1 in mice has also been implicated in regulating the expression of MHC I and II genes in CD8+ T cells demonstrating its importance in antigen presentation [97]. The role of IRF1 in cardiovascular disease has been demonstrated in coronary smooth muscle cells, specifically where phosphorylation of IRF1 has been correlated with the cell-cycle arrest in coronary smooth muscle cells [98]. Further data supporting the role for cardiovascular disease development has highlighted novel STAT1 and NF-κB binding sites that are specifically recognised by sequences within the IRF1 promoter. Binding of IRF1 to STAT1 and NF-κB has been demonstrated to regulate genes across different cell types within human atherosclerotic plaques [99].

Similarly to IRF1, IRF2 is ubiquitously expressed at low levels under physiological conditions. However, once phosphorylated IRF2 represses interferon sequence response elements in IRF1-induced IFNβ-signalling pathways [100]. IRF2 also represses NF-κB induced MHC-1 gene expression in neuroblastoma. Collectively this demonstrates the repressive roles of IRF2, in comparison to IRF1 [101].

Of all IRFs, IRF3 and IRF7 are widely known to regulate genes when bound as a heterodimer. The IRF3/7 heterodimer is involved in the progression of inflammatory disease, viral infection and in promoting sceptic shock [102]. Mice lacking IRF3 and IRF7 display an aberrant increase in viral RNA load when

infected with dengue virus [103], herpes simplex virus [104] and chikungunya infection [105], due to the disruption in IFNβ signalling.

Interestingly, recent studies have identified polymorphisms in IRF5 in patients with systemic lupus erythematosus and rheumatoid arthritis whom have an increased risk of developing cardiovascular disease [106]. The IRF5 polymorphism's in rheumatoid arthritis patients revealed protective effects against the risk of cardiovascular disease, implicating the potential role of IRF5 in autoimmune mediated cardiovascular risk [107].

IRF6 shares a similar structure to IRF3 and is widely expressed across the placenta, kidney and liver with the strongest expression observed in epithelial cells [108]. Within epithelial cells, IRF6 is important for the TLR3 mediated activation of IFNβ, IL-18 and CCL5 [109]. The importance of IRF6 within epithelial cells has also been demonstrated in a model of breast cancer, where it's known to bind the enhancer sequence of the p63 tumour suppressor gene mediating its expression [110].

Unlike the IRFs mentioned, IRF4, and 8 are crucial in leukocyte development. IRF4 is required for the proper functioning and maintenance of homeostasis of mature B and T cells, whereby mice deficient in IRF4 demonstrate a skew in B and T cell development resulting in lymphadenopathy [111]. Both IRF4 and IRF8 are crucial for development of B-cells as they heterodimerise and regulate the expression of genes necessary for B cell differentiation [112].

Similarly to IRF5, IRF9 has also been implicated in systemic lupus erythematosus (SLE). Mice with SLE lacking IRF9, demonstrate the necessity of IRF9 and STAT1 binding in the production of IgG autoantibodies [113].

Collectively, this demonstrates the diversity in structure and function amongst the individual IRFs owing to their importance in different immune processes.

1.3 Interferon Regulatory Factor 8 (IRF8)

IRF8 is an IFNγ inducible hematopoietic transcription factor that is crucial in myeloid cell development. As briefly discussed, the major functions of the IRFs involve transcriptional regulation of the immune system and cellular growth processes [114]. IRF8 functions as a transcriptional activator upon forming a heterodimer, via it's IAD, with either members of the Ets transcription factor family, eg PU.1, or members of the AP-1 family, eg BATF3, as demonstrated in **Fig 1.3** [115], [116]. The IRF8-PU.1 heterodimer promotes transcriptional activation upon binding to an EICE response element (GGAAnnGAAA) proximal to the promoter region of the target gene [117]. Similarly, the BATF3-JUN-IRF8 heterodimer also promotes transcriptional activation upon binding an AICE response element (TGAnnnGAAA or GAA ATGA), proximal to the promoter region of the target gene [118]. Upon binding to these response elements, when functioning as a transcriptional activator, IRF8 is able to regulate a select number of genes and processes that are crucial for immune effector response [86], [119]. IRF8 also functions as a transcriptional repressor, upon forming heterodimeric complexes with other IRFs, including IRF1 and IRF2, and binding an ISRE response element (GAAAnnGAAA) on its target gene [120]. This dual

transcriptional activity allows IRF8 to effectively regulate myelopoiesis and immune effector processes.

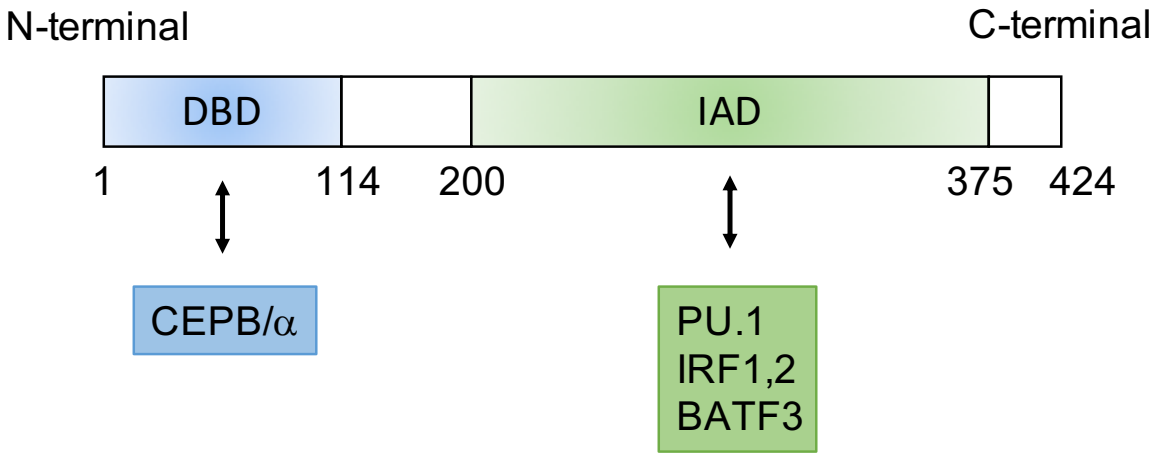

Fig 1.3 Schematic of IRF8 structure. The N-terminal harbours the DNA binding domain, which is important in the repression of C/EBPα. The C-terminal harbours the interferon association domain, which is crucial for interactions with other transcription factors, including PU.1, IRF1, IRF2 and BATF3.

1.3.1 IRF8 and myelopoiesis

IRF8 is crucial for the development of cells in the myeloid lineage (dendritic cells, monocytes, macrophages and neutrophils), as demonstrated in **Fig 1.4**. By transcriptionally regulating key lineage pathways in haematopoietic progenitor cells, IRF8 contributes to the maintenance, terminal differentiation and function of myeloid cells [121], [122]. The crucial role of IRF8 in myelopoiesis was originally discovered in global IRF8-KO mice by Holtschke and colleagues [123]. Global IRF8-KO mice displayed an aberrant increase in neutrophil accumulation, defective plasmacytoid dendritic cell (pDC) function and significant depletion in circulating conventional dendritic cells (cDCs), monocytes and macrophages, collectively mimicking a chronic myeloid-leukaemia like syndrome [123]. This has since prompted investigation into the role of IRF8 in myelopoiesis and the

resultant effect on myeloid cell function. Recent studies using IRF8-reporter mice identified the expression of IRF8 from the granulocyte-myeloid progenitors (GMP) onwards. IRF8 expression was later increased in myeloid-dendric progenitors (MDP) where cells became committed to the myeloid lineage [124]. Within MDPs, IRF8 functions to specifically inhibit continued neutrophil development and promote myeloid cell development. Previous studies by Kurotaki et al., 2014, demonstrated IRF8 transcriptionally repressed the transcription factor C/EBPα upon binding an ISRE sequence proximal to the C/EBPα promoter, via its DNA binding domain [125]. As C/EBPα is crucial in promoting neutrophil development, repression by IRF8 prevents C/EBPα from binding and transcriptionally activating genes required for neutrophil development [125]. Thus, the global-IRF8KO mouse model displays an aberrant increase in neutrophils, as IRF8 is not present to transcriptionally repress further neutrophil development. Interestingly, Kurotaki and colleagues also uncover different modes of action by which IRF8 suppresses neutrophil development and promotes development of the myeloid lineage. Upon employing two different mutations within the IAD and DBD of IRF8, Kurotaki and colleagues demonstrated mutations within the IAD, specifically hindered monocyte and macrophage development, whereas mutations in the DBD hindered neutrophil development [115], [126]. Collectively this demonstrates IRF8 transcriptionally represses C/EBPα activity via its DBD and promotes myeloid-cell lineage via interactions with its IAD.

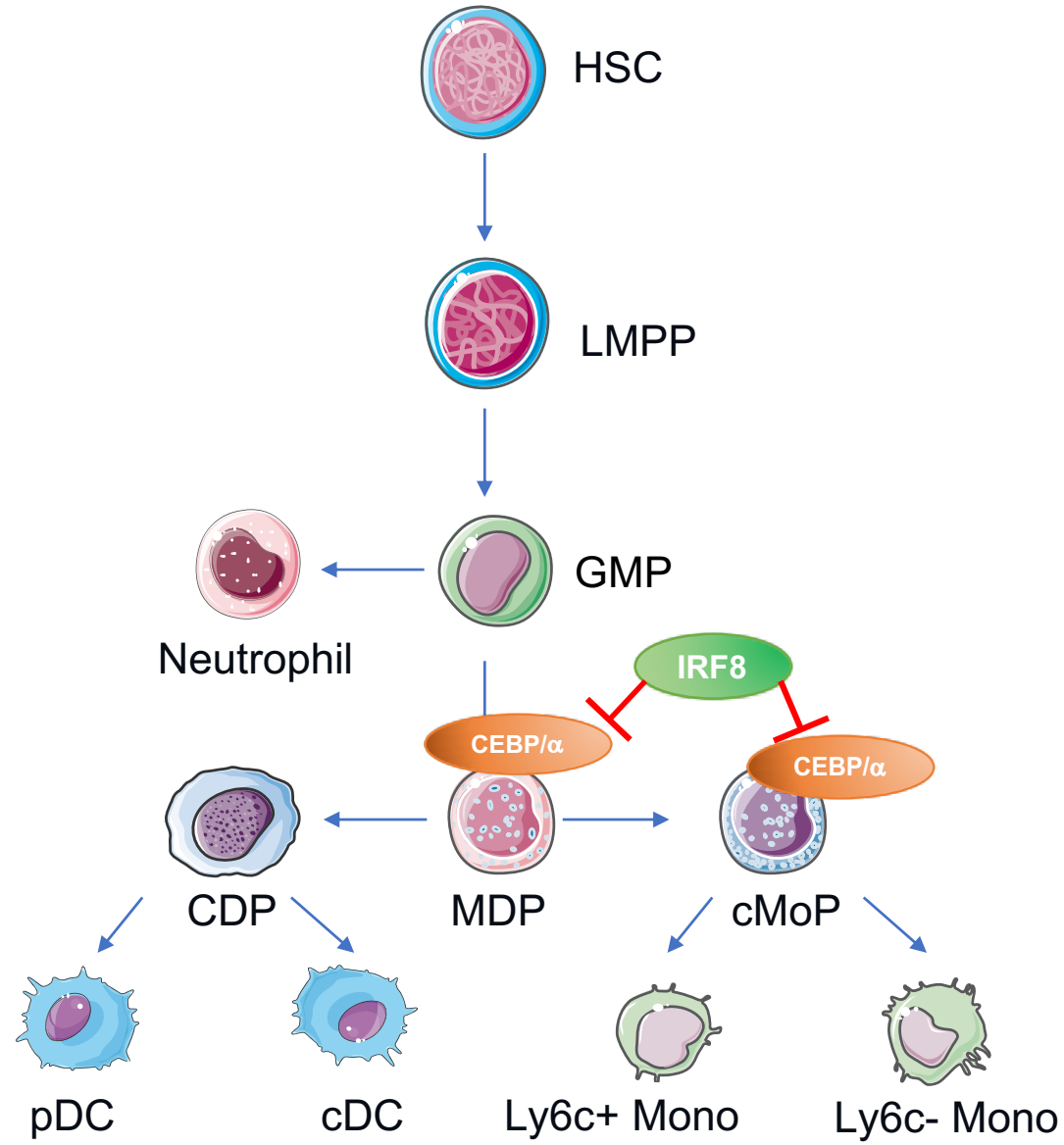

Fig 1.4 IRF8 in haematopoiesis.
IRF8 binds to and inhibits the expression of C/EBPα in MDPs and cMoPs, preventing C/EBPα mediated neutrophil differentiation. IRF8 is also required for the development of Ly6Chi and Ly6CLo monocytes, CDPs, pre-cDCs, CD8+ cDCs and pDCs (HSC – Haematopoietic stem cells, LMPP - lymphoid-primed multipotent progenitors, GMPs – Granulocyte-monocyte progenitors, MDPs – myeloid dendritic progenitors, CDPs – common dendritic progenitors, cMOPs – common monocyte progenitors, cDCs – common dendritic cells, pDCs – plasmacytoid dendritic cells). Figure adapted from [119].

As previously discussed, IRF8 activates gene transcription upon protein-protein interactions via its interferon association domain with Ets or AP-1 transcription factors. Recent studies have demonstrated the IRF8-PU.1 heterodimer is crucial in the activation of genes required for the early stages of

monocyte development [115], [116], [119], [127]. IRF8 expression within MDPs, is crucial for their differentiation into common monocyte progenitors (cMoP) which initiates monocyte and macrophage development. Kurotaki et al., 2013 demonstrate IRF8 heterodimerizes with PU.1 in cMoPs and drives the formation of H3K4me1, which is characteristic of enhancers, to induce chromatin remodelling at sites of IRF8-target genes. Of genes transcriptionally activated by IRF8-PU.1, the Kruppel-like factor 4 gene was identified as a crucial IRF8 target in the development of monocytes [128]. IRF8 induction of KLF4 promotes the development of monocytes from MDPs and cMoPs. This was supported by studies demonstrating monocyte development was defective in KLF4 deficient mice similarly to that observed in IRF8 deficient mice [129]. However, considering IRF8-KO MDPs do not express KLF4, reintroduction of KLF4 resulted in partial monocyte and macrophage development [130]. Collectively, this highlights the importance of IRF8-KLF4 in early stage monocyte development in MDPs.

Considering IRF8 is required in monocyte lineage determination, Sichien and colleagues have recently discovered IRF8 it is not required for the survival of terminally differentiated monocytes [122]. Interestingly, they also uncovered IRF8 is required for the differentiation of dendritic cells from common dendritic progenitors (CDP) that also stem from MDPs (**Fig 1.4**), enhancing our understanding on the role of IRF8 in myelopoiesis. Sichien and colleagues demonstrated IRF8 was necessary for the survival and function of conventional dendritic cells (cDCs) and plasmacytoid dendritic cells (pDCs) [122]. Upon using different conditional IRF8-KO mouse models to elucidate the role of IRF8 in early stage and terminally differentiated dendritic cells, Sichien et al., 2016 discovered

IRF8 was required for specification of CDPs to pre-cDCs and their commitment to cDC1s, via blocking their conversion to cDC2s. Global IRF8-KO mice lack pre-cDCs demonstrating the necessity of IRF8 for the commitment of CDPs to the cDC1 lineage. However, unlike monocytes, IRF8 was also required for the maintenance of terminally differentiated late stage cDC1s, as demonstrated in the $IRF8^{fl/fl}$ $Itgax^{cre}$ mice that specifically deletes IRF8 from pre-cDC cells onwards. Collectively, this demonstrates IRF8 is required for the development of pre-CDCs, from MDPs, and the terminal differentiation of pre-cDCs to cDC1s, without impacting on cDC2s [122].

In contrary, pDCs where unaffected by IRF8 deletion in global IRF8-KO and $Itgax^{cre}$ $IRF8^{fl/fl}$ mice, demonstrating IRF8 is not required for the development of pDCs, unlike cDC1s. However, Sichien and colleagues interestingly uncovered a difference in pDC function in response to IRF8 deficiency. When challenged with a pro-inflammatory TLR9 agonist, CpG, pDCs from IRF8-KO mice displayed a significant reduction in IFN-α production and failed to activate and induce the proliferation of $CD4^+$ T-cells [122]. Taken together this demonstrates IRF8 harbours distinct intrinsic cellular roles at various stages of lineage determination. Not only is IRF8 crucial for lineage determination of monocytes and cDCs but also for the optimal function of pDCs to produce type-I interferons and activate and induce T-cell proliferation in response to infection.

1.3.2 IRF8 and Interferon signalling

The interferons (IFNs) are a group of cytokines that are well characterised for their response to inflammation, apoptosis and cell proliferation, as a first line

of defence against viral infections [131], [132]. The group is separated in three classes of IFNs: Type I, Type II and Type III. The type I IFNs constitute 13 different subtypes, including IFNα, IFNβ, IFNκ, IFNω and IFNε. The Type II IFN solely consists of IFNγ and the Type III IFN subfamily is made up of IFNλ1, IFNλ2, IFNλ3, and IFNλ4 [133]. Considering all interferons mediate the anti-viral immune response, they all induce different transcriptional regulatory pathways resulting in different immune responses.

1.3.2.1 Type I IFN signalling

The Type I IFN subfamily are known to directly induce an antiviral immune response via signalling through the JAK/STAT pathway [134]. Type I IFNs are produced when pattern recognition receptors, including the toll-like receptor 9 (TLR9), recognise circulating viral DNA and RNA [135]. This stimulates the transcription of IRF3 and IRF7, via TLR9-induced activation of the MyD88 pathway [136]. The IRFs heterodimerise and bind an ISRE element proximal to the IFNα or IFNβ promoter, initiating their transcription and subsequent production. The type I IFNs produced bind to their heterodimeric receptor composed of two chains; IFNAR1 and IFNAR2. Formation of the IFNAR1/IFNAR2 complex leads to the activation of tyrosine kinase 2 (TYK2) and JAK 1 kinases. The kinases then phosphorylate and activate STAT1 and STAT2. Upon phosphorylation, STAT1 and STAT2 heterodimerise with IRF9, to form the interferon-stimulated gene factor 3 (ISGF3) transcription complex. The ISGF3 complex translocates the nucleus and binds the ISRE sequence of target genes, initiating gene transcription (**Fig 1.4**). ISGF3 is known to promote the transcription of almost 300 interferon response genes, all of which contribute to

anti-viral immunity [137]. IFNα requires the heterodimerisation of both receptors to activate JAK/STAT signalling. However, IFNβ is also able to form a stable complex with IFNAR1 independent of IFNAR2, thereby stimulating gene expression independent of the JAK/STAT pathway resulting in differential gene regulation by IFNα and IFNβ, as demonstrated in **Fig 1.5** [138].

Considering IRF3, IRF7 and IRF9 are highly involved in regulating the transcription of type I IFN-induced genes, IRF8 has also been identified as a crucial transcription factor for the production of Type I IFNs in monocytes and dendritic cells [139]–[141]. Previous work by Tailor and colleagues [140], demonstrated the importance of IFNα production in Newcastle disease virus infected pDCs and cDCs. Interestingly, IRF8 was required to amplify the production of IFNα in DCs by recruiting RNA polymerase II to the promoter of IFNs post viral infection. Deletion of IRF8, however, abrogated IFNα production even in the presence of RNA-polymerase II, therefore demonstrating the importance of IRF8 in IFN production [140]. Similarly, Li and colleagues uncovered the importance of IRF8 in promoting IFNβ production in human monocytes. IRF8 was shown to heterodimerise with PU.1 and bind the EICE response element identified upstream the IFNβ promoter site [141]. This allowed for the recruitment of IRF3 to the promoter region and induction of IFNβ gene transcription [141]. Although, both studies define the importance of IRF8 in the production of Type I IFNs, they do not define IRF-regulated expression of interferon stimulated genes in response to IFNβ. Mancino and colleagues aimed to further understand the possible role of IRF8 in downstream IFNβ signalling [86]. Upon using a mouse model that harboured a single point mutation in the interferon association domain (IAD) of IRF8, they generated an IRF8-silenced

mouse model, called Bxh2, and stimulated the bone marrow derived macrophages (BMDMs) with IFNβ. Interestingly, RNA-sequencing analysis demonstrated a significant reduction in the expression of interferon stimulated genes in Bxh2 macrophages, implying their regulation by IFNβ induction is also dependent on IRF8 expression [86]. They also identified a large overlap in the genomic occupancy of STAT1, STAT2 and IRF8 on many interferon response genes, suggesting many IFNβ inducible genes regulated by STAT activation, are also regulated by IRF8. This is amongst the first study to demonstrate that IRF8 controls the IFNβ induced response downstream of IFNβ activation [86].

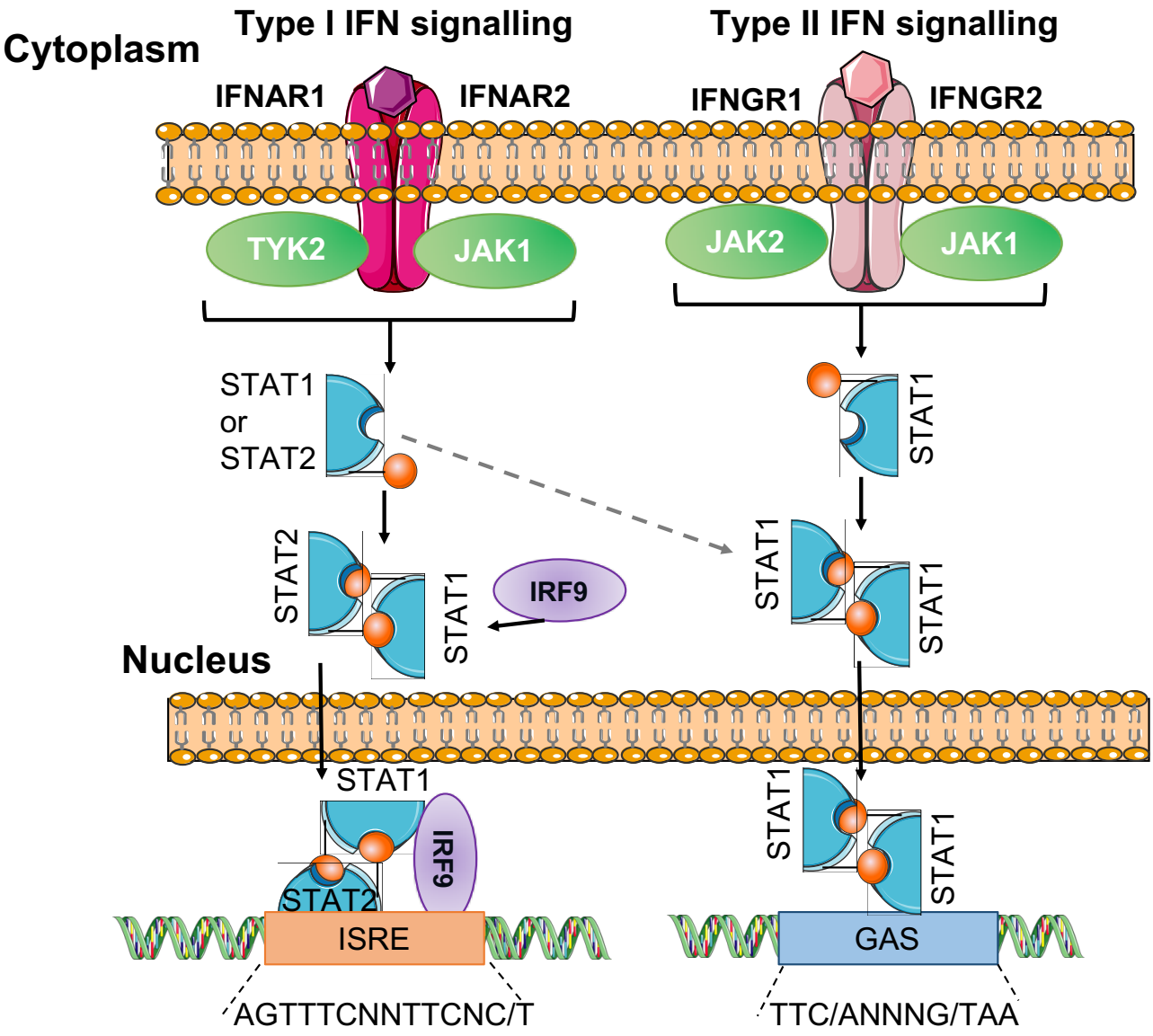

Fig 1.5 Type I and II IFN signalling transduction pathways.
Type I IFN signals via binding to the receptors; IFNAR1 and IFNAR2. This activates JAK1 and Tyk2, thus promoting the phosphorylation and activation of STAT1 or STAT2. Activated STAT1 forms either a homodimer with STAT1 or heterodimer with STAT2 and forms a heterodimeric complex with IRF9, forming the interferon stimulated gene factor-3 (ISFG3) complex. Upon nuclear translocation this complex is able to bind ISRE elements proximal to the promoter of target genes thereby regulating gene transcription. Type II IFNs bind the NFGR1 and IFNGR2 receptor subsequently activating the JAK1/JAK2 kinases. The kinases phosphorylate STAT1 thereby activating it and mediating homodimer formation. The STAT1 homodimer then translocates the nucleus where it binds specific gamma-activated sequences (GAS), proximal to the promoter of its target gene, regulating gene transcription. Image components used at the courtesy of servier medical art, Image adapted from [142].

1.3.2.2 Type II IFN signalling

The type II IFN, IFNγ, is a cytokine predominantly released when NK cells and T-cells become activated in response to viral and bacterial infection [143]. IFNγ is constitutively expressed in NK cells and NKT cells, allowing for its rapid induction in response to infection [144]. The increased production of pro-inflammatory cytokines, IL-12 and IL-18, in response to infection induces T-cells and NK-cells to enhance production of IFNγ, leading to the activation of antigen presenting cells [145], [146]. The binding of IL-12 to its receptor activates the Janus family kinases; TYK2 and JAK2. Upon activation they phosphorylate the tyrosine residues of STAT3 and STAT4 enabling their dimerization to form a STAT4 homodimer or STAT3/STAT4 heterodimer [142]. Enhanced IL-12 and IL-18 also promotes the phosphorylation of c-Jun in the nuclear compartment. Upon nuclear translocation, the STAT4 homo/heterodimers form a complex with the phosphorylated c-Jun. This STAT4/c-Jun complex subsequently binds an AP-1 site proximal to the promoter region of IL-12 responsive genes and IFNγ, thereby promoting their transcription [147]. A similar mechanism surrounding enhanced IL-18 and IL-12 has also been shown to promote IFNγ production in macrophages [148].

IFNγ exerts its anti-viral immune effects upon binding to its receptors IFNγR1 and IFNγR2 (**Fig 1.5**). Upon binding, the receptors heterodimerise and associate with JAK1 and JAK2, inducing their activation. This subsequently induces the phosphorylation of STAT1 and promotes the formation of a STAT1 homodimer. The STAT1 homodimer translocates the nucleus where it binds a gamma-activated sequence (GAS) proximal to the promoter region of its target

interferon stimulated genes and IRFs, thereby inducing their transcription, as demonstrated in **Fig 1.5** [137]. As IRF8 harbours a GAS response element upstream its promoter, IFNγ, is known to promote its expression [149]. However, IFNγ, also harbours an EICE response element of which IRF8 binds in conjunction with PU.1 thereby promoting IFNγ expression resulting in a positive feedback loop [150].

The importance of IFNγ in IRF8-mediated gene expression has been well characterised in macrophages [94]. Previous studies have demonstrated the importance of IRF8 in the response to IFNγ in various cancerous carcinoma models [151], [152]. Defective IRF8 expression, due to mutations or methylation at the promoter region, are associated with increased prevalence of chronic myeloid leukaemia, demonstrating the role of IRF8 as a tumour suppressor gene [153], [154]. However, Lee and colleagues [151] further established the defective response to IFNγ in multiple carcinoma cell lines was due to decreased expression of IRF8. Thus, confirming the importance of IFNγ in IRF8 mediated gene transcription in a cancer model [151]. However, to investigate the mechanism by which IFNγ induces IRF8 regulated gene expression, Kuwata and colleagues performed mass spectrometry on IFNγ treated macrophages [155]. Interestingly, they identified another Ets transcription factor, TEL, that was recruited to the ISRE element of IRF8 target genes, when stimulated with IFNγ. Heterodimerisation of IRF8 and TEL, led to the suppression of many interferon response genes containing an ISRE, via the IRF8/TEL mediated recruitment of histone deacetylase, HDAC3. Recruitment of HDAC3 led to the remodelling of chromatin, mediating the suppression of IFNγ induced IRF8/TEL target genes

[155]. Collectively this highlights the importance of IFNγ induction in mediating IRF8 gene regulation in conjunction with TEL and HDAC3. To further understand the biological processes that are regulated by IRF8 in response to IFNγ induction, Langlais and colleagues performed RNA-sequencing on IFNγ induced macrophages from IRF8 mutated, Bxh2 mice [94]. Many IFNγ inducible genes regulated by IRF8 where involved in processes crucial for the activation of antigen presenting cells, T-cells and inflammation. However, Langlais and colleagues also identified significant regulation of genes involved in chemotaxis and phagocytosis, processes that are crucial for macrophage function.

1.3.2.3 IFN signalling and atherosclerosis

Defective IFN signalling has been highly associated with many inflammatory diseases, in particular atherosclerosis. Enhanced interferon signalling, through type I and type II IFNs, have been shown to promote atherosclerotic plaque development via increased endothelial cell activation, foam cell formation and apoptosis of leukocytes [156], [157]. Previous studies have demonstrated increased IFNγ promotes endothelial cell activation and leukocyte adhesion via increasing the expression of endothelial adhesion molecules [158]. This was additionally supported by Stokes and colleagues whom demonstrated IFNγ deficiency abrogated monocyte and T-cell recruitment to the atherosclerotic plaque, thus highlighting the importance of IFNγ in leukocyte recruitment [159].

Macrophages are amongst the most abundant leukocyte within the atherosclerotic plaque [75] and become activated upon IFN stimulation.

Interestingly, enhanced Type I and II IFN signalling has also been implicated in altered macrophage foam cell formation [160], [161]. Previous studies have demonstrated IFNγ induced lipid-laden macrophages to exhibit reduced cholesterol efflux, due to a significant decrease in macrophage Abca1 expression [160], [162]. This was supported by studies demonstrating IFNγ negatively regulates Cyp27a1 which is known to protect against atherosclerosis development by promoting macrophage cholesterol efflux via Abca1 expression [163]. Li and colleagues [161] demonstrate IFNα priming of human macrophages promotes oxLDL uptake and subsequent foam cell formation via enhancing scavenger receptor, SR-A, gene expression [161]. Altogether this supports the concept that enhanced Type I and Type II IFN signalling contributes to increasing foam cell formation in atherosclerosis.

The IFN signalling pathway has also been shown to contribute to the regulation of genes involved in apoptosis [164], [165]. Defective clearance of apoptotic cells increases atherosclerotic plaque inflammation and contributes to the formation of a necrotic core [166]. Considering differential IFN signalling has predominantly been implicated in apoptosis within cancer models [151], [167], recent studies have highlighted a possible role in macrophage apoptosis in atherosclerosis [168]. Previous studies have demonstrated both IFNβ and IFNγ promote the expression of apoptosis inducing genes and TNF-related apoptosis inducing ligand, Fas and Fas ligand [164], [168]. Goossens and colleagues have demonstrated western diet challenged, IFN receptor deficient, $IFNAR^{-/-}$, mice display a reduction in necrotic core formation which corresponds with the decreased macrophage apoptosis identified in $IFNAR^{-/-}$ mice [169].

Altogether this demonstrates Type I and II IFN signalling affects processes crucial to atherosclerosis development. Upon promoting endothelial cell activation [159], leukocyte infiltration [169], [170] and differentiation of monocytes to activated macrophages [171], type I and II IFNs are contributing to the initial onset and development of atherosclerotic plaque formation. Additionally, their contribution to macrophage foam cell formation, via dysregulation of scavenger receptor and cholesterol transporter gene expression [160], [161], [172], alongside macrophage apoptosis [164] demonstrates their role in advanced plaque development. Collectively this demonstrates enhanced Type I and II IFN signalling contributes to atherosclerosis plaque development and progression, making them attractive targets for future therapeutic and diagnostic applications.

1.3.3 IRF8 and atherosclerosis

Considering the role of IRF8 has predominantly been characterised in myelopoiesis and myeloid immune response [115], [122], [173], [174], few recent studies have identified a possible role of IRF8 in atherosclerosis development. Doring and colleagues were amongst the first to identify an atherogenic role of hematopoetic-IRF8 deficiency in mice challenged with a high fat western diet [175]. Upon transplanting the bone marrow from $IRF8^{KO}$ mice to atherosclerosis prone $Apoe^{KO}$ mice, they generated hemaotpoetic-$IRF8^{KO}$ mice. These mice developed a CML-like phenotype, as characterised by an aberrant increase in polymononuclear neutrophils (PMNs) and significant reduction in circulating monocytes. Deletion of IRF8 from all hematopoietic cells prevented IRF8 induced repression of the transcription factor C/EBPα which is crucial for neutrophil development. For this reason, IRF8 deficient GMPs, in the haematopoetic-

IRF8^{KO} mice, were unable to commit to the myeloid lineage and prevent further neutrophil development, resulting in the expansion of PMNs. Interestingly, when challenged with a high fat western diet the hematopoetic-IRF8^{KO} mice developed significantly more atherosclerotic plaques in comparison to the WT controls. However, plaque development was attributed to the significant increase in lesional apoptotic PMNs. Interestingly, Doring and colleagues also identified IRF8^{KO} macrophages were defective in efferocytosis, as demonstrated by the reduction in macrophage CD36, and significant decrease in IL-10 production, which is induced in response to phagocytosis of apoptotic cells [176]. However, depletion of PMNs abrogated the increased atherosclerotic plaque development in haematopoetic-IRF8^{KO} mice. This suggests that the CML-like phenotype caused by IRF8 deficiency resulted in enhanced atherosclerotic plaque development. Considering IRF8 deficiency appeared to impact on the ability of macrophages to effectively phagocytose apoptotic PMNs, the altered macrophage phenotype did not appear to impact atherosclerotic plaque area in the aortic root, as the absence of lesional PMNs did not impact on plaque development [175]. Collectively, this study has demonstrated dysregulated haematopoiesis, caused by haematopoietic IRF8 deficiency, promotes atherosclerosis plaque development in mice challenged with a high fat western diet.

To understand the cell-specific effects of IRF8 on atherosclerosis development, Clement and colleagues generated a CD11c^{cre}IRF8^{KO}LdlR^{KO} mouse model and challenged mice with a high fat western diet [177]. Upon removing IRF8 from CD11c^{+} cells, Clement and colleagues aimed to understand the role of

IRF8 in dendritic cells specifically, and how IRF8 deficiency would impact on the adaptive immune response in atherosclerosis development. Intriguingly, deletion of IRF8 dependant DCs abrogated atherosclerosis plaque development, when compared to controls. Considering dendritic cells are required for T-cell homeostasis, priming and activation in response to inflammation [178], it is not surprising that $CD11c^{cre}IRF8^{KO}LdlR^{KO}$ mice displayed a significant reduction in aortic T-cell accumulation coupled with defective western diet induced T-cell activation. By removing IRF8 from $CD11c^{+}$ cells, mice lacked $CD8a^{+}$ and $CD11b^{-}$ $CD103^{+}$ DCs, resulting in the profound effect of the adaptive immune response in atherosclerosis. A subsequent reduction in IFNγ expressing $CD4^{+}$ and $CD8^{+}$ T-cells was also identified alongside a reduction in IRF8 expression in DCs from $CD11c^{cre}IRF8^{KO}LdlR^{KO}$ mice. This implies IRF8 expression is required for western diet induced T-cell priming and activation towards T-helper, T-follicular and T-regulatory cells. Interestingly, the atherosclerotic plaques developed in CD11c-$IRF8^{KO}$ mice displayed a reduction in collagen, acellular region and no difference in foam cell formation, when compared to controls. Collectively, Clement and colleagues [177] have demonstrated the necessity of IRF8 in mediating the adaptive immune response in DCs in atherosclerosis. For this reason, $CD11c^{+}$IRF8-deficiency abrogates atherosclerotic plaque development by potentially delaying progression to advanced stage plaques [177].

Considering both studies have identified a novel role for IRF8 in the development of atherosclerosis development, the models used resulted in dysregulated immune cell homeostasis which was attributed to the main cause of atherosclerosis development. Further understanding of the role of IRF8 in

myeloid cells specifically, without dysregulating immune cell homeostasis, would help uncover the functional role of IRF8 in mature myeloid cells.

1.3.3.1 IRF8 in Lupus and Atherosclerosis

Recent evidence surrounding the role of IRF8 in atherosclerosis has been identified in mouse models, however, studies by Leonard and colleagues [179] are amongst the first to identify an association of IRF8 and cardiovascular related risk in systemic lupus erythematosus (SLE) patients. SLE patients are at a significant increased risk of developing coronary heart disease, with a 50-fold increase in susceptibility in comparison to the general public [180]. Although the exact mechanism associated with increased cardiovascular risk is currently unknown, many SLE-mediated effects including increased endothelial cell apoptosis [181], improper endothelial repair [182], decreased lipoprotein lipase activity [183] and increased type I IFN production [184] are all thought to contribute to cardiovascular disease. Leonard and colleagues interestingly uncovered a significant association between three single nucleotide polymorphisms in IRF8 across two populations of SLE patients with coronary heart disease [179]. The IRF8 risk allele was associated with the presence of carotid plaques and increased intimal thickening within SLE patients. Comparative analysis against genotyping results from SLE patients across other populations demonstrated the IRF8 SNPs have not previously been linked to SLE before. This demonstrates a novel association between IRF8 and coronary heart disease in SLE patients. Interestingly, although Leonard and colleagues did not identify a significant difference in the expression of IRF8 in the PBMCs from healthy and lupus patients, they identified a reduction in the frequency of pDCs

and B-cells in patients with the IRF8 risk allele. As IRF8 is important for B-cell development and pDC function, it's possible that IRF8 contributes to cell-type specific functions, which are masked in whole PBMCs [185]. Together, this identifies a novel association of IRF8 in cardiovascular disease within mouse and human studies, ultimately raising the possibility of therapeutically targeting IRF8 in cardiovascular disease.

1.4 Non-alcoholic fatty liver disease and atherosclerosis

Non-alcoholic fatty liver disease (NAFLD) is a metabolic syndrome that encompasses a collection of several liver disorders including; steatosis, steatohepatitis, advanced fibrosis and liver cirrhosis. NAFLD is one of the most common liver diseases, affecting 25-30% of the adult population in western countries [186]. This metabolic syndrome is often caused by a variety of environmental and genetic effects that result in excessive hepatic lipid and triglyceride accumulation resulting in increased hepatic inflammation and fibrosis [187]. NALFD patients are known to have an increased risk of developing coronary artery disease, particularly due to their dysregulated hepatic lipid metabolism. The risk of cardiovascular disease in NAFLD patients has been correlated with increased calcium deposits in arteries, coronary artery stenosis and atherosclerosis [188], [189].

Differences in the expression of transcription factors known to regulate genes involved in lipid-metabolic signalling pathways, including the liver-x-receptor (LXR) regulation of Srebp2, Abcg5 and Abcg8 have been highly associated with NAFLD development [190]. Interestingly, the IRF transcription factors have also

been associated with the development of NAFLD, in particular IRF5, IRF6 and IRF9 [191]–[193]. When mice where challenged with a high fat western diet, the expression of IRF6 was crucial for the negative regulation of peroxisome proliferator-activated receptor γ (PPARγ) induced lipogenesis and fatty acid uptake, ultimately protecting against NAFLD progression [194]. Similarly, IRF9, has been shown to protect against NAFLD development when over expressed, due to its positive regulation of PPAR-α target genes known to maintain hepatic fatty acid metabolism [193], [195]. In contrast, human NAFLD patients demonstrate a significant increase in the expression of hepatocyte-IRF5, which was correlated to clinical markers of liver damage including increased bilirubin and plasma transaminase. Interestingly, mice lacking IRF5 in myeloid cells where protected from hepatic stenosis and fibrosis highlighting IRF5 as key transcription factor in NAFLD progression [196].

Collectively this demonstrates IRFs are important transcription factors in regulating signalling pathways that are differentially expressed in patients and mice with NAFLD that are also at a higher risk of developing cardiovascular disease. Although IRF8 specifically has not been implicated in NAFLD development, it is a known target gene of the nuclear receptor LXR which contributes to both NAFLD and atherosclerosis due to its regulation of genes involved in triglyceride metabolism [190], [197]. For this reason, the association of IRF8 and fatty liver disease, in the context of atherosclerosis development, will be addressed later within this thesis.

1.5 Ageing in the healthy human population

Advances in modern medicine and improvements in socio-economic status is vastly progressing the human lifespan . Current predictions estimate the global population to increase up to threefold, reaching approximately 2 billion people by 2050 [198]. Biological ageing is a multidimensional process that is established by the degradation of biological and cellular function over time. Age-related diseases account for approximately 30% of all deaths worldwide and with an increasing aged population, this is likely to increase. Many age-associated disorders include Alzheimer's disease, atherosclerosis and cancer [199], [200]. Often these are caused by a dysregulation of immune cell function, due to cellular senescence, ultimately contributing to increased susceptibility towards inflammation and infection across the aged population [201]. With a vastly increasing aged population, especially within developed countries, management strategies are required to maintain healthy ageing and reduce the prevalence of age associated diseases.

1.5.1 Ageing-associated dysregulated immune response

The process of ageing results in multiple changes at the molecular and cellular level, including senescence, telomere attrition, transcriptomic and epigenetic modifications [202]. Traditionally telomere attrition has been highly associated with increasing age and cellular senescence. Telomeres are chromatin structures located at the end of chromosomes [203]. Their associated proteins cap the ends of chromosomes therefore protecting telomeres from degradation. Cells without telomeres are highly unstable and often lost during cell growth due to degradation, leading to cell loss [204]. However, with increasing

age telomeres gradually shorten, preventing the recruitment of their associated proteins, leaving the ends of chromosomes uncapped and open to degradation. Uncapped telomeres resemble double stranded DNA breaks, which often leads to the activation of the cell stress response, upon the induction of p53, subsequently resulting in cell apoptosis and senescence [205]. The inability of telomerase, an RNA polymerase required for the replication of the terminal ends of telomeres, has been previously associated with a decline in tissue regeneration and overall accelerated ageing [206].

Differences in epigenetic and transcriptomic regulation are also hallmarks of molecular ageing [202]. Epigenetic changes involve histone post-translational modifications, differences in DNA methylation patterns and chromatin remodelling. This area has recently gained much interest, specifically as increasing evidence has emerged linking epigenetic changes and age-related disorders [207]. Differential gene expression patterns have been reported across many tissues within the aged population which has led to the further investigation into the regulation of these transcriptional differences [208]. Chromatin accessibility largely influences the ability of gene transcription, with tightly packed heterochromatin reducing the accessibility of transcription factors to bind and initiate gene transcription, whereas open euchromatin promotes gene transcription [209]. Chromatin is formed of several nucleosomes that contain structures consisting of 147bp of DNA wrapped around an octamer of histone proteins. Each octamer harbours a core of histones; H2A, H2B, H3 and H4 which undergo select post translational modifications, including acetylation, demethylation and phosphorylation [210]. As histone modifying enzymes,

including histone acetyltransferases and methyltransferases are able to subsequently deposit or remove modified histones, various histone modifications are reversible. This enables epigenetic modifications to influence chromatin structure and promote the activation or silencing of gene expression.

Ageing is associated with the aberrant transcriptional activation of many pro-inflammatory genes [211]. Gene expression comparisons performed on microarrays from young and aged tissues have uncovered many age-related transcriptional changes that are involved in inflammation, mitochondrial and lysosomal pathways [212], [213]. These age-associated transcriptional signatures largely affect how immune cells respond to infection and inflammation within the aged. Dendritic cells are amongst the central immune cells linking the innate and adaptive immune response [214]. Although previous research has heavily focused on the effect of immune-senescence on the adaptive immune response [215], little is known regarding the innate immune response. Recent immunophenotyping studies have demonstrated the aged population harbour a decrease in circulating peripheral blood dendritic cells, in particular the monocyte derived cDC subset, whereas no difference was observed in the proportion of pDCs and an increase in peripheral blood monocytes was observed [93]. This was accompanied by data demonstrating dendritic cells expressed a reduction in IL-12, which may impact upon IFNγ activation of T-cells in response to infection [216]. Rahmatpanah and colleagues explored the differences in transcriptional regulation in monocyte derived-DCs with the aim of uncovering differentially regulated pathways that may contribute to the age-associated DC dysregulation [217]. DCs are a heterogenous population of innate immune cells, comprising of

pDCs, that phenotypically resemble plasma cells, and monocyte-derived cDCs that are the largest DC subset within the peripheral blood [122]. As ageing appears to impact on the number of circulating cDCs more so than pDCs, Rahmatpanah and colleagues performed RNA-sequencing on the cDC subset of young and aged donors to understand the transcriptional differences that may contribute to altered cDC function [217]. Interestingly, they identified a number of upregulated genes involved in nutrient transport and migration alongside a decrease in genes involved in electron transport. Rahmatpanah and colleagues also identified a decrease in genes involved in mitochondrial respiration. Mitochondrial dysfunction is a hallmark of ageing and associated with many age disorders [218]. Defects in mitochondrial respiration are known to enhance inflammation, via ROS production, leading to the progressive decline of cellular function and increased susceptibility to apoptosis [219], [220]. Such reduction in mitochondrial respiration may explain the increase in expression of genes involved in solute transport, to compensate for the reduction in energy production. Collectively, this demonstrates cDCs from aged individuals exhibit metabolic changes that may contribute to the dysregulated immune cell response often associated with age.

Currently, little is known regarding the age induced transcriptional differences observed in monocytes and the mechanism by which they are evoked. Recently, few studies [221], [222] have demonstrated an expansion in circulating monocytes within the healthy aged population, where many monocytes exhibit an altered pro-inflammatory phenotype characteristic of senescent immune cells. Seidler and colleagues [221] uncovered an expansion

of non-classical monocytes within healthy aged individuals coupled with increased serum MCP-1 levels. This was further supported by Merino and colleagues [223] whom demonstrated the expansion of $CD14^{+}CD16^{+}$ monocytes, observed amongst the healthy aged resembled characteristics associated with senescent cells. This included enhanced pro-inflammatory cytokine secretion, plasma ROS levels and decreased mitochondrial membrane potential. Interestingly, Merino and colleagues suggest this pro-inflammatory status is likely due to the phosphorylation and activation of NF-KB signalling. Thus, implying age-induced transcriptional changes may underly the altered monocyte phenotype observed amongst the aged [216], [224]. Differences in the transcriptional activation of chemokine receptors important for endothelial cell adhesion were also reported by Merino and colleagues, suggesting altered monocyte function as well as phenotype [223]. The elevated pro-inflammatory phenotype and altered chemokine receptor expression of aged monocytes has prompted further investigation into the possible age-induced effect of atherosclerosis. Previous studies by Du and colleagues [225], demonstrated age-induced vascular inflammation promoted monocytosis in mice challenged with a high fat western diet. This ultimately led to increased atherosclerotic plaque development due to enhanced monocyte chemotaxis and inflammation amongst aged mice in comparison to young mice [225]. Hearps and colleagues [226] similarly show aged-induced impairment of monocyte phagocytosis, further contributing to the notion that ageing impacts upon monocyte function and phenotype. Collectively, this demonstrates that ageing induces an altered monocyte phenotype resulting in functional differences within monocytes that may contribute to age-associated disorders including atherosclerosis. Alongside

pro-inflammatory phenotypic differences in aged monocytes, Hearps and colleagues have also identified gender differences in aged monocyte phenotype. Interestingly, females exhibit an increased pro-inflammatory monocyte phenotype in comparison to men, as displayed by their elevated CXCL10 and CD163 levels. This suggests possible age-related gender differences that may impact upon gender specific disease specificity [226].

1.5.2 Gender differences in ageing

Many age-associated differences have been identified and characterised within tissues and leukocytes of the healthy aged population, however, there is still currently a lack of knowledge regarding the impact of gender related differences in healthy ageing. Historically, females generally live longer than males, yet have a greater risk of suffering from Alzheimer's and osteoporosis [227]. Previous studies have also identified several features that are continuously dysregulated with gender amongst the aged; reduced mitochondrial maintenance, enhanced inflammation, oxidative stress and proteotoxicity response [228]–[230]. However, the mechanisms underlying such age-induced sexual differences are poorly understood. To aid in the investigation of differences observed with age, gender and race, the ‘Immunomes Reference Framework’ was generated upon combining all publicly available immunological information on PBMCs and whole blood from the online database; Immport [231]. By combining the variations in serum cytokines and leukocytes of healthy young and aged males and females PBMCs and whole blood, it allows for differences to be identified amongst different genders and ages that may contribute to the disorders more commonly associated with ageing.

Comparative meta-analysis on multiple DNA microarrays from aged tissue (skeletal and nervous tissue) and senescent cells (HSCs, T-cells, endothelial cells) have also identified genes and associated pathways that are differentially regulated with age and gender [212]. In agreement with previous studies, many age-related differentially regulated processes across all tissue and cell types included metabolic processes, oxidative phosphorylation and focal adhesion. However, Voutetakis and colleagues [212] also uncover many sex-specific age-related differences. Aged healthy males demonstrate differential regulation of genes involved in cell adhesion, growth and inflammation whereas healthy aged females demonstrate an overrepresentation of genes involved in cell death, proteolysis and transmembrane transport within their skeletal muscle [212]. This study further highlights the differences in transcriptional regulation of processes that many contribute to age associated diseases, including cancer, atherosclerosis and Alzheimer's. However, knowledge of the mechanism underlying specific transcriptional differences and the resultant functional implications are yet to be clearly defined.

1.5.3 IRF8 and Ageing

Age associated differences in transcriptional regulation has become widely accepted as a hallmark of ageing [202]. However, differential regulation of the transcription factors crucial to the age-associated transcriptomic changes is yet to be uncovered. The transcription factor, IRF8, is critical for myeloid-lineage determination and protecting against infection and inflammation [127], [153]. Previous studies by Stirewalt and colleagues have interestingly uncovered a

significant reduction in the expression of IRF8 amongst healthy aged HSCs and T-cells [232]. Considering IRF8 inactivation causes the cancerous CML-phenotype [153], it's very possible that defective IRF8 expression may contribute to various cancers specifically associated with the aged population. Although IRF8 is known for its regulation of myeloid cell development [129], its regulation within aged myeloid cells has not currently been explored. Since differences in myeloid cell composition and phenotype, in particular monocytes, have been identified within the aged population [222], [224], the possibility of IRF8-induced transcriptional dysregulation within aged myeloid cells remains open.

Taken together, these data highlight the importance of myeloid cells in atherosclerosis, interferon signalling and ageing with transcriptional differences greatly impacting on myeloid-cell function. The crucial role of IRF8 in myeloid cell development and myeloid response to infection and inflammation has been well characterised. However, the functions associated with differential myeloid-IRF8 transcription in a high lipid, atherosclerosis environment is poorly understood.

1.6 Hypothesis

Within the lab, we have demonstrated IRF8-KO macrophages display reduced expression of genes known to protect against atherosclerosis development when expressed, namely Arginase 1 and Il-18bp [197], [233]. Furthermore, Doring and colleagues identified an atherogenic role of IRF8 deficiency whereby hematopoetic-IRF8 deficient mice displayed an increase in atherosclerosis plaque development when challenged with a high fat western-diet [175].

For this reason, we hypothesized that myeloid-IRF8KO^{LdlrKO} mice would develop accelerated atherosclerosis when challenged with a high fat western-diet

1.7 Project Aims

1. To develop a myeloid-IRF8KO mouse model on the atherosclerosis prone LDLR^{KO} background (M-IRF8KO^{LdlrKO}) and subsequently determine the role of myeloid-IRF8 reduction in atherosclerosis development upon challenging the mice with a high fat western-diet.

2. To identify the atherosclerotic phenotype in M-IRF8KO^{LdlrkO} mice, via histological analysis and identify the potential mechanism associated with the disease phenotype. This will be performed by determining differences in the transcriptomic profile of bone marrow derived macrophages from WT^{LdlrkO} and M-IRF8KO^{LdlrKO} mice using RNA-Sequencing.

3. To determine how myeloid-IRF8 influences IFNβ transcriptomic signalling in bone marrow derived macrophages from atherosclerosis prone WT^{LdlrKO} and M-IRF8KO^{LdlrKO} mice when challenged with a high fat western-diet, using RNA-sequencing.

4. To determine how the regulation of IRF8-target genes, identified in the atherosclerosis prone M-IRF8KO^{LdlrKO} mice differ in PBMCs and monocytes of the aged population, whom are at increased risk of Cardiovascular disease. This will be performed via comparative analysis

of the RNA-sequencing dataset generated from M-IRF8KO^{LdlrKO} mice (Aim 2) and the Immunomes microarray dataset [231] from healthy young (20-50yrs) and aged (60-100yrs) PBMCs.

Chapter 2: Materials and Methods

2.1 Generation of myeloid IRF8^{KO} mice on an atherosclerosis prone background

2.1.1 IRF8-floxed mice

Myeloid IRF8^{KO} mice, on an atherosclerosis prone background, where generated by crossing IRF8-floxed mice (stock - 014175), LysMcre$^{+/-}$ (stock - 004781) and Ldlr^{KO} mice (stock – 002207) obtained from the Jackson laboratory. The IRF8 floxed mice harbour *loxp* sites at either end of exon 2 (**Fig 2.1**). A targeting vector containing an FRT site flanked PGK-Neo selection cassette was utilized in the construction of this mutant. *LoxP* sites were inserted upstream and downstream of exon 2 and this construct was electroporated into C57BL/6 derived embryonic stem (ES) cells (Ozgene). Correctly targeted ES cells were injected into recipient blastocysts and the resulting chimeric animals were crossed to transgenic mice (on the C57BL/6 genetic background) expressing FLP recombinase. Mice that retained the *loxP* site flanked exon 2 were then bred to C57BL/6 mice to remove the FLP transgene. Heterozygotes were crossed to generate homozygotes.

2.1.2 LDLR^{KO} mice

The IRF8-floxed mice where then crossed with Ldlr^{KO} mice, performed by Dr Matthew Gage at UCL Biological Services Unit and obtained from the Jackson laboratory. Ldlr^{KO} mice develop elevated serum cholesterol levels in the region of 200-400 mg/dl, which are further increased (>2,000 mg/dl) when fed a high fat western diet. In comparison, normal serum cholesterol in mice with Ldlr is approximately 80-100 mg/dl. For this reason, Ldlr^{KO} mice are often used for

atherosclerosis studies as they develop atherosclerotic plaques when challenged with a high fat western diet. Upon crossing the IRF8-floxed and $LdlR^{KO}$ mice, this led to the generation of $IRF8^{fl/fl}LdlR^{KO}$ mice.

2.1.3 LysMcre mice

To ensure IRF8 was removed from myeloid cells specifically, $IRF8fl/fl^{LdlrKO}$ mice where crossed with mice that express cre recombinase under the Lysosyme M promoter; LysMcre mice by Dr Matthew Gage and were also obtained from the Jackson laboratory (stock - 004781) (**Fig 2.1**). In generating the LysMcre mice, a targeting vector was designed to insert a frt-flanked neomycin resistance gene and Cre recombinase cDNA sequence (with nuclear localization signal) into the ATG-start site within exon 1 of the lysozyme 2 gene (Lyz2). The construct was electroporated into 129P2/OlaHsd-derived E14.1 embryonic stem (ES) cells. Correctly targeted ES cells were transiently transfected with a Flp expression vector to remove the frt-flanked neo cassette. ES cells that had successfully undergone Flp recombination were injected in blastocysts. The resulting chimeric animals were crossed to C57BL/6 mice. The LysMcre knock-in allele has a nuclear-localized Cre recombinase inserted into the first coding ATG of the lysozyme 2 gene (Lyz2); both abolishing endogenous Lyz2 gene function and placing NLS-Cre r544 expression under the control of the endogenous Lyz2 promoter/enhancer elements. When crossed with the IRF8-floxed strain, Cre-mediated recombination results in deletion of the targeted gene in the myeloid cell lineage, including monocytes, mature macrophages, and granulocytes.

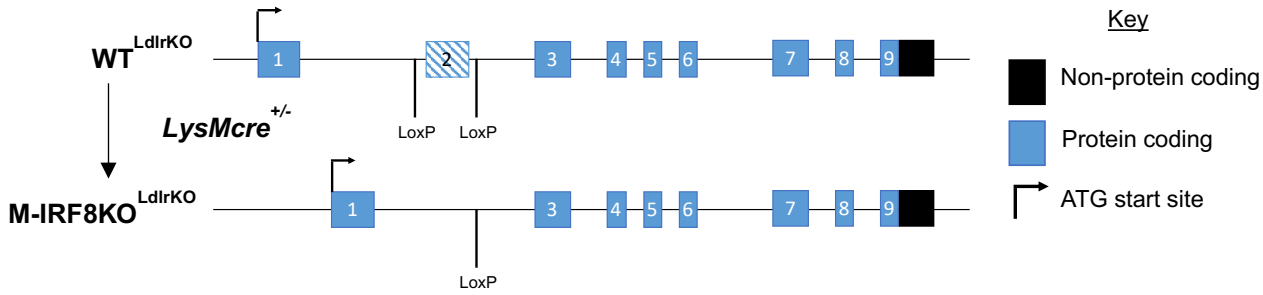

Figure 2.1 Generation of M-IRF8KO^{LdlrKO} mice.
The *Irf8* locus was engineered with LoxP recombination sites flanking exon 2. In the presence of cre recombinase, exon 2 of IRF8 is excised in Lysozyme M expressing cells.

2.2 Genetic identification of M-IRF8KO^{LdlrKO} mice

2.2.1 DNA Isolation

Genomic DNA was isolated from ear biopsies by incubating ear biopsies with 200µl of 50mM NaOH (pH = 12) at 95^{o}C for 10min. The reaction was then neutralised by placing tubes on ice and adding 20µl Tris-HCl 1 molar (M) (pH = 8). Tubes were centrifuged at 13000 revolutions per minute (rpm) for 5min 4^{o}C to remove debris and the supernatant was transferred to a clean tube. Samples were stored at 4^{o}C until analysis.

2.2.1.1 IRF8-floxed genotyping protocol

WT^{LdlrKO} and M-IRF8KO^{LdlrKO} mice where genotyped for the IRF8 floxed allele 300 base pairs (bp) and wild-type allele 214bp (**Fig 2.2**). PCR amplification was performed on the isolated DNA upon using Jumpstart Taq DNA Polymerase (Sigma Aldrich). The PCR reagents for each reaction are shown in Table 2 and the primers used to identify the IRF8-floxed alleles are as follows;
Irf8-floxed forward 5' TTGGGGATTTCCA GGCTGTTCTA 3' and reverse 5' CACAGGGAGTCCCT CTTACAAT 3'.

Amplification was undertaken by 35 cycles of 30 seconds of annealing at 60°C, and 1 minute of extension at 72°C. Samples were run on a 2% high resolution agarose gel (Sigma Aldrich) in a 1X 40 millimolar (mM) Tris, 20mM acetic acid, 1mM ethylenediaminetetraacetic acid (EDTA) TAE buffer with 1X SYBR safe DNA gel stain (Invitrogen) for 40min at 80 volts (V).

The expected band size for this IRF8-floxed PCR is 300bp and the WT PCR is 214bp.

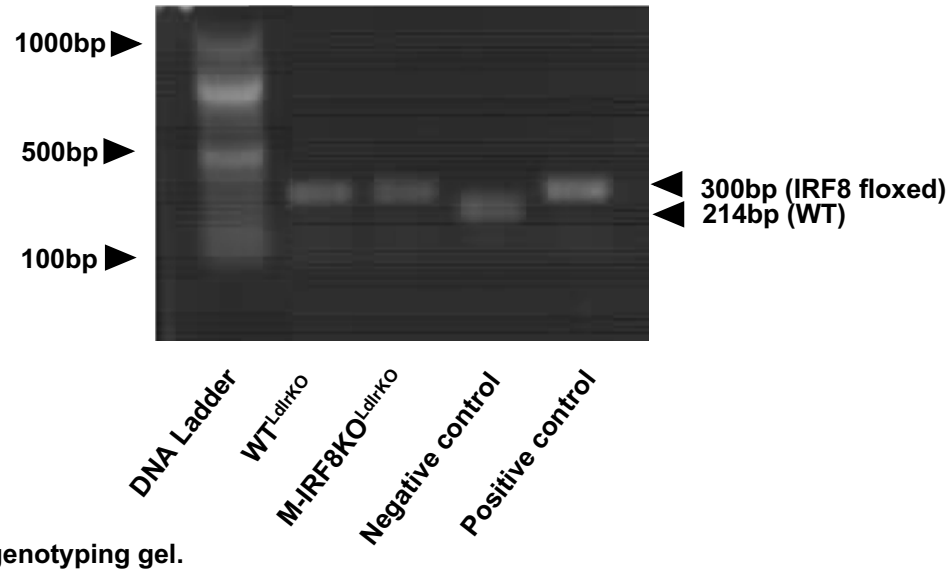

Fig 2.2 IRF8-floxed genotyping gel.
Gel electrophoresis of DNA amplified products using the corresponding primers.

2.2.1.2 LysMcre genotyping protocol

WT^{LdlrKO} and M-$IRF8KO^{LdlrKO}$ mice where genotyped for the Mutant LysM cre recombinase expressing allele (700bp) and wild-type allele (350bp) (**Fig 2.3**). PCR amplification was performed on the isolated DNA upon using the Jumpstart Taq DNA Polymerase (Sigma Aldrich). The PCR reagents for each reaction are outlined in Table 2 and the primers used to identify the LysM cre recombinase alleles are as follows; LysMcre (Mutant) forward 5' CCCAGAAATGCCAGATTACG, LysMcre (Common) 5' CTTGGGCTGCCAGA ATTTCTC and LysMcre (wild-type) 5' TTACAGTCGGCCAGGCTGAC.

Amplification was undertaken by 35 cycles of 30 seconds of annealing at 60°C, and 1min of extension at 72°C. Samples were run on a 2% high resolution agarose gel (Sigma Aldrich) in a 1X 40mM Tris, 20mM acetic acid, 1mM ethylenediaminetetraacetic acid (EDTA) (TAE) buffer with 1X SYBR safe DNA gel stain (Invitrogen) for 30min at 100V.

The expected band size for wild-type LysMcre^{+} is 350bp and the band size for Mutant LysMcre^{-} is 700bp.

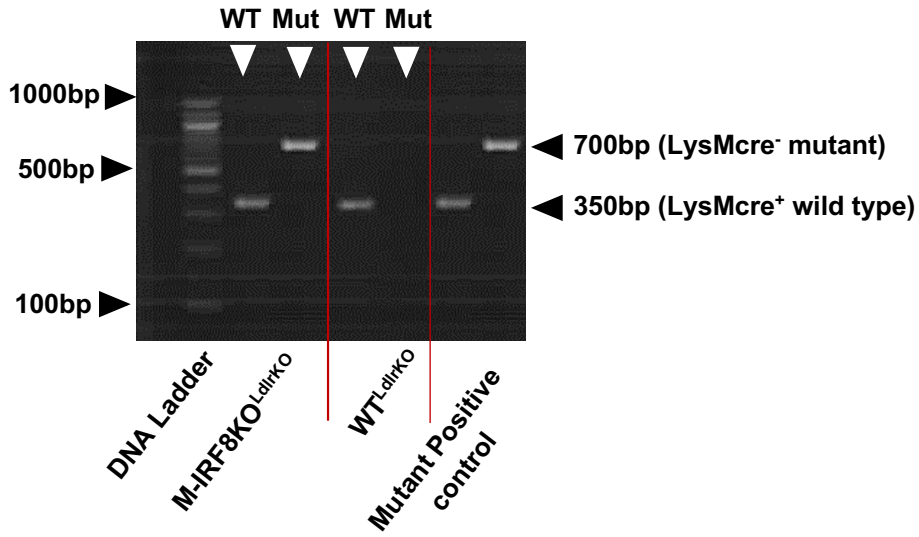

Fig 2.3 LysMcre genotyping gel.
Gel electrophoresis of DNA amplified products using the corresponding primers.

2.2.1.3 Ldlr^{KO} genotyping protocol

WT^{LdlrKO} and M-IRF8KO^{LdlrKO} mice where genotyped for the WT Ldlr allele (350bp) (**Fig 2.4**). PCR amplification was performed on the isolated DNA upon using the Jumpstart Taq DNA Polymerase (Sigma Aldrich). The PCR reagents for each reaction are outlined in Table 2 and the primers used to identify the Ldlr alleles are as follows; Ldlr (Mut) forward 5' AATCCATCTTGTTCAATGGCCGATC, Ldlr (Common) 5' CCATATGCATCCCCAGTCTT and Ldlr (wild-type) 5' GCGATGGATACACTCACTGC.

Amplification was undertaken by 35 cycles of 30 seconds of annealing at 60°C, and 1min of extension at 72°C. Samples were run on a 2% high resolution

agarose gel (Sigma Aldrich) in a 1X 40mM Tris, 20mM acetic acid, 1mM ethylenediaminetetraacetic acid (EDTA) (TAE) buffer with 1X SYBR safe DNA gel stain (Invitrogen) for 40mins at 80V.

The expected band size for Ldlr Mutant is 350bp.

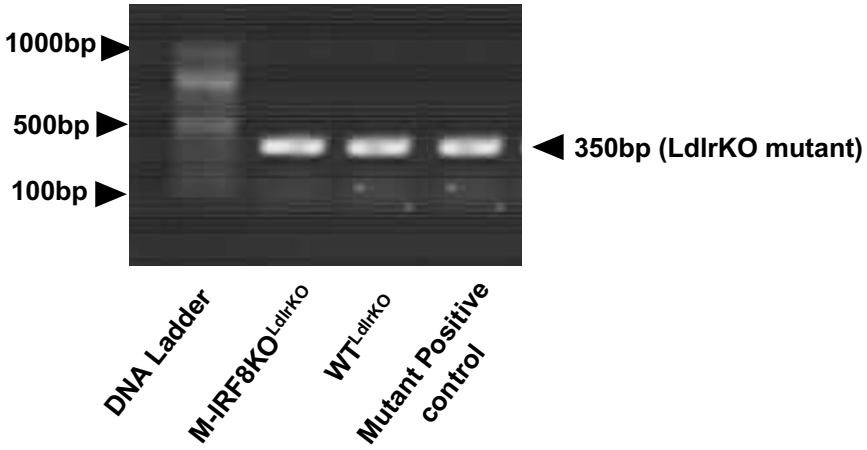

Fig 2.4 Ldlr genotyping gel.
Gel electrophoresis of DNA amplified products using the corresponding primers.

For each PCR reaction, the following reagents and DNA were added to a 0.5 mL tube:

Volume	Reagent	Final concentration
24.3μL	Water	-
3μL	10x PCR buffer (with $MgCl_2$)	1x (2mM $MgCl_2$)
0.6μL	10mM dNTPs	200μM
0.3μL	10mM Primers	1μM
0.5μL	Taq DNA Polymerase	0.083 units/μL
1μL	Template DNA	n/a
30μL	**Total reaction volume**	

Table 2 Reagent mix used for PCRs

2.3 Animal procedures

All animal experiments were carried out in accordance with the UK Animals (Scientific Procedures) Act 1986, Project License: 4776, Personal License: 12265/01.

2.3.1 Housing and diet studies

Mice were maintained in a pathogen-free animal facility in a 12-hour light-dark cycle and were housed in the same cages whenever possible. All procedures were carried under the UK's Home Office Animals (Scientific Procedures) Act 1986.

Eight-week old WT^{LdlrKO} and M-$IRF8KO^{LdlrKO}$ male mice were fed *ad libitum* a Western diet (WD) (20% Fat, 0.15% Cholesterol; #5342 AIN-7A, Test Diet Limited, UK) for 12 weeks. Mice were fasted overnight prior to sacrifice.

2.3.2 Plasma and tissue collection

Mice were fasted overnight prior to blood collection or terminal sacrifice. Animals were euthanized using increasing concentrations of CO_2 and death was confirmed by cervical dislocation or by cardiac bleeding.

For organ dissections, mice were anaesthetized, using 3.5units of isoflurane/min, after of which a small incision was made underneath the left portion of the diaphragm where the mice were euthanized upon cardiac puncture. Blood was collected into an EDTA- containing microtube (Microvette CB 300, Sarstedt), centrifuged (3000xg, 6min. at room temperature) and plasma was aliquoted and frozen at -80°C. The inferior vena cava was cut, to allow for efficient

flushing of organs with 5mL of Phosphate Buffer Saline (PBS) that was carefully inserted into the left ventricle of the heart. The PBS was slowly released to flush any remaining blood remnants from the organs. The tissues dissected post-mortem; Heart, Lung, Liver, Spleen and epididymal adipose tissue were rinsed in 1X PBS (Thermo Scientific), weighed and half were frozen at -80^{o}C and the other half placed into 10% (w/v) formalin (Sigma Aldrich). Tissues, including the aorta, placed in 10% formalin were kept at room temperature for 24hrs after being transferred into microvette cassettes and stored in 70% ethanol at 4°C until ready for processing and paraffin embedding. Finally, the femurs and tibias were dissected free of adherent tissue were cut from the mice, with the skin removed and stored in High Glucose Dulbecco's Modified Eagle Medium (DMEM) (Life Technologies).

2.3.1.1 Plasma cholesterol and blood glucose

Plasma cholesterol levels (Wako chemicals) were determined by colorimetric enzymatic assay kits as per the manufacturer's recommendations. The absorbance of each reaction product was measured at 595 nm in a TriStar2 LB 942 Multi-detection Microplate Reader (Berthold Technologies). Blood glucose measurements (Accu-Chek monitor and testing strips, Roche Diagnostics) were taken from tail blood samples before and after overnight fasting.

2.3.1.2 Blood monocyte and neutrophil composition

Animals were euthanized using increasing concentrations of CO_2 and death was confirmed cardiac puncture. Blood was collected into an EDTA-

containing microtube (Microvette CB 300, Sarstedt) and red blood cells lysed using 9mL Ammonium- Chloride-Potassium (ACK) Lysis Buffer (Lonza) for every 1mL of blood and left to lyse at room temperature for 5mins. Cells are then centrifuged at 300xg for 5mins at 4°C. The supernatant is discarded, and the pelleted cells are washed in 1x PBS (Lonza) twice. The cells were then centrifuged at 300xg for 5mins at 4°C and resuspended in 200μl of buffer (1% FCS, 2mM EDTA in PBS). 100μl of cell suspension was then transferred to a separate 1.5ml tube and supplemented with 1:100 of the following antibodies; CD115, CD11b, Ly6G, Ly6C, CD3, CD19 (Further information on antibodies are outlined in **table 2.5**). Cells were left to stain in the dark at 4°C for 30mins after of which they were centrifuged at 800xg for 3mins at 4°C. The supernatant was discarded, and cells resuspended in 300μl buffer (1% FCS, 2mM EDTA in PBS). Compensation controls for antibodies used where also prepared as outlined in section 2.9. Samples were analysed on the LSR Fortessa (Becton Dickinson) and FlowJo software (Tree Star Inc.)

2.3.1.3 Tissue macrophage and neutrophil quantification

Animals were euthanized using increasing concentrations of CO_2 and death was confirmed cardiac puncture. The aorta and spleen were dissected from mice and having removed residual fat and muscle, the tissues were placed in ice-cold PBS. A digestion mix was prepared containing the following reagents; 450U/ml collagenase type I (Sigma), 125U/mg collagenase type XI (Sigma), 60U/mg hyaluronidase (Sigma) and 60U/mg DNAse I (Sigma) in DPBS with 20mM HEPES (Sigma) up to a volume of 2.5mL/tissue. The aorta and spleen were cut into small pieces before being plunged through a 70μM cell strainer into the tissue digestion mix. The tissues were digested at 37°C for 50mins whilst

rotating. Post digestion the digestion mix was neutralised with 5ml buffer (1% FCS, 2mM EDTA in PBS) and the digested tissues where plunged through a 70μM cell strainer (Cornig). The cell suspension was then centrifuged for 10mins at 300xg, 4°C. The supernatant was discarded, and the cells were resuspended in antibody staining buffer; 1:100 CD45, CD115, Ly6g, CD11b, F4/80 and CD64 in 300μl buffer (1% FCS, 2 mM EDTA in PBS) (further details on antibodies are outlined in table 2.5). The cells where left to stain in the dark at 4°C for 30mins after of which they were centrifuged at 800xg for 3mins at 4°C. The supernatant was discarded, and cells resuspended in 300μl buffer (1% FCS, 2mM EDTA in PBS). Compensation controls for antibodies used where also prepared as outlined in section 2.9. Samples were analysed on the LSR Fortessa (Becton Dickinson) and FlowJo software (Tree Star Inc.)

2.4 Histology and image analysis

2.4.1 Slide preparation and staining

Mouse hearts and the left lobe of the livers were dissected and fixed in 10% (w/v) formalin (Sigma Aldrich) for 24-48 hours, processed in a TP 1050 Tissue Processor (Leica) and embedded in paraffin wax. Paraffin-embedded hearts and livers were cut into 4μM sections. The paraffin-embedded hearts were sectioned until the aortic root was visible. Sections were stained with haematoxylin and eosin (H&E) in an automatic multiple slide stainer (Tissue-Tek DRS 2000, Sakura). Stained sections were scanned with NanoZoomer Digital slide scanner (Hamamatsu) and image analysis performed using Image J software.

For aortic macrophage content, CD68 staining was performed on the paraffin-embedded heart sections. Immunohistochemistry staining was performed at the UCL IQPath Laboratory using the Ventana Discovery XT instrument, using the Ventana DAB Map detection Kit (760-124). For pre-treatment Ventana Protease 1 (equivalent to pronase, 760-2018) was used. CD68 primary antibody (AbD Serotec #MCA1957), followed by Rabbit anti Mouse (#E0354 Dako). Stained sections were scanned with NanoZoomer Digital slide scanner (Hamamatsu) and image analysis performed using Image J v2.0 software.

2.4.2 En face analysis of aorta

Mice were perfusion-fixed with phosphate-buffered paraformaldehyde (4% [wt/vol.], pH 7.2) under terminal anaesthesia. The entire aortic tree was dissected free of fat and other tissue. Peripheral adipose tissue was removed from the aorta and an incision was made across the inner aortic arch. The aorta was then stained with a 60% working dilution of the diazol dye, Oil-Red-O (Sigma Aldrich), which stains neutral lipids and triglycerides red. The aorta was initially rinsed in MilliQ water for 1min, to remove excess PFA, before washing in 60% isopropanol for 2mins; this facilitates staining as the isopropanol sustains the neutral lipids. The aorta was then placed into 1.5mL of 60% oil-red-o and placed on a nutator for 12mins. The excess stain was removed, using 60% isopropanol and the aorta stored in MilliQ water ready for imaging. The aorta was then mounted onto a glass slide before imaging (Leica, DFC310FX) under a dissection microscope (Leica, MZ10F). Lesion area of whole aorta was analysed using Image J v2.0.

2.4.3 Aortic sinus atherosclerotic plaque quantification

Paraffin embedded hearts where sectioned from the apex upwards, until reaching the aortic root which is characterized by the tricuspid valve. From this point, 5μM sections were mounted onto Superfrost Plus microscope slides (Thermo Scientific) and stained with hematoxylin and eosin (H&E) in an automatic multiple slide stainer (Tissue-Tek DRS 2000, Sakura). Stained sections were scanned with a NanoZoomer Digital slide scanner (Hamamatsu). The percentage of atherosclerotic lesions where determined as %plaque area within the aortic root. This was performed using Image J by averaging 3 sections from each mouse with 30-50μM intervals between sections [234].

2.4.4 Plaque complexity

Plaque severity was determined by categorising plaques into early stage, moderate stage and advanced stage as outlined on the American heart association guidelines, adapted for mouse models [31]. The advance stage plaques were analysed for necrotic core and fibrous cap formation. To determine the acellular (%) necrotic core area, the H&E stained aortic root image was opened on the Image J software and converted to an RGB stack. The threshold of the image was subsequently adjusted to ensure only the acellular regions were left unhighlighted. The proportion of the unhighlighted acellular region of each plaque was calculated as a % of the plaque area and an average of all plaques within the root from each section was taken as the final acellular (%) necrotic core area. To determine the (%) fibrous cap area the % area of the fibrous cap was determined as per the total area of the plaque, after which an average of all fibrous cap areas from each plaques within the root from each section was taken

as the final fibrous cap (%) area [31], [235]. The diameter of the fibrous caps identified in the advance stage plaques was recorded at the widest point of each fibrous cap.

2.4.5 Image processing for hepatic lipid droplet identification

The identification and quantification of lipid droplets were made with the help of Eli (Easy Lipids) v1.0, an in-house software developed in collaboration with Dr. Vanessa Diaz and Dr. Cesar Pichardo at the Multiscale Cardiovascular Engineering (MUSE) (University College London, UK). Scans of H&E stained liver sections were used as input. This software uses a method based on the Hough Transform [236] for the identification of the droplets estimating the centres and radii of each of them. A final report is generated with the dimensions of the droplets (i.e. diameter and area) including a histogram describing the frequency of lipid vacuoles within specified diameter ranges (**Fig 2.5**). A trial of Eli v1.0 is currently available upon request on the MUSE website at UCL (www.ucl.ac.uk/muse/software).

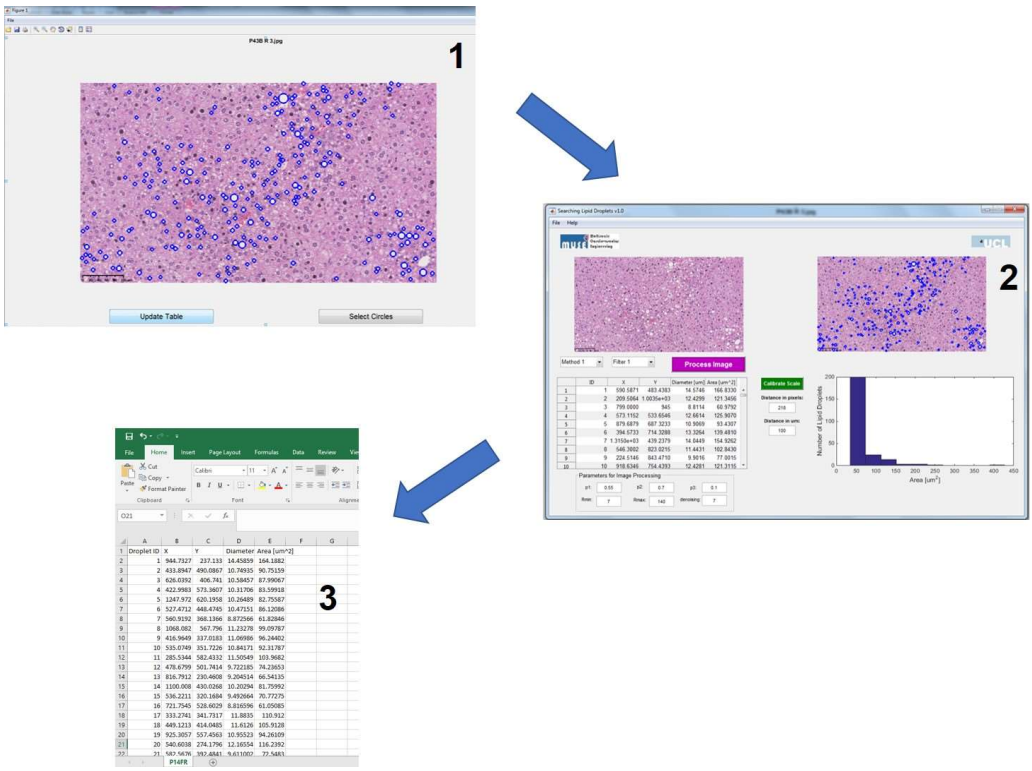

Fig 2.5 Identification of lipid droplet areas using the Eli (Easy Lipids) v1.0 software.
(1) The lipid droplets are highlighted by drawing blue circles around them. (2) the number of blue circles were quantified as per the area of the liver section. (3) The results are exported into an excel file, to allow for statistical analysis.

2.5 Cell culture

All bone marrow derived macrophages (BMDMs) and blood cell isolations and cell culture were performed using aseptic technique in a class II laminar flow hood. Where available, purchased reagents were sterile. If needed, reagents were sterilised by using a high temperature and high-pressure autoclave and/or a 0.22μM filter (EMD Millipore). Cells were incubated at 37°C in a 5% CO_2 atmosphere unless otherwise stated.

2.5.1 Cell enumeration

To enumerate cells and assess viability trypan blue dye exclusion staining was performed. This involved adding equal volumes of cell suspension to 0.4% (v/v) trypan blue solution and cells that absorbed the dye were considered non-

viable. Cells were counted using a manual haemocytometer (Digital Bio) with a conventional light microscope (Primo Vert, Zeiss).

2.5.2 Bone marrow derived macrophage culture

BMDMs were prepared as in [237] using L929 Conditioned Medium (LCM) as a source of M-CSF for the differentiation of the macrophages. After 6 days of differentiation, LCM-containing medium was removed, and cells were washed three times in warm 1X PBS (Lonza).

2.5.2.1 BMDM stimulation

For treatment experiments, cells were incubated in Glucose Dulbecco's Modified Eagle Medium (DMEM) (Life Technologies), supplemented with 1% low-endotoxin (≤10 EU/mL) Fetal Bovine Serum (FBS) (Life Technologies), 2mM glutamine (Lonza) and 20μg/mL gentamycin (Sigma Aldrich), without any LCM, before being treated. Cells where then treated with DMSO (Sigma), 10ng IFNβ, 50ng native LDL (nLDL) (Bio-Rad), 50ng, acetylated LDL (acLDL) (Bio-Rad) or varying concentrations of BMS309403 inhibitor (1mM, 5mM, 10mM, 25mM, 50mM - Tocris) for 6 or 24 hours (mRNA quantification, protein isolation).

2.5.1.1 Bone marrow derived macrophage purity

The purity of harvested BMDMs was determined by measurement of the macrophage cell surface marker; F4/80, using flow cytometry [238] (**Fig 2.6**). Harvested BMDMs where washed twice with wash buffer (PBS with 2% FCS and 2mM EDTA) and stained using an antibody mix of 1:100 F4/80 and 1/200 Live/Dead (details provided in **table 2.5**). Cells where stained in the dark at 4^{o}C

for 30mins. They were then washed twice with wash buffer before finally being resuspended in 150µL wash buffer and transferred to a 1mL FACS tube. Samples were analysed on the LSR Fortessa (Becton Dickinson) and FlowJo software v10.0 (Tree Star Inc.)

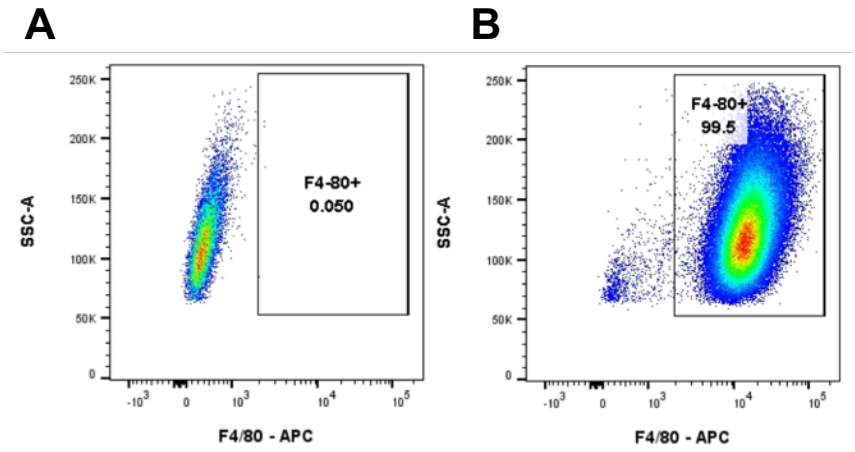

Fig 2.6 Purity of F4/80 stained BMDMs.
(A) Unstained live BMDMs demonstrating 0.05% of cells are F4/80+. (B) F4/80 stained live cells demonstrating, 99.5% of BMDMs are F4/80+.

2.5.3 In vitro macrophage migration assay

To investigate macrophage migration, BMDMs were cultured, as described in 2.4.2. Cells were then washed twice in warm 1x PBS (Lonza), gently lifted from the cell surface using a cell scraper (Thermo fisher), transferred to a 1.5mL tube and centrifuged for 5mins, 300xg at room temperature. Cells were counted, as described in section 2.4.1, and resuspended in DMEM containing 10% low endotoxin (≤10 EU/mL) FBS (Life Technologies), 2mM glutamine (Lonza) and 20µg/mL gentamycin (Sigma Aldrich), without any LCM, before being treated, to reach a total concentration of $1x10^6$ cells/mL. For cell stimulations, the following treatments where added to each Eppendorf; DMSO, 50ng nLDL (Bio-Rad), 50ng acLDL (Bio-rad) with or without 10µM, 25µM

BMS309403 inhibitor (Tocris) and 10μM, 25μM BMS309403 inhibitor (Tocris) alone. A total volume of 600μL of conditioned medium, containing 100ng/μL MCP-1 (Bio-Rad), was inserted into each well of a 24-well plate (Starsedt, non-coated). Following this, 300μL of BMDM cell suspension, with various treatments, was inserted into a 8μM pore transwell (Corning) and this was placed in each well of a 24-well plate. Cells were left to migrate over 20 hours.

Post 20 hours, the transwells were removed from the 24-well plate and their medium discarded. A cotton bud was used to remove any residual BMDMs from the inside of the transwell, that did not migrate across the membrane. The transwells were then fixed and stained, according to the manufacturers protocol (Reastain kit – Gentaur). The transwells were left to dry at room temperature for 24 hours after being imaged (Leica, DFC310FX) under a microscope (Leica, MZ10F) and migrated cells were subsequently counted at a magnification of 8x on four individual areas of the transwell.

2.5.4 *In vitro* macrophage foam cell assay

To investigate macrophage foam cell formation, BMDMs were cultured, as mentioned in 2.4.2. Cells were then gently lifted from the 6-well plates (Starsedt, non-coated), using a cell scraper (Thermo Fisher), transferred to a 1.5mL tube and centrifuged for 5mins, 300xg at room temperature. Cells were counted, as described in section 2.4.1, and later resuspended in DMEM containing 10% low endotoxin (≤10 EU/mL) FBS (Life Technologies), 2mM glutamine (Lonza) and 20μg/mL gentamycin (Sigma Aldrich), without any LCM, before being treated, to reach a total concentration of $1x10^6$ cells/mL. For treatment experiments, resuspended BMDMs were supplemented with either; DMSO (Sigma), 50ng

nLDL (Bio-Rad), 50ng, acLDL (Bio-Rad) with or without 5μM, 10μM or 25μM BMS309403 inhibitor (Tocris). 300μL of cells was transferred into each well of a chamberwell slide (Thermo Fisher), plating triplicates/condition and incubated for 24 hours.

After 24 hours, cells were washed twice with warm 1X PBS (Lonza) and fixed using 200μL of 4% paraformaldehyde (Sigma) for 10mins at room temperature. Cells were then rinsed with 1X PBS for 1min to remove excess paraformaldehyde and 100μL of 60% isopropyl alcohol was added to each well for a further 15mins. Cells were then stained with 100μL of 60% oil-red-o for 1min in the dark. Cells were rinsed in 100μL of 60% isopropyl alcohol for 15 seconds and subsequently washed in 1x PBS for 1min three times. The chamberwells were removed, as per the manufacturer's instructions and slides were later imaged under a conventional light microscope (Primo Vert, Zeiss) with camera attached. Foam cell formation was quantified, as the density of red oil-red-o stain/macrophage using Image J analysis.

2.5.5 *In vitro* macrophage cholesterol ester content

BMDMs were cultured, as described in 2.4.2 in 6-well plates (Starsedt, non-coated). BMDMs were treated with either; DMSO, 50ng nLDL, 50ng acLDL with or without 5μM, 10μM or 25μM BMS309403 inhibitor (Tocris) in for 24 hours. After 24hours macrophages were washed twice in warm 1x PBS before being fixed in 1mL of 2% paraformaldehyde for 15mins. Cells were then washed three times in 1x PBS. Lipids were then extracted from the macrophages by incubating them with 200μL of 3:2 hexane/isopropyl alcohol for 30mins at 4^{o}C. The protocol was then continued as per the manufacturer's instructions (A12216 –

ThermoFisher). The plate was gently mixed, and absorbance read on a spectrophotometer at 590nm.

2.6 RNA extraction and analysis

2.6.1 RNA extraction and cDNA synthesis

Total Ribonucleic acid (RNA) was extracted with TRIzol Reagent (Invitrogen) following manufacturer's protocol. Briefly, $1x10^6$ BMDMs was homogenized in 350µL of TRIzol Reagent. Homogenates were either stored at -80^{o}C until further processing or used for RNA extraction immediately after cell lysis. Homogenates were vortexed (1min at maximum speed) after which, 70µL of chloroform (Acros organics) was added to homogenates. These were vortex-mixed and incubated at room temperature for 2-3mins before centrifugation (13,000xg, 15mins at 4^{o}C). Following centrifugation, the entirety of the aqueous phase was transferred onto a new pre-chilled 1.5mL tube and 175µL of cold isopropyl alcohol was added to precipitate the RNA. Tubes were then stored at -20^{o}C for 18 hours. The following day, the precipitated RNA was pelleted by centrifuging samples at 13,500rpm, 20mins at 4^{o}C. The supernatant was discarded, and RNA was washed twice with 500µL of cold 70% molecular grade ethyl alcohol (Sigma Aldrich) and centrifuged (13,500rpm, 20mins at 4^{o}C). After the last wash, supernatants were removed completely, and pellets were allowed to dry by leaving tubes uncapped at room temperature for 5mins. Pellets were then resuspended with 20µL of molecular biology water (Sigma Aldrich). Sample concentration and purity was determined using a NanoDropTM 1000 Spectrophotometer. Sample purity was assessed by 260/280 ratio and presence of contaminants by the 260/280 ratio. The minimum 260/230 ratio accepted was

1.80. 500µg of RNA was retrotranscribed using the qScript cDNA Synthesis Kit (Quantabio) following manufacturer's protocol.

2.6.2 Quantitative real-time PCT

Specific genes were amplified and quantified by PCR, using the PerfeCTa SYBR Green FastMix, Low ROX (Quanta) on an MX3000p system (Agilent) under the following conditions: 95°C for 30 seconds followed by 40 cycles of 55°C for 5 seconds and 60°C for 30 seconds. Amplicon specificity was assessed after every run by performing a dissociation (melt) curve: 95°C for 1min, 55°C for 30 seconds and 95°C for 30 seconds.

For a single reaction, the following reagents and cDNA were added to a single well in a 96-well plate:

Quantity	Reagent	Final concentration
6.2µL	Water	-
7.5µL	2x Reaction Buffer	1X
0.15µL	10µM Primers	100nM
1µL	100ng of cDNA	-
15µL	**Total reaction volume**	

Table 2.1 The concentration of reagents required for each individual qPCR reaction

All samples were run in duplicates and the relative amount of mRNAs was calculated using the comparative Ct method and normalized to the expression of Cyclophylin [197]. This gene is not regulated by IRF8, as previously established in the lab (data not shown). The following formula was used to quantify relative mRNA levels:

$\Delta Ct = Ct_{gene} - Ct_{cyclophylin}$

$\Delta\Delta Ct = \Delta Ct_{sample}$- average $\Delta Ct_{control}$

Fold induction= $2^{-\Delta\Delta Ct}$

2.6.3 Primer design

Transcript sequences were obtained from the from the University of California, Santa Cruz (UCSC) Genome Browser database (https://genome.ucsc.edu) [239]. Primers were obtained using the Primer3 (v. 0.4.0) online software [240], under the following parameters: amplicon size of 60-120 base pairs, primer size of 18-25 base pairs and melting temperature of 60^{o}C. In order to avoid amplification of contaminating genomic DNA, primers were designed where one half hybridized to the 3′ end of one exon and the other half to the 5′ end of the adjacent exon (exon spanning). Primer efficiency was determined by running a standard curve with known cDNA concentrations, and only those primers with an efficiency of 90-110% were used. All primer sequences used are in **Table 2.2** and **Table 2.3**.

Gene Name	Forward sequence (5'-3')	Reverse sequence (5'-3')
Abca1	GGACATGCACAAGGTCCTGA	CAGAAAATCCTGGAGCTTCAAA
Ccl12	GAAGATTCACGTCCGGAAGC	GGGTCAGCACAGATCTCCTT
Ccl3	CCAGCCAGGTGTCATTTTCC	CCTCCAAGACTCTCAGGCAT
Ccl4	TTTCTCTTACACCTCCCGGC	TCTGTCTGCCTCTTTTGGTCA
Ccl8	AGTCACCTGCTGCTTTCATGT	CCCTGCTTGGTCTGGAAAaC
Ch25h	GCTATGACTTCCCGTGGTCC	GAGAGTGATGCATGTCGTGG
Cxcl10	TTTCTGCCTCATCCTGCTGG	CATTCTCACTGGCCCGTCAT
Cxcl11	CAAGCTCGCCTCATAATGCA	ACGTTCCCAGGATGTCACAT
Cxcl16	CTGGATGTCGGCTAGGTGAC	AGCAGCGCCAACAAGAAAAG
Cyclophilin	GGCCGATGACGAGCCC	TGTCTTTGGAACTTTGTCTGCAA
Fabp4	ATGAACTTCTCCGGCAAGTACC	CTGACACCCCCTTGATGTCC
Fabp5	CGGAAGGTCAAGTCACTGGT	TTAGTGTTGTCTCCTGCCCG
Irf8	CAATCAGGAGGTGGATGCTT	GGGTGGTTCAGCTTTGTCTC
P2ry12	TTCAGCAGAACCAGGACCAT	GGGAGAAGGTGGTATTGGCT
P2ry13	TCACACAAAAGGTGCCATGT	ACACAGTGGTCAGGCTAGGG
P2ry14	TTCTGTTGACGAAGCTTGCC	CTGTGGTGGTGGAGTTGTTC
Scd1	TGTCAAAGAGAAGGGCGGAA	CGGGCTTGTAGTACCTCCTC

Table 2.2 Mouse gene primers used for qPCR.

Oligo Name	Forward sequence (5'-3')	Reverse sequence (5'-3')
Abcd2	ACTGGCTTTGCAGATGGTGA	ATCAGCTCCAGAGGCCAGTA
Ctsc	AGACCCCAATCCTAAGCCCT	TGGGCGTACTTTCCTGCAAT
Cxcl16	CGCCATCGGTTCAGTTCATG	GGAGCTGGAACcTCGTGTAG
Cyclophilin	GCATACGGGTCCTGGCATCTTGTCC	ATGGTGATCTTCTTGCTGGTCTTGC
Cyp27a1	TCAGCTGTTCGTTCAAGGCT	CATTGGACCGTACTTGGCCT
Gab1	ACACCTGGAAACTCTTGGCA	ATGCGTTCTGGTGGGTTCG
Irf8	ATTTTTAAGGCCTGGGCAGT	ATTTTTAAGGCCTGGGCAGT
P2ry13	GCCGCCATAAGAAGACAGAG	CACCGCTCAGATCTGTTGAA

Table 2.3 Human gene primers used for qPCR.

Oligo Name	Forward sequence (5'-3')	Reverse sequence (5'-3')
Fabp4	GGTGTAGCCTAGGACTGGAC	ACCACCCACCACAACTGTAA
Fabp5	GTTCTGGAAACTGCCCTGTG	AGTCTCTCCAAGGTGTCTGG
Pry13	TTCACTTCACCGTTCTTGCC	TAGCCAAACCCTGAAGACGG
Pry14	ACTGATGTGCGAGACTAGGG	TGTTTTGGGGAAGTGGCTTG

Table 2.4 Mouse primers used for ChiP-qPCR.

2.7 Protein Isolation and Western Blot analysis

Bone marrow cells from WTLdlrKO and M-IRF8KOLdlrKO were seeded, at a cell density of $5x10^6$ cells/ 10cm dish in complete DMEM and left to differentiate into macrophages over 6-7 days. Cells were washed twice in ice cold 1X PBS, scraped from the dishes and centrifuged at 1200rpm, for 10mins at 4^{o}C, after which the supernatant was discarded. Total protein was isolated from the cell pellets using radioimmunoprecipitation assay (RIPA) buffer, supplemented with 1mM sodium orthovanadate (Sigma Aldrich) and 1x phosphatase inhibitor cocktail IV (Sigma Aldrich). The cells where agitated for 30mins at 4^{o}C, before being centrifuged for 10mins at 13500rpm at 4^{o}C. The eluted protein was quantified using the BCA protein assay (Thermo Fisher). This assay uses the reduction of Cu^{2+} to Cu^{1+} by protein in an alkaline medium and produces a colorimetric reaction of the cuprous cation (Cu1+) by bicinchoninic acid (BCA), which was measured at 590nm on a TriStar² LB Multidetection Microplate Reader. Proteins were denaturalised by being boiled in a buffer containing 2% Sodium Dodecylsulfate (SDS) and 5% β-mercaptoethanol for 10mins and separated on a 10% acrylamide gel (BioRad) for 2 hours 30mins at a constant voltage of 100V. Proteins were then transferred to a PVDF membrane (Millipore) by wet transfer at 100V for 1 hour. After transfer, membranes were blocked with

StartingBlock™ Blocking Buffer (Thermo Fisher) for 1 hour at room temperature, and then blotted with primary antibody overnight at 4ºC. Rabbit IRF8 monoclonal antibody (Cell signalling, D20D8), rabbit Cyp27a1 monoclonal antibody (Abcam, ab126785) and Hsp90 polyclonal (Santa Cruz, sc-7947) were used as primary antibodies. Anti-rabbit (Dako, PO448) horseradish-peroxidase-tagged antibodies were used for secondary binding and chemiluminescence (EMD Millipore Immobilon™ Western Chemiluminescent HRP Substrate, Thermo Scientific) was used to visualise proteins.

2.8 Chromatin Immunoprecipitation

$50x10^6$ BMDMs from WTLdlrKO were cultured and directly double crosslinked with 2mM Di(N-succinimidyl) glutarate (Sigma) for 20mins at room temperature, followed by 1% formaldehyde (Thermo Scientific) for 10mins at room temperature. The crosslink reaction was quenched upon the addition of glycine, at a final concentration of 200mM, for 10mins whilst agitating at room temperature. The cells were washed twice with ice cold PBS, scraped into a 1.5mL tube and centrifuged for 10mins at 800xg, 4ºC. Nuclei were isolated by rotating cell preparations for 10mins at 4ºC with the following lysis buffers: Buffer 1 (50mM Hepes-KOH, pH 7.5, 140mM NaCl, 1mM EDTA, 10% glycerol, 0.5% NP-40 and 0.25% Triton X-100), Buffer 2 (10mM Tris-HCl, pH 8.0, 200mM NaCl, 1mM EDTA and 0.5mM EGTA), and Buffer 3 (10mM Tris-HCl, pH 8.0, 100mM NaCl, 1mM EDTA, 0.5mM EGTA, 0.1% Nadeoxycholate and 0.5% N-Lauroylsarcosine). Pellets were resuspended in 300µL of lysis buffer 3 and sonicated for 25 cycles (30 seconds ON/OFF) in the UCD-300 Bioruptor (Diagenode), to generate DNA-fragment sizes of 0.2–0.5 kilo bases (kb).

Successful sonication was confirmed by running products on a 2% agarose gel, in a 1X TAE buffer with 1X SYBR safe DNA gel stain (Invitrogen) for 30mins at 80V (**Fig 2.7**).

The concentration of sheared DNA was calculated using the NanoDropTM 1000 Spectrophotometer and multiplied by the total volume of DNA extracted from the undiluted sheared chromatin sample. Upon quantification of sheared DNA, 10µg of chromatin was immunoprecipitated with the following antibodies: 5µg IRF8 (ab, Cell Signalling) and 3µg H3K27ac (07-449, Merck), where antibody specificity was assessed against the same amount of IgG from rabbit serum (I5006, Sigma).

After proteinase K (Sigma) treatment, the immunoprecipitated DNA was purified using the QIAquick PCR purification kit (Qiagen) and analysed by quantitative real-time PCR with corresponding primers (sequences are listed in Table 2.4). Relative occupancies were normalized to input DNA (fold difference = 2–Ct-sample-Ct-input).

To determine the % Input of each IP sample the following calculation was used;

Average Ct of IP'ed samples – Average Ct of Input = dCt

% Input = (POWER(2,-dCt)) x 100

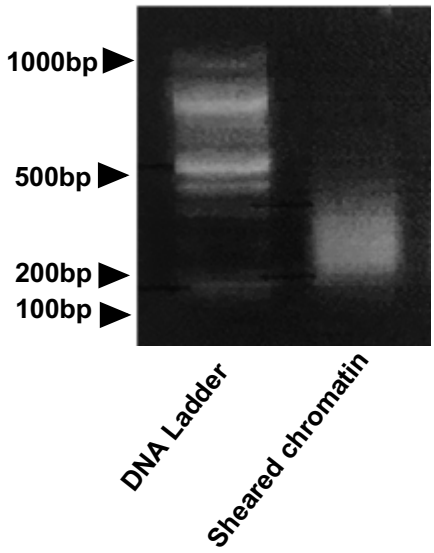

Fig 2.7 Sheared BMDM chromatin post sonication.
50x106 BMDMs where sonicated for 25 cycles at 30 seconds ON and 30 seconds OFF.

2.9 RNA Sequencing

RNA-Sequencing (RNA-Seq) is a method of high throughput sequencing of the whole transcriptome that offers many additional benefits over other gene screening methods including microarrays. These benefits include the ability to detect novel transcripts, reveal splice variants and increased efficacy of low abundance transcript detection are some of the reasons that make RNA-seq a more attractive method of high throughput sequencing over others [7].

2.9.1 RNA preparation and sequencing

WT^{LdlrKO} and M-$IRF8KO^{LdlrKO}$ mice where fed a high fat western-diet for 12 weeks after which their bone marrow was isolated and cultured with LCM (see section 2.5.2) to generate bone marrow derived macrophages from a total of n=6 mice (n=3/genotype). The macrophages were cultured with either DMSO (basal) or IFNβ for 6hrs and the total RNA was extracted using TRIzol reagent (see section 2.5.1). The RNA was then used for sequencing, where pipeline analysis were performed by UCL Genomics (London, UK). cDNA libraries were prepared

from the total RNA provided using reagents and protocols supplied with the Stranded mRNA-Seq Kit (Kapa Biosystems). Briefly, poly-A tailed RNA was purified using paramagnetic oligo-dT beads from 200ng of total RNA, with a RNA Integrity Number above 7.5 as determined by the Agilent Bioanalyzer (Agilent). The purified RNA was fragmented chemically by heating samples in the presence of Mg2+ and cDNA was synthesised using random primers supplied in the kit (Kapa Biosystems). Adapter-ligated DNA library was then amplified with 12 cycles of PCR and library fragment was estimated using the Agilent TapeStation 2200 and confirmed to be ~150bp (~280bp when including the Illumina adapters). Lastly, Library concentration was determined using the Qubit DNA HS assay (Life Technologies). Libraries were sequenced at a concentration of 1.8pM on a Illumina NextSeq 500, NCS v2.1.2 (Illumina), with a 43bp paired end protocol. Base calling was performed using the standard Illumina parameters (RTA 2.4.11).

2.9.2 RNA-Seq computational analysis

Reads were de-multiplexed using Illumina bcl2fastq v2.17 (Illumina) and then were aligned using STAR-2.5.3a to the mouse GRCm38/mm9 reference sequence. The reads where then filtered to removed singletons and unaligned reads. Gene counts where then quantified using the Partek E/M Annotation Model to mm9 - RefSeq Transcripts 83 - 2017-11-01 and differential expression analysis performed with DESeq2-3.5 (using Wald hypothesis test and parametric fit type with FDR step-up). To correct for multiple comparisons, a false discovery rate (FDR) of 0.05 was applied, to reduce the probability of false positives being included in the differentially regulated gene list [241] and a fold change cut off of 1.3 was applied to all gene lists produced.

2.9.3 RNA-Seq pathway and comparative analysis

All pathway analysis was performed using the web-based platform 'Metascape' [242]. This online tool combines functional enrichment, interactome analysis, gene annotation, and membership search from over 40 independent knowledgebases. Additionally, it facilitates comparative analyses of datasets across multiple independent experiments [242]. To perform the pathway analyses, individual gene lists were uploaded onto the Metascape website. Metascape is a platform that provides combined gene annotation, functional enrichment and interactome analysis by comparing an input gene list against 40 independent knowledgebases, where each knowledgebase contains curated genes under specific gene modalities. For example, Gene Ontology harbours gene annotations according to their molecular function, biological process or cellular component, whereas Reactome represents gene annotations according to different disease states and associated infections. By combining such breadth of knowledgebases, Metascape provides a platform by which pathway analysis can be performed across multiple knowledgebases, instead of one, thereby generating maximal information from a specific gene set. Although other online tools are available that combine gene annotation data similarly to Metascape, including g:Profiler and Webgestalt, they do not cover as many knowledgebases, are not as user friendly or as regularly updated as Metascape [243], [244]. For this reason, all pathway analysis performed within this thesis has been done through Metascape. For pathway analysis, all gene ontology (GO) processes, KEGG and Reactome annotation memberships were selected under the 'Enrichment' tab to allow for enriched pathways across all three membership tools

to be identified. Metascape generates a list of significant pathways, outlining their significance, enrichment ratio, gene members within each pathway and the relationship between the genes within each pathway as demonstrated in a cluster graph. Upon downloading the results, further detailed analysis sorting through upregulated and downregulated pathways and genes was performed using Microsoft Excel. Heatmaps of genes within each pathway was generated using either the online tool 'Heatmapper' (http://www.heatmapper.ca), using raw Deseq2 gene counts, or the statistical software 'GraphPad Prism version 7' when plotting the linear fold change.

Comparative analysis with multiple gene lists was also performed using 'Metascape' [242]. Multiple gene lists were uploaded to the website and analysed using the 'Enrichment' settings previously mentioned. Generated results included circus plots that highlight the degree of overlap between significantly regulated genes and genes that undercome the same function. Additional cluster graphs were also generated that highlight the proportion of each independent gene list that is enriched for a specific functional cluster. Analysis was performed on the downloaded pathway lists to generate heatmaps and Venn diagrams (using the online tool http://bioinformatics.psb.ugent.be/webtools/Venn) of significantly regulated genes that were identified in both independent gene lists.

2.10 Flow Cytometry

Flow cytometry samples were analysed using the LSR Fortessa (Becton Dickinson) and FlowJo software (Tree Star Inc.)

2.10.1 Antibodies

The list of antibodies used, including the fluorescent conjugate. concentration (where given) and clone is given in **Table 2.6**.

	Flurochrome	Target	Clone	Dilution	Supplier
CD11b	V500	Mouse	M1/70	100	BioLegend
CD14	A700	Human	HCD14	100	BioLegend
CD16	BV786	Human	3G8	100	Sirigene
CD19	FITC	Human	H1B19	100	BioLegend
CD20	FITC	Human	2H7	100	BioLegend
CD3	FITC	Human	UCHT1	100	BD Bioscience
CD45	PerCP Cy5.5	Mouse	30-F11	100	BioLegend
CD56	FITC	Human	HCD56	100	BioLegend
CD64	APC	Mouse	X54-5/7.1	100	BioLegend
F4/80	FITC	Mouse	BM8	100	BioLegend
HLA-DR	V500	Human	G46-6	100	BioLegend
Ly6g	PeCy7	Mouse	1A7	100	BioLegend

Table 2.5 List of antibodies used for flow cytometry

2.10.2 Compensation controls

Compensation controls are employed in multicolour flow cytometry to account for the spectral overlap of certain fluorochromes. Samples stained with single fluorochrome are run through the flow cytometer and the compensation matrix is calculated by the FACSDiva Software (BD Biosciences). Generally, compensation beads (BD Biosciences) consist of beads that do not bind antibody to provide a baseline fluorescence signal, and beads specific for the appropriate isotype are used. For each fluorochrome in the panel, one drop of negative control beads and one drop of antibody-binding beads were mixed in a 5mL FACS tube (BD Biosciences). This reproducibly added up to a total volume of

120µL. Antibodies were directly added at the right concentration and the mixture was incubated for 30mins at 4°C in the dark. Beads were washed twice with wash buffer at 1000xg, 3mins, 10°C before being resuspended in 500µL of wash buffer containing 0.01% sodium azide. Beads were stored at 4°C in the dark for up to two weeks.

2.11 Human participant recruitment

2.11.1 Ethics Statement

This study was approved by the UCL Research Ethics Committee (Refs: 2907/002 and 5061/001). Written informed consent was obtained from all volunteers prior to their participation in the study.

2.11.2 Inclusion and Exclusion Criteria

Volunteers were non-smoking adult males and females aged 18 and over (≥65 years was considered aged). It was difficult to recruit aged volunteers who had no chronic medical problems and/or are not on any medication, even though they described themselves as healthy. In addition, it was imperative to avoid a sampling bias by assessing ≥65 years participants with no co-morbidities nor taking regular medications.

No screening tests were performed on recruited participants. All medical evaluation was done using a questionnaire. Participants were asked to avoid heavy alcohol consumption and intense exercise during the study. A summary of the cohort is given in **Table 2.6**.

Age Group	Young	Aged
Mean Age	26.5	76.3
Age SD	3.58	11
Recruited	8	3
Gender (M/F)	(2/6)	(0/3)
Medication		
Antihypertensives	0	3
Anticoagulants	0	2
Miscellaneous*	4	0
HRT**	0	3

Table 2.6 Demographic data for the monocyte-ageing study.
*Includes supplements and contraceptive pills. **Includes tibolene and levothyroxine.

2.11.3 Monocyte isolation

For the purpose of this study, monocytes were isolated by an MSc student; Nadia Nozari. Monocytes where freshly isolated from peripheral, venous blood whole blood that was obtained from the median cubital vein of healthy, consented volunteers using a 20-gauge butterfly needle and aseptic non- touch technique. EDTA BD Vacutainer tubes (2mM final, Becton Dickinson) were used. To isolate peripheral blood monocytes, the red blood cells were lysed by adding 1mL of blood to 9mL of Ammonium- Chloride-Potassium (ACK) Lysis Buffer (Lonza) for 7mins before centrifugation at 300xg, 10mins, room temperature. Pellets were washed twice in ice-cold PBS and spun at 300xg, 10mins, 10^{o}C. The cells where then resuspended in 10mL of Hank's balanced salt solution (HBSS) and counted as mentioned in section 2.4.1. Monocytes where subsequently isolated upon use of a negative pan monocyte isolation kit (Miltenyi biotec) whereby classical ($CD14^{++}CD16^{-}$), intermediate ($CD14^{++}CD16^{+}$) and non-classical ($CD14^{+}CD16^{++}$) monocytes where obtained by depletion of magnetically labelled non-monocytic cells. Isolated monocytes where then lysed in 350μL of TrIZOL for RNA extraction

and analysis as outlined in section 2.5. The primers used for gene expression studies are outlined in **Table 2.3** and antibodies used for flow cytometry are outlined in **Table 2.5**.

Isolated monocyte purity was assessed using a simple flow cytometry panel (**Table 2.5**). A lineage cocktail consisting of CD3 (T cells), CD19 (B cells), CD20 (B cells) and CD56 (NK cells) was used to exclude potential contaminants. This method of isolation routinely resulted in >90% pure monocyte populations from both young and aged donors (**Fig 2.8**).

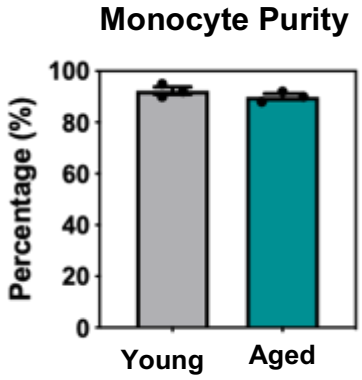

Fig 2.8 The purity of isolated peripheral blood monocytes.
Representation of the purity of monocytes as a % of single cells from young and aged healthy donors (n=3).

2.12 Statistical analysis

Data were analysed and plotted using GraphPad Prism v7.0 (GraphPad Software). Statistical tests were also performed using this software. The tests performed are given in the figure legends. P values of < 0.05 were considered statistically significant. When two datasets were compared the two-tailed students t-tests were applied unless stated. When comparing more than two groups a one-way ANOVA was applied unless stated. In calculating differences between liver lipid droplet size (Chapter 3), the area under the curve was calculated and compared across both genotypes. In generating the RNA-

Sequencing data, differential expression was performed using Deseq 2-3.5 where the Wald hypothesis test and parametric fit type with an FDR of <0.05 was set up. When performing pathway analysis on the differentially regulated genes identified in the RNA-sequencing dataset, the online platform 'Metascape' was used to sort statistically significant pathways and cluster them into groups using Kappa-based statistics [242]. The p-value generated in determining the statistical significance of the pathways identified in Metascape was generated based on the accumulative hypergeometric distribution [242].

Chapter 3: Results - Effect of myeloid-IRF8 reduction on Atherosclerosis

3.1 Introduction

Interferon regulatory factor 8 (IRF8) is an interferon inducible transcription factor that is crucial for haematopoietic lineage determination. The importance of IRF8 in determining granulocyte and monocyte cell fate has been demonstrated amongst a variety of models of global IRF8 deficiency in both mouse and human [121], [123]. IRF8 is pivotal in promoting the differentiation of myeloid cells whilst simultaneously inhibiting further neutrophil development [125]. Previous studies by Watanabe et al., 2013, demonstrate global-IRF8 deficiency promotes severe immunodeficiencies and a chronic myeloid leukaemia-like (CML) syndrome [153]. The CML syndrome is characterised by an aberrant expansion of circulating neutrophils and significant depletion of circulating monocyte subsets; Ly6C^{hi} and Ly6C^{lo} [129], [153], [245] A reduction in circulating myeloid cells results in impaired immune responses to IFN-γ and production of inflammatory cytokines leading to increased susceptibility to bacterial and viral infection [121].

IRF8 has been well characterised for its role in mediating immune cell response to infection and inflammation [121], [246]. Adams et al., 2018 demonstrated the importance of IRF8 in the anti-viral immune response of NK-cells, where IRF8 was necessary to promote the proliferation of virus-specific NK-cells [246]. Although IRF8 has been well characterised for its role in promoting myeloid-cell differentiation and development, it's role in monocyte and macrophage function, in relation to atherosclerosis development, is poorly understood.

Atherosclerosis is an inflammatory lipid mediated disorder that is largely influenced by myeloid cells – including macrophages [48]. Previous studies, investigating the role of IRF8 in atherosclerosis development have reported conflicting results [175], [177]. Doring et al., 2012 report haematopoetic-IRF8 deficiency accelerates atherosclerosis development, whereas Clement et al., 2018 demonstrates deletion of IRF8 in CD11c+ dendritic cells protects against atherosclerosis development. Considering IRF8 has been investigated in both hematopoietic stem cells and dendritic cells, its function in macrophages has received less attention within an atherosclerosis context. Previous studies by Pourcet et al., uncover a novel role for macrophage-IRF8 in modulating the expression of genes known to be involved in atherosclerosis: IL-18 binding protein and Arginase-1 [197], [233]. Both are known to protect against the development of atherosclerosis by preventing inflammation and nitric oxide induced cytotoxicity [197], [233]. Interestingly, both IL-18bp and Arginase-1 where modulated by an LXR-IRF8 crosstalk, as demonstrated in Fig 3.1. Because of the known role of LXR nuclear receptor in atherosclerosis [247]–[249], this led to further postulation of a possible role for macrophage-IRF8 in atherosclerosis progression.

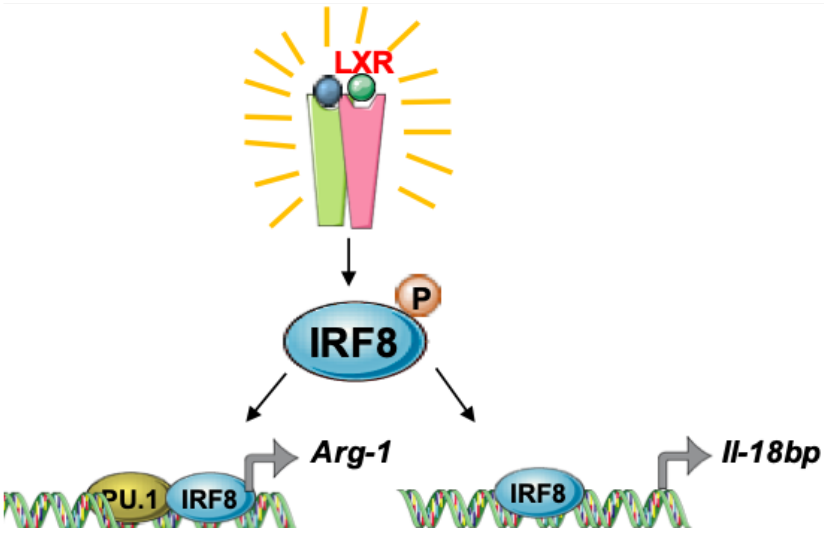

Figure 3.1 Schematic diagram of the LXR-IRF8 crosstalk.
LXR becomes activated via endogenous ligand allowing the receptor to bind and activate IRF8, via IRF8 phosphorylation. This enables IRF8 to heterodimerise with binding partner, PU.1, and promote gene expression of Arginase-1 and Il-18bp.

This chapter establishes the role of myeloid-IRF8 in atherosclerosis development using a novel myeloid specific IRF8^{KO} mouse model generated on the LDLR^{KO} background (M-IRF8KO^{LdlrKO}), using WT^{LdlrKO} mice as controls. Previous studies by Doring et al., 2012, demonstrated hematopoietic-IRF8 deficiency resulted in a CML-like phenotype, due to the dysregulation of myelopoiesis, which ultimately contributed to increased atherosclerotic plaque development [175]. To prevent any undesired phenotype, such as CML, that may independently contribute to atherosclerosis development, it is crucial that we better characterise the blood immune cell composition and metabolic profile of hyperlipidaemic IRF8-deficient mice [21].

Interferon regulatory factors, including IRF5, IRF6 and IRF9 have also been implicated in the development of other metabolic diseases [192]–[194], [250], some of which are known to contribute to atherosclerosis progression [193]. Non-alcoholic fatty liver disease (NAFLD) is one such disease that is highly associated with cardiovascular disease, in particular atherosclerosis by

promoting inflammation, stenosis and vascular calcification [251], [252]. Therefore, further investigation is important to determine whether myeloid-IRF8 deficiency affects the development of fatty liver disease that may also contribute to atherosclerosis development.

Considering Doring and colleagues, identified an atherogenic phenotype of hematopoetic-IRF8 deficiency, via deletion of IRF8 from all bone marrow derived immune cells, including myeloid cells, they have not characterised a cell specific role of IRF8 in atherosclerosis [175]. Thus, we aimed to decipher the role of IRF8 in myeloid cells specifically within atherosclerosis, without impacting on non-myeloid immune cells. This will enable us to gain a clearer insight into the possible targeting of myeloid-IRF8 in future clinical applications.

3.1.1 Objectives and aims

The objective for Chapter 3 is to determine the effect of myeloid-IRF8 reduction on the development of atherosclerosis.

Aims:

1. Confirm IRF8 depletion in myeloid cells and determine the metabolic profile of western diet fed WT^{LdlrKO} and M-$IRF8KO^{LdlrKO}$ mice.
2. Determine the impact of myeloid-IRF8 reduction on atherosclerosis progression.
3. Determine whether myeloid-IRF8 reduction impacts on the metabolic Non-alcoholic fatty liver disease that could influence atherosclerosis development.

3.2 IRF8 is reduced in bone marrow derived macrophages of M-IRF8KO^{LdlrKO} mice

Myeloid-cells, specifically macrophages have a pivotal role in the development of atherosclerosis [48]. Thus, to investigate the role of myeloid-IRF8 reduction in atherosclerosis development, Dr Matthew Gage, generated a conditional myeloid-IRF8 knock out mouse model (M-IRF8KO^{LdlrKO}), prior to my joining the lab. To specifically delete IRF8 from myelomonocytic cells, we employed the cre-loxP recombination approach. Upon crossing IRF8 floxed mice with mice that expressed cre recombinase under the lysozyme M promoter, we were able to remove IRF8 from lysozyme M expressing cells, specifically myeloid cells [253]. This approach of conditional-IRF8 removal from myeloid-cells has been successfully used in other studies [254], lending to our adoption of this approach.

First, to validate the depletion of IRF8, qPCR primers were designed that specifically flank the region of IRF8 that was removed - exon 2. As displayed in **Fig 3.2**, the gene expression of *Irf8* was significantly reduced (95%) in bone marrow derived macrophages of M-IRF8KO^{LdlrKO} mice, when compared to WT^{LdlrKO} mice. This was further confirmed at the protein level as shown in western blot and protein densitometry analysis (**Fig 3.2 B & C**). Relative mRNA expression of an unrelated gene used as negative control, *Caspase-1*, further supports LysMcre induced reduction of *Irf8* in the bone marrow derived macrophages, as no difference was observed in *Caspase-1* gene expression (**Fig 3.2 D**). Collectively, this demonstrates the bone marrow derived macrophages from M-IRF8KO^{LdlrKO} mice display significantly reduced expression of IRF8 at

both the gene and protein level, when compared to WT^{LdlrKO} mice. This, therefore, validates our conditional model of myeloid-IRF8 reduction.

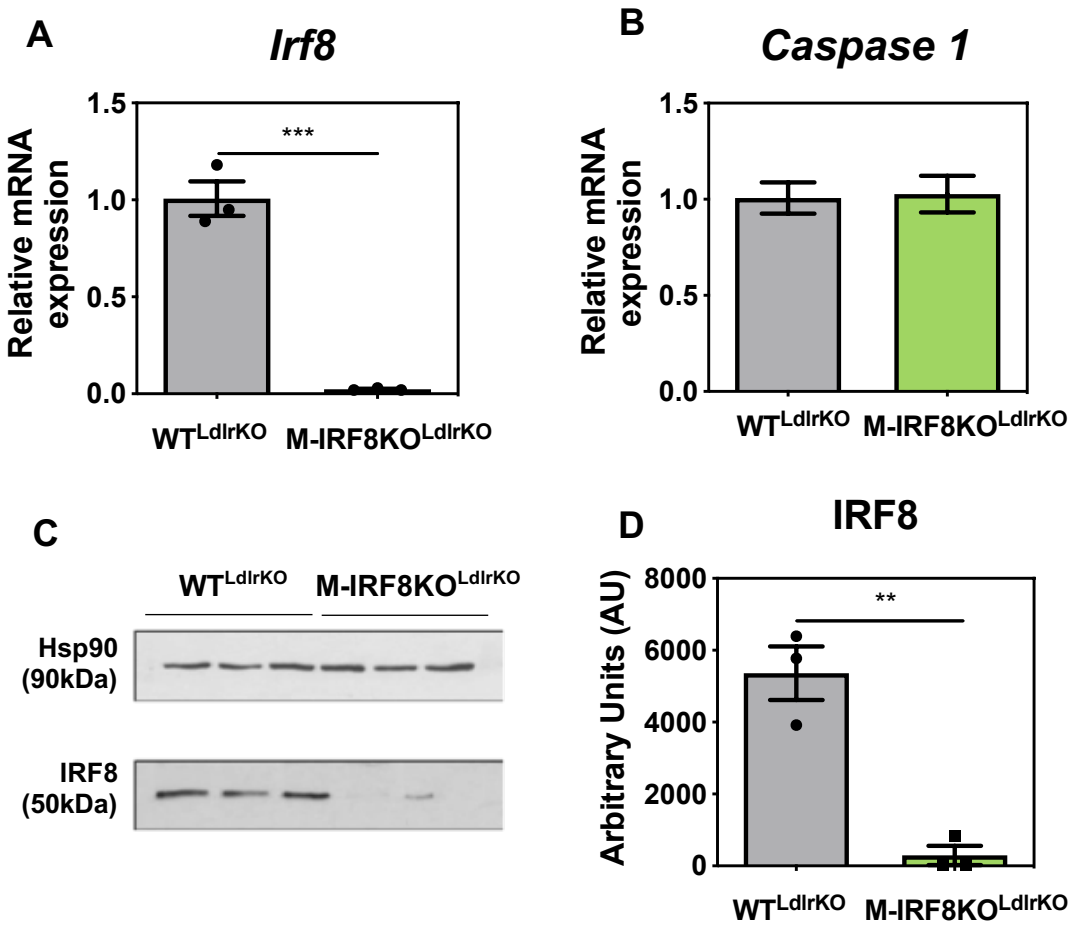

Fig 3.2 IRF8 expression is depleted in bone marrow derived macrophages of M-$IRF8KO^{LdlrKO}$ mice.
(A) *Irf8* mRNA expression determined by quantitative-PCR of bone marrow derived macrophages. (B) *Caspase 1* mRNA expression determined by quantitative-PCR of bone marrow derived macrophages. (C) IRF8 protein expression analysed by western blot of bone marrow derived macrophages (n=3 per group) with subsequent (D) densitometry quantification of the western blot bands. Data are presented as mean ± SEM, statistical analysis performed using unpaired students t-test (**P < 0.01, ***P<0.0001, relative to $WT^{Ldlr\text{-}KO}$ mice).

3.3 Investigation of myeloid-IRF8 reduction on Atherosclerosis development

3.3.1 Myeloid-IRF8 reduction protects against atherosclerosis development

Upon validating the depletion of IRF8 in the bone marrow derived macrophages of M-IRF8KO^{LdlrKO} mice, we went on to further explore the effect of myeloid-IRF8 reduction on the development of atherosclerosis. The atherosclerotic plaque initially develops in regions of perturbed blood flow and reduced sheer laminar stress [10]. In mice, this is often initiated within the aortic sinus before progressing to the aortic arch, thoracic and abdomen [31]. For this reason, we investigated plaque development within these regions by staining the aortic roots with haematoxylin and eosin. Upon quantifying the percentage of stained plaque area, we observed M-IRF8KO^{LdlrKO} mice developed significantly less plaque in comparison to WT^{LdlrKO} (**Fig 3.3.1 A & B**).

The location of plaque development is often an indication on the stage of atherosclerosis, specifically as differences in lesional development within the descending aorta is often seen in moderate-advanced atherosclerosis. This is frequently due to the reduced curvature of the aorta, in comparison to the aortic root. To investigate whether myeloid-IRF8 reduction also affects plaque development in the descending aorta, lipids were stained with oil-red-o and subsequently quantified as a percentage of the total aorta, aortic arch, descending thoracic or abdomen. Interestingly, we did not observe a significant difference in the percentage of plaque developed in the descending aorta as a whole or within the arch, abdomen or thoracic areas (**Fig 3.3.1 C, D & E**).

Although this implies possible early-stage atherosclerosis development, specifically due to plaque formation primarily occurring within the aortic sinus prior to advancement into the descending aorta, studies investigating the type and severity of plaques developed would further confirm this. Interestingly, Doring et al., 2012, identified significant differences in plaque development within the descending aorta, as well as aortic sinus in the hematopoietic-IRF8KO^{ApoeKO} mice. However, such differences are likely to be attributed to the differences in lipoprotein profile between Apoe^{KO} and Ldlr^{KO} mice. Mice on the Ldlr^{KO} background are less likely to develop plaque within the descending aorta, after 12 weeks of western diet, due to the reduced plasma cholesterol levels in comparison to Apoe^{KO} mice [255], [256]. Alongside differences in lipoprotein profile, perturbed blood flow is also known to contribute to the site-specific development of atherosclerotic plaques. This may contribute to the differences observed in plaque development between the aortic sinus and descending aorta [257].

In comparison to studies investigating hametopoetic-IRF8 deficiency [175], we have identified an athero-protective phenotype of myeloid-IRF8 reduction upon reduced plaque development within the aortic root. This demonstrates myeloid-IRF8 reduction retards atherosclerosis development, complementing studies by Clement et al., 2018 whom also demonstrate myeloid CD11c-IRF8 deficiency abrogates atherosclerosis development.

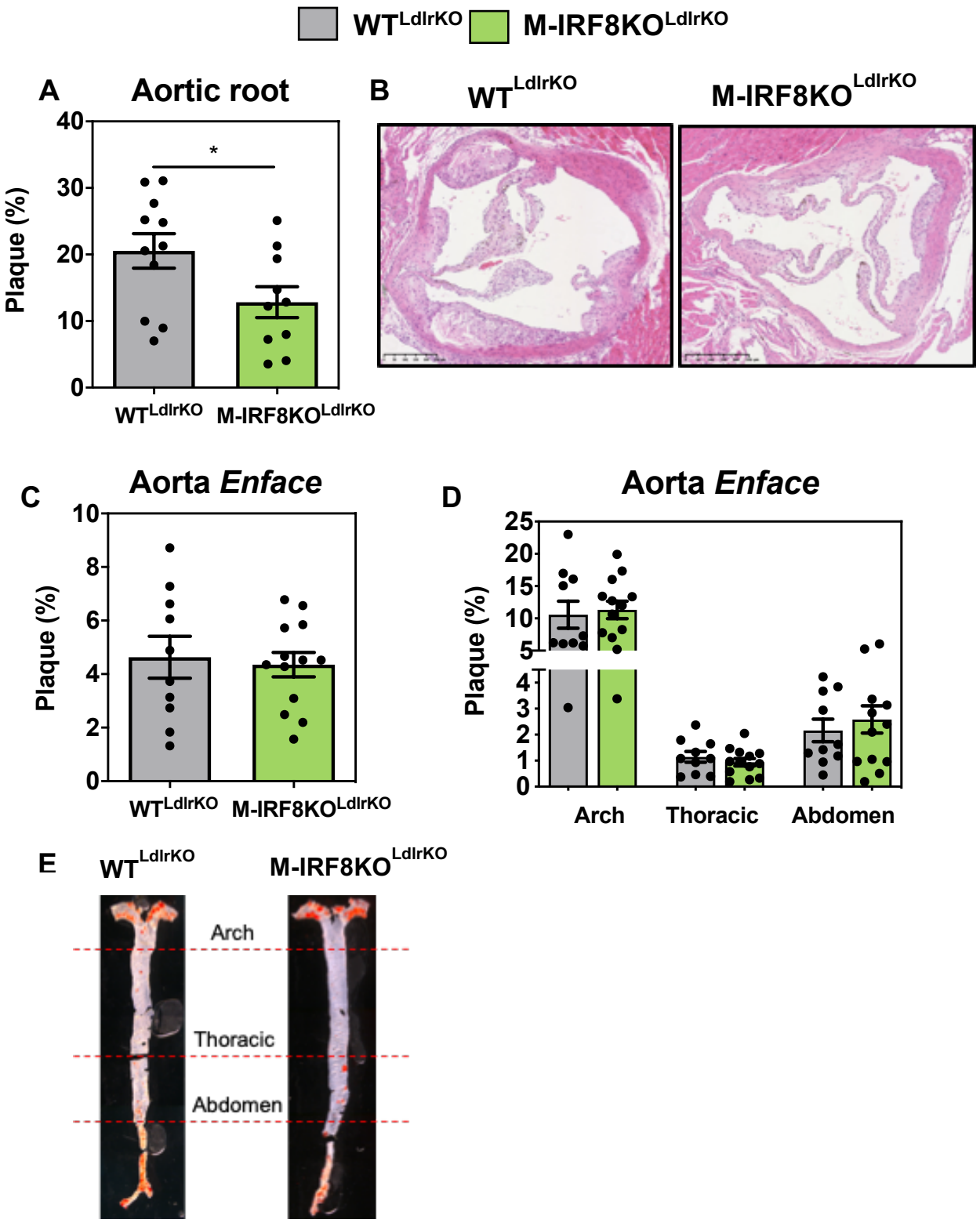

Fig 3.3.1 Myeloid-IRF8 reduction protects against atherosclerotic plaque development in the aortic roots of western diet fed mice, without having an effect in the descending aorta. (A) Quantification of atherosclerotic plaque developed in the (B) H&E stained aortic roots of western diet fed mice (n=10-11/group), 20x magnification. Quantification of Oil-Red-O lipids in the (C) total aorta enface and (D) aortic arch, thoracic and abdomen of western diet fed mice (n=10-11/group). (E) Representative images of Oil-Red-O stained aortas. Data presented as mean±SEM, statistical analysis conducted using unpaired students t-test, *$p<0.05$ relative to $WT^{Ldlr\text{-}KO}$ mice.

3.3.2 M-IRF8KO^{LdlrKO} mice develop fewer advanced stage plaques with no apparent physiological differences

Atherosclerotic plaque severity is often used as an insight into possible clinical manifestations [258]. Further investigation into the phenotype and severity of lesions developed may also highlight possible mechanisms by which myeloid-IRF8 reduction retards the development of atherosclerosis. Therefore, we performed lesion severity analysis, according to the American Heart Association guidelines, adjusted to animal models, [31], [259] to identify whether myeloid-IRF8 affected lesion severity. As demonstrated in **Table 3**, early stage atherosclerotic lesions are classified by the formation of macrophage foam cells and their subsequent accumulation across the arterial sub-endothelium forming a fatty streak [31]. Moderate stage plaques are characterised by an increase in foam cell accumulation and apoptosis of foam cells. The resultant release of lipids contributes to the formation of an extracellular lipid core and a thickened artery wall. Advanced stage plaques, however, display an increase in calcification, foam cell apoptosis and defective clearance of apoptotic cells leading to an enlarged necrotic core. Increasing smooth muscle cell proliferation and collagen formation result in an increase in fibrous tissue leading to the development of a fibrous cap. The relative thickness of the fibrous cap contributes to plaque stability, particularly as thinning of the fibrous cap has been associated with increased risk of plaque rupture [31], [260] (**Table 3**). Upon quantifying the different types of lesions present we identified no difference in the number of early stage plaques developed in the M-IRFK8KO^{LdlrKO} mice, when compared to WT^{LdlrKO}. However, the number of moderate and advanced stage plaques increasingly declined in M-

IRF8KO^{LdlrKO} mice in comparison to the WT^{LdlrKO} mice. This was further highlighted upon combining the number of moderate and advanced stage plaques developed (**Fig 3.3.2 A & B**). This suggests myeloid-IRF8 reduction may prevent the development of mature advanced stage plaques.

To better define the type and severity of the advanced stage plaques developed, analysis on the area of plaque necrotic cores and the area and diameter of fibrous cap formation was performed. Advanced stage plaques are characterised by the accumulation of apoptotic foam cells due to defective efferocytosis, ultimately resulting in the formation of lipid-rich necrotic cores [261]. Continued plaque progression can result in thinning of the fibrous cap leading to a vulnerable rupture prone plaque [262]. To determine the severity of the advanced stage plaques developed, the area of necrotic cores and fibrous caps formed within was determined. Intriguingly, myeloid-IRF8 reduction made no significant difference to necrotic core formation, fibrous cap area or fibrous cap diameter (**Fig 3.3.2 C, D & E**).

Overall, this data suggests that myeloid-IRF8 reduction prevents the development of mature advanced stage plaques, without affecting the formation of necrotic cores or fibrous caps which are characteristic of advanced stage plaque development.

Plaque type	Stage	Description	Image
Type I-II	Early	Formation of isolated macrophage foam cells that begin to aggregate across the arterial sub endothelium to form a fatty streak	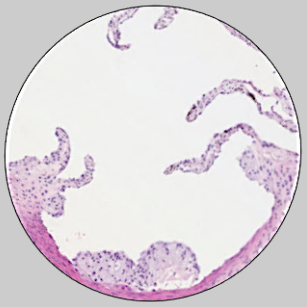
Type III-IV	Moderate	Apoptotic foam cells release lipids to form intracellular lipid pools within the fatty streak. Ineffective clearance of apoptotic cells results in a growing plaque with a mature extracellular lipid core	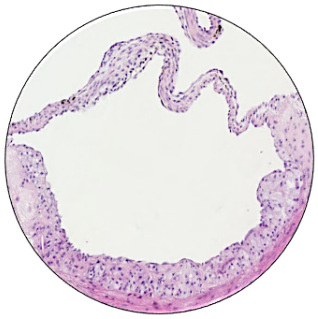
Type V-VI	Advanced	Large lipid core with increasing plaque fibrosis and calcification. Thinning of the fibrous cap contributes to plaque vulnerability and possibility of plaque rupture	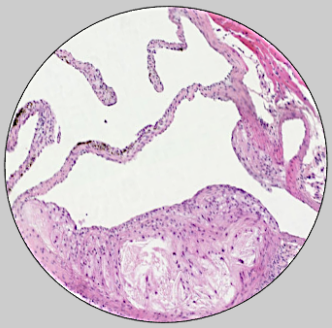

Table 3. Characteristics of plaque type and severity at different stages of atherosclerosis development.
Plaque images are from H&E stained aortic roots of western diet-fed 20wk old WT^{LdlrKO} and M-$IRF8KO^{LdlrKO}$ mice.

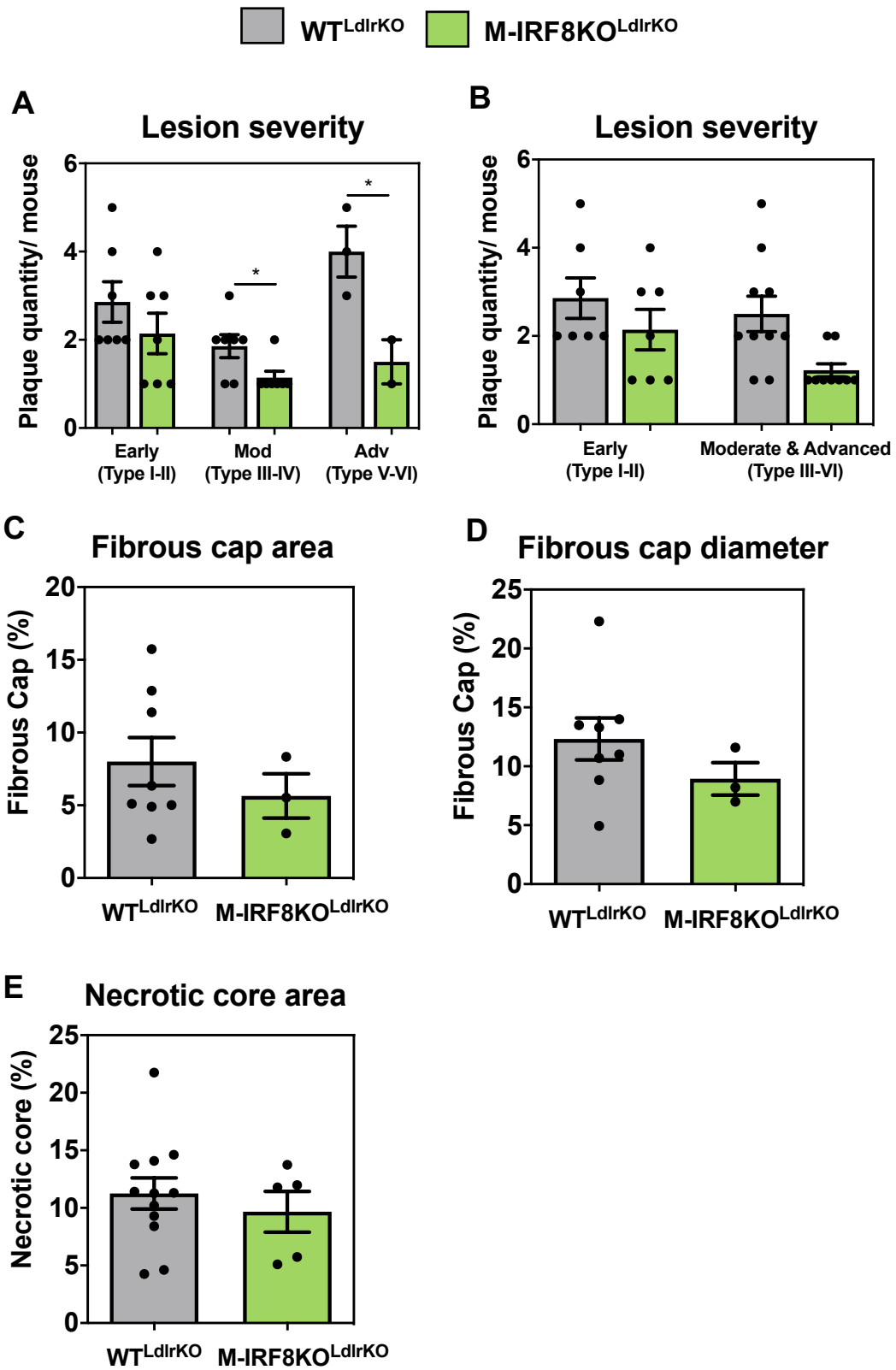

Fig 3.3.2 M-IRF8KO^{LdlrKO} mice develop fewer advanced stage plaques with no difference in the severity of advanced stage plaques developed.

(A) Lesion severity scoring of atherosclerotic plaques within the aortic root (n=10+11/group), separated as early, moderate or advanced or with moderate and advanced stage plaques combined (B). Scoring was conducted according to the American Heart Association guidelines. (C) Fibrous cap area and (D) thickness measured in the advanced stage atherosclerotic lesions in the aortic root. (E) Necrotic core analysis conducted on the advanced stage atherosclerotic plaques in the aortic root (n=11 WT^{LdlrKO}, n=5 M-IRF8KO^{LdlrKO}).. Data are representative of mean±SEM, statistical analysis conducted using the unpaired students t-test *p<0.05 relative to WT$^{Ldlr\text{-}KO}$ mice.

3.3.3 M-IRF8KO^{LdlrKO} mice display reduced macrophage content within their atherosclerotic plaques

Macrophages have a pivotal role in the progression of atherosclerotic plaques, and they are found in increased abundance with increasing plaque severity [48]. Having previously identified myeloid-IRF8 reduction retards the development of advanced stage plaques (**Fig 3.3.1**), we next investigated plaque macrophage content. CD68 is a cell surface marker, often used in the identification of macrophages in aortic root samples [263], [264]. To identify for possible differences in plaque CD68+ cellular content, paraffin embedded aortic root sections where stained for CD68+ cells. Interestingly, M-IRF8KO^{LdlrKO} mice display a significant decrease in the percentage of plaque CD68+ cells in comparison to WT^{LdlrKO} by approximately 43% (**Fig 3.3.3 A & B**). This suggests myeloid-IRF8 reduction may impair the balance of plaque macrophage infiltration, proliferation and apoptosis within the atherosclerotic plaque, resulting in reduced plaque macrophage content.

To confirm the differences identified in plaque macrophage content, we quantified the number of aortic macrophages from western diet fed mice, using the same gating strategy as shown in (**Fig 3.3.3 D**). Due to the low cell numbers, aorta from n=4 mice where pooled for one point and aorta from n=2 mice where pooled for the other point. This resulted in only two plotted values therefore preventing possible statistical analysis. Nevertheless, M-IRF8KO^{LdlrKO} mice display a reduction in the percentage of aortic macrophages, (**Fig 3.3.3 C**) as

expected, lending support to a novel regulation of plaque macrophage content by myeloid-IRF8.

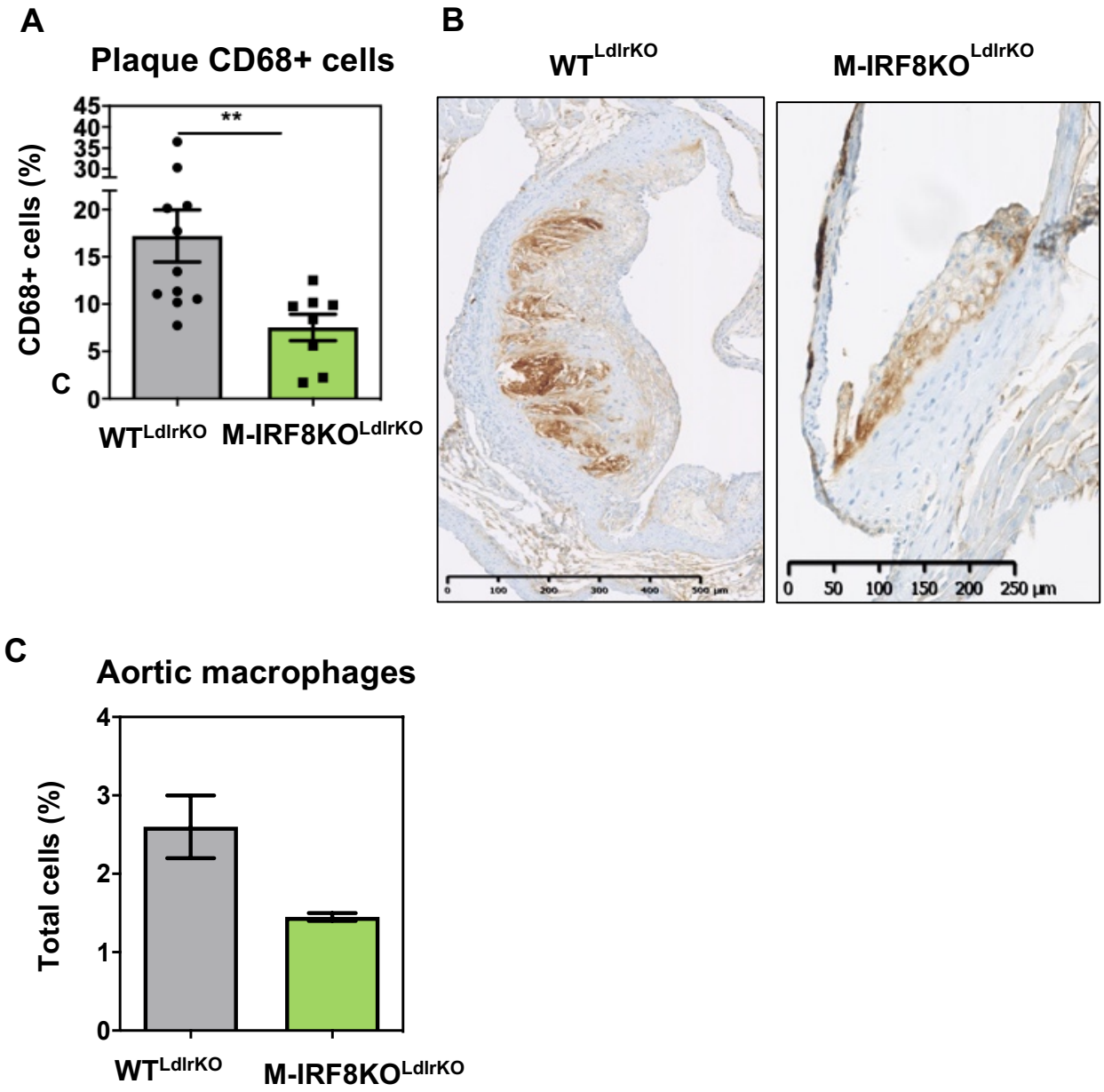

Fig 3.3.3 M-IRF8KO^{LdlrKO} mice display decreased CD68+ cell content within their atherosclerotic plaques.
(A) Quantification of CD68+ cells in the aortic root of western diet fed mice, as depicted by the (B) brown stain within the plaques (n=10-11/group). (C) Quantification of total aortic macrophages (CD45+CD64+CD11b+F4/80), aortae from n=2 and n=3 mice were pooled in two individual experiments (totalling n=5/group), resulting in only two data points for WT^{LdlrKO} and M-IRF8KO^{LdlrKO} mice and preventing possible statistical analysis on these samples. Data presented as mean±SEM, statistical analysis conducted using the unpaired students t-test, **p<0.01 relative to WT$^{Ldlr\text{-}KO}$ mice.

3.4 Characterisation of metabolic profile and development in western diet fed mice

3.4.1 Myeloid-IRF8 reduction does not affect the metabolic profile of mice

IRF8 has been well characterised for its role in myelopoiesis across multiple species [119]. However, previous studies have suggested a possible role for IRF8 in regulating genes involved in both glucose and lipid metabolism within the granulocyte monocyte progenitors in leukaemia [265]. Previous studies by Pourcet et al., have demonstrated IRF8 regulation of genes known to affect the development of atherosclerosis, namely Arginase-1 and IL-18bp [197], [233]. Interestingly, previous studies by Clement et al., investigating IRF8 deficiency in $CD11c^{+}$ cells in atherosclerosis, had demonstrated an increase in plasma cholesterol levels in CD11c-$IRF8^{KO}$ mice [177]. Thus, we explored the effect of myeloid-IRF8 reduction on plasma cholesterol. In contrast to Clement et al., 2012, we did not observe a difference in total plasma cholesterol levels between M-$IRF8KO^{LdlrKO}$ and WT^{LdlrKO} mice (**Fig 3.4.1 A**).

As previous studies have identified a role for IRF8 in regulating genes involved in glucose metabolism [265], we further determined whether this association was mirrored by myeloid-IRF8 reduction and initially measured blood glucose. A 30% reduction in blood glucose of both WT^{LdlrKO} and M-$IRF8KO^{LdlrkO}$ was observed when fasted, however myeloid-IRF8 reduction had no effect on blood glucose levels at both rested and fasted state (**Fig 3.4.1 B).** Despite previous studies have demonstrated global-IRF8 deficiency to impact on the expression of genes involved in glucose homeostasis [265], we have demonstrated myeloid-IRF8 reduction does not impact overall blood glucose

levels. Work by Scheller et al., 2013, that identified IRF8-associated differences in glucose homeostasis, did so in the granulocyte-monocyte progenitors of human chronic myeloid-leukaemia (CML) patients [265]. This suggests, the IRF8-mediated differences observed by Scheller and colleagues may be due to differences in IRF8 expression in immune cells other than myeloid-cells, since their model depletes IRF8 from all cells. In agreement, Shaffer et al., 2008 demonstrated CML patients that presented with altered glucose metabolism was due to the differential regulation of glucose-related genes by IRF4 in B-cells [266]. Although IRF4 is a different interferon regulatory factor, these studies suggest regulation of glucose metabolism related genes in CML patients may be due to differential expression of interferon regulatory factors in non-myeloid cells.

This work demonstrates that high-fat western diet-fed M-IRF8KO^{LdlrKO} mice do not develop impaired total plasma cholesterol or blood glucose homeostasis, when compared to WT^{LdlrKO}.

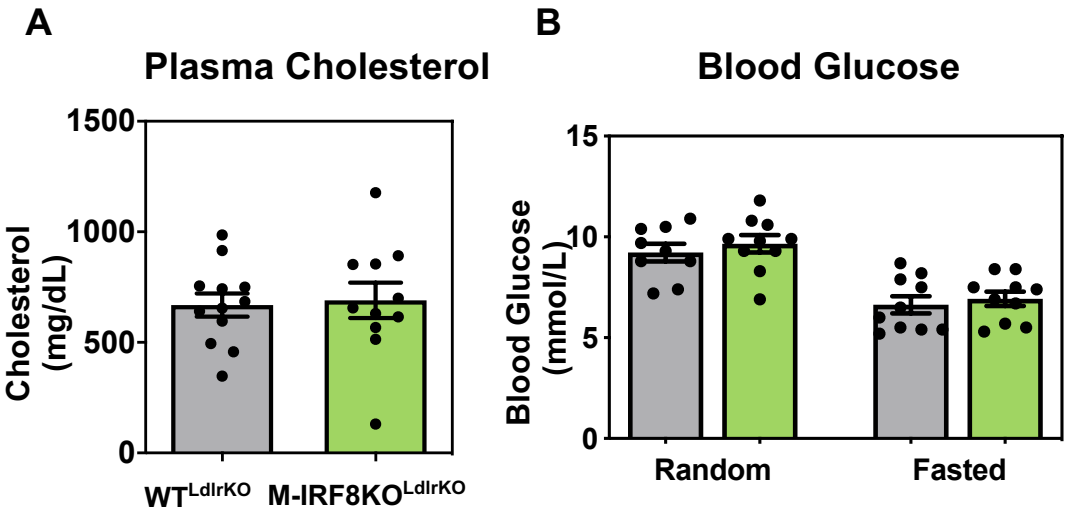

Fig 3.4.1 Myeloid-IRF8 reduction does not impair the metabolic profile of western diet fed mice.
(A) Plasma cholesterol concentration of western diet fed mice. (B) Blood glucose measurements recorded from the tail vein of western diet fed M-IRF8KO^{LdlrKO} and WT^{LdlrKO} mice at basal rate and fasted basal rate post 12weeks of western diet feeding. All data are representative of n=10-11/group, no significance identified upon performing statistical analysis using unpaired students t-test.

3.4.2 M-IRF8KO^{LdlrKO} mice display normal development

Upon confirming myeloid-IRF8 reduction did not impact on plasma cholesterol and blood glucose, we next aimed to further investigate whether myeloid-IRF8 reduction impacted on mouse development. Body and organ mass, are often used to detect growth and metabolic related disorders than can affect the overall development of the mouse [267]. To determine whether myeloid-IRF8 reduction affects the growth and development of the mice, body and organ mass where recorded. As expected for the type of western diet used [268], the body mass of both WT^{LdlrKO} and M-IRF8KO^{LdlrKO} increased by approximately 40% upon feeding the mice a western diet [267]. However, myeloid-IRF8 reduction had no effect on the overall body mass pre- or post-western diet feeding (**Fig 3.4.2 A**).

Further investigation into organ mass, demonstrates myeloid-IRF8 reduction appeared to have no impact on the development of the liver, epididymal fat, lung, kidney or heart (**Fig 3.4.2 B & C**). However, M-IRF8KO^{LdlrKO} mice developed significantly larger spleens in comparison to WT^{LdlrKO} (**Fig 3.4.2 C**) representing a modest increase of 13% in mass. Interestingly, IRF8 reduction has been previously associated with splenomegaly [269], [270]. IRF8 has been shown to negatively regulate the expansion of myeloid-derived suppressor cells within the spleen, known to cause splenomegaly within the global-IRF8 deficient mouse model [269]. However, when depleted from myeloid cells, including dendritic cells or mature macrophages from chow fed mice, this phenotype is no longer apparent [177], [270]. This is suggestive of a possible diet-induced splenomegaly phenotype.

To explore the overall effect of myeloid-IRF8 reduction on splenomegaly development, we determined the % of cre expressing mature macrophages and neutrophils within the spleen, characterised as ($CD45^+CD11b^+CD64^+F4/80^+$) and ($CD45^+Ly6G^+$) (**Fig 3.4.2 D, Methods 2.5**). Surprisingly, we do not see a difference in the percentage of total splenic macrophages (**Fig 3.4.2 E)** nor in the percentage of total splenic neutrophils (**Fig 3.4.2 F)** in western diet-fed mice. This suggests that myeloid-IRF8 reduction may affect spleen size via dysregulation of other cre-expressing cells, including monocytes or myeloid derived suppressor cells, that have not been explored.

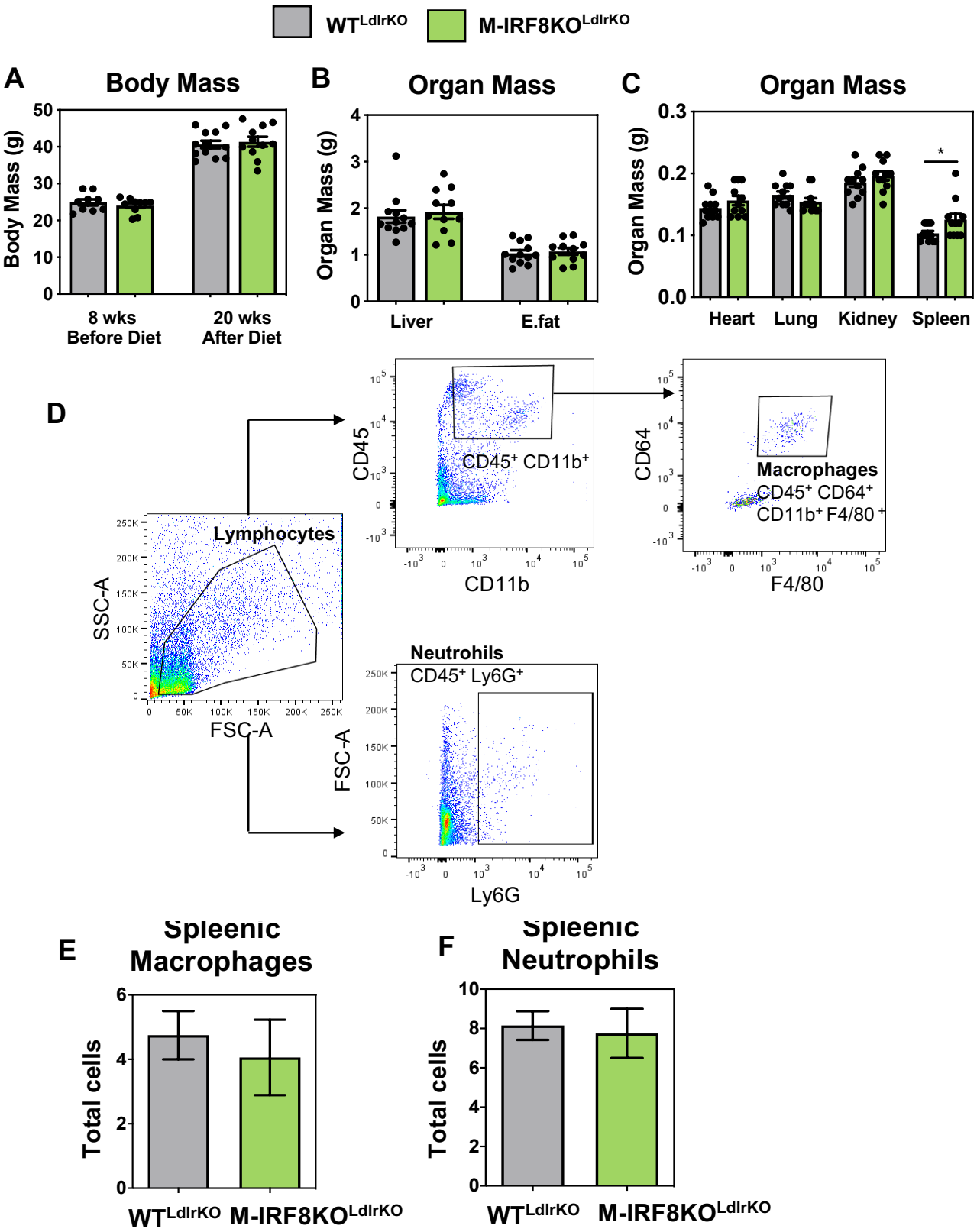

Fig 3.4.2 Myeloid-IRF8 reduction does not impact on the body mass or organ development of western diet fed mice.

(A) Total body mass of mice recorded pre and post western diet feeding. (B+C) Organ mass of mice recorded post 12weeks of western diet feeding (n=10+11/group). (D) Gating strategy implemented to decipher (E) macrophages (CD45+CD64+CD11b+F4/80) and (F) neutrophils (CD45+Ly6G+) from spleens of western diet fed mice (pooled n=5/genotype). Data are presented as mean ± SEM, statistical analysis conducted using unpaired students t-test, *p<0.05, relative to $WT^{Ldlr\text{-}KO}$ mice.

.

3.4.3 Myeloid-IRF8 reduction does not affect the number of circulating blood monocytes and neutrophils

Global IRF8 deficiency is known to disrupt myelopoiesis resulting in a chronic myeloid-leukaemia like syndrome resulting in a significant reduction in circulating monocytes and an aberrant increase in circulating neutrophils [121], [245]. Previous work by Doring and colleagues, demonstrated hematopoeitc-IRF8 deficient mice develop this CML-like phenotype, that ultimately contributed to atherosclerotic plaque development [175]. As lysozyme M is solely expressed in mature myeloid cells, not haematopoietic progenitors, it is not expected to affect myelopoiesis, resulting in a CML-phenotype similar to that observed in Doring et al., 2012. To confirm this, we determined the number of circulating blood monocytes and neutrophils (**Fig 3.4.3 A, Methods 2.6**). There was no significant difference in the number of the circulating neutrophils or monocytes in the M-IRF8KO^{LdlrkO} mice, when compared to WT^{LdlrKO} mice (**Fig 3.4.3 B & C**).

Overall, this data suggests that myeloid-IRF8 reduction does not impede myelopoiesis or subject the mice to a phenotype similar to that of chronic myeloid leukaemia like syndrome. This demonstrates the atherosclerotic phenotype observed in M-IRF8KO^{LdlrKO} mice is not likely to be due to the formation of a CML like phenotype, as previously demonstrated in the atherosclerosis prone hematopoetic-IRF8 deficient mouse model [175].

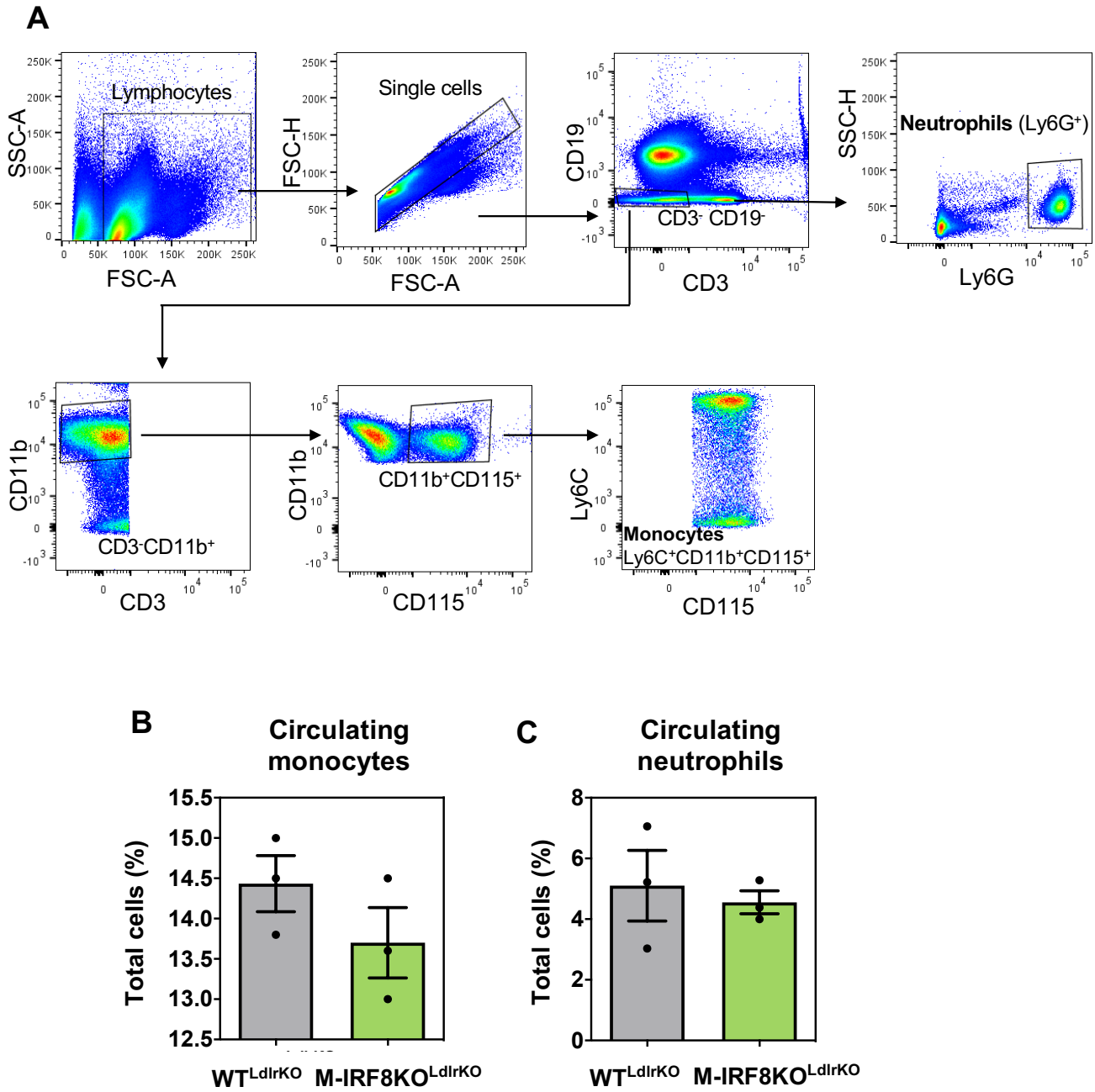

Fig 3.4.3 Myeloid-IRF8 reduction does not affect the total number of circulating blood monocytes or neutrophils.
(A) Gating strategy implemented to identify monocytes (Ly6C+CD11b+CD115+) and neutrophils (Ly6G+) from the blood (Lineage – CD3, CD19). (B) Total frequency of (B) circulating monocytes and (C) circulating neutrophils (n=3/group). Data are presented as mean ± SEM, no significance identified upon performing statistical analysis using unpaired students t-test.

3.5 Western diet fed mice do not develop a liver metabolic syndrome often associated with atherosclerosis

Non-alcoholic fatty liver disease (NAFLD) is a classic example of a hepatic metabolic syndrome that is often associated with coronary artery disease [251], [252]. NAFLD is characterised by an increase in hepatic triglyceride accumulation resulting in increased hepatic inflammation and fibrosis [187]. Increases in systemic inflammation, fibrinogen, C-reactive protein and disturbances in lipoprotein metabolism associated with NAFLD are also risk factors for cardiovascular disease. For this reason, it is thought many NAFLD patients are often at an increased risk of developing cardiovascular complications, including atherosclerosis [187], [271].

However, select interferon regulatory factors, including IRF6 and IRF5, have also been implicated in the development of NAFLD [191], [192]. The negative regulation of peroxisome proliferator-activated receptor γ (PPARγ) induced lipogenesis and fatty acid uptake, by IRF6 has been shown to protect against NAFLD, when rodents are challenged with a high-fat diet [191]. Induction of macrophage-specific IRF5, also contributes to inflammation resulting in hepatocyte apoptosis in models of NAFLD [192]. IRF9, however, is known to protect against NAFLD development when over expressed, due to its positive regulation of PPAR-α target genes known to maintain hepatic fatty acid metabolism [193], [195]. Although IRF8 has not been associated with the regulation of peroxisome proliferator-activated receptor, it is a known target gene of the nuclear receptor LXR, also known to contribute to NAFLD due to its regulation of genes involved in triglyceride metabolism [190], [197].

Therefore, we next aimed to investigate myeloid-IRF8 reduction in the development of NAFLD. To investigate this, the diameter and area of lipid droplets present within the H&E stained livers of both M-IRF8KO^{LdlrKO} and WT^{LdlrKO} mice where quantified as described in section **2.3.5** [190]. Due to the sporadic nature of both macro and microvesicular lipid droplets present within the livers of mice fed a high fat diet, lipid droplets were quantified at four different regions using an unbiased randomized approach. Interestingly, there was no significant difference observed in the number and size of lipid droplets present within the liver of M-IRF8KO^{LdlrKO} mice when compared to WT^{LdlrKO} mice (**Fig 3.5**).

Overall, this suggests myeloid-IRF8 reduction does not impact upon NAFLD development, however, the amount of cholesterol present within the western diet used is significantly lower than the traditional high fat high cholesterol diets generically used to study fatty liver disease. To gauge a clearer understanding on the effect of myeloid-IRF8 reduction on NAFLD specifically, it would be more suitable to challenge mice with a high fat high cholesterol diet, that is more suited to NAFLD-specific studies.

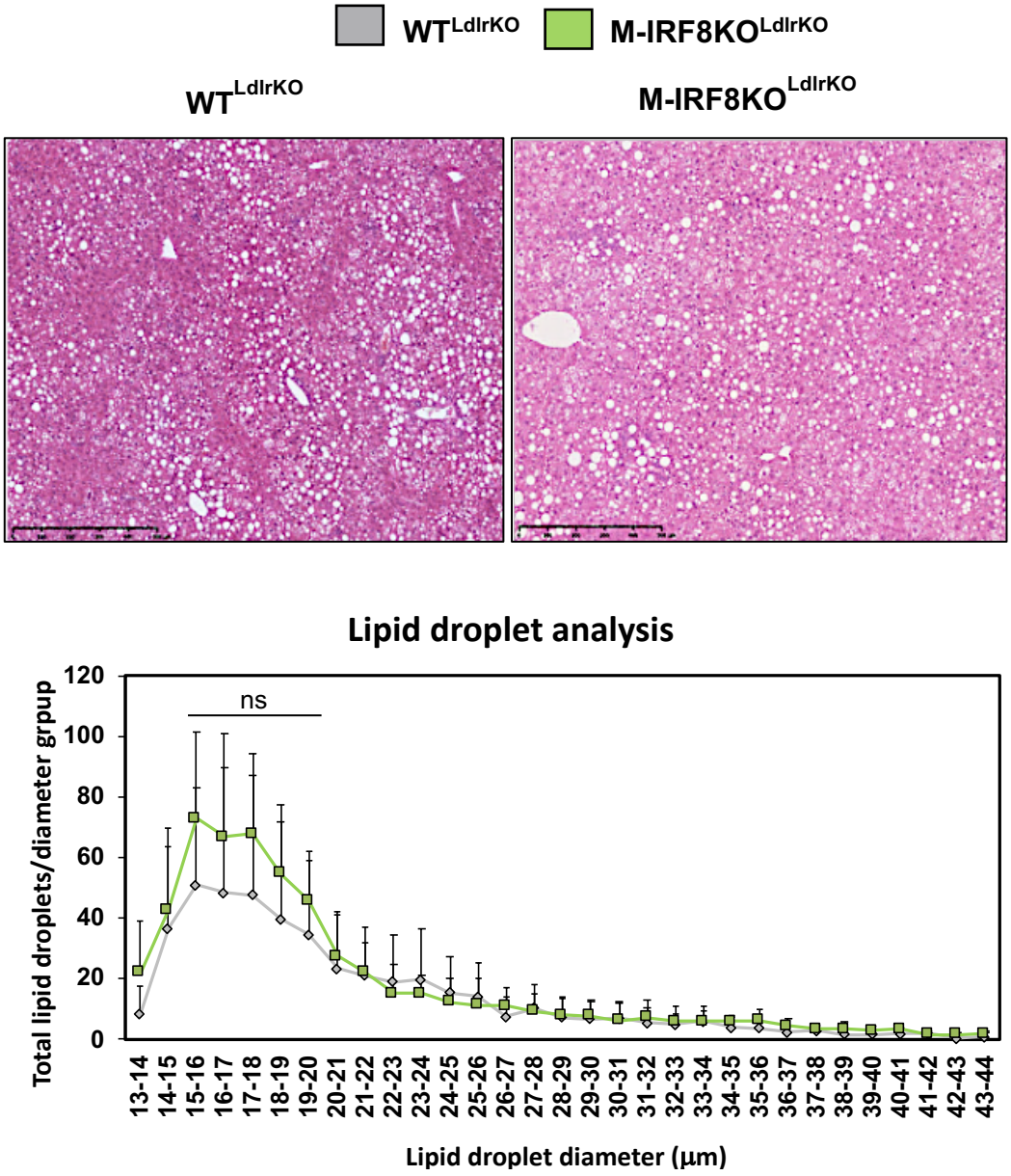

Fig 3.5. M-IRF8KO^{LdlrKO} mice display no difference in hepatic lipid droplet in comparison to WT^{LdlrKO} mice fed a western diet.
(A) Images of H&E stained livers from western diet fed mice. (B) Quantification of lipid droplets in the livers of western diet fed mice, using Eli 2.0 analysis software (n=5/group). Data presented as mean+SEM. No statistical significance was identified upon performing statistical analysis using the ROC – Area under the curve test on GraphPad Prism v8.0.

3.6. Summary

1. When challenged with a high fat western diet, myeloid-IRF8 reduction retards atherosclerotic plaque formation within the aortic root.
2. M-IRF8KO^{LdlrKO} mice develop fewer advanced stage plaques. However, the severity of advanced stage plaques developed, as quantified by necrotic core and fibrous cap area and thickness, in both WT^{LdlrKO} and M-IRF8KO^{LdlrKO} mice does not differ.
3. M-IRF8KO^{LdlrKO} mice have significantly fewer plaque CD68+ cells within their aortic roots alongside fewer aortic macrophages.
4. Myeloid-IRF8 reduction does not impact on hepatic lipid droplet formation, a characteristic of NAFLD, when challenged with a high fat western diet.

3.6.2 Discussions and Limitations

3.6.2.1 IRF8 and myelopoiesis in atherosclerosis

IRF8 has been well characterised for its role in the regulation of the type II interferon immune response against infection and inflammation [272]. Throughout this study we have uncovered a novel protective role of myeloid-IRF8 reduction in protecting against the inflammatory, lipid-mediated development of atherosclerosis (**Fig 3.3.1)**. Upon generating a model that selectively reduces IRF8 from mature myeloid cells, using cre/loxP recombination in lysozyme M expressing cells, we have been able to investigate the myeloid-specific role of IRF8 in atherosclerosis development. Our findings demonstrate, when challenged with a high fat western diet, M-IRF8KO^{LdlrKO} mice develop significantly less atherosclerotic plaque within the aortic root in comparison to WT^{LdlrKO} mice

(**Fig 3.3.1**). In contrast to previous studies by Doring et al., 2012, M-IRF8KO^{LdlrKO} mice do not display a chronic myeloid leukaemia like syndrome, which has previously been reported to promote atherosclerosis due to the expansion of circulating neutrophils and reduction in circulating monocytes, which is not apparent in the M-IRF8KO^{LdlrKO} mice (**Fig 3.4.3**). Due to IRF8 deletion in mature myeloid-cells, differences in neutrophil and monocyte number are not expected. This is due to the role of IRF8 in preventing further neutrophil production, when expressed in granulocyte-monocyte progenitors (GMPs). IRF8 binds and transcriptionally represses the activation of the transcription factor, Cepb/α, that is crucial for neutrophil development. This allows for subsequent activation of the transcription factor KLF4, of which IRF8 forms a heterodimeric complex with and is able to promote further development of myeloid-cells, [129], [174]. Impairment of IRF8 expression in GMPs, has been shown to disrupt myelopoiesis, resulting in an aberrant increase in circulating neutrophils and decrease in monocytes, as demonstrated in human and mouse IRF8-silenced immunodeficiencies [121]. For this reason, differences are not expected and have not been observed in the proportion of circulating monocytes and neutrophils in M-IRF8KO^{LdlrKO} mice.

3.6.2.2 Myeloid-IRF8 and atherosclerotic plaque development

Interestingly, we observed myeloid-IRF8 reduction has no impact on atherosclerotic plaque development within the total or subsections of the descending aorta (**Fig 3.3.1**). Atherosclerosis is known to develop in a site-specific manner, where increased plaque development is often identified in regions with lesser curvature, in particular at aortic branch points [257].

Therefore, differences in plaque development are often observed within the aortic root and arch during the initial months of western diet feeding [273]. However, fluid sheer stress is also known to have a large impact on atherosclerosis site specificity, particularly as laminar blood flow impacts on endothelial cell morphology and subsequent gene expression. Aortic endothelial cells exposed to disturbed blood flow demonstrate an activated, pro-inflammatory phenotype due to an increase in NF-kB signalling resulting in enhanced inflammation (IL-1α, reactive oxygen species) and pro-atherogenic gene expression (ICAM-1, V-CAM1, MCP-1, VEGF). Collectively this has been shown to promote endothelial cell permeability and lipid uptake rendering sites exposed to disturbed blood flow prone to atherosclerotic plaque development. This suggests that differences in sheer stress blood flow may contribute to differences observed in atherosclerotic plaque development in the aortic root, arch and descending thoracic and abdomen (**Fig 3.4.2**).

3.6.2.3 The impact of myeloid-IRF8 reduction on atherosclerotic plaque severity

However, plaque burden alone is often not enough to decipher the risk of potential clinical events. Investigating the severity of atherosclerotic lesions, using tools including histopathological analysis have proven highly beneficial in understanding the type and severity of plaques generated. This can therefore be used in identifying risk of clinical events [274]. To have a clearer understanding on whether myeloid-IRF8 reduction impacted on lesion severity as well as plaque burden, histopathological analysis was performed on the aortic root plaques.

Considering both WT^{LdlrKO} and M-$IRF8KO^{LdlrKO}$ mice develop a similar number of early stage plaques, the number of moderate and advanced stage plaques developed were much fewer in the M-$IRF8KO^{LdlrkO}$ mice (**Fig 3.3.2**).

Previous studies have demonstrated IRF8 regulation of key processes involved in advanced lesion formation, namely efferocytosis and neointima formation via phenotypic switching of smooth muscle cells (SMCs) [175], [275]. Defective efferocytosis is typically associated with enhanced acellular necrotic core formation due to the inability of plaque macrophages to effectively remove apoptotic cells and lipids. This combined with the formation of a fibrous cap surrounding the plaque, due to an increase in fibrotic collagen formation, is known to contribute to advanced plaque formation [276]. Enhanced necrotic cores due to defective efferocytosis has been observed in hematopoetic-$IRF8^{KO}$ mice, as characterised by decreased macrophage expression of scavenger receptor CD36 and removal of apoptotic neutrophils [175]. However, M-$IRF8KO^{LdlrKO}$ mice do not display differences in necrotic core formation (**Fig 3.3.2**). It must be noted, however, that hematopoetic-$IRF8^{KO}$ mice displayed an aberrant increase in apoptotic plaque neutrophils which also contributed to increased plaque size. On the contrary, M-$IRF8KO^{LdlrKO}$ mice do not display a difference in aortic neutrophil content which may contribute to the lack of difference observed in necrotic core formation.

Alongside plaque necrosis, fibrous cap area and thickness largely contribute to plaque severity and stability. Historically, fibrous caps predominately form at the advanced stage plaque, once atheroma has been established. The thickness of

the fibrous cap indicates the probability of plaque rupture, specifically as plaques with thin fibrous caps are more prone to rupture than plaques with large fibrous caps [277]. IRF8 is known to regulate phenotypic switching of smooth muscle cells when over expressed, from a quiescent to synthetic proliferative phenotype and proliferative smooth muscle cells form a large component of the fibrous cap [275], [278]. Previous studies investigating hematopoetic-IRF8 and CD11c-specific IRF8 in atherosclerosis, have shown IRF8 expression to modulate collagen formation and hence fibrous cap area [175], [177]. However, we interestingly observe no difference in the area or diameter of fibrous cap formation within advanced plaques (**Fig 3.3.2**). It is possible the study is not powered enough to detect differences in the the formation of the fibrous cap and necrotic core. To determine the sample size required to gain significance, we performed a sample size and power calculations based on a priori determined outcome, using the GPower online software. Using this software, we generated an effect size of of 0.64, based on the mean and standard deviations of the plaque necrotic core area in WT^{LdlrKO} and M-$IRF8KO^{LdlrKO}$ mice, combined with a power of 0.8, demonstrating a further 31 mice would be required for significance to be achieved. Although a larger sample size is required, the data currently suggests myeloid-IRF8 reduction alone may not be enough to impact on atherosclerotic fibrous cap development. It is possible that expression of IRF8 in other cells including $CD11c^{+}$ plaque cells and smooth muscle cells may be sufficient to maintain for instance collagen formation, involved in fibrous cap formation. Overall, this implies myeloid-IRF8 reduction may delay the onset of atherosclerotic plaque development. However, as studies where performed on mice after only 12 weeks of western diet feeding, it raises the possibility that

plaque formation may be delayed in M-IRF8KO^{LdlrKO} mice. To further explore this, studies could be performed on mice after different periods on western diet.

3.6.2.4 Macrophage composition within the atherosclerotic plaque

Although myeloid-IRF8 reduction does not promote differences in plaque severity, the differences elicited in plaque area and burden may be due to differences in plaque immune cell composition as demonstrated by the significant decrease in CD68+ cell content within the plaques. CD68 is a cell surface marker highly expressed on monocytes, macrophages and to some degree on smooth muscle cells also [279]. Considering the important role of macrophages in atherosclerosis development from the initial onset to advanced lesion formation, plaque macrophage content is also used as an indicator to possible processes that may be influencing plaque progression. Intriguingly, M-IRF8KO^{LdlrKO} mice display a significant reduction in plaque CD68^{+} content in comparison to WT^{LdlrKO} mice and this is further supported by the decrease in aortic macrophages present within M-IRF8KO^{LdlrKO} mice. This highlights a novel role for myeloid-IRF8 reduction in modulating the CD68+ cell content within the plaques. Considering the frequency of circulating monocytes does not change between the genotypes, the differences in aorta and plaque macrophage content may suggest differences in macrophage apoptosis or a functional inability of myeloid-IRF8 macrophages to be able to migrate across the subendothelial membrane and into the growing plaque. Further investigation into chemotaxis-related gene expression and migration of IRF8KO^{LdlrKO} macrophages would help clarify this, as discussed later within the thesis.

3.6.2.5 Myeloid-IRF8 reduction and NAFLD

Atherosclerosis is often associated with many other metabolic disorders due to shared risk factors. NAFLD is one such example of a metabolic disease often associated with patients with coronary artery disease. Interestingly, interferon regulatory factors have also been implicated in NAFLD development, specifically IRF6 and IRF9. Both IRF6 and IRF9 deficiency has been shown to promote liver steatosis via dysregulation of PPAR-alpha and gamma signalling pathways [194], [280]. Although IRF8 has not been implicated in fatty liver disease before, its known positive regulation by PPAR-γ in alveolar macrophages prompted us to further explore its possible role in fatty liver disease when deficient in myeloid-cells in mice fed a high fat western diet [281]. Upon quantifying the diameter of micro-vesicular and macro-vesicular lipid droplets in the livers of M-IRF8KO^{LdlrKO} and WT^{LdlrKO} mice, we interestingly, did not observe any difference in lipid droplet formation. This suggests myeloid-IRF8 reduction is not likely to impact on fatty liver disease when challenged with a high fat western diet. However, it must be noted that the high-fat western diet used in this study, is not designed to promote NAFLD [282]. Therefore, to explore the role of myeloid-IRF8 in NAFLD, specifically, it would be more suited to use a high fat high cholesterol diet, that is designed for NAFLD studies. Collectively, this demonstrates the atherosclerosis phenotype identified in the M-IRF8KO^{LdlrKO} mice is not likely to be associated with NAFLD. In order to investigate the role of myeloid-IRF8 reduction in atherosclerosis and NAFLD, the mice would need to be challenged with a high fat high cholesterol diet.

3.6.2.5 Conclusion

Overall, this chapter has demonstrated that myeloid-IRF8 reduction retards the development of atherosclerosis, when challenged with a high fat western diet. Myeloid-IRF8 reduction also hindered the development of advanced stage plaques alongside reducing plaque macrophage content. Overall, this highlights a novel athero-protective role for myeloid-IRF8 reduction in atherosclerosis development.

Chapter 4: Results - Potential mechanisms underlying the athero-protective role of myeloid-IRF8 reduction

4.1 Part A: Identifying intracellular signalling pathways affected by myeloid IRF8-knock down.

4.1.1 Introduction

IRF8 is a transcriptional regulator of a large network of genes involved in mediating the innate and adaptive inflammatory immune response [94], [283]. The ability of IRF8 to regulate various signalling pathways, largely depends on the transcription factor of which it forms a heterodimeric complex [119]. Structurally, IRF8 consists of an interferon association domain, to which it binds to its partner transcription factor, and a DNA binding domain, to which it binds a unique IRF response element within the regulatory regions of its target gene, as demonstrated in **Fig 1.1**. Upon binding and forming a heterodimeric complex with a partner transcription factor, IRF8 can either activate or repress gene expression, as shown in table 3 [284]. Typically, IRF8 acts as a transcriptional activator when bound to the E26 transformation-specific or E-twenty-six (Ets) transcription factor PU.1, of which it binds a unique Ets-interferon consensus elements (EICE). IRF8 also functions as a transcriptional activator when bound to an activating protein-1 family member (AP-1), such as BAFT3, to which it binds a unique AICE response element. However, when in a heterodimeric complex with either IRF1 or IRF2, IRF8 becomes a transcriptional repressor and specifically represses genes upon binding an interferon stimulated response element (ISRE).

Co-transcription factor	Motif name	Function	Sequence
PU.1	EICE	Activation	GGAAnnGAAA
AP-1	AICE	Activation	TGAnnnGAAA
IRF1/ IRF2	ISRE	Repression	GAAAnnGAAA

Table 4. The co-transcription factors that form a heterodimeric complex when bound to IRF8 and their regulation of gene expression.

Through these modes of action, IRF8 regulates a wide range of processes, that when dysregulated, result in increased susceptibility to infection and an impaired inflammatory response [153], [285].

My findings in Chapter 3 demonstrate myeloid-IRF8 reduction retards atherosclerotic plaque development in mice challenged with a western diet. The **aim** of this chapter is to determine potential mechanisms by which myeloid-IRF8 reduction confers this athero-protection. Considering the role of IRF8 as a transcriptional activator and repressor, the focus of this chapter is to elucidate how the differences in transcriptional regulation elicited by myeloid-IRF8 may functionally impact on atherosclerosis development. To investigate this, I analysed genome wide transcriptomic differences in bone marrow-derived macrophages from western diet-fed WT^{LdlrKO} and M-$IRF8KO^{LdlrKO}$ mice by RNA-Sequencing (RNA-Seq).

4.1.2 Myeloid-IRF8 reduction reprograms macrophage gene expression

The bone marrow from n=3 western diet-fed WT^{LdlrKO} and M-$IRF8KO^{LdlrKO}$ mice were isolated and differentiated into macrophages *in vitro.* RNA was subsequently isolated from the untreated macrophages and used for RNA-Sequencing. RNA-Seq analysis, using the online platform Metascape, demonstrate significant transcriptional differences between the WT^{LdlrKO} and M-$IRF8KO^{LdlrKO}$ mice (**Fig 4.1.2**). Overall, we discovered 366 genes that were more than or equal to 1.3-fold differentially regulated in M-$IRF8KO^{LdlrKO}$ mice, when compared to controls. We identified 167 upregulated genes (orange) and 199 downregulated (blue) genes in the IRF8-KO macrophages as demonstrated in the volcano plot (**Fig 4.1.2 A**), with the grey dots displaying the proportion of genes that did not meet the applied cut offs. Additionally, the heatmap displays the differential regulation of genes within each triplicate sample that was sequenced from the macrophages of WT^{LdlrKO} and M-$IRF8KO^{LdlrKO}$ mice (**Fig 4.1.2 B**).

To identify the biological pathways associated with the differentially regulated genes, gene set enrichment analysis was performed using the online web-based tool, Metascape (described in 2.8.3). Metascape is a platform that provides combined gene annotation, functional enrichment and interactome analysis by comparing an input gene list against 40 independent knowledgebases, including KEGG, Reactome, Gene Ontology and MSigDB [242]. Each knowledgebase contains curated genes under specific gene modalities (as described in Methods section 2.8.3). Identification of pathways selectively enriched in the uploaded differentially expressed gene list can help

elucidate critical molecular functions and processes that may contribute to the protective phenotype that myeloid-IRF8 reduction confers against atherosclerosis.

This analysis identified 'Cancer' ($Log_{10}P = -7$) and 'Response to growth factor stimulus' as the most significantly upregulated pathways, implying IRF8 regulates genes involved in cell growth. However, many genes within these pathways; including *Bcl2, Bmp2, Fos, Ednrb, Sort1, Vegfa, Nr4a1*, are also associated with 'Positive regulation of cell death', 'Cell adhesion' and 'Cell chemotaxis'. This demonstrates that these genes also contribute to other atherosclerosis-related pathways [286]–[290] that may contribute to the athero-protective phenotype exerted by myeloid-IRF8 reduction. We also identified 'Fatty acid transmembrane transport' as the most enriched upregulated pathway (Enrichment Ratio = 48). The enrichment score is a measure of the number of IRF8-target genes identified divided by the number of genes annotated to this pathway [291] (**Fig 4.1.2 C**). Alongside this, 'Inflammatory response' and 'Leukocyte migration' were the most significantly ($Log_{10}P = -12$) downregulated pathways with 'Lipid metabolism' being the most enriched downregulated pathway (Enrichment ratio = 29) (**Fig 4.1.2 D**).

To effectively visualise the degree of association between each pathway, a clustergraph was produced for each set of upregulated and downregulated pathways. An additional benefit of generating clustergraphs is the ability to visually cluster pathways hierarchically based on their similarity in function. Hierarchically clustering each functional term into a tree, based on Kappa-

statistical similarities among their gene memberships, prevents repetition of associated pathways generated from different knowledgebases. The subset of similar representative terms within each cluster form the subtrees. More specifically, each term is represented by a circle node, where its size is proportional to the number of input genes that fall into that term, and its colour represents its cluster identity, as indicated on the bar chart (**Fig 4.1.2 C & E**).

The clustergraphs demonstrate the degree of overlap between the genes in enriched pathways, as shown by the interconnecting purple lines. Interestingly, the most significant downregulated pathway 'Inflammation' has more interconnecting purple lines, and hence greater gene overlap, with other downregulated pathways (**Fig 4.1.2 F**). This indicates, many downregulated 'Inflammatory' genes are also present in other pathways, in comparison to the 'Response to growth factor' related genes. Collectively, this implies there is a greater functional overlap between genes that are downregulated in response to IRF8-reduction than genes that are upregulated in response to IRF8-reduction. In addition, the genes present in the most enriched upregulated (Lipid transport) and downregulated (Lipid metabolism) pathways share minimal overlap with other pathways. This indicates the IRF8 regulated genes within these pathways are only, reportedly, specifically involved in this process when compared to all other IRF8-regulated genes. The high enrichment ratio of 48 for upregulated genes involved in 'Lipid transport', is due to 50% of the genes annotated to this pathway also being regulated by IRF8. The enrichment ratio of 29 for downregulated genes reported in 'Lipid metabolism', is due to 75% of genes annotated to this pathway being regulated by IRF8, as displayed in **Fig 4.1.1**.

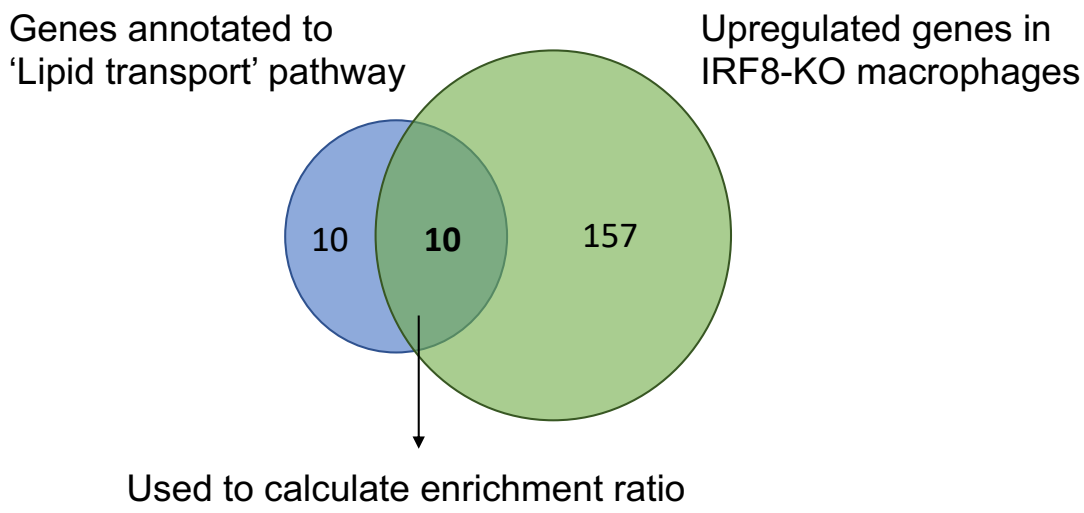

Fig 4.1.1 Derivation of enrichment score.

This demonstrates IRF8 regulates a niche subset of genes specifically involved in lipid homeostasis. However, whether the differential regulation of these genes by IRF8 has direct functional implications on atherosclerosis development remains to be further explored.

Collectively, these results demonstrate IRF8 acts as both a transcriptional activator and repressor in macrophages from western diet fed M-IRF8KO^{LdlrKO} mice, as shown by the 199 downregulated and 167 upregulated genes. Although a similar number of up and downregulated genes were uncovered, the pathways associated with the downregulated genes were more significantly enriched (highest downregulated pathway Log10P = -12) when compared to the upregulated ones (highest upregulated pathway Log10P = -7). This may be due to the larger number of downregulated genes sharing similar functions and being associated to a specific pathway in comparison to the upregulated ones. This information allows us to investigate the mechanism by which IRF8 regulates the

identified significantly enriched pathways and explore their potential contribution to atherosclerosis development.

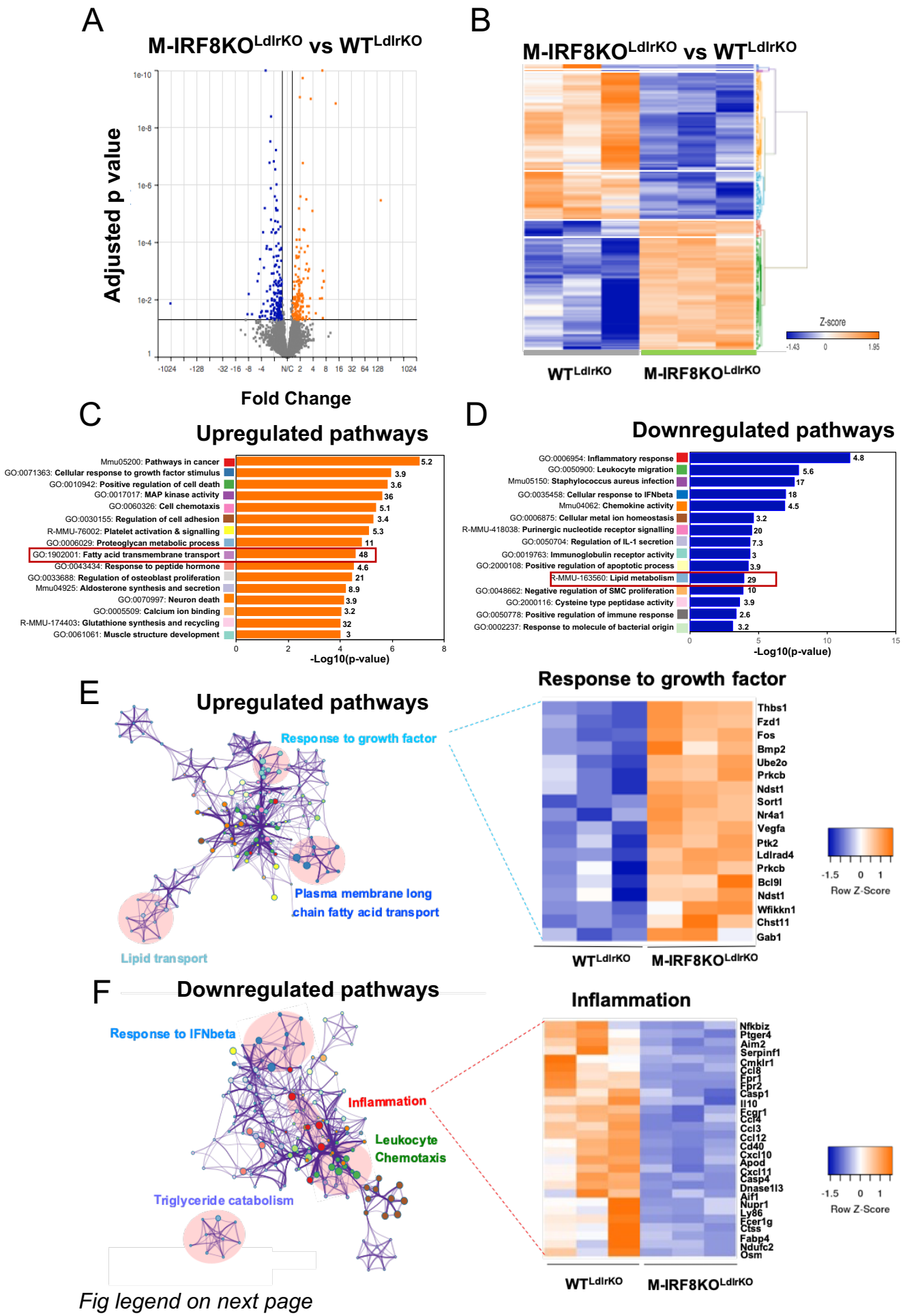

Fig legend on next page

Fig 4.1.2 Myeloid-IRF8 deficiency reprograms macrophage gene expression.
(A) Volcano plot of fold change vs. P value of differentially expressed genes comparing 12-wk-old, WD-fed M-IRF8KO^{LdlrKO} and WT^{LdlrKO} bone marrow-derived macrophages (n = 3/group). The grey line indicates an adjusted P value threshold of 0.05 (Wald test for logistic regression). (B) Clustered heat map of RNA-seq normalised gene counts in WD-fed macrophages (n = 3 mice/group). Gene set meta-analysis demonstrating most significant (C) upregulated and (D) downregulated pathways of genes differentially regulated by myeloid-IRF8 deficiency with their corresponding enrichment score indicated. The red box indicates the largest enrichment score. Pathway enrichment network visualisation showing the intra-cluster and inter-cluster similarities of enriched terms for (E) upregulated and (F) downregulated pathways. Novel atherosclerosis specific IRF8 regulated pathways, when compared to WT^{LdlrKO}, are highlighted in light pink, where the degree of regulation in the most significant differentially regulated pathway is further highlighted in the corresponding heatmap, showing normalized gene counts. Remaining cluster annotations are shown in colour code on the (C) upregulated and (D) downregulated pathway analysis bar chart. Pathway analysis and enrichment visualisation was performed using Metascape. Data presented are Linear fold change 1.3, FDR 0.05, $p<0.01$.

4.1.3 Myeloid-IRF8 positively regulates inflammatory gene expression

The 'Inflammatory response' pathway was the most significant IRF8-downregulated pathway ($Log_{10}P$ = -12) identified amongst the differentially expressed genes in IRF8-KO macrophages. This pathway encompasses 40 genes, where the top 4 differentially regulated genes include the pro-inflammatory chemokines (*Cxcl11* FC -7.3*, Cxcl10* FC -3*, Ccl8* FC -4.6*, Ccl12* FC-3.5) all known to contribute to atherosclerosis development when their expression is induced [292]–[294] (**Fig 4.1.3 A**).

The hyperlipidaemic, atherosclerosis-prone environment, caused by the deficiency of the LDL-receptor in M-IRF8KO^{LdlrKO} mice, combined with the fat-rich diet, contributes to the altered regulation of pro-inflammatory genes and signalling pathways. As IRF8 is known to be crucial for macrophage response to infection and inflammation, we next interrogated whether the hyperlipidaemic environment of M-IRF8KO^{LdlrKO} mice impacts on the regulation of IRF8-target genes. To do this, we compared IRF8-target genes identified in western diet-fed M-IRF8KO^{LdlrKO} mice to IRF8-target genes identified in an independent study in

normolipidemic mice [86], [94]. The Bxh2 mouse model harbours a single point mutation within the interferon association domain of IRF8, effectively silencing IRF8 expression, mimicking the global-IRF8KO mouse model [86], [94]. Differences in transcriptional regulation elicited by IRF8 deficiency was explored in the macrophages from Bxh2 mice by Langlais et al., 2016 and Mancino et al., 2015. To identify for differences in the regulation of 'Inflammatory' genes identified in macrophages from M-IRF8KO^{LdlrKO} mice and Bxh2 mice, comparisons of genes, with a linear fold change cut of off ≥ 1.3, were performed using Metascape.

Interestingly, we identified a 50% overlap of inflammatory genes regulated by IRF8 in western diet challenged, hyperlipidaemic M-IRF8KO^{LdlrKO} mice when compared to normolipidemic Bxh2 mice (**Fig 4.1.3 B**). This 50% overlap encompasses a limited number of 21 genes and demonstrates a select number of 'inflammatory' genes that are regulated by IRF8 in both a hyperlipidaemic and normolipidemic environment.

With advances in next generation sequencing, recent studies have investigated the transcriptional profile of macrophages from the aorta of western diet fed LDLR^{KO} mice [78]. Plaque macrophages arise from both circulating monocytes and the proliferation of local aortic macrophages [57]. However, the majority of proliferating aortic macrophages originate from circulating monocytes [22]. The hyperlipidaemic environment of western diet-fed mice promotes monocytosis in the bone marrow, leading to increased circulating bone marrow-derived monocytes that ultimately contributes to the aortic plaque macrophage

content [21], [295]. Therefore, we aimed to determine how the regulation of the 366 IRF8 target genes identified in hyperlipidaemic M-IRF8KO^{LdlrKO} mice, compare to aortic macrophages from atherosclerosis prone LDLR^{KO} mice from an independent study by Cochain and colleagues [78]. To investigate this, comparisons were performed between the aortic macrophage subsets identified by Cochain et al., 2018 that are enriched in pro-inflammatory markers (TNF-α, IL-6, IL-1β); trem2hi and inflammatory [78], and the myeloid-IRF8 target genes identified in our study. The inflammatory macrophage subset is enriched in classic pro-inflammatory genes, including; *Il-1β, TNFα, IL-6, Nf-κb*, whereas the trem2hi macrophage subset display enriched expression of genes involved in lipid metabolism, oxidation and calcification, including *Cxcl16, Lpl, Lgmn, Fabp5, Fcer1g* [78]. Interestingly, 174 out of a total 582 genes that were enriched in inflammatory aortic macrophages overlapped with genes enriched in trem2hi aortic macrophages, with IRF8 being one of them. This demonstrates IRF8 is differentially regulated in the macrophages from atherosclerosis-prone mice and warrants further investigation of IRF8-target genes within the inflammatory and trem2hi aortic macrophage subsets (**Fig 4.1.3 C**). Upon performing comparative analysis with Metascape, we identified 14 IRF8 target genes from M-IRF8KO^{LdlrKO} macrophages are enriched in lipid-associated trem2hi aortic macrophages and 26 IRF8 target genes macrophages are enriched in inflammatory aortic macrophages (**Fig 4.1.3 C**). Although these are a limited number of genes, a large degree of functional overlap between the IRF8 target genes that were not differentially regulated within inflammatory and trem2hi aortic macrophages was revealed. This is demonstrated by the light blue overlapping lines on the circos plot (**Fig 4.1.3 C**). Collectively these results show a greater proportion of IRF8-

target genes share functional similarities to both inflammatory and trem2hi aortic macrophages.

To determine the regulation of the overlapping 24 IRF8-target genes with inflammatory and trem2hi aortic macrophages, a heatmap of the fold changes from each gene list was generated (**Fig 4.1.3 D**). Interestingly, a striking majority of genes in IRF8-KO macrophages showed reduced expression in comparison to aortic and trem2hi macrophages. This uncovers the anti-inflammatory properties of IRF8-KO macrophages and implies IRF8 may contribute to the regulation of differentially expressed pro-inflammatory genes enriched in the aortic inflammatory and trem2hi macrophages of $LDLR^{KO}$ mice [78]. Overall, this identifies a role for myeloid-IRF8 in regulating a select subset of pro-inflammatory genes, that are enriched in an atherosclerosis-prone environment.

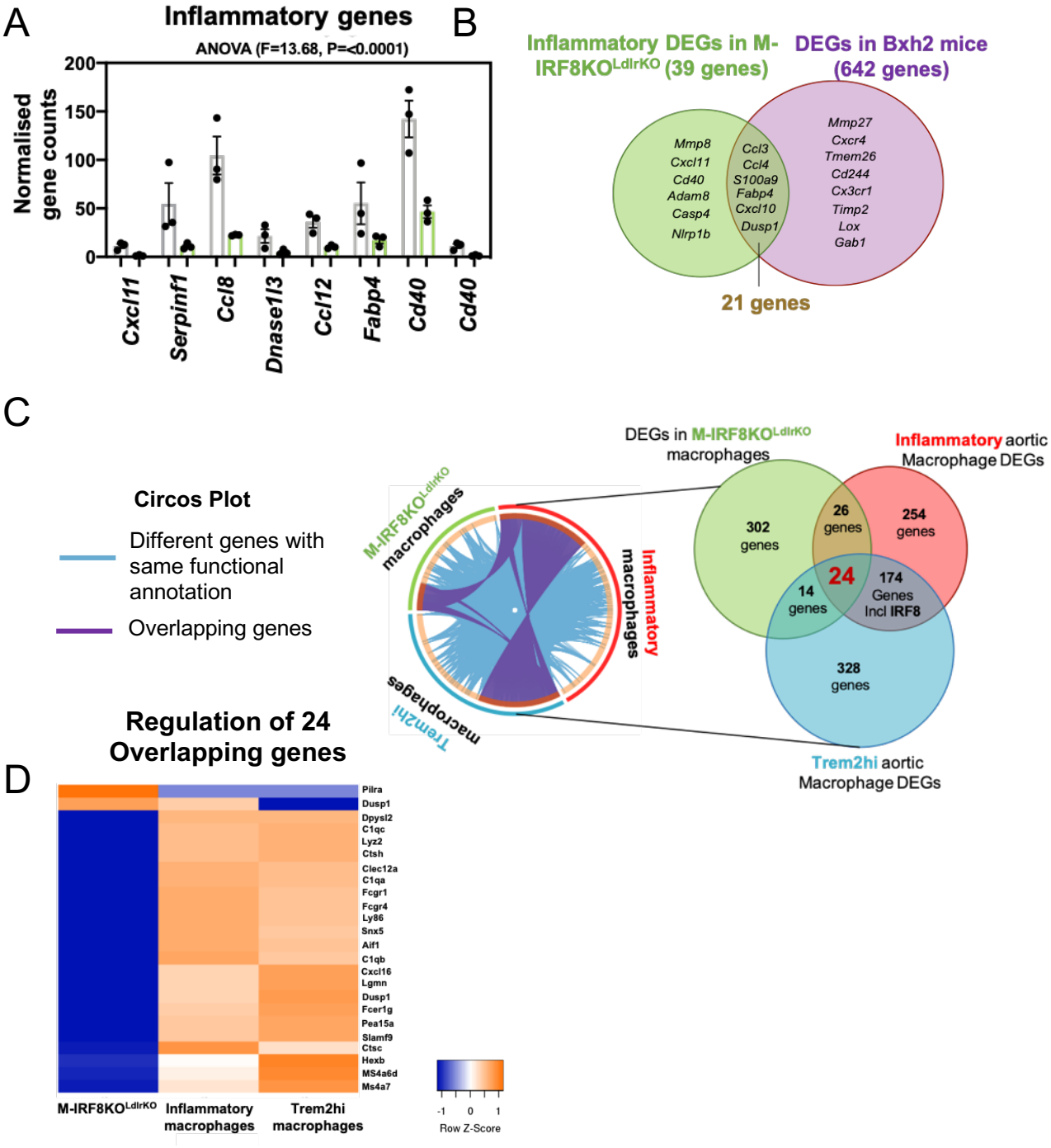

Fig 4.1.3 Macrophage-IRF8 positively regulates inflammatory gene expression.
(A) RNA-seq normalised gene counts of the topmost significantly downregulated pro-inflammatory genes in Western Diet-fed M-IRF8KO^{LdlrKO} and WT^{LdlrKO} macrophages (n=3/group, grey = WT^{LdlrKO}, green = M-IRF8KO^{LdlrKO}). (B) Venn diagram comparing the differentially regulated genes identified in basal IRF8-KO macrophages (green) and IRF8 target genes from normolipidemic IRF8-silenced Bxh2 mice (Langlais et al, 2016) (purple). The most significantly regulated genes (fold change) are highlighted in each Venn section. (C) Circos plot highlighting the overlap of differentially regulated genes (purple lines) identified in untreated IRF8-KO , inflammatory aortic and trem2hi aortic macrophages (as described in Cochain et al., 2018). The blue lines link the different genes that share the same gene ontology, whereas the purple lines link overlapping genes. The attached Venn (*right*) further highlights the number of differentially regulated genes that overlap between the (C) three input gene lists. (D) Heatmap of fold changes of the 24 genes present in the three gene lists. Fold changes shown (Linear, 1.3+ for all gene lists). Data presented are Linear fold change 1.3, FDR 0.05, p<0.01.

4.1.4 Myeloid-IRF8 promotes macrophage migration via regulation of chemotaxis-related genes

Aberrant chemotaxis of leukocytes is one of the hallmarks of atherosclerotic plaque initiation [48]. Amongst the top regulated pathways, 'Leukocyte chemotaxis' was the second most significantly reduced ($Log_{10}P$ =-8) in BMDMs from M-IRF8KO^{LdlrKO} mice. Due to the pivotal role of chemotaxis in atherosclerotic plaque progression, we further explored the regulation of IRF8-target genes involved in this pathway. A total of 26 pro-chemotactic genes implicated in atherosclerotic plaque progression were down regulated in M-IRF8KO^{LdlrKO} macrophages. The most strongly regulated genes (*Ccl3* FC -1.6 fold*, Ccl4* FC -2.3 fold*, Ccl8* FC -4.6 fold*, Ccl12* FC -3.5 fold*, Cxcl10* FC -3 fold*, Cxcl16* -1.6 fold) were validated in a separate independent set of animals (**Fig 4.1.4 A & B**). This demonstrates myeloid-IRF8 positively regulates pro-chemotactic gene expression. However, among the most significantly regulated pro-chemotactic genes, we uncovered a subset of G-protein coupled receptors that have not been previously associated with macrophage migration in atherosclerosis (*P2ry12, P2ry13, P2ry14*). To determine the regulation of these purinergic receptors by IRF8, we performed chromatin immunoprecipitation, to detect IRF8 occupancy of these genes. As shown (**Fig 4.1.4 C & D**), we observed increased IRF8 occupancy at an IRF-site proximal to the promoter and enhancer region of P2ry12 and P2ry13, when compared to the IgG control. These regions of IRF8 binding, originally identified as IRF8 binding sites by Natoli and colleagues, using chromatin immunoprecipitation sequencing [86], also demonstrated increased acetylation of H3K27 which is representative of open

chromatin often identified in promoter and enhancer regions of active transcription (**Fig 4.1.4 C & D**) [296].

Having shown the regulation and occupancy of pro-chemotactic *P2ry13* and *P2ry14* by IRF8, we next questioned the functional impact this may have on macrophage migration. Enhanced myeloid-cell chemotaxis contributes to atherosclerotic plaque initiation [297]. Upon investigating whether the differential regulation of pro-chemotactic genes by IRF8 influences migratory ability of BMDMs from M-IRF8KO^{LdlrKO} mice, would guide us towards the potential mechanism by which myeloid-IRF8 deficiency retards atherosclerotic plaque development.

The pro-atherosclerotic macrophage chemotactic protein, MCP-1, plays a crucial role in the recruitment of myeloid cells to the atherosclerotic plaque [298]. The hyperlipidaemic environment, caused by the western diet, promotes MCP-1 expression, resulting in enhanced monocyte recruitment [51]. For this reason, we used MCP-1 as a chemoattractant to monitor changes in macrophage migration. Interestingly, we observed a significant decrease in the number of IRF8-KO macrophages, migrating towards MCP-1, in comparison to WT macrophages, under basal conditions over 20 hours (**Fig 4.1.4 E**). This demonstrates a novel functional role of myeloid-IRF8 deficiency impairing the migratory capacity of macrophages.

To determine whether myeloid-IRF8 deficiency impacted on the migration of macrophage foam cells towards MCP-1, BMDMs from M-IRF8KO^{LdlrKO} and WT^{LdlrKO} mice were also exposed to native or acetylated LDL for 24 hours, thus

inducing foam cell formation. Interestingly, in this experimental setting addition of acLDL had no impact on the number of migrating macrophages, as demonstrated by the similar number of WT-Basal and WT-acLDL macrophages migrating towards MCP-1 **(Fig 4.1.4 E**). Similarly to basal macrophages, myeloid-IRF8 reduction also impaired the migration of macrophage foam cells by ~50% (**Fig 4.1.4 E & F**). This suggests that, myeloid-IRF8 reduction impairs the migration of macrophages irrespective of foam cell formation, *in vitro*.

Overall, these results uncover a role for myeloid-IRF8 reduction in negatively regulating chemotactic gene expression that may contribute to the impaired macrophage migration under basal conditions and in response to native and acetylated LDL. Therefore, these results imply myeloid-IRF8 reduction may lead to the reduced recruitment of myeloid-cells to the atherosclerotic plaque, resulting in reduced plaque CD68+ cellular content (**Fig 3.3.3 B**) thereby contributing to the observed reduced atherosclerosis development (**Fig 3.3.1**).

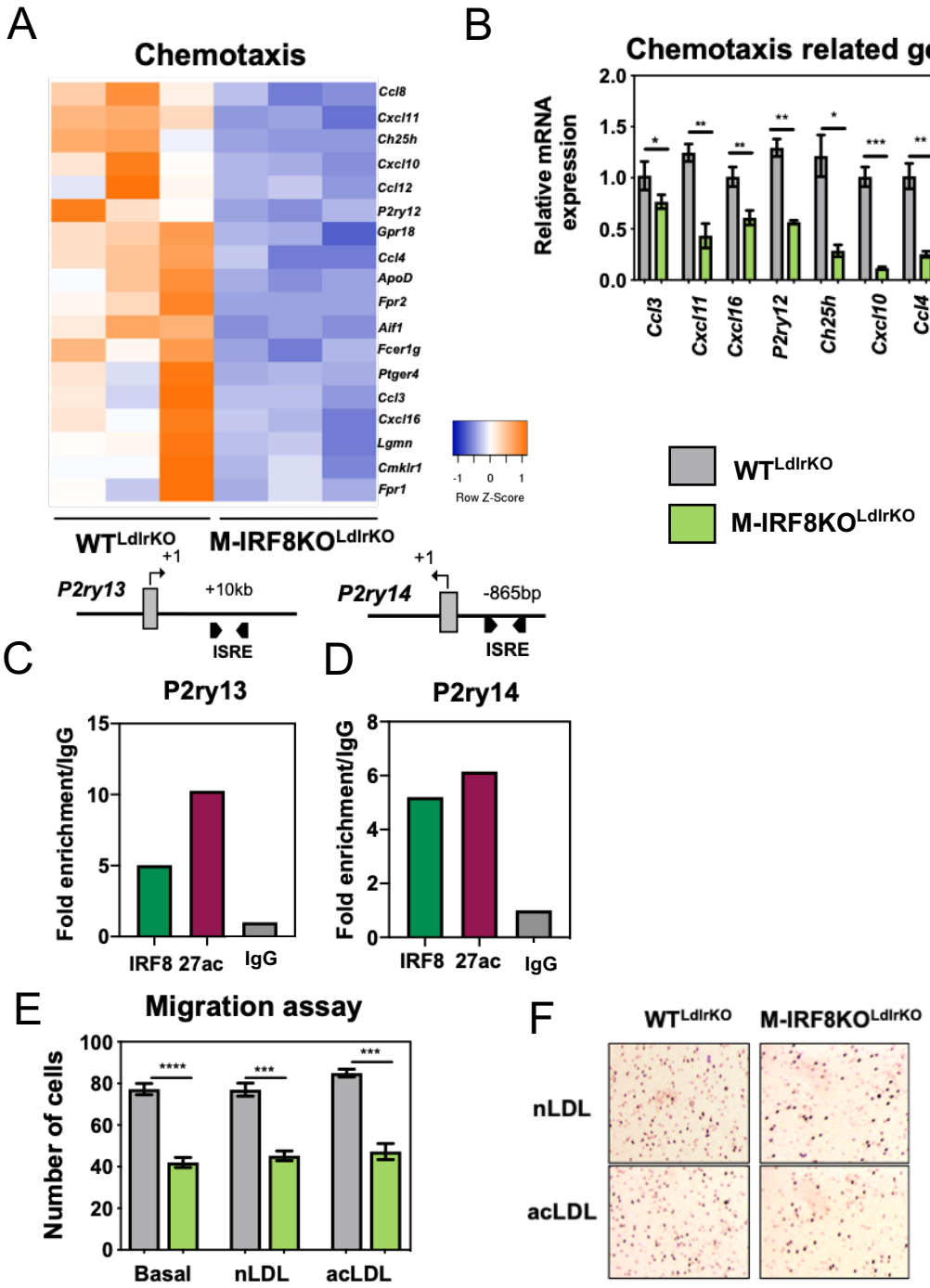

Fig 4.1.4 Myeloid IRF8 positively regulates chemotaxis-related gene expression and macrophage migration.

(A) Clustered heatmap of RNA-seq chemotaxis related normalised gene counts in macrophages from Western diet-fed mice (n = 3/group). (B) Relative gene expression of chemotaxis-related genes validated in an independent experiment, Western diet-fed macrophages (n=3/group). IRF8 occupancy and H3K27 acetylation (H3K27Ac) at the P2ry13 (C) and P2ry14 (D) identified IRF8 binding sites [86] at chromatin from BMDMs from WT^{LdlrKO} Western diet-fed mice are shown. Data are normalized to input compared with IgG as a negative control. One representative experiment of two (each using n = 2/genotype) is shown. (E) Macrophage migration assay demonstrating number of Western diet-fed $M\text{-}IRF8KO^{LdlrKO}$ and WT^{LdlrKO} macrophages migrating over 8μm membrane towards 100ng MCP-1 over 20hrs, at basal (untreated) and challenged with nLDL and acLDL (n=3/group, grey = WT^{LdlrKO}, green = $M\text{-}IRF8KO^{LdlrKO}$). (F) Representative images of PFA-fixed, violet stained macrophages post migration (40x optical zoom). Statistical significance calculated using unpaired Student's t-test *p>0.05, **p>0.01, ***p>0.001, ****p>0.0001, relative to $WT^{Ldlr\text{-}KO}$ mice.

4.1.5 Myeloid-IRF8 regulates macrophage foam cell formation via regulation of lipid-biosynthesis genes.

Overrepresented functional pathways, obtained from differentially regulated gene lists, are often categorized according to their level of significance. Therefore, categorizing pathways according to their enrichment score provides an alternative effective method to elucidate critical pathways that may contribute to the phenotype observed, in this case atherosclerosis. Upon ranking pathways according to their level of enrichment, 'Fatty acid transmembrane transport' was the most enriched upregulated pathway, with the highest enrichment score of 48, (**Fig 4.1.2 C**). 'Lipid metabolism' was the most enriched downregulated pathway, with an enrichment score of 29 (**Fig 4.1.2 D**). Due to the importance of dysregulated lipid metabolism within the pathogenesis of atherosclerosis [29], [299], IRF8 regulation of genes identified within these pathways was also confirmed. Investigating the differential regulation of these pathways may uncover functional differences in lipid-mediated processes important in atherosclerosis progression, such as foam cell and cholesterol ester formation, that could contribute to the athero-protective phenotype observed in myeloid-IRF8 reduced mice.

Genes involved in reverse cholesterol transport (*P2ry12, P2ry14*) [300], [301] cholesterol metabolism (*Ch25h, Cyp4f18*) [302], [303] and lipid transport (*Fabp4, Fabp5, Scd1*) [304]–[306] are downregulated in IRF8-knock down mice (**Fig 4.1.5 A**). Their regulation by IRF8 was confirmed in a separate independent experiment (**Fig 4.1.5 B**). The fatty acid binding proteins Fabp4 (FC -3.2) and Fabp5 (FC -2.5) are known to promote macrophage foam cell formation and

cholesterol ester content, contributing to atherosclerotic plaque formation [307], [308]. They have the largest fold decrease within the 'Lipid transport' pathway and have not been previously associated with IRF8 in an atherosclerosis context. For this reason, we additionally confirmed their regulation by IRF8, upon performing chromatin immunoprecipitation on the WT^{LdlrKO} macrophages, to identify for IRF8 occupancy. Our collaborator (Dr Antonio Castrillo) kindly provided us with the sequence of the ChIP-Seq peak for Fabp4, Fabp5, P2ry13 and P2ry13 (taken from Langlais et al., 2016 datasets) that was used to detect IRF8 binding. Using ChIP-qPCR, we identified 32% increased IRF8 binding, when compared to the IgG control, proximal to the sequence of the peaks provided for Fabp4 and 45% increased IRF8 occupancy at Fabp5 (**Fig 4.1.5 C & D**). The amplified sequences – 84bp in length, where also regions associated with increased H3K27 acetylation, a marker of chromatin accessibility.

This work demonstrates IRF8-reduction promotes macrophage foam cell formation (**Fig 4.1.5 F & G**), whilst inhibiting macrophage migration, towards the pro-atherogenic chemoattractant MCP-1, when compared to WT^{LdlrKO} (**Fig 4.1.4 E**) Considering IRF8-KO macrophages show the same concentration of cellular free cholesterol after treatment with acLDL (**Fig 4.1.5 E**), they become significantly foamier than WT^{LdlrKO} macrophages. This is consistent with reports showing that foamy aortic macrophages are in fact less inflammatory [79] which we also show for IRF8-KO macrophages when compared to aortic plaque macrophages (**Fig 4.1.3**),

Altogether we have identified IRF8-regulation of genes involved in lipid metabolic processes, that may contribute to the enhanced foam cell formation identified in IRF8-KO macrophages. Since these findings have not been previously associated with IRF8 in macrophages from a hyperlipidaemic environment, it would be informative to additionally measure foam cell formation within the aortic root, via oil-red-o staining of plaques [309] to determine if the foaminess of plaque macrophages differs with IRF8 reduction.

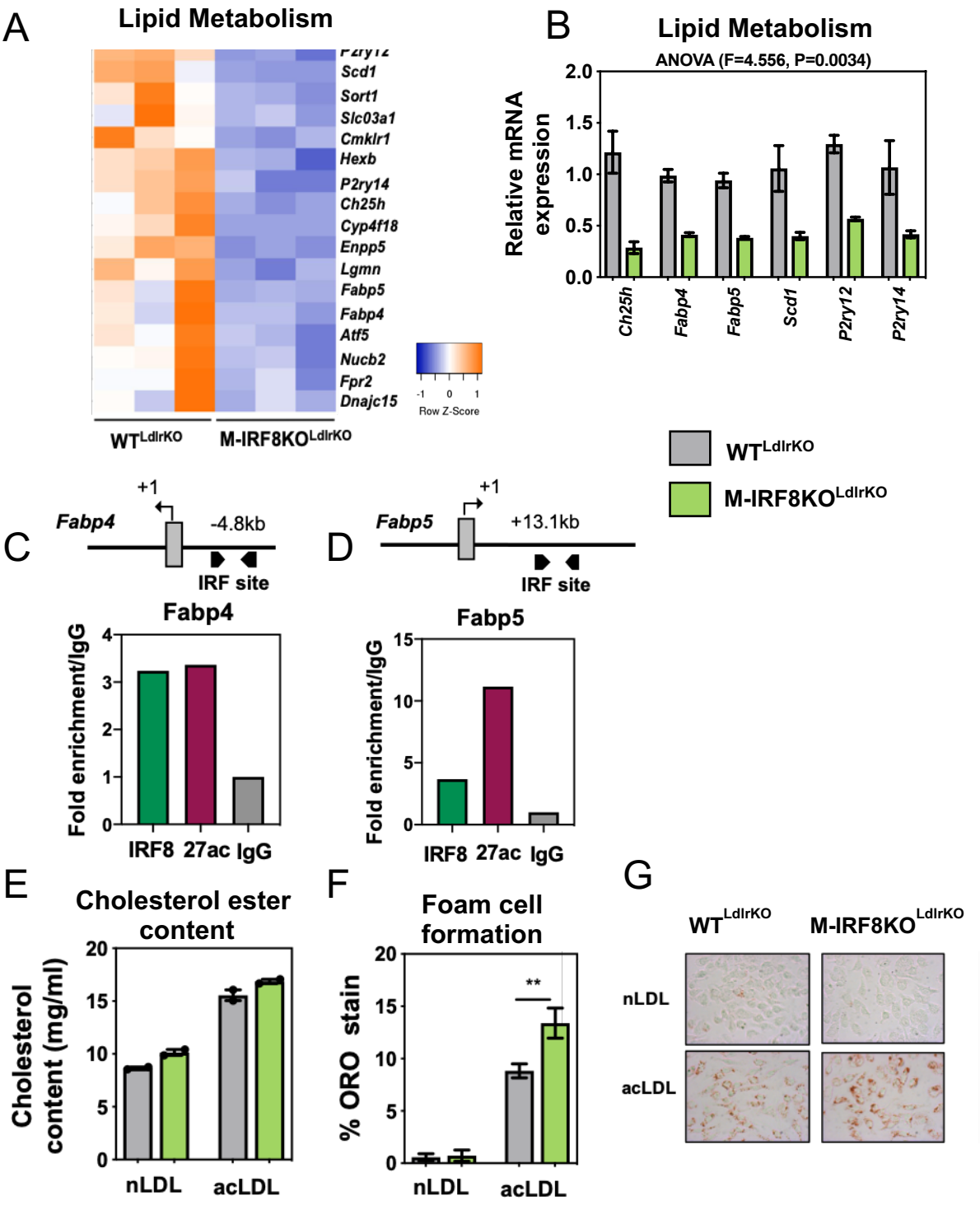

Fig 4.1.5 Macrophage-IRF8 regulates macrophage cholesterol content and foam cell formation via its association with lipid metabolism related genes.
(A) Clustered heatmap of RNA-seq normalised gene counts, for lipid metabolic processes, Western diet-fed macrophages (n = 3/group). (B) Relative gene expression of lipid metabolism related genes validated in an independent experiment, Western diet-fed macrophages (n=3/group). IRF8 occupancy and H3K27 acetylation (HK27Ac) at the Fabp4 (C) and Fabp5 (D) identified IRF8 binding sites in BMDMs from WT^{LdlrKO} Western diet-fed mice are shown. Data shown are normalized to input compared with IgG as a negative control. One representative experiment of two (each using n=2/genotype) is shown. (E) Cholesterol ester content of Western diet-fed macrophages post 24hr culture with 50ng nLDL or acLDL. (F) Macrophage foam cell formation after 24hr culture with 50ng nLDL, and acLDL. (G) Quantification of oil-red-o stain performed using Image J, images taken at 40x optical zoom. Data representative of n=3/group, statistical analysis conducted using one-way ANOVA or unpaired students t-test, *p<0.05, **p<0.01, ***p<0.0001, ****p<0.00001, relative to $WT^{Ldlr-KO}$ mice.

4.1.6 Impaired macrophage foam cell, cholesterol ester content and macrophage migration by Fabp4 and Fabp5 inhibition is dependent on IRF8.

Pharmacological and genetic inhibition of Fabp4 and Fabp5 has been shown to prevent macrophage foam cell formation by limiting the transfer of lipids into macrophages [310], [311]. Selective inhibition of both Fabp4 and Fabp5 using the competitive inhibitor BMS309403, in western diet-fed mice, has been shown to abrogate foam cell formation *in vivo* and *in vitro* as well as reduce cellular cholesterol content via enhanced reverse cholesterol transport [307], [311]. Having shown both *Fabp4* and *Fabp5* gene expression is regulated by IRF8, we aimed to investigate their role in the IRF8-mediated athero-protection in M-IRF8KO^{LdlrKO} mice.

Of the genes previously shown [307], [312] to be affected by Fabp4 and Fabp5 inhibition, we observed a significant increase in the expression of ATP binding cassette cholesterol transporter *Abca1* [310] in response to 10μM of the competitive Fabp4/5 inhibitor, BMS309403, when cells were cultured with acLDL to mimic foam cell formation. Interestingly, this significant upregulation of *Abca1* was only apparent in WT^{LdlrKO} but not IRF8-KO macrophages, proposing the increased expression of *Abca1* in response to Fabp4 and Fabp5 inhibition is dependent on IRF8 expression (**Fig 4.1.6 A**).

To investigate whether known functional atherosclerosis-related pathways impacted by Fabp4 and Fabp5 inhibition were also dependant on IRF8 expression, we next assessed the cholesterol and neutral lipid content of

macrophages subject to acLDL treatment and the Fabp4/5 BMS309403 inhibitor. As expected based on previous reports [307], we observed a significant reduction in cholesterol content with increasing, optimised, concentrations of the BMS309403 inhibitor at 10μM and 25μM in the WT^{LdlrKO} but not in the IRF8-KO^{LdlrKO} macrophages (**Fig 4.1.6 B**). This implies macrophage cholesterol ester levels are regulated by IRF8 induced Fabp4 and Fabp5 expression. This intriguing discovery prompted additional investigation into the impact of IRF8 mediated regulation of Fabp4 and Fabp5 on foam cell formation. Here, we identified a significant reduction in foam cell formation using 25μM BMS309403 inhibitor in the WT^{LdlrKO} but not IRF8-KO^{LdlrKO} macrophages (**Fig 4.1.6 C & D**). This demonstrates Fabp4 and Fabp5 inhibition prevents macrophage cholesterol ester content accumulation and foam cell formation in the presence of IRF8. However, as both Fabp4 and Fabp5 is regulated by IRF8, their expression is subsequently reduced in IRF8-KO macrophages (**Fig 4.1.5 B**) and the inhibitor is unable to prevent the Fabp4 and Fabp5 mediated effect on macrophage cholesterol ester content and foam cell formation (**Fig 4.1.6 B & C**). This may be due to the remaining genes differentially regulated by IRF8- reduction, known to promote cholesterol ester content and foam cell (*Scd1* [313]*, Sort1* [286]*, Hcar2* [314]). Their differential expression, due to IRF8-deficiency may contribute to the enhanced foam cell formation and cholesterol ester content observed in IRF8-KO macrophages.

We previously identified differential regulation of chemotaxis-related genes in IRF8-KO macrophages. When combined with previous reports demonstrating a role for Fabp4 in mediating cancerous cell invasion and

migration [315] this led us to explore the impact of IRF8-Fabp4/5 inhibition on macrophage migration. Upon subjecting the macrophages to increasing concentrations of BMS309403 inhibitor, we identified a significant reduction in the migration of WT^{LdlrKO} macrophages (**Fig 4.1.6 E & F**). To investigate whether this difference in macrophage migration was sustained in macrophage foam cells, cells where treated with acLDL and increasing concentrations of the BMS309403 inhibitor. This resulted in a significant 40% reduction in macrophage migration specific to WT^{LdlrKO} and not the IRF8-KO^{LdlrKO} macrophages (**Fig 4.1.6 G & H**).

This implies the athero-protective benefits of Fabp4/5 inhibition is dependent on the expression of macrophage-IRF8. This work has increased our understanding of how IRF8 impacts on cellular lipid accumulation, foam cell formation and macrophage migration, via its regulation of Fabp4 and Fabp5.

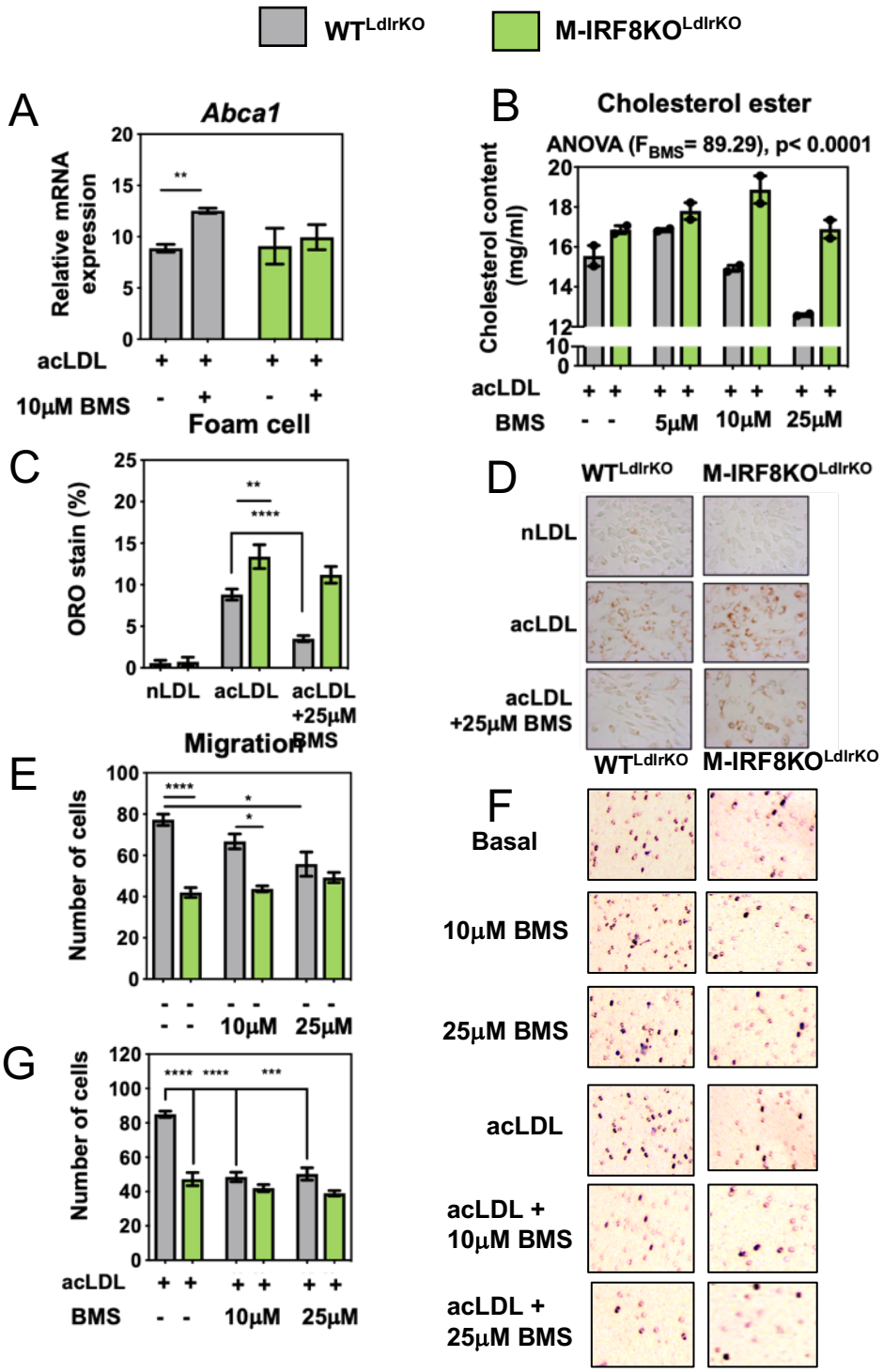

Fig 4.1.6 Athero-protective role of Fabp4/5 inhibition is dependent on macrophage-IRF8 expression.

(A) Relative gene expression of *Abca1,* validated in an independent experiment, in western diet-fed macrophages (n=3/group), challenged with or without 50ng acLDL and Fabp4/5 inhibitor BMS309406 at 10μM. (B) Cholesterol ester content of western diet-fed macrophages post 24hr culture with 50ng acLDL in the presence of BMS309406 at either 5μM, 10μM or 25μM (n=3/group). (C) Quantification of oil-red-o stain performed using Image J, images taken at 40x optical zoom. (D) Macrophage foam cell formation after 24hr culture with 50ng nLDL, acLDL and 25μM BMS. Number of macrophages migrating towards 100ng MCP-1 over 20hrs with (E) 10μM or 25μM BMS309406 and when challenged with (G) 50ng acLDL. (F) Representative images captured at 20x optical zoom. Data representative of n=3/group, statistical analysis conducted using paired students t-test, *p<0.05, **p<0.01, ***p<0.0001, ****p<0.00001, relative to WT$^{Ldlr-KO}$ mice.

.

4.2 Part B: Identification of IRF8 target genes that are differentially regulated in lipid-laden aortic macrophages: comparison with published datasets

4.2.1 Introduction

Next generation sequencing has revolutionised the amount of genomic data obtainable from molecular biology experiments [316]. The huge advances in sequencing over the past 10 years have led to increased availability of sequencing tools at an overall reduced cost. This has led to many researchers adopting sequencing methods to maximise the amount of data obtained from their experiments [316]. Upon taking advantage of publicly available recent sequencing data, it has become possible to perform comparisons against different datasets. Each dataset may have been generated using different methodologies; RNA-Sequencing, microarrays or single cell-RNA sequencing. However, by taking into consideration the different parameters used to correct for multiple comparisons, it is still possible to identify trends in similarities or differences in gene expression that are as a result of impaired genomic or cell-specific gene regulation, age or disease phenotype.

The focus of this section of the chapter is to maximise our understanding of myeloid-IRF8 regulation in atherosclerosis. We aim to do this by comparing how the differentially regulated genes identified in the macrophages of M-IRF8KO^{LdlrKO} mice differ from aortic macrophage subsets (inflammatory, resident like, trem2hi) [78], foamy macrophages [79] and IRF8-silenced macrophages [86], [94] in a non-atherosclerotic background, as demonstrated in **Fig 4.2.1.** The

differences between the experimental methods used to generate the gene lists are outlined in **Table 4.1**.

In order to investigate the following:

1. Whether the hyperlipidaemic environment and diet of M-IRF8KO^{LdlrKO} mice alters the regulation of IRF8 target genes, in comparison to known IRF8-regulated genes from macrophages in a normolipidemic environment, identified in IRF8-silenced Bxh2 macrophages [86], [94].
2. Determine whether IRF8KO^{LdlrKO} macrophages share transcriptional similarities to aortic macrophage subsets; resident-like, trem2hi and inflammatory from western diet fed mice as identified in Cochain et al, 2018 [78].
3. Determine whether the regulation of IRF8-target genes identified in our studies resembles changes in foamy aortic macrophages from western diet fed mice as described in Kim et al, 2018 [79].

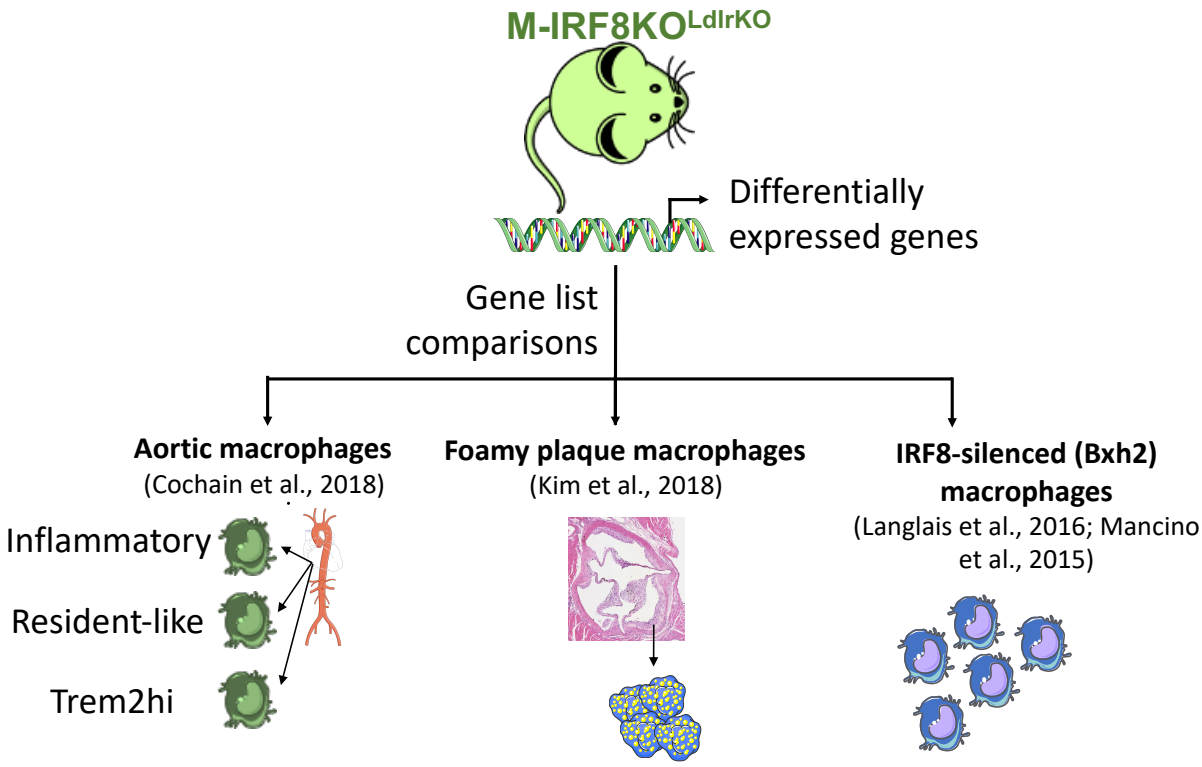

Fig 4.2.1 Summary of RNA-Seq gene list comparisons.
Genes differentially regulated in M-IRF8KO^{LdlrKO} macrophages will be compared to differentially regulated genes in inflammatory, resident-like, trem2hi aortic macrophage subsets, alongside foamy aortic macrophages and IRF8-silence macrophages.

Publication	RNA-seq type	Experimental conditions	Platform used	Cut offs applied
Langlais et al., 2016 [94]	Bulk RNA-Seq	• Chow-fed mice	• Sequencing performed on HiSeq 2000 Sequencer (Illumina). • Reads were mapped to the mouse UCSC mm9 reference • Normalisation and differential expression analysis were conducted using edgeR Bioconductor package	• Genes were retained that had a minimum of five counts per million reads in at least 2 of the 12 samples • Genes that were 2-fold change differentially expressed and had adjusted p-values of $<10^{-5}$ were considered significant
Mancino et al.,21015 [86]	Bulk RNA-Seq	• Chow-fed mice	• Sequencing performed on HiSeq 2000 Sequencer (Illumina). • Reads were mapped to the mouse UCSC mm9 reference • Differentially expressed genes were called using cufflinks 1.2.1	• Genes that were 2-fold change differentially expressed and had adjusted p-values of <0.05 were considered significant
Kim et al., 2018 [79]	Bulk RNA-Seq	• High fat western diet-fed mice for 28 weeks • $Apoe^{KO}$ mice were used	• Sequencing performed on HiSeq 3000 Sequencer (Illumina).	• Differential expression was obtained by DeSeq2 guidelines (all P-values corrected for testing multiple genes using Bonferonni correction) • Genes with an adjusted p-value of <0.05 were considered significantly differentially expressed
Cochain et al., 2018 [78]	Single-cell RNA-Seq	• High fat western diet-fed for 11weeks • $Apoe^{KO}$ female mice used	• Single cells were encapsulated in droplets using 10X Genomics GemCode Technology • Sequencing was performed on rhe Illuminase HisEq 2500	• Differential expression was identified using the Bayesian approach where genes with absolute adjusted z-score of >1.96 or <-1.96 and a p value <0.01 where identified as statically significant

Table 4.1 Summary of the different RNA-Seq and experimental methods used in articles used for gene list comparisons.

4.2.2 Myeloid-IRF8 transcriptomic regulation is different in normolipidemic to hyperlipidaemic mice

We next investigated whether the hyperlipidaemic environment of M-IRF8KO^{LdlrKO} mice alters the regulation of IRF8 target genes. Although it would have been more ideal to compare the transcriptomes of western diet fed M-IRF8KO^{LdlrKO} mice and chow fed M-IRF8KO^{LdlrKO} mice, it was not possible within the time frame of this thesis. As an alternative approach we performed gene comparisons with a published dataset from normolipidemic IRF8-silenced (Bxh2) mice, as described in Mancino et al., 2015 and Langlais et al., 2016 [86], [94]. The Bxh2 mice, carry a single point mutation in the interferon association domain of IRF8, preventing it from forming protein-protein interactions with its binding partners and hence silencing IRF8 function [285]. By comparing the M-IRF8KO^{LdlrKO} gene list with two independent studies reporting basal IRF8 regulation in normolipidemic Bxh2 mice, we identified 42 genes that were present in all three lists (**Fig 4.2.2 A**). Interestingly, of these, about 80% showed decreased expression in macrophages from M-IRF8KO^{LdlrKO} mice and the Bxh2 mice from the Mancino et al., 2015 and Langlais et al., 2016 studies. This confirms the basal regulation of these IRF8 targets is the same across different models of IRF8 reduction (**Fig 4.2.2 B**).

To elucidate the functional pathways associated with these 42 overlapping genes, Metascape pathway analysis was performed. The most significant enriched pathways included ‘Cellular defence response to external stimuli and IFNβ’ alongside ‘Complement activation’ and ‘Cell migration’ (**Fig 4.2.2 C**). This implies inflammatory, defence response related IRF8-target genes are regulated

in both a normolipidemic and hyperlipidaemic, atherosclerosis prone environment. The increased number of blue lines within the circus plot (**Fig 2.2.2 B**), in comparison to the purple lines, indicates a greater proportion of non-overlapping genes share the same function. Whether these genes are similarly regulated across hyperlipidaemic atherosclerosis prone M-IRF8KO^{LdlrKO} mice and normolipidemic Bxh2 mice is yet to be investigated.

Upon identifying the 'Defence response' pathways are subject to IRF8 regulation in macrophages from both normolipidemic and hyperlipidaemic environment, we aimed to understand how the pathways that are significantly enriched in hyperlipidaemic M-IRF8KO^{LdlrKO} mice and normolipidemic IRF8-silenced Bxh2 mice, compare with each other. As demonstrated in **Fig 4.2.2 D**, the heatmap of significance displays pathways that are enriched in macrophages from M-IRF8KO^{LdlrKO} and Bxh2 mice. Interestingly, although 'Inflammation', 'IFN response' and 'Chemotaxis' are regulated in both M-IRF8KO^{LdlrKO} and Bxh2 mice, they are much more significantly regulated in macrophages from M-IRF8KO^{LdlrKO} mice, thus implying the hyperlipidaemic atherosclerosis prone environment of M-IRF8KO^{LdlrKO} mice promotes IRF8 regulation of these pathways more strongly than in mice from a normolipidemic environment.

To determine the proportion of genes that contribute to the significant pathways highlighted in **Fig 4.2.2 D,** a Metascape clustergraph was generated. This demonstrates how each pathway cluster is connected (**Fig 4.2.2 E**). Each node within the clustergraph, is presented as a pie chart where the colour of slice relates to a corresponding gene list (blue – M-IRF8KO^{LdlrKO}, green, Bxh2

macrophages from Mancino et al.,2015 and red – Bxh2 macrophages from Langlais et al., 2016). The clustered pie chart further highlights the proportion of genes that are differentially regulated within a cluster from each specific gene list or study. Overall, this analysis shows that considering inflammatory-related pathways are regulated by IRF8 in both hyperlipidaemic and normolipidemic mice, the number of genes regulated by IRF8 in these pathways is somewhat higher in atherosclerosis prone mice, (44 genes in M-IRF8KO^{LdlrKO} macrophages, 16 genes in Bxh2 macrophages from Langlais et al.,2016 and 30 genes in Bxh2 macrophages from Mancino et al., 2015). Therefore, owing to the increased significance of the inflammatory-related pathways in atherosclerosis prone M-IRF8KO^{LdlrKO} mice. This is consistent with previous reports demonstrating the hyperlipidaemic environment of atherosclerosis prone mice promotes the induction of inflammatory related genes [317]. Interestingly, we have also identified 234 genes that are preferentially regulated in M-IRF8KO^{LdlrKO} mice, proposing their regulation may be promoted by the hyperlipidaemic environment. However, studies would be required to confirm regulation of IRF8-target genes is specific to a hyperlipidaemic environment by directly comparing to transcriptomes in macrophages from non-western diet fed M-IRF8KO^{LdlrKO} mice. This would help identify how the hyperlipidaemic environment of atherosclerosis prone mice alters the regulation of inflammatory IRF8 target genes that are crucial to atherosclerosis development.

A

Circos Plot

Different genes with same functional

Overlapping genes

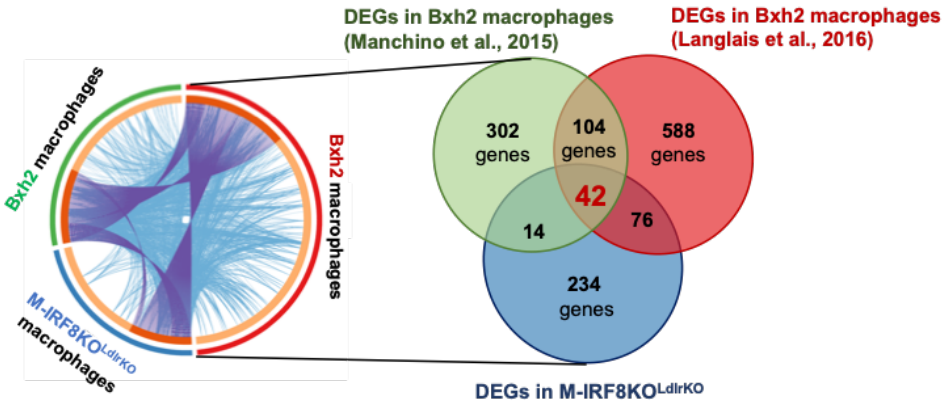

B

Top differentially regulated genes in normo and hyperlipidemia

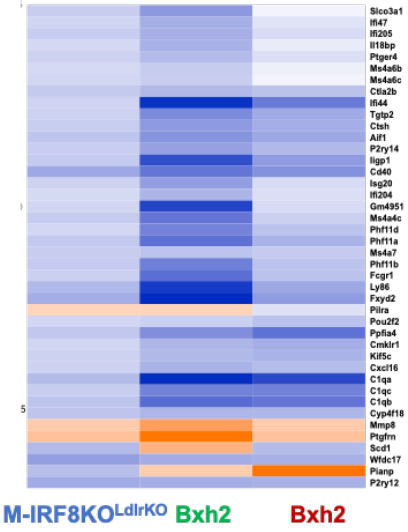

C

Top differentially regulated overlapping pathways

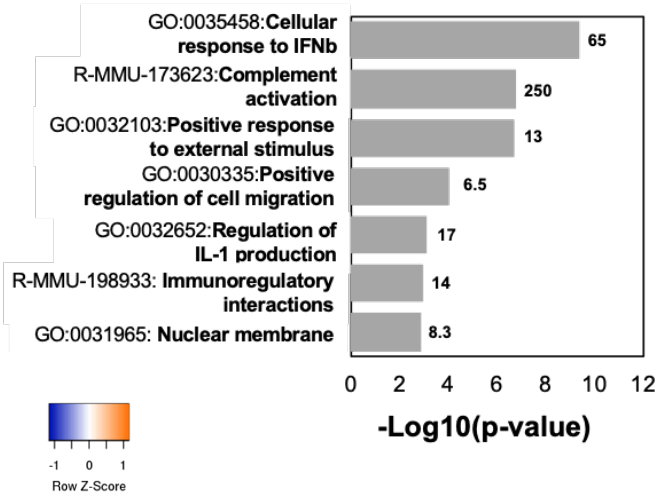

D

Most significant pathways

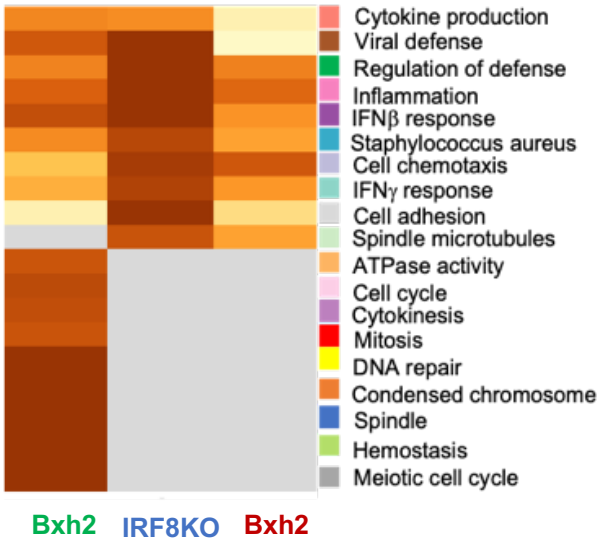

E

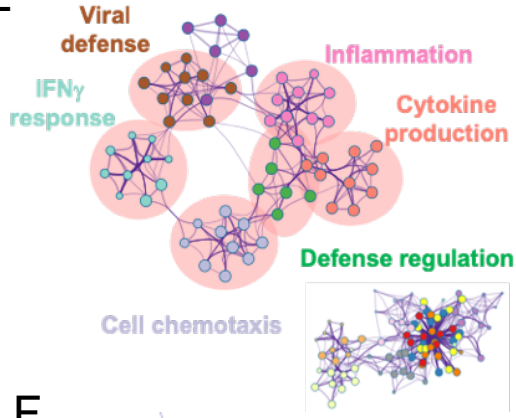

F

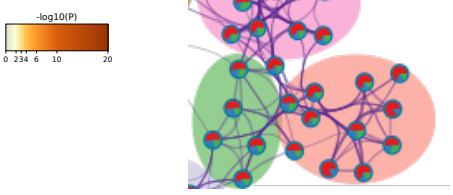

Figure legend on next page

Fig 4.2.2 High lipid atherosclerosis environment influences IRF8-target gene expression when compared to a normolipidemic environment.
(A) Circos plot highlighting the overlap of differentially regulated genes (purple lines) identified in Western diet-fed untreated IRF8-KO BMDMs and two independent studies (Langlais et al., 2015 in red and Mancino et al., 2016 in green) investigating the IRF8 transcriptome in chow-fed basal IRF8-silenced BMDMs from Bxh2 mice. The purple lines connect overlapping genes across each dataset and blues lines connect the different genes that fall into the same ontology. Corresponding Venn diagram highlights the number of overlapping genes from all 3 lists of differentially expressed genes. (B) Clustered heatmap of linear fold changes of overlapping genes in IRF8-deficient macrophages. (C) Gene set meta-analysis of overlapping IRF8-target genes, displaying the most significantly regulated pathways with enrichment ratio to the right of each bar. (D) Heatmap displaying the p-value of the most statistically enriched pathways across all four gene lists. Grey areas indicate lack of enrichment for that term in the corresponding gene list. (E) Pathway enrichment network visualisation showing the intra-cluster and inter-cluster similarities of enriched terms across all three gene lists. Pathways with a proportion of differentially regulated genes in M-IRF8KO^{LdlrKO} mice are highlighted in light pink. Remaining cluster annotations are shown in colour code on the (D) 'Most significant pathways' heatmap. (F) The same enrichment network whereby nodes display the proportion of genes from each gene list within that specific pathway node. Colour code for pie sector follows; Red = Langlais et al., 2016, Green = Mancino et al., 2015, Blue = IRF8-KO macrophages. Pathway analysis and enrichment visualisation was performed using Metascape. Data presented are Linear fold change 1.3, FDR 0.05, $p<0.01$.

4.2.3 Myeloid-IRF8 regulates genes enriched within aortic macrophage subsets

Macrophages present within the atherosclerotic plaque have been shown to exhibit differential phenotypes, owing to their pro-inflammatory and anti-inflammatory functions within the plaque [25], [75], [318]. Recently, differences in the phenotype of macrophage subsets have been thought to contribute to atherosclerosis progression whilst providing an indication on plaque phenotype and atherosclerosis severity [319]. Cochain et al., 2018, have discovered a novel transcriptomic signature of three aortic macrophage subsets; Resident-like, Inflammatory and trem2hi, from western diet-fed mice that may individually contribute to select processes that promotes atherosclerosis development [78]. The resident-like subset identified are transcriptionally similar to aortic macrophages from non-western diet-fed mice, [78] whereas the inflammatory subset display enriched pro-inflammatory gene expression (*NF-κB, IL-1β*). The novel trem2hi macrophage subset, identified by Cochain and colleagues [78],

demonstrate a gene expression signature reminiscent of osteoclasts, advocating a potential role in lesion calcification. The trem2hi macrophages also display enrichment of genes involved in lipid metabolism and catabolism and oxidative stress, processes that are vital to atherosclerosis plaque development [78], [320], [321].

Using this information, we aimed to determine whether the genes enriched within the macrophage subsets, where also identified as IRF8-target genes in M-IRF8KO^{LdlrKO} mice. Therefore, possibly identifying a macrophage subset enriched in IRF8-target genes [78]. This would help identify transcriptional signatures unique to aortic macrophage subsets from western diet-fed mice that are regulated by IRF8, thereby having the potential to be targeted in future clinical applications.

Meta-analysis of all four gene lists using Metascape demonstrated a large degree of gene overlap, as shown by the purple lines in the circus plot (**Fig 4.2.3 A**). This was largely observed between the three macrophage subsets; Resident-like, inflammatory and trem2hi, suggesting many genes are enriched in all three aortic macrophage subsets. However, there was a greater degree of functional overlap between the genes enriched in the three macrophage subsets and IRF8-KO macrophages as shown by the blue connecting lines on the circos plot (**Fig 4.2.3 A**). This indicates, many non-overlapping genes share functional similarities. By investigating the regulation of IRF8 target genes, identified in M-IRF8KO^{LdlrKO} mice, compared to the genes enriched within the inflammatory macrophage subset (**Fig 4.2.3 B**), we discovered ~80% of genes enriched within

the inflammatory subset where negatively regulated in IRF8-KO macrophages. This implies IRF8-KO macrophages are less inflammatory than inflammatory aortic macrophages. Interestingly, ~80% of genes enriched within resident-like aortic macrophages where negatively regulated in IRF8-KO macrophages (**Fig 4.2.3 C**), whereas only ~60% of genes enriched in lipid-associated trem2hi macrophages where negatively regulated in IRF8-KO macrophages (**Fig 4.2.3 D**). However, upon comparing genes IRF8-target genes enriched in all macrophage subsets, we identified IRF8-KO macrophages negatively regulates all enriched target genes within inflammatory, resident-like and trem2hi aortic macrophages (**Fig 4.2.3 E**).

Overall, this shows IRF8 differentially regulates genes that are also enriched within inflammatory, resident-like and trem2hi macrophage subsets from hyperlipidaemic mice. IRF8-KO macrophages show negative regulation of most target genes that are enriched in both inflammatory and resident-like aortic macrophages. However, we demonstrate IRF8-KO macrophages positively regulates a greater proportion of target genes that are also positively regulated within the lipid-associated trem2hi macrophages. Collectively, this has increased our understanding of IRF8-regulated genes that are enriched within aortic macrophages from western diet-fed mice. This provides an insight into future potential therapeutic targets aimed at macrophage lipid metabolism within atherosclerosis development.

As a large proportion of non-overlapping genes between the aortic macrophage subsets and M-IR8KO^{LdlrKO} mice share functional similarities (light

blue lines in **Fig 4.2.3 A**), we aimed to determine the significance of pathways enriched amongst these genes. Interestingly, 'Inflammation' and 'Defence response' were the most significant regulated pathways across all gene lists (**Fig 4.3.2 F & G**), demonstrating the atherosclerosis prone environment promotes these processes across all macrophage subsets.

To identify the proportion of genes that contribute to the significant pathways highlighted in **Fig 4.2.3 F**, a Metascape clustergraph was generated. This shows how each pathway cluster is connected **(Fig 4.2.3 G).** Each node within the clustergraph is shown as a pie chart where the colour of each slice relates to a corresponding gene list (blue – Inflammatory macrophages, Green, resident-like macrophages, red – IRF8-KO macrophages and purple – trem2i macrophages). This further highlights the proportion of genes that are differentially regulated within that cluster from each specific list. As shown in **Fig 4.2.3 H**, an equal proportion of genes are involved in IL-1 production, inflammation, migration and MAPK signalling, indicating these processes are not only enriched amongst all atherosclerotic macrophage subsets but also regulated by IRF8.

Overall, this comparative meta-analysis has identified a total of 22 IRF8-target genes, from M-IRF8KO^{LdlrKO} BMDMs, that are differentially regulated in aortic inflammatory, trem2hi and resident-like macrophage subsets from western diet-fed mice. This demonstrates that IRF8 regulates genes that may contribute to macrophage functional processes that are key in atherosclerosis development. This work also proposes profiling BMDMs could provide an alternative method to

investigating aortic macrophages directly. Although direct comparative studies of aortic macrophages and BMDMs from the same animals would need to be performed to confirm this.

A

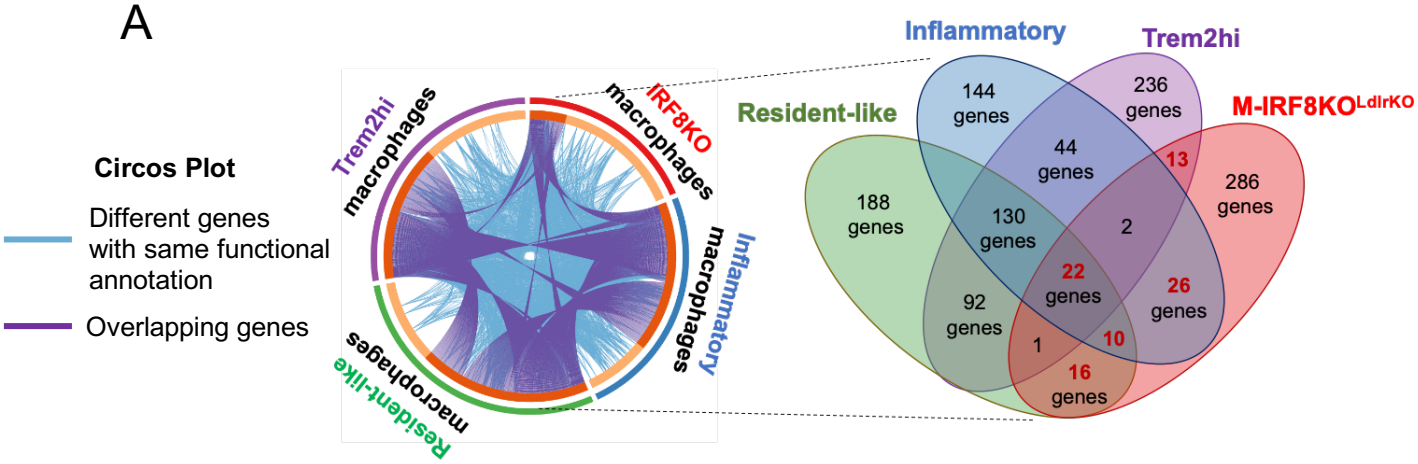

B

Inflammatory

Gene	Fold change
Egr2	1.56
Nr4a1	1.9
Txnrd1	1.63
Cxcl10	-2.9
St3gal6	-2.5
Ccl4	-2.3
Gm63777	-2.1
Scimp	-1.9
Nfkbiz	-1.7
Herpud1	-1.7
Casp4	-1.7
Ccl3	-1.6
Gadd45b	-1.6
Cd83	-1.5
Ifi204	-1.3
Sifn2	-1.4

C

Resident

Gene	Fold change
F13a1	2.7
Dusp6	1.8
Slc43a2	1.4
Aoah	-1.3
Rsrp1	-1.4
Ms4a6b	-1.4
Pros1	-1.4
Cmklr1	-1.5
Cept1	-1.5
Zfp385a	-1.5
Slc31a2	-1.9
Ctla2b	-1.9
Lyz1	-2.3
Fxyd2	-2.9
P2ry12	-4.9

D

Trem2hi

Gene	Fold change
Itgax	2.8
Gclm	1.7
Lhfpl2	1.6
Adam8	1.5
Sgk1	1.4
Nucb2	-1.5
Pkib	-1.5
Cpq	-1.5
Sdhb	-1.6
Ndufc2	-1.6
Pnp	-1.7
Ppfia4	-2
Fabp5	-2.5

E

All

Gene	Fold change
Lyz2	-2.6
Ly86	-2.5
C1qa	-2.4
Slamf9	-2.1
C1qb	-2.1
Aif1	-2.1
Ctsh	-1.8
C1qc	-1.8
Fcgr4	-1.8
Ms4a7	-1.8
Fcgr1	-1.7
Fcer1g	-1.7
Cxcl16	-1.6
Dpysl2	-1.6
Ctsc	-1.6
Clec12a	-1.5
Pea15a	-1.4
Ms4a6d	-1.4
Ctss	-1.4
Lgmn	-1.4
Hexb	-1.3
Snx5	-1.3
Pilra	1.6
Dusp1	1.8

F

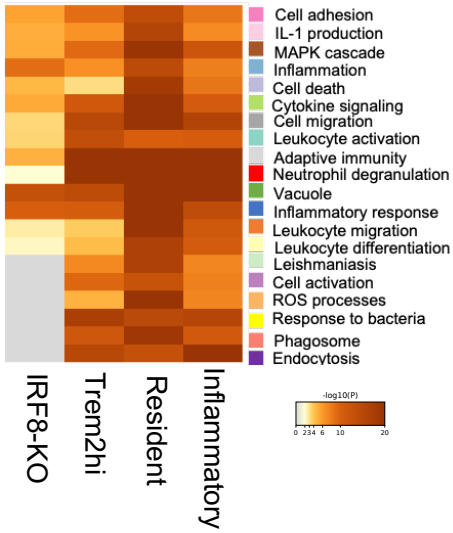

G

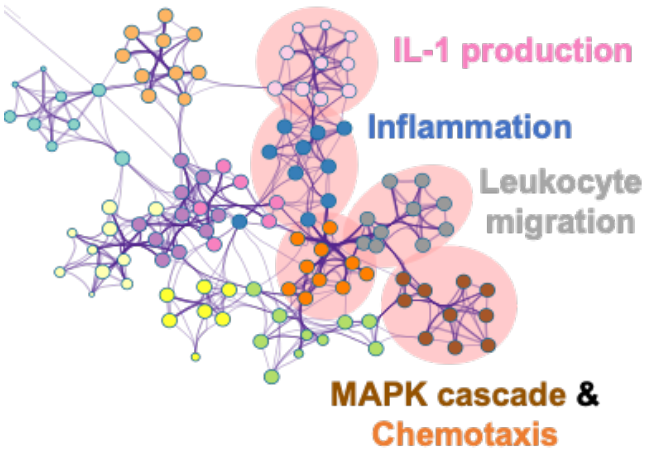

H

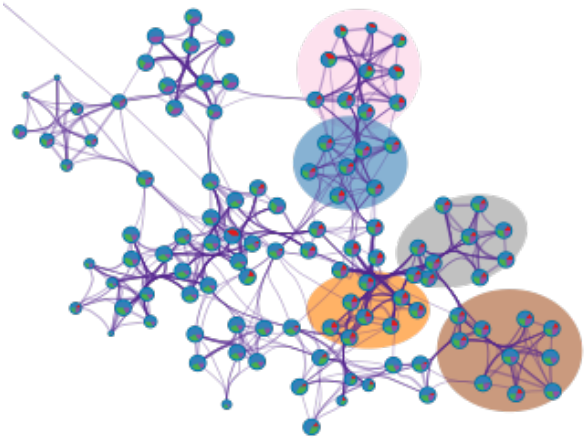

Figure legend on next page

Fig 4.2.3 Myeloid-IRF8 regulates genes enriched within aortic inflammatory macrophage subsets.
(A) Circos plot highlighting the overlap of differentially regulated genes (purple lines) identified in Western diet-fed IRF8-KO macrophages, inflammatory macrophages, resident-like macrophages and trem2hi macrophages. The purple lines connect overlapping genes across each dataset and blues lines connect the different genes that fall into the same ontology. The corresponding Venn diagram highlights the number of overlapping genes from all 4 input gene lists. Table with the fold changes of IRF8 target genes in IRF8-KO macrophages that are differentially regulated in (B) inflammatory macrophages, (C) Resident-like macrophages, (D) trem2hi macrophages and (E) all four gene lists (Cochain et al., 2018). (F) Heatmap displaying the p-value of the most statistically enriched pathways across all four gene lists. Grey cells indicate the lack of enrichment for that term in the corresponding list. (G) Pathway enrichment network visualisation showing the intra-cluster and inter-cluster similarities of enriched terms across all four gene lists. Pathways with a proportion of differentially regulated genes in M-IRF8KO^{LdlrKO} mice are highlighted in light pink. (F) Remaining cluster annotations are shown in colour code on the 'Most significant pathways' heatmap. (H)The same enrichment network is shown where the nodes display the proportion of genes from each list that are present within the same pathway. Colour code for pie sector; Blue = inflammatory macrophages, green = resident-like macrophages, red = IRF8-KO macrophages. Pathway analysis and enrichment visualisation was performed using Metascape.

4.2.4 IRF8-KO macrophages are transcriptionally similar to aortic foamy macrophages

Macrophage foam cell formation is a hallmark in the initiation of atherosclerosis, were the foam cell content of atherosclerotic plaques often contributes to plaque phenotype and severity [31], [79], [320]. We have identified a signature of IRF8 target genes that are differentially regulated in inflammatory, resident-like and trem2hi aortic macrophage subsets that may contribute to atherosclerosis progression (section 4.2.3). Upon combining this knowledge with our previous data, identifying a role for IRF8 reduction in promoting macrophage foam cell formation (**Fig 4.1.5 F**), we questioned whether IRF8 differentially regulates genes that are enriched within foamy aortic macrophages, as identified by Choi et al., 2018 [79].

To determine this, comparative meta-analysis was performed on the differentially regulated genes identified in IRF8-KO macrophages and foamy aortic macrophages by Choi et al., 2018 [79]. Interestingly, we observed an

increase in the number of genes that shared the same function, in comparison to the number of over-lapping genes between IRF8-KO macrophages and foamy aortic macrophages (**Fig 4.2.4 A**). This suggests IRF8 may regulate select functional pathways that are enriched in aortic foamy macrophages. To determine the functional pathways that are enriched within the over-lapping genes present in both foamy and IRF8-KO macrophages, gene set enrichment analyses was performed as before. 'Inflammatory response' and 'Lipid metabolic processes' were the two most significant enriched pathways in this gene list. Of these pathways, 65% of genes (9 out of 14 genes) involved in 'lipid metabolic processes' were positively regulated in both IRF8KO^{LdlrKO} and foamy macrophages, whereas 80% of genes (14 out of 17 genes) involved in inflammation were downregulated in IRF8KO^{LdlrKO} macrophages and upregulated in the foamy macrophages (**Fig 4.2.4 B**). This demonstrates IRF8 differentially regulates genes that are enriched within foamy aortic macrophages. Taken together this indicates, IRF8-KO macrophages regulate select genes involved in lipid metabolism that are similarly regulated in foamy aortic macrophages. However, the regulation of IRF8 target pro-inflammatory genes are negatively regulated within foamy aortic macrophages.

To identify the pathways that were significantly regulated amongst the genes that share functional similarities, as depicted by the blue lines on the circus plot (**Fig 4.2.4 A**), in both IRF8-KO and foamy macrophages, comparative analysis was performed. Pathway analysis results showed genes involved in 'Chemotaxis', 'Cell death' and 'Inflammation' were significantly regulated in both IRF8-KO and foamy macrophages. This suggests, IRF8 may also regulate

chemotaxis and cell death processes in foamy macrophages that are crucial in atherosclerotic plaque development.

In summary, our studies imply IRF8-KO macrophages share a similar transcriptional profile to foamy aortic macrophages. IRF8 differentially regulates genes involved in lipid-biosynthetic processes, similarly to foamy macrophages whilst negatively regulating pro-inflammatory genes. This implies the genes involved in lipid-metabolic processes that are enriched in foamy macrophages and regulated by IRF8, may contribute to the increased foam cell formation previously identified in IRF8-KO macrophages (**Fig 4.1.5 H**).

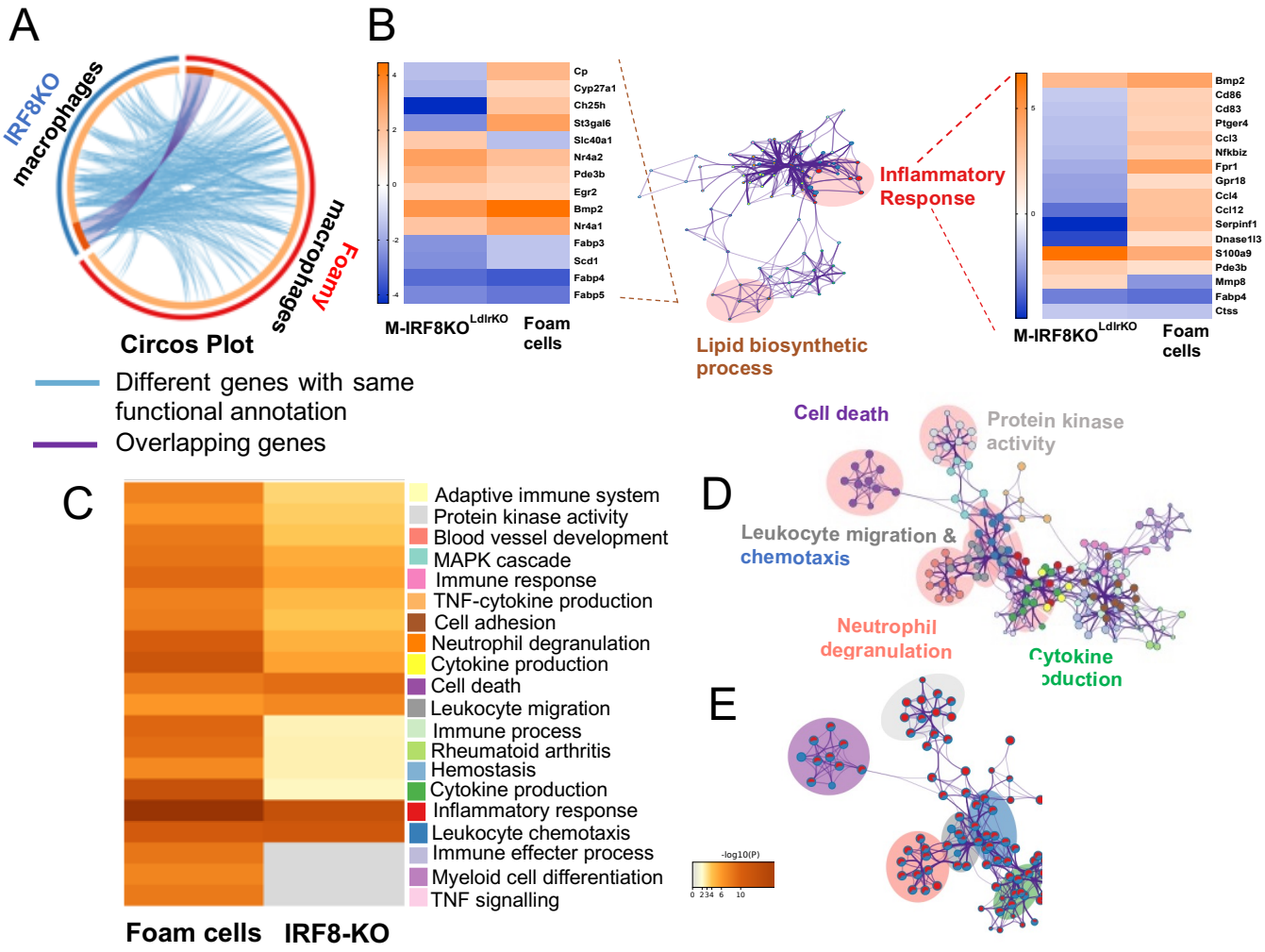

Fig 4.2.4 IRF8 differentially regulates genes enriched in foamy aortic macrophages.
(A) Circos plot highlighting the overlap of differentially regulated genes (purple lines) identified in Western diet-fed basal IRF8-KO macrophages and foamy aortic macrophages. The purple lines connect overlapping genes across each dataset and blues lines connect the different genes that fall into the same ontology. The corresponding Venn diagram highlights the number of overlapping genes from IRF8-KO macrophages and foamy aortic macrophages (Kim et al., 2018). (B) Pathway enrichment network visualisation of overlapping IRF8-target genes present in aortic foamy macrophages, showing the intra-cluster and inter-cluster similarities of enriched terms across both gene lists. Highlighted in light pink are two of the most significantly regulated pathways with differential gene expression within the pathway presented in a clustered heatmap of fold changes (M-IRF8KO^{LdlrKO} vs WT^{LdlrKO} and Foamy macrophages vs non-foamy macrophages) for lipid biosynthetic processes (*Left*) and Inflammatory response (*Right*). (C) Heatmap displaying the p-value of the most statistically enriched pathways across both gene lists. Grey cells indicate the lack of enrichment for that term in the corresponding gene list. (D) Pathway enrichment network visualisation showing the intra-cluster and inter-cluster similarities of enriched terms across both lists. Pathways with a proportion of differentially regulated genes in M-IRF8KO^{LdlrKO} mice are highlighted in light pink. Remaining cluster annotations are shown in colour code on the (C) 'Most significant pathways' heatmap. (E) The same enrichment network as (D), where significant pathways are highlighted, and nodes display the proportion of genes from each gene list within that specific pathway. Colour code for pie sector; blue = IRF8-KO macrophages and red = foamy macrophages. Pathway analysis and enrichment visualisation was performed using Metascape. Data presented are Linear fold change 1.3, FDR 0.05, p<0.01.

4.3 Summary

As summarised in **Fig 4.3**, this chapter has established the following;

1. Myeloid-IRF8 reduction transcriptionally reprograms macrophage gene expression in bone-marrow derived macrophages.
2. IRF8 positively regulates inflammatory, chemotactic and lipid-metabolic pathways.
3. Inhibition of Fabp4/5 retards foam cell formation, macrophage cholesterol ester accumulation and macrophage migration.
4. The *in-vitro* athero-protective effects of Fabp4/5 inhibition are dependent on myeloid-IRF8 expression.
5. The regulation of IRF8-target genes differs between hyperlipidaemic M-IRF8KO^{LdlrKO} mice and normolipidemic IRF8-silenced (Bxh2) mice [86], [94].
6. Myeloid-IRF8 differentially regulates genes that are enriched within the aortic resident-like, inflammatory and trem2hi subsets from western diet-fed mice [78].
7. IRF8-KO macrophages share a similar transcriptional profile to foamy aortic macrophages [79], in regards to genes involved in lipid-biosynthetic processes.

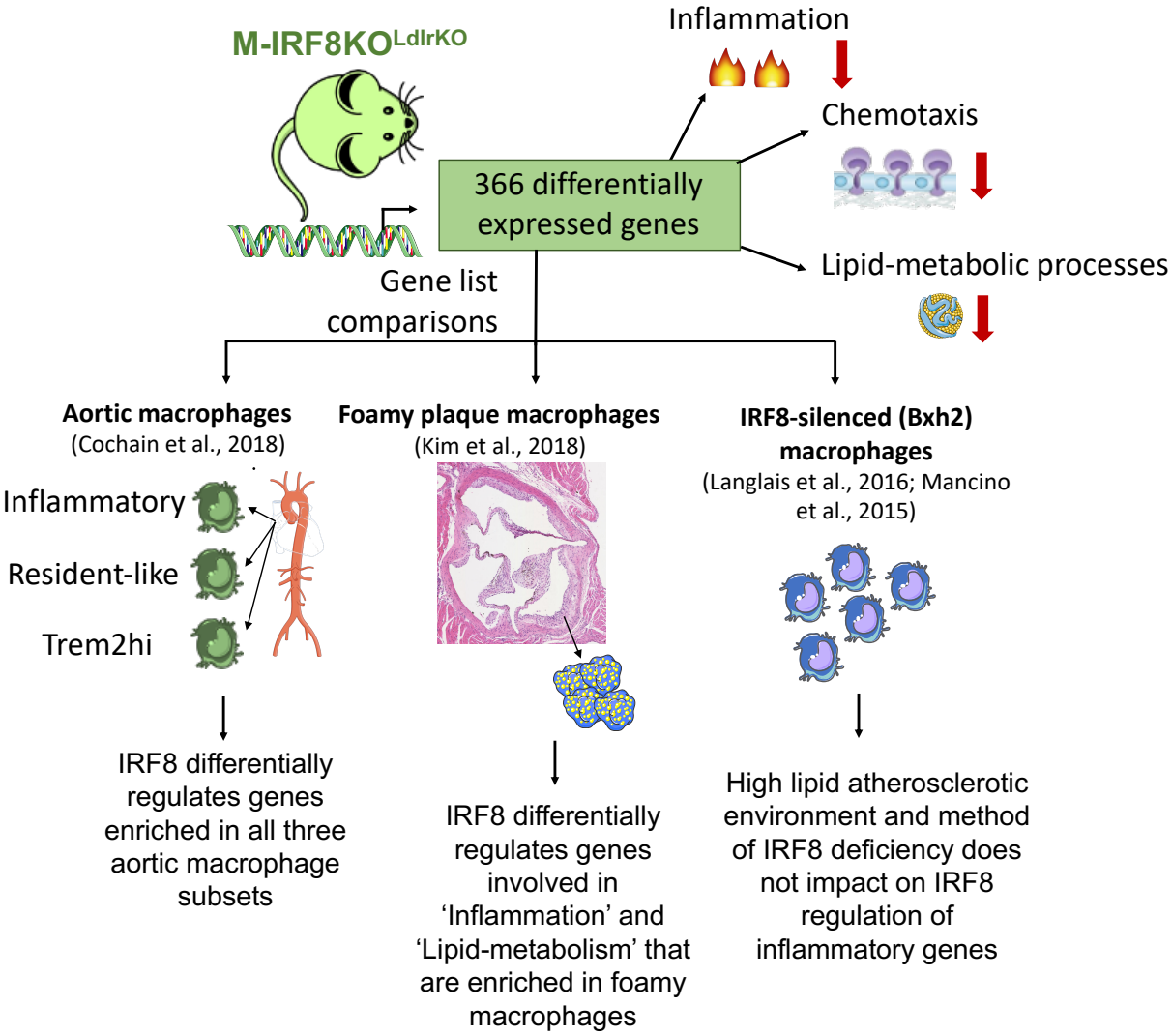

Fig 4.3 Summary of key findings.
The most significant differentially regulated pathways identified from the differentially expressed genes in BMDMs from M-IRF8KO^{LdlrKO} mice. Summary of gene list comparisons performed and the main outcomes from each comparison.

4.4 Discussion

The results in this chapter demonstrate a novel dual-transcriptional role of myeloid-IRF8 reduction in the activation and repression of multiple biological pathways, that may collectively contribute to the athero-protective phenotype of myeloid-IRF8 reduction. To understand the potential athero-protective mechanism elicited by myeloid-IRF8 reduction, we investigated the transcriptional differences in the bone marrow derived macrophages (BMDMs) from western diet fed WT^{LdlrKO} and M-$IRFK8KO^{LdlrKO}$ mice by performing high throughput RNA-seq.

Aortic leukocyte infiltration is a hallmark of atherosclerosis [48], [322], with many infiltrating cells, in particular monocytes, originating from the bone marrow [279]. Previous studies have demonstrated that during the initiation of atherosclerosis and early stage plaque development, a large proportion of lesional macrophages originate from the circulation [22], [57]. The hypercholesteraemic environment of $LDLR^{KO}$ mice, results in an expansion of circulating monocytes, in comparison to chow fed mice, contributing to the increase in monocyte-macrophage differentiation and transmigration across the arterial wall [21]. The pro-inflammatory environment of the atherosclerotic plaque has been shown to promote macrophage heterogeneity [75], [78]. Previous studies have uncovered the benefits of using BMDMs to increase our understanding of macrophage dynamics in atherosclerosis [323]. For this reason and the increased availability of BMDMs in comparison to plaque macrophages, RNA-Seq analysis was performed on the BMDMs of western diet fed mice.

Analysis of the RNA-Seq datasets uncovered 366 differentially regulated genes in IRF8KO^{LdlrKO} macrophages, with 167 genes upregulated and 199 genes downregulated, when compared to WT^{LdlrKO}. Gene set enrichment analysis identified 16 upregulated enriched biological pathways and 15 downregulated enriched biological pathways amongst the differentially regulated genes. Of the upregulated pathways, the most significant biological processes involved 'Cell growth' ($Log_{10}P$ = -5.8), 'Cancer' ($Log_{10}P$ = -7) and 'Lipid transport' ($Log_{10}P$ = -4.5) (**Fig 4.1.2**). This is possibly due to the tumour suppressor properties of IRF8 [324], coupled with the decreased global-IRF8 expression being highly associated with multiple cancers, including breast, myeloma and chronic myeloid leukaemia [153], [324], [325]. For this reason, it is not surprising that many 'Growth factor' and 'Cancer' related pathways are amongst the most significantly upregulated. It must, however, be noted that many of the differentially regulated genes (*Bmp2, Fos, Dusp1, Ednrb*) within the growth pathways are highly associated with other pathways including 'Cell chemotaxis' and 'Cell death'. This is also shown by the large degree of overlap in pathway nodes on the upregulated clustergraph (**Fig 4.1.2 E**). This suggests that myeloid-IRF8 reduction transcriptionally reprograms macrophages to display an increased enrichment of pathways associated with growth and development. However, the genes present within such pathways are also associated with other pathways, including 'Cell chemotaxis' and 'Cell death', that may collectively contribute to the athero-protective function of myeloid-IRF8 reduction.

Alongside the upregulated pathways, a further 15 downregulated pathways were identified in the IRF8-KO macrophages. The downregulated

pathways displayed an increased level of significance in comparison to the upregulated pathways. Interestingly, 'Inflammation' ($Log_{10}P$ = -11.7) and 'Leukocyte chemotaxis' ($Log_{10}P$ = -7.6) were the most significantly downregulated pathways, indicating a possible anti-inflammatory and anti-migratory transcriptional phenotype of the IRF8-KO macrophages. The dual activation and repressive transcriptional activity of IRF8 is determined by the cofactor of which it forms a heterodimeric complex with and the subsequent sequence to which it binds proximal to the promoter region of its target genes [115], [326]. Previous studies investigating IRF8 genomic occupancy in macrophages, show the majority of constitutive IRF8 binding was at sites harbouring an EICE sequence, characteristic of transcriptional activation [94]. It is for this reason, IRF8 reduction has been predominantly associated with pathways that are negatively regulated in the absence of IRF8, including impaired innate immune response [116] and increased susceptibility to infection [121], as IRF8 promotes the expression of genes that are crucial for the maintenance of these processes. We next aimed to investigate the pathways and genes that were downregulated in IRF8-KO macrophages and understand how they may contribute to the athero-protective phenotype of myeloid-IRF8 reduction.

4.4.1 IRF8 and Inflammation

Of the most significant regulated genes within this pathway; Chemokine interferon-γ inducible protein 10 kDa (*Cxcl10,* FC -2.99*),* Chemokine like receptor 1 (*Cmklr1,* FC -1.51), Absent in melanoma 2 *(Aim2,* FC -1.34) and Fc Fragment Of IgE Receptor Ig (*Fcerg1* FC -1.66), have been implicated in the promotion of atherosclerosis. The chemokine ligand Cxcl10 is known to promote chemotaxis,

cell proliferation, plaque instability and inflammation, whereby reduction in Cxcl10 significantly reduce atherosclerotic plaque progression [327], [328]. Similarly, *Aim2* and *Fcer1g,*have been associated with enhanced inflammatory NF-κB signalling, promotion of lesion size when overexpressed and increased apoptosis [329], [330].

Previous studies have demonstrated the importance of IRF8 binding and regulation of inflammatory processes in the macrophages of IRF8 mutated (Bxh2; $IRF8^{m/m}$) mice on a normolipidemic environment [86], [94]. Using this information, we aimed to determine whether the regulation of IRF8 target genes identified in hyperlipidaemic M-$IRF8KO^{LdlrKO}$ mice, differed to those identified in normolipidemic Bxh2 mice. This would enhance our understanding on the previously uncharacterised area of how IRF8 regulation differs in a high lipid atherosclerosis prone environment. The Bxh2 mice used in the studies conducted by Langlais et al., 2016 and Mancino et al., 2015, carry a single point mutation (Arg294>Cys) in the IRF8 interferon association domain (IAD), that's crucial for making protein-protein interactions with its binding partners. Mutations within this domain significantly impair IRF8 function, rendering the mice phenotypically similar to global $IRF8^{KO}$ mice, as they harbour a CML-like phenotype and lack CD8α+ conventional DCs [331], [332]. Upon comparing the inflammatory IRF8-target genes identified in IRF8-KO macrophages from western diet-fed mice, to the differentially regulated genes identified in the $IRF8^{m/m}$ macrophages from Bxh2 mice, we observed a 50% overlap of genes (**Fig 4.1.3 B**). Many of the overlapping genes were involved in atherosclerosis-related processes including chemotaxis and vascular calcification in conjunction with inflammation. However,

pathway analysis performed on the 18 inflammatory genes specific to M-IRF8KO^{LdlrKO}, displays their enrichment in processes surrounding apoptosis and inflammation. This suggests, IRF8-regulation of select apoptotic genes may be specific to the hyperlipidaemic environment of M-IRF8KO^{LdlrKO} mice. We then determined the pathways that were enriched across all differentially regulated genes in IRF8-KO and Bxh2 macrophages. Although, the Bxh2 mouse model used by both Langlais et al., 2016 and Mancino et al., 2015 are genetically the same, they both applied different parameters to generate a list of significantly regulated genes; Langlais et al., 2016 selected genes with a fold change>2 and p-value <10^{-5} whereas Mancino et al., 2015 selected genes with a fold change of >2 and p-value 0.05 For this reason, the number of differentially regulated IRF8-target genes reported are different between the two reports.

Comparisons of IRF8-target genes identified in M-IRF8KO^{LdlrKO} mice and the Bxh2 mice from Langlais et al., 2015 and Mancino et al., 2016, uncovered a total of 42 overlapping genes across all gene lists. Pathway analysis of the 42 overlapping genes, show significant regulation of genes involved in 'Inflammation' and 'External stimulus response' (**Fig 4.2.2**). All 42 overlapping genes were negatively regulated in the absence of IRF8, in macrophages from M-IRF8KO^{LdlrKO} mice and Bxh2 mice. This shows IRF8 regulation of select genes involved in inflammation does not differ based on the hyperlipidaemic environment of atherosclerosis prone mice, when compared to normolipidemic mice and in the different models of IRF8 reduction. The pathway analysis also uncovered a greater number of non-overlapping genes that shared functional similarities (**Fig 4.2.2 A**). This implies macrophage-IRF8 may regulate other functional processes, outside of inflammation, in both normolipidemic and

hyperlipidaemic environment. However, to enhance our understanding on the differential regulation of IRF8-target genes in response to a normolipidemic or hyperlipidaemic environment, additional studies comparing IRF8 gene regulation would be required in chow diet-fed M-IRF8KO^{LdlrKO} mice. Collectively, we have identified an anti-inflammatory transcriptional phenotype of IRF8KO^{LdlrKO} macrophages, from a hyperlipidaemic environment, which share similar transcriptional characteristics to other models of IRF8 reduction.

IRF8- reduction has been well characterised in enhancing susceptibility to infection within a normolipidemic environment, via impairment of myeloid inflammatory signalling pathways [121]. However, recent insight into the transcriptional differences in aortic macrophage subsets from western diet fed LDLR^{KO} mice, highlighted significant enrichment of IRF8 expression within an inflammatory subset of aortic macrophages that was only identified in atherosclerotic mice [78]. Using this information, we aimed to explore how the regulation of IRF8-target genes identified in M-IRF8KO^{LdlrKO} mice, compared to the aortic macrophage subsets from atherosclerotic LDLR^{KO} mice. Cochain et al, 2018 performed unsupervised clustering on the single-cell sequencing analysis from the aortic macrophages and identified two distinct subsets of aortic macrophages exclusively within atherosclerotic LDLR^{KO} mice. These included the inflammatory subset; highly enriched for inflammatory markers (Il1β, Nlrp3, Il1a) and trem2hi subset; highly enriched for the trem2 macrophage marker which is involved in phagocytosis and lipid metabolism [333] as well as regulating oxidative stress and lipid metabolism [78]. Interestingly, IRF8 was amongst the most enriched genes in the inflammatory (FC -2) and trem2hi (FC -1.8)

macrophage subsets. This proposes a potential role for IRF8 in the inflammatory and trem2hi aortic macrophage subsets.

To determine whether the number and regulation of IRF8-target genes, identified in M-IRF8KO^{LdlrKO} mice, differed in aortic macrophages, we performed comparative analysis amongst IRF8-KO, inflammatory and trem2hi macrophages. Intriguingly, we identified a large degree of functional overlap amongst the gene lists. This implies many IRF8-target genes share functional similarities in inflammatory and lipid associated macrophages that may contribute to atherosclerosis development. We also identified 22 downregulated IRF8 target genes that were significantly enriched in, resident-like, inflammatory and trem2hi macrophage subsets (**Fig 4.1.3**). This discovery implies IRF8 transcriptionally regulates select genes that are enriched within aortic macrophages from hyperlipidaemic mice. The negative regulation of pro-inflammatory genes in IRF8-KO macrophages, in comparison to inflammatory aortic macrophages further highlights the anti-inflammatory nature of IRF8-KO macrophages from an hyperlipidaemic environment.

4.4.2 IRF8 and chemotaxis

Chemotaxis is a crucial process in the development and progression of atherosclerosis. It involves the movement of leukocytes, including monocytes, along a chemical gradient, allowing for their adherence to the arterial wall and ultimate transmigration into the intima [48]. Many IRF8-target genes identified in the chemotaxis pathway are crucial in the development of atherosclerosis. Of the

top regulated genes, Ccl3 deficiency has been shown to prevent atherosclerosis progression via inhibition of neutrophil accumulation [334]. Enhanced expression of Ccl4, Ccl8 and Ccl12 have also been identified in the atherosclerotic plaques of mice and human, where they have been shown to promote leukocyte transmigration [335].

We became increasingly interested in the IRF8 regulated purinergic receptors; P2ry12, P2ry13 and P2ry14 since they have not previously been associated with IRF8 in an atherosclerosis context. These purinergic receptors have been well characterised for their role in reverse cholesterol transport, specifically within hepatocytes and endothelial cells. In an atherosclerotic environment, the lipid-free apolipoprotein A-1 (ApoA-I) binds to the ecto F1 ATPase, on endothelial cells, stimulating hydrolysis of ATP. The purinergic receptors are subsequently activated by the ADP generated, allowing for HDL transcytosis, involving cholesterol uptake, within the arterial intima and cholesterol efflux from foam cells via the activation of ABC cholesterol transporters [300], [336]–[338]. The released cholesterol is taken up by HDL and transported to the liver for removal. The hepatocyte purinergic receptors are also activated upon the generation of ADP, allowing for cytoskeleton reorganisation and subsequent uptake of HDL holoparticles. Therefore, the purinergic receptors; P2ry13, P2ry14, have been deemed as athero-protective and many studies have displayed their protection upon using global P2ry-KO mouse models fed a high fat western diet [300], [339], [340]. Interestingly, recent studies have identified a novel role for purinergic receptor signalling in macrophage migration in a spinal cord injury model [341]. Kobayakawa et al., 2019 had shown the importance of

IRF8-regulated purinergic signalling, by using a cocktail of inhibitors targeted towards all P2X and P2Y receptors. This work revealed the reduction in P2X/P2Y mediated macrophage migration along a C5a chemical gradient, was dependent on IRF8 expression [341]. This is amongst the first study to identify a crucial role of IRF8 in purinergic signalling, however, little information is currently known on the regulation of specific purinergic receptors by IRF8 within a hyperlipidaemic, atherosclerotic environment.

This thesis demonstrates IRF8 transcriptional regulation of P2ry12, Pry13 and P2ry14 and also identifies increased binding of IRF8 at a distinct site proximal to the promoter of both P2ry13 and P2ry14, in hyperlipidaemic mice. Our studies also show IRF8- reduction impairs the ability of macrophages to migrate towards the pro-atherosclerotic chemoattractant; MCP-1, by ~50%. Collectively, we have discovered myeloid-IRF8 reduction functionally impairs the migration of macrophages from a hyperlipidaemic environment, *in vitro*, via its regulation of key chemotactic ligands and purinergic receptors that are crucial for macrophage chemotaxis. This may also explain the reduced CD68+ cellular plaque content in M-IRF8KO^{LdlrKO} mice and raises the possibility that reduced macrophage migration, may contribute to the reduced atherosclerotic plaque development identified in M-IRF8KO^{LdlrKO} mice. Considering macrophage migration has currently been assessed *in vitro*, it would be necessary to confirm the reduced migratory capacity of IRF8-KO macrophages *in vivo* by recruitment of radiolabelled macrophages in the atherosclerotic plaque [58]. Additional investigation into the definitive role of purinergic receptor signalling and chemokines, using specific inhibitors [342], [343]to these receptors, would help

further clarify the mechanism by which myeloid-IRF8 reduction inhibits macrophage migration.

4.4.3 IRF8 and lipid metabolism

Alongside the regulation of inflammatory and chemotaxis-related pathways, genes involved in lipid metabolism where also amongst the most enriched (Enrichment ratio = 29) downregulated pathways in IRF8-KO macrophages (**Fig 4.1.2 D**). Dysregulated lipid metabolic processes are one of the key hallmarks for atherosclerosis progression and this study identifies a novel regulation of lipid metabolic gene expression by macrophage-IRF8 in hyperlipidaemic mice. Of the genes involved in 'Lipid metabolism', many are involved in the metabolism of cholesterol, including *Cyp27a1* and *Ch25h*, known to hydroxylate cholesterol at different carbon chains, resulting in the production of 27-hydroxycholesterol (27-HC) and 25-hydroxycholesterol (25-HC) respectively. Due to their high polarity, in comparison to cholesterol, they are much easily transferred across the phospholipid membrane and removed from macrophages [344]. They have also been implicated in impacting atherosclerotic plaque development by promoting inflammation via iNOS, and macrophage chemotaxis [69], [345]. Previous studies have demonstrated both 25-HC and 27-HC activate liver X receptors and promote macrophage cholesterol efflux via the ATP binding cassette transporters, ABCA1 and ABCG1 [346]. Other IRF8-regulated genes involved in lipid metabolism include, the purinergic receptors; *P2ry12, P2ry13, P2ry14* [336], [339], [347] and Lgmn, which suppresses oxLDL induced apoptosis of macrophages in atherosclerotic plaques, promoting plaque instability [348].

The ‘Lipid metabolism’ pathway encompasses genes that are involved in the promotion and reduction of atherosclerotic plaque development. To determine the overall impact of this differential gene expression on key lipid metabolic functions crucial to atherosclerotic plaque development, we assessed the generation of macrophage foam cells and cholesterol esters, *in vitro*, when challenged with acetylated LDL. Considering myeloid-IRF8 reduction retards atherosclerotic plaque development in M-IRF8KO^{LdlrKO} mice, we surprisingly identified a significant increase in foam cell formation of IRF8-KO macrophages in comparison to the WT^{LdlrKO} macrophages. This proposes, myeloid-IRF8 reduction increases the ability of macrophages to become foamy in response to acLDL. Interestingly, recent studies by Kim et al., 2018, uncovered an enriched anti-inflammatory gene signature in foamy aortic macrophages from western diet-fed LDLR^{KO} mice, in comparison to non-foamy aortic macrophages [79]. Interestingly, we also identified a decreased inflammatory gene signature in the BMDMs from M-IRF8KO^{LdlrKO} mice (**Fig 4.1.3**). When challenged with acLDL *in vitro,* there was a significant increase in foam cell formation in IRF8-KO macrophages in comparison to controls. However, to confirm this in aortic plaque macrophages it would be necessary to stain aortic plaques with oil-red-o to identify differences in plaque macrophage foam cell formation. Based on this information, we aimed to determine how the regulation of IRF8-target genes in M-IRF8KO^{LdlrKO} macrophages compared to foamy macrophages in hyperlipidaemic LDLR^{KO} mice [79]. Interestingly, we identified IRF8 differentially regulates genes enriched within foamy aortic macrophages, in particular those involved in ‘Inflammation’ and ‘Lipid metabolism’ (**Fig 4.2.4**). The differential

regulation of these IRF8-target genes may, therefore, contribute to the increased foam cell formation, identified in acLDL treated IRF8-KO macrophages (**Fig 4.1.5 F**).

The cholesterol ester content of foamy macrophages is another important indicator of cellular cholesterol content and is often measured when assessing foam cell formation. Foam cells are generated upon the uptake of modified lipoproteins via cell-surface scavenger receptors, CD36 and SR-A. The cholesterol ester associated with ingested lipoproteins is hydrolysed by lysosomal acid lipase to form free cholesterol. The free cholesterol is then re-esterified by the enzyme ACAT1 to form cholesterol esters which are stored in lipid droplets, resulting in macrophage foam cell formation [38], [162]. Therefore increased macrophage cholesterol ester content is generally associated with increased foam cell formation [349]. While the IRF8-KO macrophages display significantly increased foam cell formation, they show no difference in cholesterol ester content when compared to WT^{LdlrKO} macrophages. This may be due to the expression of other lipid metabolism related genes regulated by IRF8, known to promote cholesterol uptake, including Sortillin-1 (FC 2.5) [286]. It is possible that during in vitro cell culture, these genes may have a larger net impact as the number of macrophages used per condition and genotype are the same, in comparison to *in vivo* where we have identified fewer aortic plaque CD68+ macrophages.

Many IRF8-target genes involved in lipid metabolism are crucial in macrophage cholesterol uptake, efflux and metabolism - processes that are critical in atherosclerosis plaque development. We identified IRF8-regulation of

the fatty acid binding proteins which are known for their role contribution to macrophage foam cell formation in atherosclerosis. The fatty acid binding proteins; Fabp3, Fabp4 and Fabp5, function as intracellular lipid chaperones that bind saturated and unsaturated long chain fatty acids and facilitate their transport [350]. Recent studies displayed inhibition of Fabp4 inhibits macrophage foam cell formation, therefore reducing atherosclerotic plaque development, as shown in table 5 [307]. For this reason, Fabp inhibition has been deemed an attractive therapeutic target in the prevention of atherosclerosis. However, inhibition studies indicate global-Fabp4/5 inhibition can promote the levels of circulating free-fatty acids due to decreased hepatic uptake and metabolism [308].

Gene	Inhibitor	Outcome	Role in atherosclerosis	Reference
Fabp4	8g (Synthetic small molecule inhibitor)	Reduced macrophage foam cell formation ↓	Inhibitor reduces atherosclerosis ↓	[307]
		Reduced cholesterol ester content ↓		
		Reduced inflammation ↓		
	Genetic macrophage deletion	Increased cholesterol efflux ↑	Inhibitor reduces atherosclerosis ↓	[310], [311]
		Decreased inflammation ↓		
Fabp5		Increased serum expression in atherosclerosis ↑	Biomarker of increased atherosclerosis ↑	[305]
Fabp4 and Fabp5	BMS-309403	Reduced plasma triglycerides ↓	Inhibitor reduces atherosclerosis ↓	[312], [351]
		Reduced foam cell formation ↓		
		Inhibits macrophage MCP-1 release ↓		
		Reduced inflammation ↓		

Table 5. Summary of fatty acid binding proteins implicated in atherosclerosis

We investigated whether IRF8 regulates the athero-protective properties of Fabp4/5 inhibition in IRF8-KO macrophages from M-IRF8KO^{LdlrKO} mice. This may potentially provide an insight into the mechanism by which IRF8 reduction reduces atherosclerotic plaque burden in M-IRF8KO^{LdlrKO} mice. We used the selective, cell permeable Fabp4/5 inhibitor, BMS-309403, that interacts with the

fatty-acid-binding pocket within the interior of the protein, competitively inhibiting binding of endogenous fatty acids. Interestingly, we observed a significant decrease in foam cell formation when using 25μM of BMS-309403 only in the WT^{LdlrKO} macrophages. This was mirrored by macrophage cholesterol ester content that was reduced upon increasing concentration of BMS-309403. This suggests IRF8-regulation of Fabp4 and Fabp5 may contribute to the athero-protective phenotype of myeloid-IRF8 reduction (summarised in **Fig 4.4**).

Alongside inflammation and lipid metabolism, Fabp4 and Fabp5 inhibition is also known to impact on the expression of chemoattractant MCP-1. We therefore interrogated whether inhibition of Fabp4 and Fabp5 impacted on the impaired migratory phenotype of IRF8-KO macrophages. We identified increasing concentrations of BMS-309403 reduced the migratory ability of WT^{LdlrKO} but not IRF8-KO macrophages towards MCP-1 (**Fig 4.1.6 E**). This decreased migratory phenotype of WT^{LdlrKO} macrophages remained with the addition of acLDL, while IRF8-KO macrophages displayed no difference in macrophage migration under these conditions. This highlights a role for Fabp4/5 inhibition in negatively regulating macrophage migration, that is dependent upon IRF8. Considering MCP-1 gene expression is not dependent on IRF8, it is possible that Fabp4/5 regulation of macrophage migration, to the atherosclerotic plaque, occurs by impacting on chemokines regulated by IRF8, including *Ccl3* [334]*, Cxcl10* [327]*, P2ry13 or P2ry14* [341] that have not yet been identified as genes affected by Fabp4/5 inhibition.

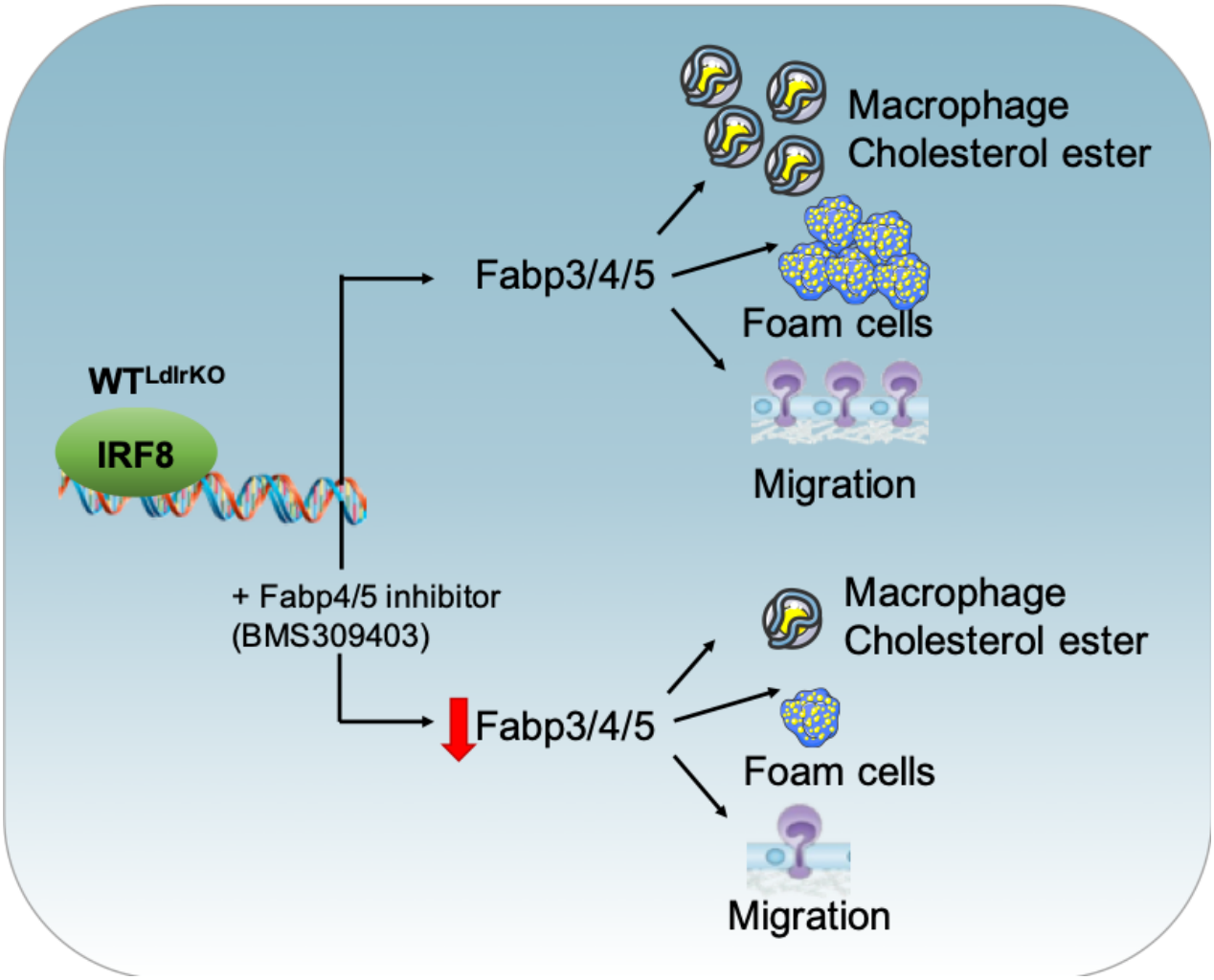

Fig 4.4 Schematic demonstrating the athero-protective benefits of Fabp4/5 inhibition are dependent on IRF8 expression.
Expression of Fabp3,4 & 5 (Top) promote macrophage cholesterol ester content, foam cell formation and migration. Whereas, inhibition (bottom) using the BMS309403 inhibitor, prevents macrophage cholesterol ester content, foam cell formation and macrophage migration.

Collectively, we have identified IRF8-regulation of 'Inflammatory', 'Chemotaxis' and 'Lipid-mediated' pathways that may all contribute to the athero-protective mechanism of myeloid-IRF8 reduction. We have also shown the athero-protective properties of Fabp4/5 inhibition are dependent upon IRF8 expression. Overall this implies IRF8 reduction may prevent the development of atherosclerosis via its transcriptional regulation of pro-chemotactic and lipid-

metabolic genes that are crucial for atherosclerosis promoting processes including; macrophage migration, foam cell formation and cholesterol ester content.

Chapter 5: Results - IRF8 regulates macrophage responses to IFNβ in an atherosclerotic environment

5.1 Introduction

Type 1 interferon (IFN) signalling (IFNα and IFNβ) has been well characterised for its role in host defence against viral infection [352]–[354]. Recent evidence uncovering a type-1 IFN signature amongst inflammatory disorders, including atherosclerosis, has prompted our investigation into the role of type 1 IFNs in atherosclerosis. Previous reports have shown type 1 IFNs to promote atherosclerosis and increase cardiovascular risk in systemic lupus erythematous patients, by inducing endothelial dysfunction, which was reversed upon silencing the type 1 IFN receptor [355]. IFNβ has emerged as an important regulator of inflammation and atherosclerosis, and has been studied to a greater extent, in the context of atherosclerosis, in comparison to other type 1 IFNs, such as IFNα [169]. Previous studies have demonstrated the crucial role of IFNβ in promoting TNF and IL-6-induced inflammation both of which are known to contribute to atherosclerosis development [356], [357]. Goossens et al, 2010, demonstrated an increase in IFNβ promotes atherosclerosis development upon enhanced macrophage recruitment and adhesion to atherosclerotic lesions via increased CCL5/CCR5 and MCP-1/CCR2 signalling [169]. This study also complemented reports demonstrating unstable human atherosclerotic plaques, that were prone to rupture, displayed increased expression of type-1 IFN induced interferon stimulated genes, due to an increase in IFN-signalling[169]. This highlights the importance of IFNβ signalling in atherosclerotic plaque development across both mouse and human studies.

The type 1 IFN signalling pathway regulates a selection of genes known to form an IFN signature, as described below [358]. This signature includes a host of interferon stimulated genes (ISGs) that actively promote inflammation, predominantly via IFN binding to the IFN receptor and subsequent activation of the JAK/STAT pathway. Activation of STAT1 and STAT2 are known to form heterodimeric complexes with IRF3 and IRF9, forming transcriptional activators [134], [359]. These transcriptional activators bind and regulate a selection of interferon associated genes (*Ifit1, Ifit2, Trem1, Mmp14, Ccl2, Ccl3*), that contribute to the interferon-mediated inflammatory response [138].

IRF8 has been shown to promote the production of type I IFNs in models of infectious Newcastle Lyme disease as well as in monocytes from healthy human adults [141]. Although Mancino and colleagues have uncovered differential IFNβ signalling in macrophages [86], little is known regarding the role of IRF8 in IFNβ signalling in an atherosclerotic environment.

IRF8 and IFNβ individually display an important role in atherosclerosis development [169], [175], [177]. The focus of this chapter is to understand how myeloid-IRF8 influences IFNβ regulated gene expression in BMDMs from hyperlipidaemic WT^{LdlrKO} and M-$IRF8KO^{LdlrKO}$ mice by comparing IFNβ-stimulated differentially regulated genes, as demonstrated in **Fig 5.1**.

This chapter aims to determine:

1. The impact of myeloid-IRF8 reduction on macrophage IFNβ signalling by identifying IRF8 target genes and pathways that are induced/repressed by IFNβ. To determine this bone marrow derived macrophages from western

diet-fed WT^{LdlrKO} and M-$IRF8KO^{LdlrKO}$ (n=3/group) were stimulated with 10ng IFNβ for 6hrs after of which the RNA was extracted and used for RNA-Sequencing.

2. Upon performing pathway analysis on the differentially regulated IRF8-target genes that have been identified in Aim 1, I aim to investigate the pathways that have been induced/repressed by IFNβ in M-$IRFK8KO^{LdlKO}$ BMDMs, when compared to WT^{LdlrKO}, that may be used as future therapeutic targets.

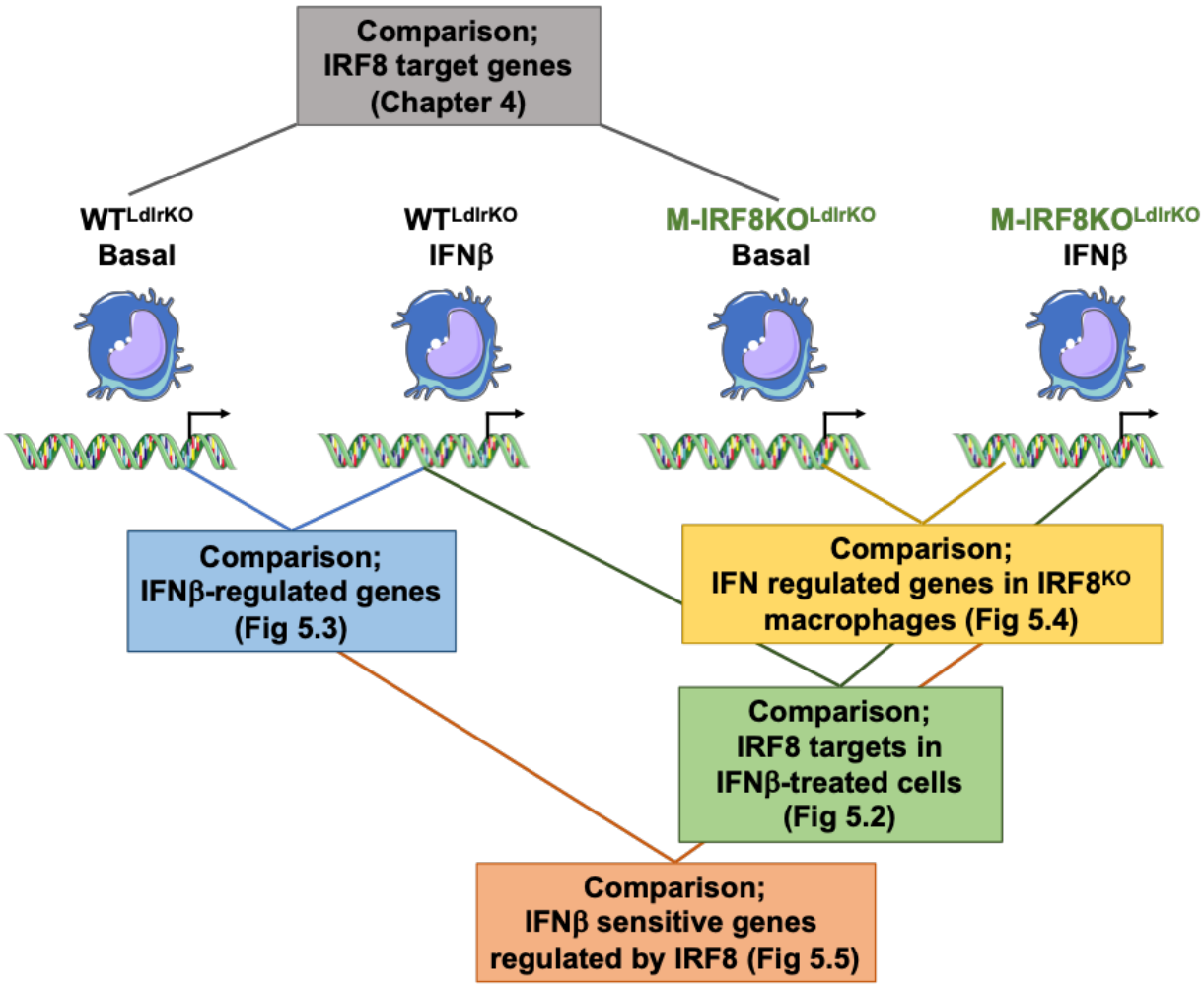

Fig 5.1 Summary of RNA-seq comparisons between untreated and IFNβ treated WT^{LdlrKO} and M-IRF8KO^{LdlrKO} transcriptomes.
Differential gene expression was assessed between; untreated WT macrophages and IFNβ treated WT macrophages (Fig 5.3 – blue), untreated IRF8-KO macrophages and IFNβ treated IRF8-KO macrophages (Fig 5.4 - yellow), IFNβ treated WT and IFNβ treated IRF8-KO macrophages (Fig 5.2 – green) and IFNβ sensitive genes regulated by IRF8 (Fig 5.5 – orange).

5.2 IRF8 differentially regulates macrophage response to IFNβ

To understand the effect of myeloid-IRF8 reduction on IFNβ signalling we compared genes that were differentially regulated in IRF8-KO macrophages in comparison to WT^{LdlrKO} macrophages, when treated with 10ng IFNβ for 6hrs. We generated a list of differentially regulated genes, using the same parameters as previously discussed in the analysis of untreated BMDMs from M-$IRF8KO^{LdlrKO}$ macrophages (Chapter 4) (FDR = 0.05, FC = 1.3) to keep uniformity amongst comparison parameters. We identified a total of 373 differentially regulated genes, in response to IFNβ treatment, in macrophages from M-$IRF8KO^{LdlrKO}$ mice when compared to IFNβ-treated WT^{LdlrKO} macrophages. This is demonstrated in the volcano plot (**Fig 5.2 A)** and in the heatmap where the degree of differential regulation is highlighted amongst samples (**Fig 5.2 B**). To explore the biological pathways enriched within the gene set, we performed pathway analysis on the differentially regulated genes. 'Leukocyte chemotaxis' (**Fig 5.2 C**) was identified as the most significant upregulated pathways ($Log_{10}P$ = -7.9) and TGF-beta signalling as the most significant downregulated pathway ($Log_{10}P$ = -5.8) (**Fig 5.2 D**). This reveals IFNβ treatment reverses the positive regulation of IRF8-target genes involved in chemotaxis, as previously identified in untreated macrophages (**Fig 4.1.4**). This is also highlighted in the clustergraph with the corresponding heatmap, where certain chemotaxis-related genes (*Ccl12, Ccl22, Tnfsf14)* that were previously downregulated in $IRF8KO^{LdlrKO}$ macrophages are now significantly upregulated (**Fig 4.1.4 E**).

Overall, we have demonstrated myeloid-IRF8 reduction alters the macrophage transcriptome in response to IFNβ stimulation, as demonstrated by the 373 differentially regulated genes in IFNβ-treated IRF8-KO macrophages, in comparison to IFNβ-treated WT cells. We have uncovered a series of IFNβ inducible pathways that are positively regulated by IRF8, including 'Chemotaxis', 'ABC transport' and 'GAP-junction formation'. As these processes have not been previously associated with IFNβ stimulation, this work implies that IRF8 reduction may alter cellular response to IFNβ in hyperlipidaemic mice which may contribute to atherosclerosis development.

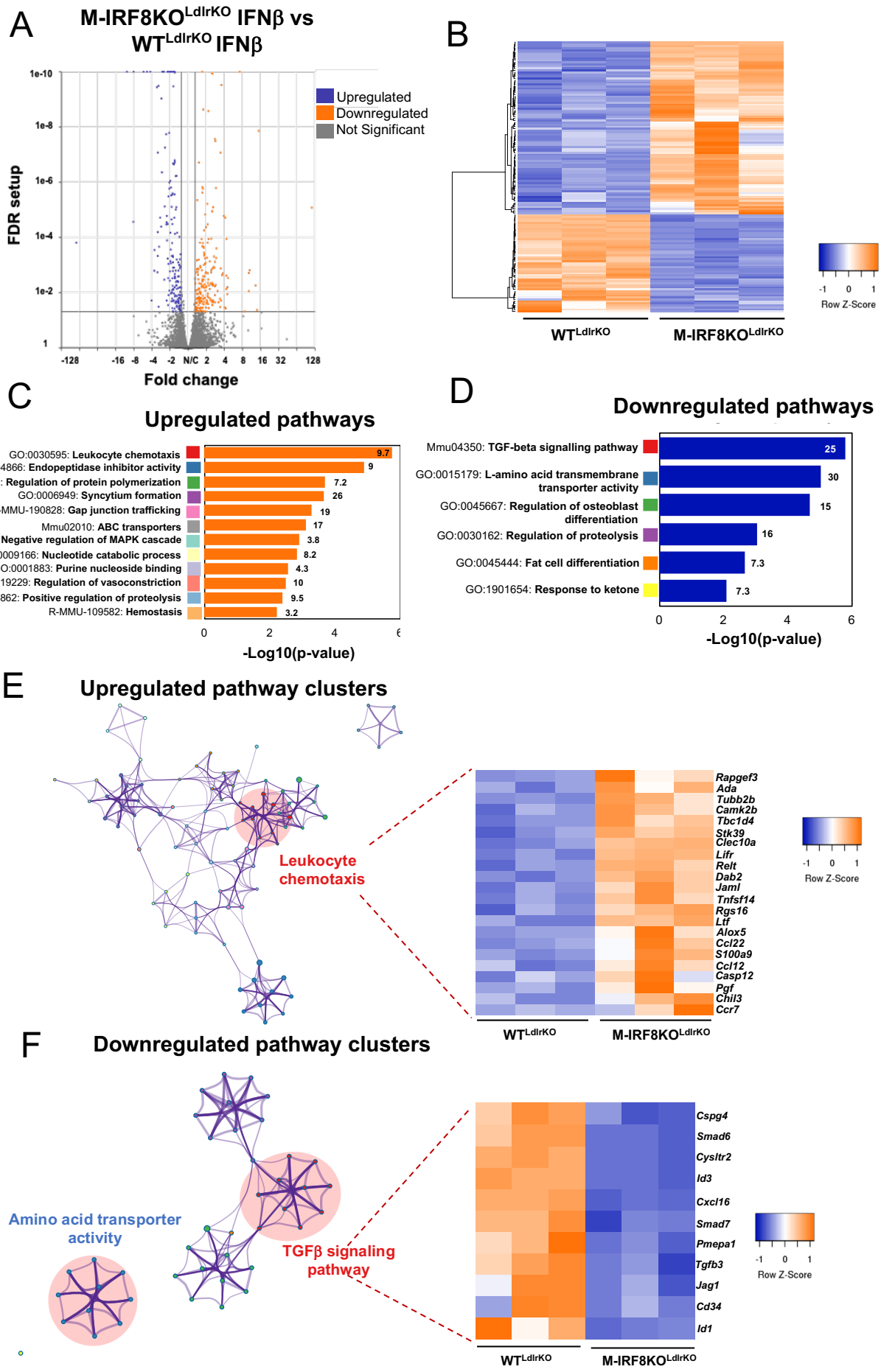

Figure legend on next page

Fig 5.2 IRF8-reduction alters macrophage response to IFNβ stimulation in a hyperlipidaemic environment.
(A) Volcano plot of fold change vs. P.value of differentially expressed genes comparing 12-wk-old, Western diet-fed M-IRF8KO^{LdlrKO} and WT^{LdlrKO} BMDMs (n = 3/group). The grey line indicates an adjusted P value threshold of 0.05 (Wald test for logistic regression). (B) Clustered heatmap of RNA-seq normalised gene counts in Western diet-fed macrophages (n = 3/group). Gene set enrichment analysis demonstrating the most significant (C) upregulated and (D) downregulated pathways of genes differentially regulated by myeloid-IRF8 reduction with their corresponding enrichment score at the end of each bar. Pathway enrichment network visualisation showing the intra-cluster and inter-cluster similarities of enriched terms for (E) upregulated and (F) downregulated pathways. Novel atherosclerosis specific IRF8 regulated pathways, in response to IFNβ treatment, when compared to WT^{LdlrKO}, are highlighted in light pink, where the degree of regulation in the most significant differentially regulated pathway is further highlighted in the corresponding heatmap, showing normalized gene counts. Remaining cluster annotations are shown in colour code on the upregulated and downregulated pathway analysis bar chart. Pathway analysis and enrichment visualisation was performed using Metascape. Data presented are Linear fold change 1.3, FDR 0.05, p<0.01.

5.3 IFNβ stimulated macrophages from hyperlipidaemic WT^{LdlrKO} mice are pro-inflammatory

To determine the impact of IFNβ stimulation on the gene expression of WT^{LdlrKO} macrophages, from a hyperlipidaemic environment, we compared the differentially regulated genes identified in IFNβ treated WT^{LdlrKO} macrophages to untreated WT^{LdlrKO} macrophages. Altogether we identified 1923 differentially regulated genes in response to IFNβ stimulation in WT^{LdlrKO} macrophages, when compared to untreated BMDMs, as highlighted in both the volcano plot and heatmap (**Fig 5.3 A & B**). We identified 1000 upregulated genes in response to IFNβ treatment that were significantly enriched in pathways including 'Inflammation' ($Log_{10}P$ = -20) and 'Response to IFN' ($Log_{10}P$ = -33) (**Fig 5.3 C**). This implies IFNβ treatment significantly induces inflammatory response pathways in macrophages from a hyperlipidaemic environment.

We also identified 923 downregulated genes in IFNβ stimulated WT^{LdlrKO} macrophages, that were significantly associated with 'Cholesterol biosynthesis' ($Log_{10}P$ = -7.8) and "Fatty acid metabolism' ($Log_{10}P$ = -7.2) (**Fig 5.3 D**). This

suggests, IFNβ may have a role in defective macrophage cholesterol metabolism in atherosclerosis, by negatively regulating genes crucial for atherosclerosis-related lipid metabolic processes [313], [360].

To determine the degree of overlap between genes in different significantly regulated pathways, a clustergraph was produced using Metascape. The upregulated clustergraph displays a clear overlap in genes involved in 'IFN response', 'Cell adhesion' and 'Cytokine production', as demonstrated by the purple interconnecting lines between the different coloured nodes. This implies, genes upregulated in response to IFNβ are involved in multiple processes surrounding cell defence (**Fig 5.3 E**). However, the genes involved in each downregulated pathway do not appear to overlap with many other pathways, as demonstrated by the disparate clustering of each coloured tree with few purple interconnecting lines between the nodes (**Fig 5.3 F**). This suggests, genes downregulated in response to IFNβ treatment are enriched in singular pathways. This provides insight into the IFNβ-negatively regulated signalling pathways that may contribute to atherosclerosis progression with the potential for future investigation as a therapeutic target.

To summarise, we have demonstrated IFNβ treatment promotes the expression of genes involved in pro-inflammatory and defence response pathways in macrophages from a hyperlipidaemic environment. Alongside this, we have identified a role for IFNβ in negatively regulating genes involved in lipid metabolism and transport, many of which are known to protect against atherosclerosis development [307], [361]. Collectively this suggests that IFNβ

treatment transcriptionally reprograms macrophages, from a hyperlipidaemic environment, to become more inflammatory and less responsive to lipid metabolism and transport.

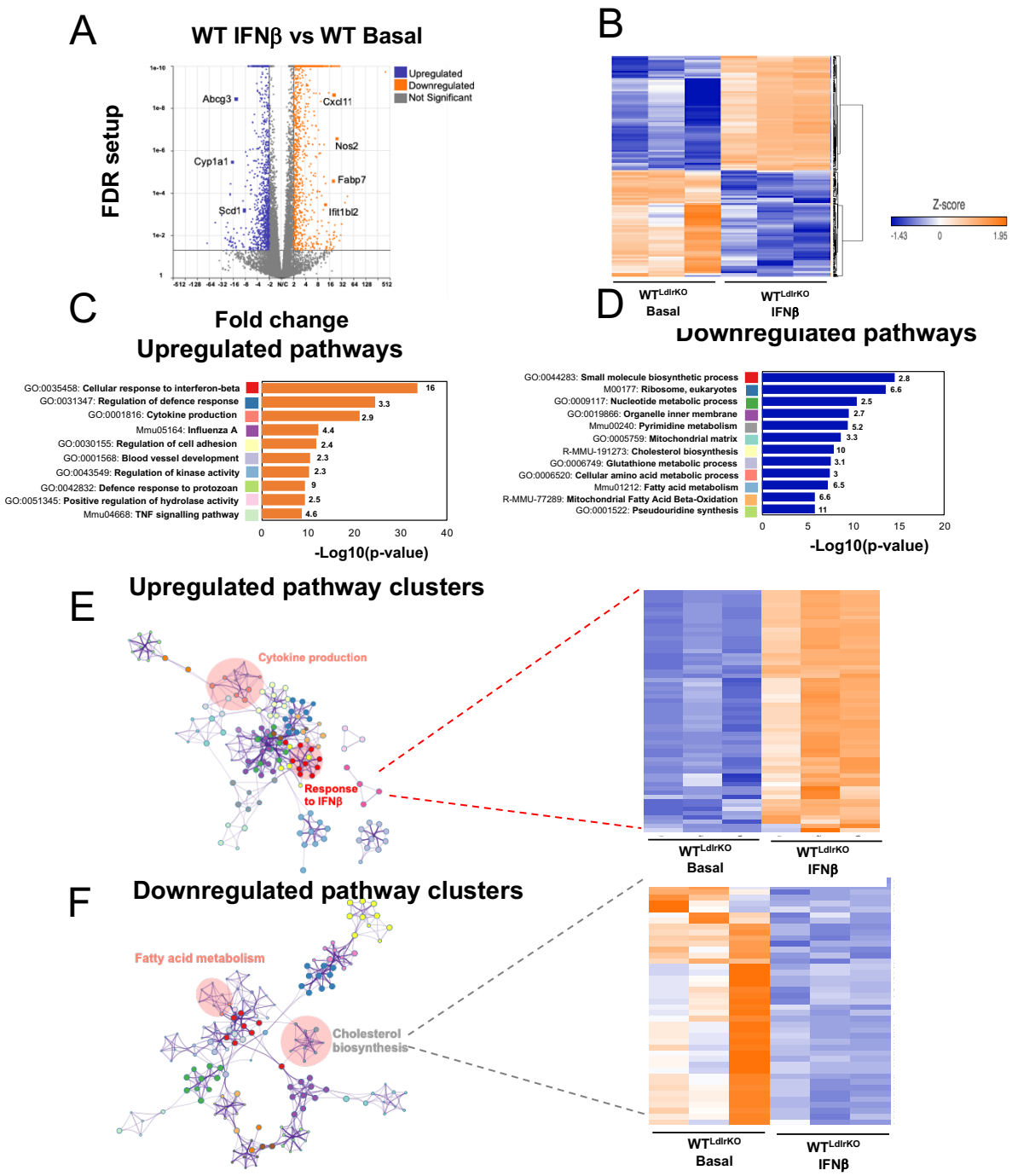

Fig 5.3 IFNβ–stimulated WT^{LdlrKO} macrophages are more inflammatory and less responsive to lipid-metabolic processes in hyperlipidaemic mice.
(A) Volcano plot of fold change vs. P.value of differentially expressed genes comparing 12-wk-old, Western diet-fed WT^{LdlrKO} BMDMs challenged with or without 10ng IFNβ (n = 3/group). The grey line indicates an adjusted P value threshold of 0.05 (Wald test for logistic regression). (B) Clustered heat map of RNA-seq normalised gene counts in Western diet-fed macrophages (n = 3/group). Gene set enrichment-analysis demonstrating the most significant (C) upregulated and (D) downregulated pathways of genes differentially regulated by IFNβ stimulation with their corresponding enrichment score at the end of each bar. Pathway enrichment network visualisation showing the intra-cluster and inter-cluster similarities of enriched terms for (E) upregulated and (F) downregulated pathways. The most significant and enriched pathways are highlighted in light pink, where the degree of gene regulation in the most significant differentially regulated pathway is highlighted in the attached clustered heatmap of the RNA-seq normalized gene counts. Remaining cluster annotations are shown in colour code on the upregulated and downregulated pathway analysis bar chart. Pathway analysis and enrichment visualisation was performed using Metascape. Data presented are Linear fold change 1.3, FDR 0.05, p<0.01.

5.4 Myeloid-IRF8 reduction promotes IFNβ stimulation of pro-apoptotic genes whilst negatively regulating fatty acid biosynthesis

Upon identifying differentially regulated pathways in response to IFNβ in WT^{LdlrKO} macrophages from a hyperlipidaemic environment, we next investigated whether the response to IFNβ in hyperlipidaemic IRF8-KO macrophages was any different. We analysed the differentially regulated genes identified in IFNβ-treated IRF8-KO macrophages when compared to basal IRF8-KO macrophages. RNA-seq analysis identified 1698 genes were differentially regulated in IFNβ-treated IRF8-KO macrophages, in comparison to untreated IRF8-KO macrophages (**Fig 5.4 A & B**). Although the number of genes induced by IFNβ-stimulation in IRF8-KO macrophages was similar to WT^{LdlrKO} macrophages (983 in IRF8-KO vs 1000 in WT^{LdlrKO}), slightly fewer where repressed in IRF8-KO macrophages (784 repressed in IRF8-KO vs 923 in WT^{LdlrKO}), as shown in the heatmap. This shows IRF8 is specifically required for the induction of 139 genes in response to IFNβ, in macrophages from western diet-fed mice that may also contribute to the previously identified IFNβ-induced pro-atherogenic phenotype [169].

Pathway analysis demonstrated 'Response to IFNβ' ($Log_{10}P = -37.8$) was the most significantly upregulated pathway, similarly to that identified in IFNβ treated WT^{LdlrKO} macrophages (**Fig 5.4**). This implies the genes involved in 'IFNβ response' that are differentially regulated in response to IFNβ, may not be dependent on IRF8 expression. 'Cell death' (*Casp1, Casp2, Casp3, Bcl-2*) was also amongst the most upregulated ($Log_{10}P = -10$) pathway (**Fig 5.4 C & E**), suggesting IRF8 may regulate IFNβ-stimulation of macrophage cell death in a

hyperlipidaemic environment. In comparison, IFNβ treatment significantly downregulates genes involved in the 'RNA metabolic processes' (*Rps14, Rps15, Rps16, Rcl-1*) ($Log_{10}P = -19.7$) and 'Fatty acid biosynthesis' (*Acat1, Acat2, Acat3, Abcd1*) ($Log_{10}P = -4.8$) (**Fig 5.4 D**). This shows, IFNβ treatment induces pathways associated with cell death, preferentially in the absence of IRF8, in hyperlipidaemic mice. Whereas, IFNβ treatment represses genes associated with pathways that are involved in RNA and fatty acid metabolism, in macrophages from both WT^{LdlrKO} (**Fig 5.3 D & F**) and M-$IRF8KO^{LdlrKO}$ mice (**Fig 5.4 D & F**). This suggests IRF8 regulates IFNβ inducible genes involved in cell death and lipid metabolic-related processes that may contribute to the role of IFNβ in atherosclerosis development.

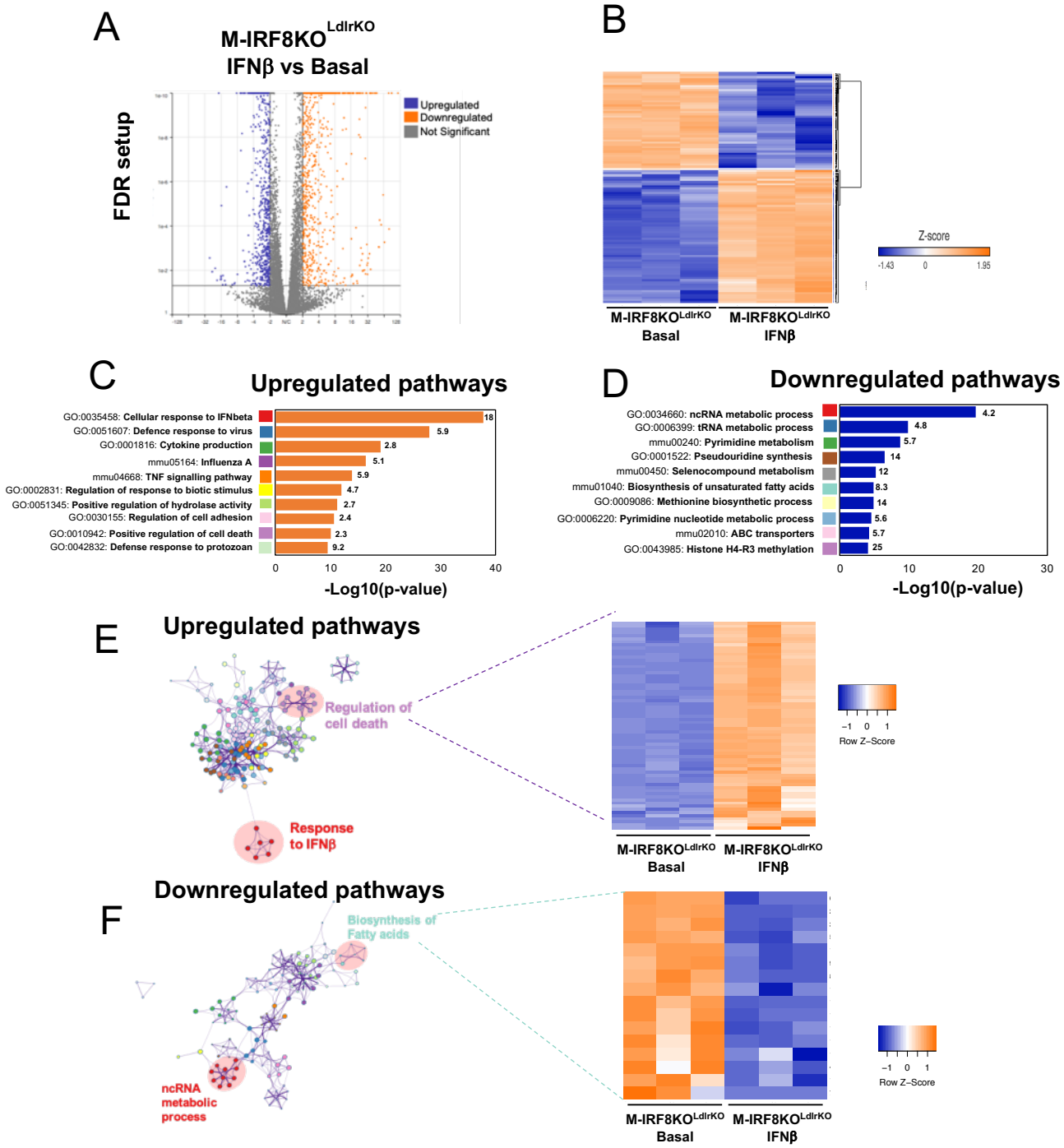

Fig 5.4 IFNβ differentially regulates 'Cell death' and 'Fatty acid' related genes in the absence of IRF8.

(A) Volcano plot of fold change vs. P value of differentially expressed genes comparing 12wk old, Western diet-fed M-IRF8KO^{LdlrKO} BMDMs challenged with or without IFNβ (n=3/group). The grey line indicates an adjusted P value threshold of 0.05 (Wald test for logistic regression). (B) Clustered heatmap of RNA-seq normalised gene counts in Western diet-fed macrophages (n=3/group). Gene set enrichment analysis demonstrating the most significant (C) upregulated and (D) downregulated pathways of genes differentially regulated by IFNβ with their corresponding enrichment score at the end of each bar. Pathway enrichment network visualisation showing the intra-cluster and inter-cluster similarities of enriched terms for (E) upregulated and (F) downregulated pathways. The most significant and enriched pathways are highlighted in light pink, where the degree of gene regulation, for that pathway, is highlighted in the attached clustered heatmap of the RNA-seq normalized gene counts. Remaining cluster annotations are shown in colour code on the upregulated and downregulated pathway analysis bar chart. Pathway analysis and enrichment visualisation was performed using Metascape Data presented are Linear fold change 1.3, FDR 0.05, p<0.01.

5.5 IFNβ regulation of lipid metabolism, chemotaxis and apoptosis related genes is dependent on IRF8

Thus far, we have identified genes and pathways that are differentially regulated in response to IFNβ treatment and myeloid-IRF8 reduction. To better understand the pathways associated with genes that are dependent on IRF8-expression and differentially regulated in response to IFNβ treatment, comparisons were performed on the list of differentially regulated genes in IFNβ treated WT^{LdlrKO} (1923 genes – **Fig 5.3**) and IFNβ-treated IRF8-KO (1698 genes – **Fig 5.4**) macrophages.

In total, we uncovered 1036 genes that were not dependant on IRF8 expression, as they were regulated in both IFNβ-treated WT^{LdlrKO} and IRF8-KO macrophages, when compared to untreated macrophages (**Fig 5.5 A**). Pathway analysis on the 1036 overlapping genes, demonstrated significant enrichment of processes including; 'Response to IFNβ' ($Log_{10}P$ = -33), 'Response to virus' ($Log_{10}P$ = -27) and 'Cytokine production' ($Log_{10}P$ = -12) (**Fig 5.5 C**). The increased significance of these pathways is further demonstrated in the heatmap of significance in **Fig 5.5 E**. This implies IRF8 does not regulate IFNβ-induced pathways involved in inflammation and defence response, in hyperlipidaemic mice. Alternatively, we identified a number of genes differentially regulated in response to IFNβ treatment that were either regulated in response to IRF8 expression (887 genes), or in the absence of IRF8 expression (667 genes), with the most significant genes highlighted in the Venn diagram (**Fig 5.5 A**).

Pathway analysis revealed genes regulated by IFNβ treatment preferentially in IRF8-KO macrophages, were highly enriched in processes surrounding 'Leukocyte migration' ($Log_{10}P$ = -5.8), 'Cell death' ($Log_{10}P$ = -5.8) and 'Cell adhesion' ($Log_{10}P$ = -4.9) (**Fig 5.5 B**), with the top regulated genes included on the Venn (**Fig 5.5 A**). This supports previous studies demonstrating the importance of IFNβ in modulating monocyte cell migration and promoting FasL mediated cell death in dendritic cells and thyroid follicular cells [165], [167]. However, this study is the first to suggest IFNβ regulation of these processes is negatively regulated by IRF8, in macrophages from western diet-fed mice.

In comparison, the 887 genes differentially regulated in response to IFNβ treatment that were dependent on IRF8 expression, as identified preferentially in WT^{LdlrKO} macrophages, where highly enriched in processes including; 'Cholesterol biosynthesis' ($Log_{10}P$ = -7), 'Small molecule metabolism' ($Log_{10}P$ = -9.6) and 'Lipid metabolism' ($Log_{10}P$ = -5) (**Fig 5.5 D**). This suggests, IRF8 regulates pathways associated with cholesterol biosynthesis and metabolism, that are enriched in response to IFNβ-treatment, in macrophages from western diet-fed mice.

Collectively, we have identified IFNβ treatment modulates many pathways independently of IRF8 and the significance of these pathways is highlighted in the 'Significant pathways heatmap' (**Fig 5.5 E**). The clustergraphs represent the overlap of genes present within each pathway (**Fig 5.5 F**) where the proportion of genes from each gene list is presented as a slice of the pie chart in each node (Blue = WT^{LdlrKO} IFNβ vs basal and red = M-$IRF8KO^{LdlrKO}$ IFNβ vs basal). The

blue highlighted cluster represents small molecule processes and the purple highlighted cluster represents amino acid metabolism (**Fig 5.5 G**).

Altogether this data demonstrates, IRF8 significantly regulates the following pathways; 'Cholesterol Biosynthesis', 'Lipid metabolism', 'Migration' and 'Apoptosis', in response to IFNβ treatment in western diet-fed mice. These pathways are pivotal in the development and progression of the atherosclerotic plaque [38], [52], [162], [362]. Their differential regulation by IRF8 in response to IFNβ, has increased our understanding of IRF8-IFNβ signalling pathways that are enriched in macrophages from an atherosclerosis-prone environment.

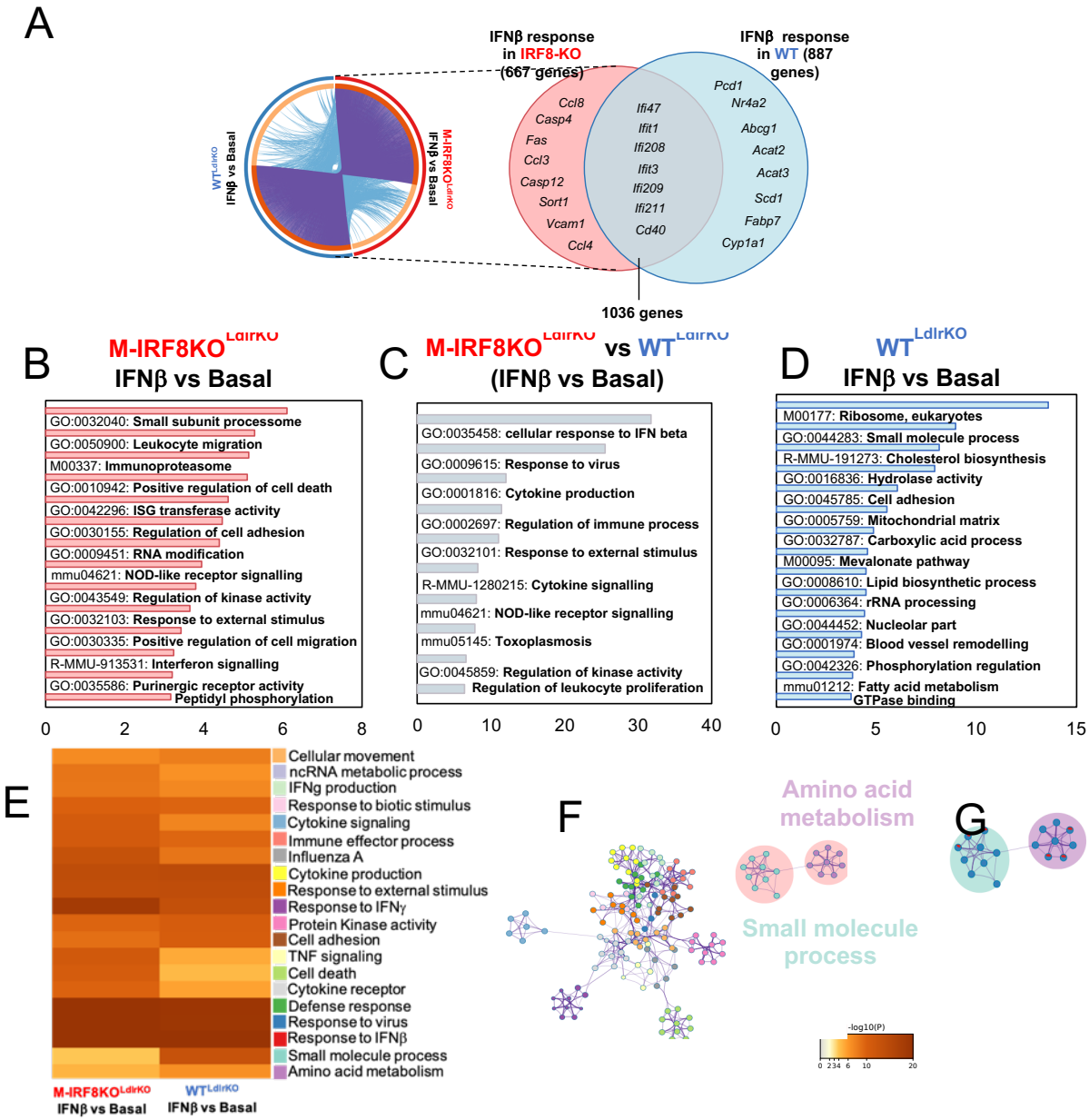

Fig 5.5 IFNβ-induction of genes involved in 'Cholesterol metabolism', 'Apoptosis' and 'Migration' are regulated by IRF8.

(A) Circos plot highlighting the overlap of differentially regulated genes (purple lines) identified in Western diet-fed WT^{LdlrKO} BMDMs stimulated with 10ng IFNβ for 6hrs and IRF8-KO BMDMs stimulated with 10ng IFNβ for 6hrs. The purple lines connect overlapping genes across each dataset and blues lines connect the different genes that fall into the same ontology. The corresponding Venn diagram highlights the number of overlapping genes from both input gene lists. Gene set enrichment analysis highlighting the most significantly enriched pathways of genes differentially regulated solely in (B) IFNβ stimulated IRF8-KO macrophages (667 genes), genes differentially regulated in (C) both IRF8-KO and WT^{LdlrKO} macrophages (1036 genes) and genes differentially regulated solely in (D) IFNβ stimulated WT^{LdlrKO} macrophages (887 genes). (E) Clustered heatmap of significance displaying the most statistically enriched pathways across all genes in both lists. (F) Pathway enrichment network visualisation showing the intra-cluster and inter-cluster similarities of enriched terms across both lists. Pathways with a proportion of differentially regulated genes in both lists are highlighted in light pink. Remaining cluster annotations are shown in colour code on the (E) 'Significant pathways' heatmap. (G) The same enrichment network where nodes display the proportion of genes from each gene list within that specific pathway node. Color code for pie sector; blue = IFNβ stimulated WT^{LdlrKO} macrophages, red = IFNβ stimulated IRF8-KO macrophages. Pathway analysis and enrichment visualisation was performed using Metascape. Data presented are Linear fold change 1.3, FDR 0.05, $p<0.01$.

5.6 Myeloid-IRF8 reduction transcriptionally reprograms macrophage response to IFNβ stimulation

In total, the RNA-sequencing performed on IFNβ-stimulated BMDMs from western diet-fed mice uncovered over 4000 IRF8-target genes that were differentially regulated in response to IFNβ stimulation in WT and IRF8-KO macrophages (**Fig 5.6.1**). Hierarchical clustering of normalised gene counts identified four distinct clusters of genes (**clusters A-D**) that are differentially regulated by IRF8 and/or IFNβ–treatment. To understand the biological pathways enriched amongst the differentially regulated genes, pathway analysis was performed on the genes in each cluster.

Genes that are downregulated in response to IFNβ, in the absence of IRF8, are highlighted in cluster A of the heatmap. The top GO term associated with these genes include 'Aminoacyl tRNA biosynthetic processes' that is crucial for protein translation. In this pathway, *Cxcr4* and *Il-17ra* were the most significant and are known to contribute to atherosclerosis via promoting endothelial cell integrity and leukocyte migration respectively [363], [364]. Altogether, this demonstrates genes involved in protein translation are differentially regulated by IRF8 in response to IFNβ-treatment. When stimulated with IFNβ, genes involved in protein translation are significantly downregulated in IRF8-KO macrophages. This implies, increased IFNβ-induced JAK-STAT signalling may promote the interaction of STATs with co-repressors and their subsequent recruitment to the gene promoter site [365], [366], of which they are only able to access in the absence of IRF8 expression.

Cluster B highlights a subset of IRF8 target genes that are positively regulated preferentially in response to IFNβ and are enriched in the pathway 'Fat cell differentiation'. Within this pathway, the pro-inflammatory *Smad7* and scavenger receptor *Cxcl16*, show a significant decrease in expression in the WT^{LdlrKO} macrophages when stimulated with IFNβ (**Fig 5.6**). This suggests, IFNβ regulation of 'Fat cell differentiation' in macrophages from an atherosclerosis environment is dependent on IRF8 expression.

On the contrary, cluster C highlights a subset of genes that are negatively regulated by IRF8 irrespective of IFNβ. Genes within this cluster are enriched in processes involving macrophage cholesterol efflux, as demonstrated by the term 'ABC transporters' [367]. ABC transporters have a crucial role in macrophage cholesterol efflux, where their deficiency has been shown to promote foam cell formation and atherosclerosis progression [65], [70]. This demonstrates, IRF8 reduction reverses IFNβ-induced repression of select genes, many of which are involved in ABC-mediated cholesterol transport.

Genes in cluster D, were significantly enriched in 'Inflammatory response' ($Log_{10}P$ = 2.6E-10). Most genes within this cluster are positively regulated by IFNβ, with increased regulation evident in IRF8-KO macrophages. This implies many IFNβ-inducible genes involved in the 'Inflammatory response' are negatively regulated by IRF8 in macrophages from an atherosclerosis prone environment.

Overall, we have identified a series of IRF8 target genes and pathways that are both responsive and non-responsive to IFNβ treatment. Interestingly, many IFNβ-regulated genes that are dependent on IRF8 expression are enriched in lipid associated pathways (**Clusters B and C**) suggesting IRF8 may regulate IFNβ induction of such pathways in macrophages from western diet-fed mice.

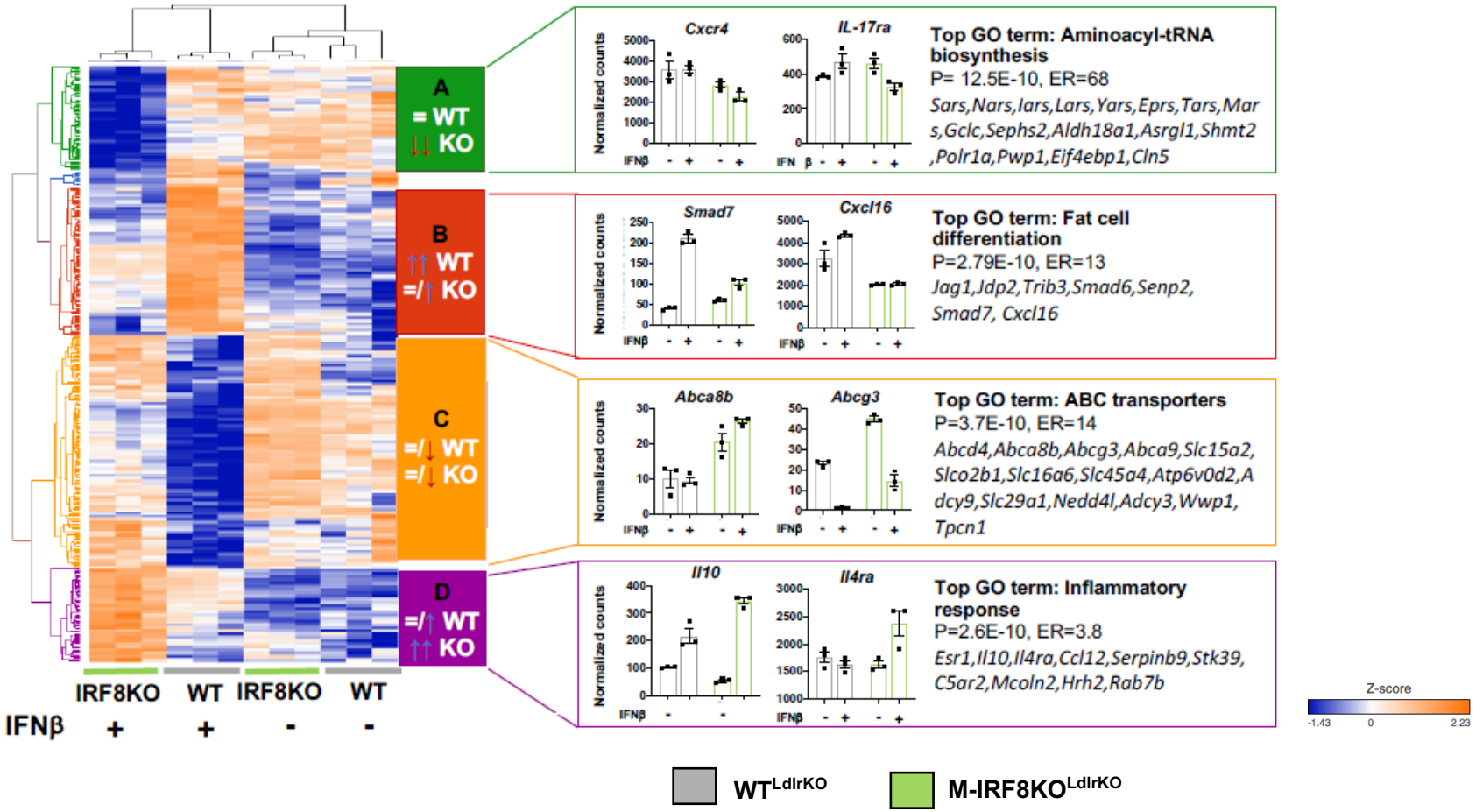

Fig 5.6 Myeloid-IRF8 reduction transcriptionally reprograms macrophage response to IFNβ stimulation.
Log2 transformed normalized RNA-seq gene counts, from Deseq, of WD-fed BMDMs from M-IRF8KO^{LdlrKO} and WT^{LdlrKO} mice (n=3 per group) at basal or treated with 10ng IFNβ for 6hrs. Four patterns of gene expression (clusters A-D) were identified amongst differentially expressed genes by hierarchical clustering of normalised gene counts. Bar graphs of counts of two representative genes from each cluster are displayed alongside the most significantly enriched gene ontology term and genes present within the cluster of this term. Data presented are raw gene counts. Statistical significance calculated using the Wald parametric test, FDR 0.05, p<0.01.

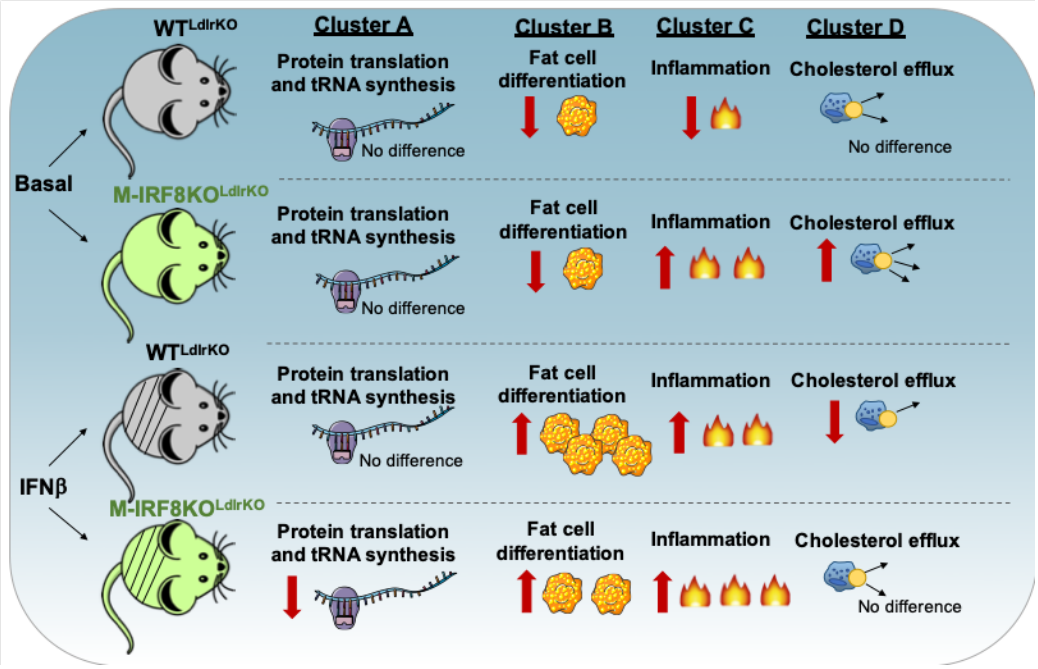

Fig 5.6.1 Summary schematic of IRF8-regulated pathways in response to IFN□.
Images adapted from Servier Medical Art.

5.7 Summary

As summarised in **Fig 5.7**, this chapter has established the following;

1. IRF8 reduction differentially regulates macrophage response to IFNβ treatment in hyperlipidaemic mice.
2. IRF8 does not regulate IFNβ induction of genes involved in 'Defence response' pathways in macrophages from a hyperlipidaemic environment.
3. IRF8 differentially regulates the expression of genes, in response to IFNβ treatment, that are involved in 'Cholesterol biosynthesis', 'Apoptosis' and 'Migration' in macrophages from a hyperlipidaemic environment.

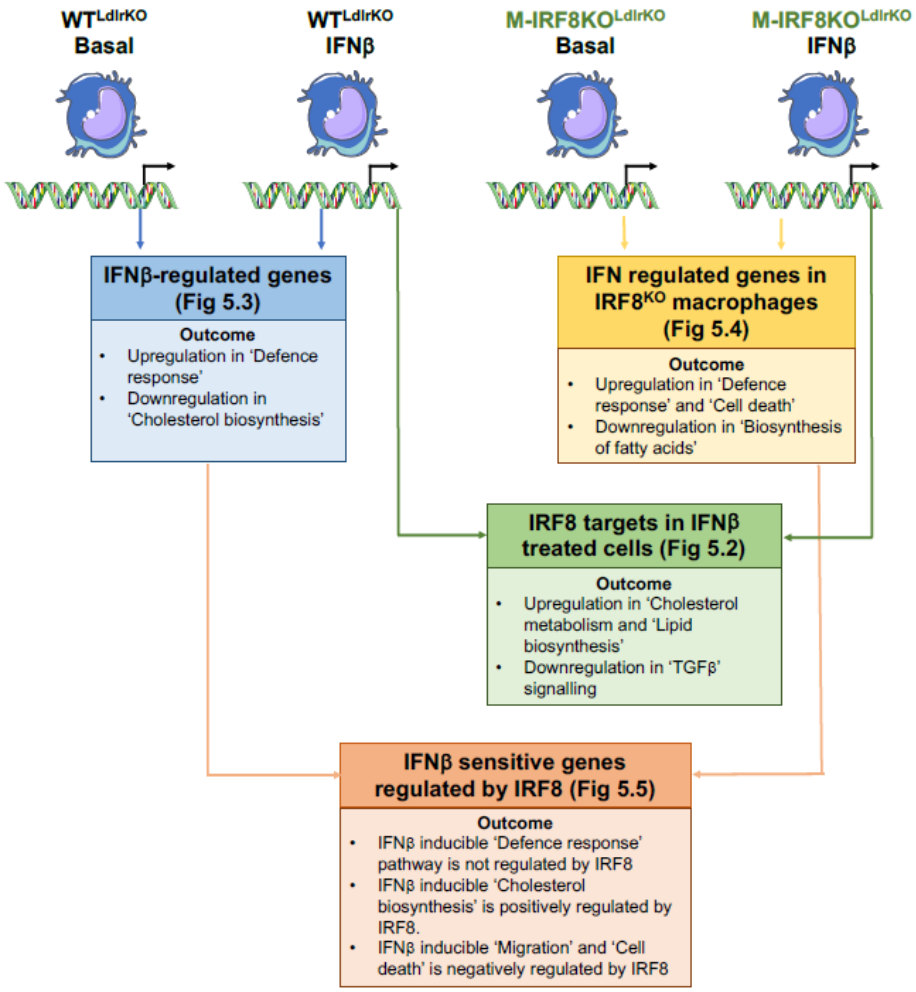

Fig 5.7 Summary diagram of key findings from gene list comparisons of IFNβ stimulated macrophages from WT^{LdlrKO} and M-IRF8KO^{LdlrKO} mice.

5.8 Discussion

IFNβ has been well characterised for its role in mediating the immune cell response to inflammation and bacterial infection [131], [352], [354]. Recent studies by Goossens and colleagues [169] have identified an atherogenic role of myeloid-IFNβ signalling via the promotion of plaque macrophage infiltration, impaired cholesterol efflux via *Abca1* and increased cholesterol uptake via scavenger receptor *Sr-A* [172]. The atherosclerosis-inducing western diet is known to trigger IFN-signalling pathways in myeloid cells [169]. Previous studies have demonstrated IRF8 positively regulates type I IFN production in monocytes

and plasmacytoid dendritic cells [140], [141]. Furthermore, studies by Mancino and colleagues have demonstrated IRF8 differentially regulates macrophage response to IFNβ simulation in normolipidemic mice [86]. Considering IRF8 and IFNβ are independently implicated in atherosclerosis development [169], [175], [177], and IRF8 regulated IFNβ signalling has been identified in normolipidemic mice [86], we aim to determine whether IRF8 reduction impacts the IFNβ induced gene expression in macrophages from hyperlipidaemic western diet-fed mice. This information would enhance our understanding of IRF8 regulation of IFNβ signalling in atherosclerosis, providing insight for future possible therapeutic targets. For this reason, RNA-sequencing was performed on IFNβ treated BMDMs from M-IRF8KO^{LdlrKO} and WT^{LdlrKO} mice.

5.7.1 IRF8 differentially regulates macrophage response to IFNβ

To determine the transcriptional effect of myeloid-IRF8 reduction on macrophage response to IFNβ treatment, we compared differentially regulated genes in IFNβ stimulated IRF8-KO macrophages to IFNβ stimulated WT macrophages. Altogether, we identified 373 differentially regulated genes in response IFNβ treatment in IRF8-KO macrophages (**Fig 5.2**). Pathway analysis demonstrated genes enriched for processes involving 'Leukocyte migration' and 'ABC transport' where significantly upregulated in IRF8-KO macrophages, suggesting IRF8 reduction positive regulates IFNβ induction of pathways known to promote atherosclerosis. Increased IFNβ signalling has been highly associated with modulating chemotaxis of monocytes, dendritic cells and macrophages in various models of inflammation [169], [170], [368]. However, many chemotactic ligands upregulated by IFNβ (*Ccl12, Ccl8*) in IRF8-KO macrophages, were

previously downregulated in untreated IRF8-KO macrophages. This suggests their regulation by IFNβ may involve another IFN-induced transcription factor that is negatively regulated by IRF8 in basal macrophages [86]. Amongst the upregulated pathways, genes involved in ABC-cholesterol transport, syncytium formation and gap junction trafficking where also significantly enriched. Syncytium formation involves the fusion of cells, often in response to viral infections and has been shown to amplify the IFNβ elicited immune response [369]. Similarly, genes involved in gap junction trafficking also mediate cell-cell interaction and are important in monocyte-endothelial cell adhesion [370] and the formation of immunological synapses [371]. The differential regulation of these pathways in macrophages from hyperlipidaemic mice, suggest, IFNβ-induction, may impact on macrophage cholesterol efflux and its ability to form interactions with other cells. Such processes are crucial during the early stages of atherosclerotic plaque progression [249] and these results uncover a previously unknown route by which IRF8 modulates macrophage response to IFNβ in atherosclerosis. To confirm these results, macrophage cholesterol efflux assays and measurement of cellular adhesion (using methods such as fluidic-probe force microscopy) in response to IFNβ, would be required [372].

In contrast, there was a 30% decrease in the total number of upregulated genes in IFNβ treated IRF8-KO macrophages, when compared to IFNβ treated WT macrophages (**Fig 5.3** and **Fig 5.4**). This may be due to the main role of IFNβ in the activation of genes, via the JAK/STAT pathway, rather than repression of gene expression [138], [359]. Pathway analysis of downregulated genes in IFNβ-treated IRF8-KO macrophages, when compared to WT, demonstrated high enrichment in processes including 'TGF-β signalling' and

'Amino acid transporter activity'. Previous studies have demonstrated IRF3-induced TGF-β signalling promotes IFNβ signalling, via the binding of IRF3 to the interferon response element present upstream the IFNβ promoter [373].

5.7.2 IFNβ stimulation of 'Defence response' genes are not dependent on IRF8

Comparative analysis on the differentially regulated genes identified in IFNβ stimulated WT macrophages, when compared to untreated WT macrophages, allowed us to determine the transcriptional impact of IFNβ treatment on macrophages from a hyperlipidaemic environment. As expected [353], IFNβ significantly induced genes enriched in processes surrounding ' Response to virus', 'Response to external stimulus and IFNβ' in WT^{LdlrKO} macrophages. However, we became interested in the negative regulation of lipid-metabolic pathways by IFNβ stimulation in WT macrophages, particularly as previous studies have reported conflicting results in the role of type-1 IFNs in lipid induced processes, including foam cell formation [161], [169]. Goossens et al., 2010 demonstrated IFNβ priming of myeloid cells had no impact on oxLDL uptake in vitro [169], whereas Li et al., 2011 demonstrated IFNα promoted oxLDL uptake in THP-1 cells [374]. Enhanced oxLDL uptake was also mirrored in atherosclerotic $LDLR^{KO}$ macrophages that harboured an altered heparan sulphate structure, which was linked to increased type-I IFN signalling [375]. Upon considering the impact of IFNβ stimulation in lipid-mediated processes crucial for atherosclerosis development, it was intriguing to discover a large proportion of downregulated genes are in fact involved in cholesterol biosynthesis (*Cyp1a1, Scd1, Acat2, Acat3*), fatty acid metabolism (*Scd1, Scd2, Acot2, Acot 3*) and fatty acid beta-oxidative pathways (*Acad12, Pccb, Hacd3, Acot13*). Reduced

expression of genes within these pathways, in particular the Acyl-CoA:cholesterol acyltransferases (ACATs), have been shown to reduce the progression of pre-existing atherosclerotic lesions [30], [38]. Therefore, our data suggests, in western diet-fed mice, IFNβ treatment results in the negative regulation of genes important for macrophage cholesterol metabolism that may contribute to atherogenesis. To determine whether the differential gene regulation elicited by IFNβ stimulation, impacts on atherosclerosis development, it would be beneficial to measure *in vivo* macrophage cholesterol uptake, efflux, ester content and foam cell formation in response to IFNβ to increase our understanding on the functional implications elicited by this differential gene regulation.

5.7.3 IFNβ differentially regulates 'Cell death' and 'Fatty acid' related genes in the absence of IRF8

To determine the regulation of IFNβ-treated genes in IRF8-KO macrophages from a hyperlipidaemic environment, comparative analysis was performed on IFNβ treated IRF8-KO macrophages, when compared to untreated. Similarly, to IFNβ treated WT macrophages, we identified an increased enrichment of genes involved in 'Response to IFNβ' and 'Viral response'. We also discovered increased enrichment of genes involved in 'Cell death' pathways, suggesting myeloid-IRF8 reduction may negatively regulate IFNβ-induced pro-apoptotic genes. Considering studies by Yang and colleagues demonstrate IFNβ promotes cell survival via activation of NF-KB signalling [347], others have reported no differences in macrophage cell death in atherosclerosis prone mice lacking the IFNβ receptor, IFNAR [169]. This data demonstrates, IRF8 transcriptionally regulates IFNβ-induced cell death related genes that may contribute to the role of IFNβ in apoptosis within atherosclerosis. However,

additional functional experiments would be required to assess aortic macrophage cell death, for instance via TUNEL staining [376]. Considering previous studies have demonstrated IRF8 to positively regulate Fas mediated apoptosis in non-haematopoietic cells, via IFNγ activation [377], this is the first study to suggest IRF8 regulates IFNβ-induced macrophage cell death in an atherosclerotic environment.

5.7.4 IFNβ-induction of genes involved in 'Cholesterol metabolism', 'Apoptosis' and 'Migration' are regulated by IRF8

Having identified transcriptional differences elicited by myeloid-IRF8 reduction in response to IFNβ treatment, we aimed to determine which differentially regulated processes where specific to IRF8 expression. Additional comparative analysis was performed on the list of differentially regulated genes identified in the IFNβ treated IRF8-KO vs untreated IRF8-KO macrophages and the IFNβ treated WT vs untreated WT macrophages (**Fig 5.6**). Interestingly, we identified a large degree of overlapping genes that were differentially regulated in both IFNβ treated WT macrophages, when compared to untreated, and IFNβ treated IRF8-KO macrophages, when compared to untreated. We demonstrated IFNβ induction of genes involved in Viral response (*Ifit1, Ifit2, Ifit3, IL-1b*), Cytokine production (*Il-10, Il-12, Il-1, Il-7*) and Immune response (*Dnas1l3, Fcgr1, Tlr9, Tlr3*), was not dependant on IRF8 expression, in hyperlipidaemic mice. We also discovered an increased enrichment of genes involved in 'Lipid-metabolic' and 'Cholesterol biosynthesis' processes, in response to IFNβ treatment that were also dependant on IRF8 expression. This suggests IRF8 is important for the regulation of IFNβ-induced lipid metabolic processes in atherosclerosis (**Fig 5.6 D**). Interestingly, the Acyl-CoA cholesterol transferase enzymes, *Acat1, Acat2*

and *Acat3* were amongst the most significantly regulated within the lipid-metabolic pathways. These enzymes are crucial in the esterification of macrophage free cholesterol, to form cholesterol esters that are stored in lipid droplets, contributing to macrophage foam cell formation [38]. Interestingly, previous studies demonstrated IFNβ induced activation of *Acat1* was associated with decreased cholesterol efflux via the ABC transporter; ABCA1 in macrophages stimulated with acLDL [38]. In contrast, we observe a reduction in the ACAT enzymes and ABC cholesterol transporters in IFNβ treated IRF8-KO macrophages, when compared to untreated macrophages. The western diet has also been shown to induce epigenetic reprogramming of innate immune cells that subsequently alters cellular response to secondary stimulus [378]. Upon taking this into consideration, it's possible that macrophages from western diet fed mice, may be epigenetically reprogrammed allowing for differences in IFNβ-induced gene expression between western diet fed mice and non-western diet fed mice.

In contrast, many genes differentially regulated in response to IFNβ treatment, in the absence of IRF8 expression, were highly enriched in processes surrounding 'Leukocyte migration' (*Ccl3, Ccl4, Ccl8, P2ry12*) and 'Cell death' (*Fas, Bmp2, Casp8, Casp12*). Interestingly, Mancino et al., 2015 demonstrated genomic IRF8-occupancy in IFNβ treated BMDMs from normolipidemic $IRF8^{m/m}$ mice for several genes highly enriched in these pathways, including *Ccl3, Ccl4, Ccl8, Casp8* and *Casp12* [86]. The lack of IRF8 occupancy at Fas, however, suggests IRF8 regulation of Fas in a hyperlipidaemic environment, may be dependent on the potential epigenetic reprogramming of IRF8-KO macrophages by the western diet. To investigate this epigenetic reprogramming, it would be beneficial to determine differences in binding of transcription factors, such as

IRF8, via ChIP-sequencing [379] and measure the activity of the enhancer and promoter landscape using ATAC-sequencing [209]. It would also prove beneficial to couple this data with differences in gene regulation, identified using RNA-sequencing, on M-IRF8KO^{LdlrKO} and WT^{LdlrKO} mice challenged with a western and chow diet. This would increase our understanding of the diet induced epigenetic effects on IRF8 reduction and the impact this has on secondary IFNβ signalling.

In conclusion, this data has demonstrated that IRF8 is required for the regulation of several previously uncharacterised pathways, that are differentially expressed in response to of IFNβ stimulation in atherosclerosis. These pathways include; chemotaxis, apoptosis and lipid-metabolism related genes and are often dysregulated in atherosclerotic plaque formation [334], [362], [380]. This data has increased our understanding of IRF8-regulated IFNβ signalling in macrophages from an atherosclerosis prone environment, identifying pathways that could be further explored in therapeutic applications aimed at atherosclerosis.

Chapter 6:Results - Investigation into the emerging role of myeloid-IRF8 signalling in ageing

6.1 Introduction

Human life expectancy is vastly increasing, with the population aged over 60 years predicted to increase more than threefold by 2050 in more economically developed industrialised countries [198]. Ageing is associated with a plethora of diseases, including Cardiovascular disease, Stroke and Alzheimer's disease [199], [200], [381]. This is due to the age-related dysfunction of the innate and adaptive immune response, in particular for age-associated Cardiovascular disease [226]. Currently, the mechanisms underlying this dysregulated immune response are unclear. However, recent evidence has emerged indicating impaired monocyte function may contribute to the dysregulated innate immune response identified amongst the aged population [224], [226].

Peripheral blood monocytes are a heterogenous population of bone marrow derived cells that constitute between 10-20% of the total blood leukocyte population [382]. Three individual subsets have been identified; Classical pro-inflammatory monocytes ($CD16^{-}CD14^{+}$) that are the most abundant (90%), intermediate monocytes ($CD16^{lo}CD14^{+}$) and non-classical monocytes ($CD14^{lo}CD16^{+}$) [383], [384]. Collectively, they protect against infection via the activation of pattern recognition receptors (PRRs), including toll-like receptors (TLRs) [385]. They also support the adaptive immune response via the production of pro- and anti-inflammatory mediators whilst differentiating into antigen presenting cells. Previous studies, have identified an expansion in $CD16^{+}$ monocytes within the aged human population; a characteristic resembling the

response to bacterial infection, alongside decreased expression of cell surface markers (CX_3CR1 and CD62L) that may affect monocyte survival and migration to inflammatory sites [221], [386]. This, therefore, demonstrates defective monocyte function within the aged population.

To elucidate the potential mechanism of immune cell dysregulation, studies have investigated the transcriptomic differences amongst select aged immune cells. Stirewalt and colleagues identified a significant association between reduced IRF8 expression in hematopoietic stem cells (HSCs) and mature $CD34^+$ T-cells in aged humans and mice, suggesting a possible role for dysregulated IRF8 in these aged cells [232]. Due to the crucial role of IRF8 in monocyte function [121] combined with the dysregulated monocyte phenotype observed in the aged, we interrogated whether the expression of IRF8 and its target genes, differ in aged monocytes.

The 10,000 immunomes project consists of a human immunology reference database, publicly available from ImmPort, of young and aged genes identified within the PBMCs and whole blood of males and females [231]. This provides a platform allowing for the study of age and gender related differences to be identified within the healthy human population. This information can be used in comparative studies to help identify specific genes and signalling pathways that may potentially be used as age-related biomarkers. Currently, little information in known regarding gender differences within the aged population, however, studies have implied the innate immune response may differ with gender as well as age [228], [230]. Interestingly, healthy aged women display a reduction in the proportion of circulating $CD16^+$ monocytes, with no difference in

phagocytic function when compared to men [387], [388]. Hearps et al., 2012 also identified women to exhibit an increase in plasma CXCL10, characteristic of monocyte/macrophage activation, in comparison to men. Collectively, this data implies the innate immune response is altered amongst different genders within the aged population, however, the mechanism underlying such differences is poorly understood. With many age-related inflammatory disorders impacting men and women differently, it's important to further understand the transcriptional differences amongst different aged genders, to help identify potential biomarkers that could be used for certain gender-specific age-related diseases.

This chapter establishes how the regulation of IRF8-target genes, identified in hyperlipidaemic M-IRF8KO^{LdlrKO} mice, differ in the monocytes and PBMCs of different age and gender healthy human populations. This analysis would help identify IRF8-regulated genes that have the potential to be used as biomarkers of cardiovascular disease in the healthy aged population in a sex-specific manner.

Aims:

1. Determine the regulation of IRF8 in human monocytes from young and aged individuals
2. Identify IRF8-target genes that are differentially regulated in aged PBMCs from males, and females as identified in the 10,000 human immunomes project [231].
3. Confirm differential regulation of IRF8-target genes, identified in the above comparative analysis, in human monocytes from young and aged individuals.

6.2 Aged human monocytes and monocyte subsets, display reduced expression of IRF8

Differences in transcriptional regulation of immune cells, including; hematopoietic stem cells, mature T-cells, peripheral blood mononuclear cells (PBMCs) and monocytes, are one of the seven hallmarks of ageing [202]. Previous studies by Stirewalt et al., 2009, identified a significant reduction in IRF8 expression within healthy aged HSCs and cells of the adaptive immune response, including mature T-cells [232]. Although age-induced differential gene expression within innate immune cells are less well reported, few studies have displayed differential gene expression within aged monocytes and their subsets. This prompted our investigation into the expression of IRF8 and its target genes within healthy aged monocytes. Interestingly, we identified a striking decrease in the gene expression of IRF8 within aged monocytes, when compared to young, thus, implying an age-induced reduction in myeloid-IRF8 signalling (**Fig 6.1 A**).

Age-related differences in the quantity and cell-surface expression of monocyte subsets has also been previously reported [221]. This prompted our investigation into the expression of IRF8 in monocyte subsets. Similarly, to the total monocyte population, we also identified a decrease in IRF8 expression in classical (**Fig 6.1 B**), intermediate (**Fig 6.1 C**) and non-classical monocytes (**Fig 6.1 D**). Collectively, this shows an age-associated reduction in IRF8 expression within monocytes and monocyte subsets of healthy human subjects. This may impact on the ability of aged monocytes to respond to bacterial and viral infection. However, to confirm this it would be beneficial to determine the regulation of previously identified IRF8-target genes in monocytes from healthy aged individuals at baseline and in response to inflammatory stimuli, including LPS and

interferon at gene and protein level [389], [390]. This would help underpin the role of IRF8 in healthy ageing.

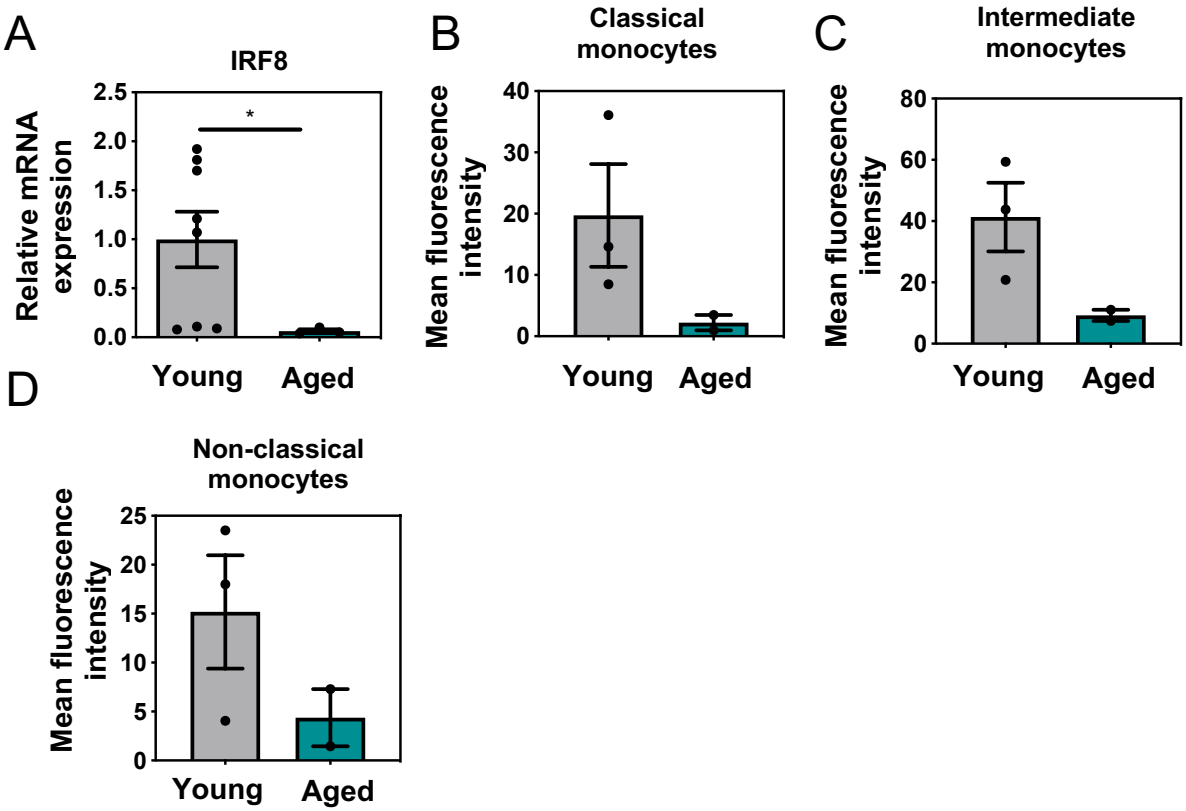

Fig 6.1 IRF8 expression is reduced in aged monocytes and monocyte subsets.
(A) Relative IRF8 gene expression in human aged monocytes compared to young (n=8 young, n=3 old). (B) Mean fluorescence intensity of IRF8 expression in classical monocytes from young and old donors. (C) Mean fluorescence intensity of IRF8 expression in intermediate monocytes from young and old donors. (D) Mean fluorescence intensity of IRF8 expression in non-classical monocytes from young and old donors. Monocyte subset data generated from MSc student Nadia Nozari. Monocyte subset data is representative of n=3 young and n=2 old. Statistical significance calculated using an unpaired students t-test, *p>0.05, due to sample size of n=2 for aged monocyte subsets in (B), (C) and (D), statistical analysis was not possible.

6.3 Age and gender impact on IRF8-regulated transcriptional network

Myeloid-IRF8 regulates a network of genes that are crucial for monocyte and macrophage response against inflammation and infection [285]. Having identified reduced IRF8 expression in aged monocytes and monocyte subsets (**Fig 6.1**), we aimed to explore whether differences in IRF8 expression impacted on the regulation of previously identified IRF8-target genes in aged monocytes. This would allow us to identify a possible age-induced difference in IRF8-regulated pathways. The 10,000 immunomes project encompasses a human immunology reference network, formed from the combination of 242 independent studies. Collectively this database highlights a number of genes and proteins that are regulated in the PBMCs or whole blood amongst a population of >10,000 individuals aged between 20-100 years [231].

Amongst the ~20,000 genes identified in PBMCs of young males and females (20-50years) and aged males and female (60-100years) [231], we identified 1795 differentially regulated genes with age and 4127 genes differentially regulated with gender (**Fig 6.2 A**). This demonstrates, gender-related gene differences are more prominent amongst PBMCs from a healthy human population. To determine whether previously identified IRF8 target genes, from M-IRF8KO^{LdlrKO} mice, were differentially regulated with age and gender in human PBMCs, comparative analysis was performed on the list of IRF8-target genes against the list of genes that were differentially regulated with age and gender in PBMCs (**Fig 6.2 B**). Interestingly, many IRF8-target genes appeared to share functional similarities between differentially regulated genes in 'Young vs Old' PBMCs, as shown by the overlapping blue lines on the circus plot (**Fig 6.2 B**). This implies genes regulated by IRF8 and genes differentially regulated

with age are involved in similar functional processes. However, a significant proportion of differentially expressed genes (DEGs), identified in 'Men vs Women' PBMCs, displayed an absence of functional overlap between the gene lists (**Fig 6.2 B**). This indicates that most genes differentially regulated with gender are enriched in functional processes that are different to those in M-IRF8KO^{LdlrKO} mice and those enriched in the aged population. These functional differences could potentially contribute to gender-related differences in disease development such as Sepsis [391].

Investigation into the quantity of IRF8-target genes that overlap between the two gene lists, identified a total of 70 overlapping IRF8 target genes, with only 5 genes regulated amongst all three lists (**Fig 6.2 B**). Of the 69 overlapping genes, many are significantly different in young males, young females or aged females, with altering patterns of regulation amongst the groups (**Fig 6.2 C**). Pathway analysis of the differentially regulated overlapping genes, highlighted many where significantly enriched for terms including 'Chemotaxis', 'Inflammatory response' and 'Fat cell differentiation' to name a few (**Fig 6.2 D**). Understandably, there may be cross-species differences that may contribute to the relatively low number of IRF8 target genes identified in the human PBMCs. However, such comparative analysis allows for the identification of genes that are differentially regulated in healthy aged monocytes.

Collectively, we have identified a total of 4405 genes that are differentially regulated by either age or gender in PBMCs from the healthy human population. Although only 70 genes overlap with myeloid-IRF8 target genes, they are highly enriched in process that are known to be dysregulated in the aged population,

specifically the ‘Inflammatory response’ [226], [392]. Therefore, this comparative analysis highlights a series of IRF8-target genes that, with validation in human monocytes, may provide as useful biomarkers in healthy ageing.

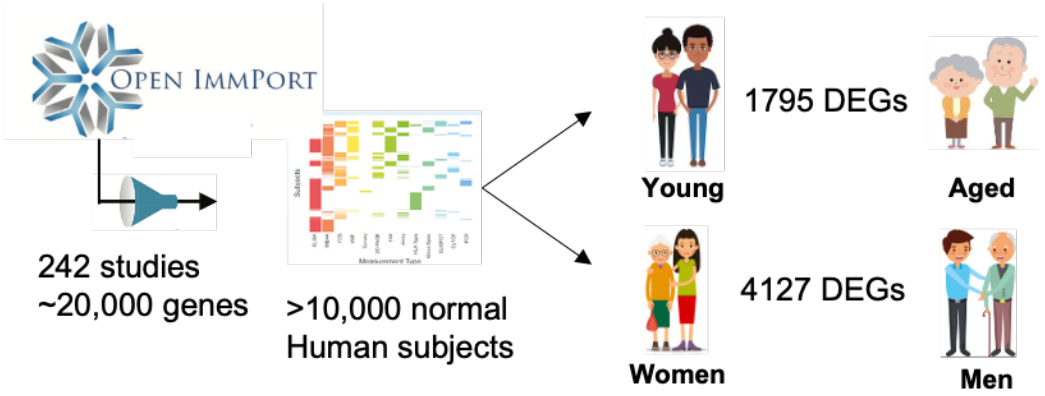

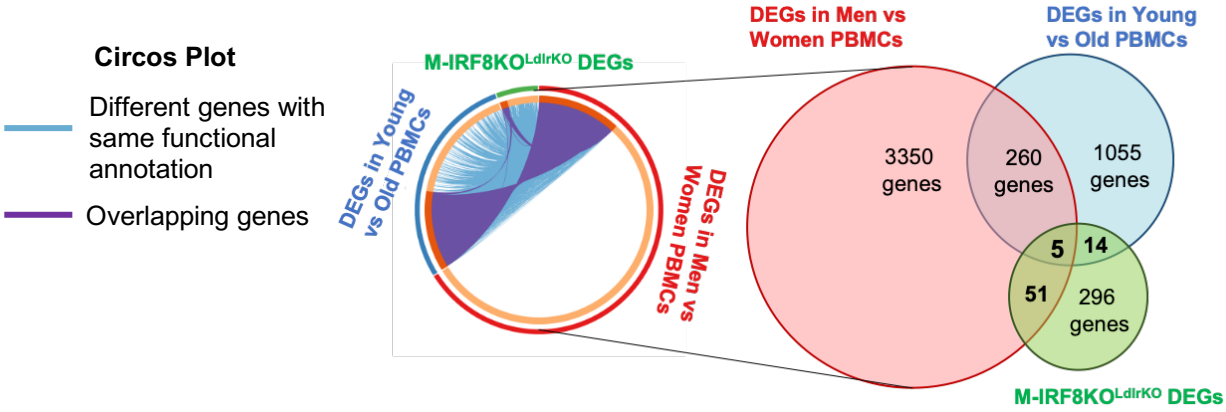

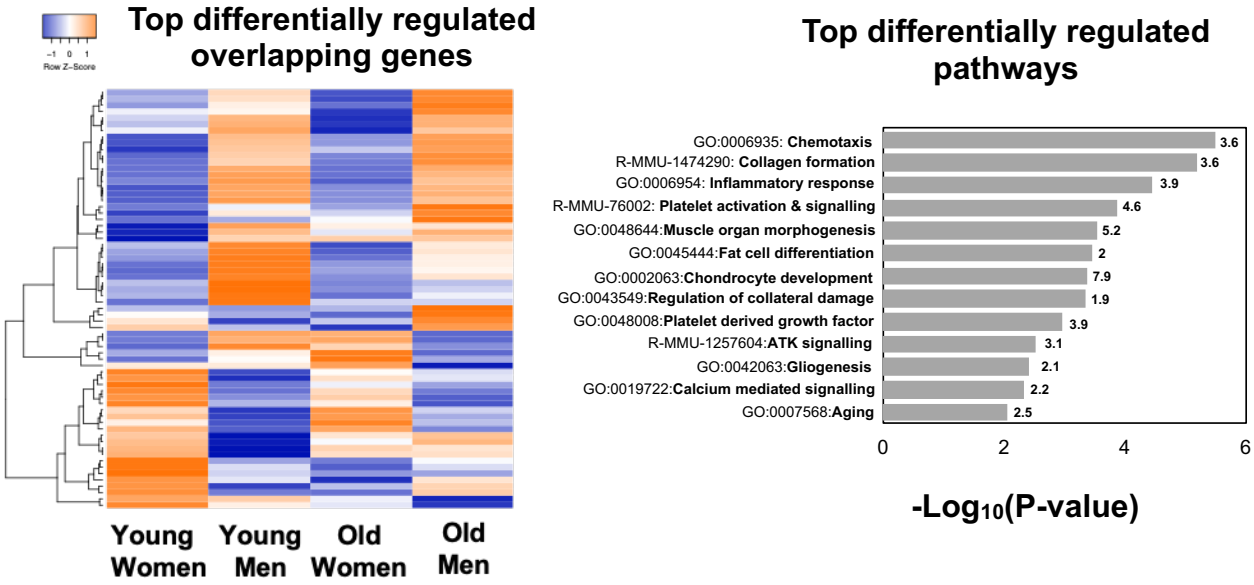

Fig 6.2 IRF8 target genes are differentially regulated with age and gender.
(A) Overview of differentially regulated genes identified in the Immunomes PBMC database [231] comparing genes from young (20-50yrs) males and females and aged (60-100yrs) males and females. (B) Circos plot highlighting the overlap of differentially regulated genes (purple lines) identified in Western diet-fed BMDMs from M-IRF8KO^{LdlrKO} mice (n=3/group) and DEGs identified in the Immunomes male vs female PBMCs and Old vs Young PBMCs. (C) Clustered heatmap displaying the raw gene counts of DEGs in PBMCs of young males, females and old males and females that are also regulated by IRF8. (D) Pathway analysis of the top differentially regulated overlapping genes, highlighting the most significant pathways with corresponding enrichment score at the end of each bar.

6.4 Transcriptional regulation of key genes involved in lipid-mediated disorders are differentially expressed with age and gender

Age-related disorders, including atherosclerosis and Alzheimer's, are often associated with a dysregulated immune response due to impaired transcriptional regulation of key metabolic processes [200], [225]. Within this study, we have uncovered a role for myeloid-IRF8, in retarding the development of atherosclerosis, when deleted from myeloid cells, possibly due to its transcriptional reprogramming of macrophages (Chapters 3 and 4). Of the IRF8-target genes differentially regulated with age and gender in PBMCs, identified in **Fig 6.2**, many were enriched in lipid-associated 'Fat cell differentiation' (GAB1, CTSC, CYP27A1) ($Log_{10}P$ = -3.8). This implies, IRF8 regulation of genes involved in lipid metabolic processes could be altered in the healthy ageing of immune cells.

Having identified a significant decrease in IRF8 expression within healthy aged monocytes (**Fig 6.3 A**), we aimed to determine whether the downstream IRF8 target genes, identified in IRF8-KO macrophages, where also differentially regulated in human monocytes from healthy young (18-30yrs) and aged (65+yrs) humans. This would allow for identification of IRF8-regulated age-associated differences in healthy monocytes that may contribute to certain age-related diseases. We identified a significant decrease in the expression of cholesterol transport receptor, P2RY13 (**Fig 6.3 A**), and atherosclerosis associated cathepsin, CTSC (**Fig 6.3 B)** and protein kinase adaptor GAB1 (**Fig 6.3 C**) in aged monocytes [393], [394].

To compare how the regulation of these IRF8 target genes differed amongst men and women, we plotted their expression in PBMCs, taken from the Immunomes raw data set [231]. The expression profile of *Gab1* (**Fig 6.3 H**) was very similar in aged men and women PBMCs, when compared to the young. However, CTSC (**Fig 6.3 I**) was significantly increased, by 45%, in aged PBMCs of males and females and P2RY13 (**Fig 6.3 G**) displayed no difference in aged PBMCs. Considering monocytes only form between 10-20% of the population of PBMCs [382], it's possible that some age-related differences observed in human monocytes may be masked in the immunomes PBMC data due to different expression profiles within other cells including T-, B- and NK cells.

In comparison, although not significant, a trend to decrease was observed in the expression of cholesterol metabolizing enzyme, CYP27A1, (**Fig 6.3 F**) with no difference observed in the scavenger receptor, CXCL16, (**Fig 6.3 E**) or the fatty acid transporter, ABCD2, (**Fig 6.3 D**) in aged monocytes. CYP27A1 and ABCD2 show age-related differential expression in PBMCs (**Fig 6.3 K & L**), however, CXCL16, (**Fig 6.3 J**) only shows gender related differences in PBMCs from the young.

This implies genes, previously identified as IRF8 targets in a mouse model of atherosclerosis, are also differentially regulated in the PBMCs of young and aged individuals. Interestingly, 3 genes are negatively regulated in aged monocytes (GAB1, CTSC, P2RY13) also. However, due to the low sample size of male-only aged donors, it's not possible to infer gender related differences from the monocyte data. To determine the sample size required to gain significance, power calculations were conducted based on a priori determined outcome, using

the GPower online software. This generated an effect size of 1.65 from the mean and standard deviation of IRF8 in both young and old donors (**Table 6**). Upon increasing the sample size, to a minimum of 9 individuals per group, using an effect size of 1.65, it would be possible to determine the age-associated and possible gender associated regulation of lipid-associated genes in monocytes, that may collectively contribute to the increased prevalence of lipid-mediated disorders amongst the aged population.

Power analysis and test	Effect size	α-err probability	Power	Degrees of freedom	Sample size/group
A priori, T-test	1.65	0.05	0.9	16	9

Table 6. Sample size required to generate significance in genes differentially regulated in monocytes from young and aged individuals.

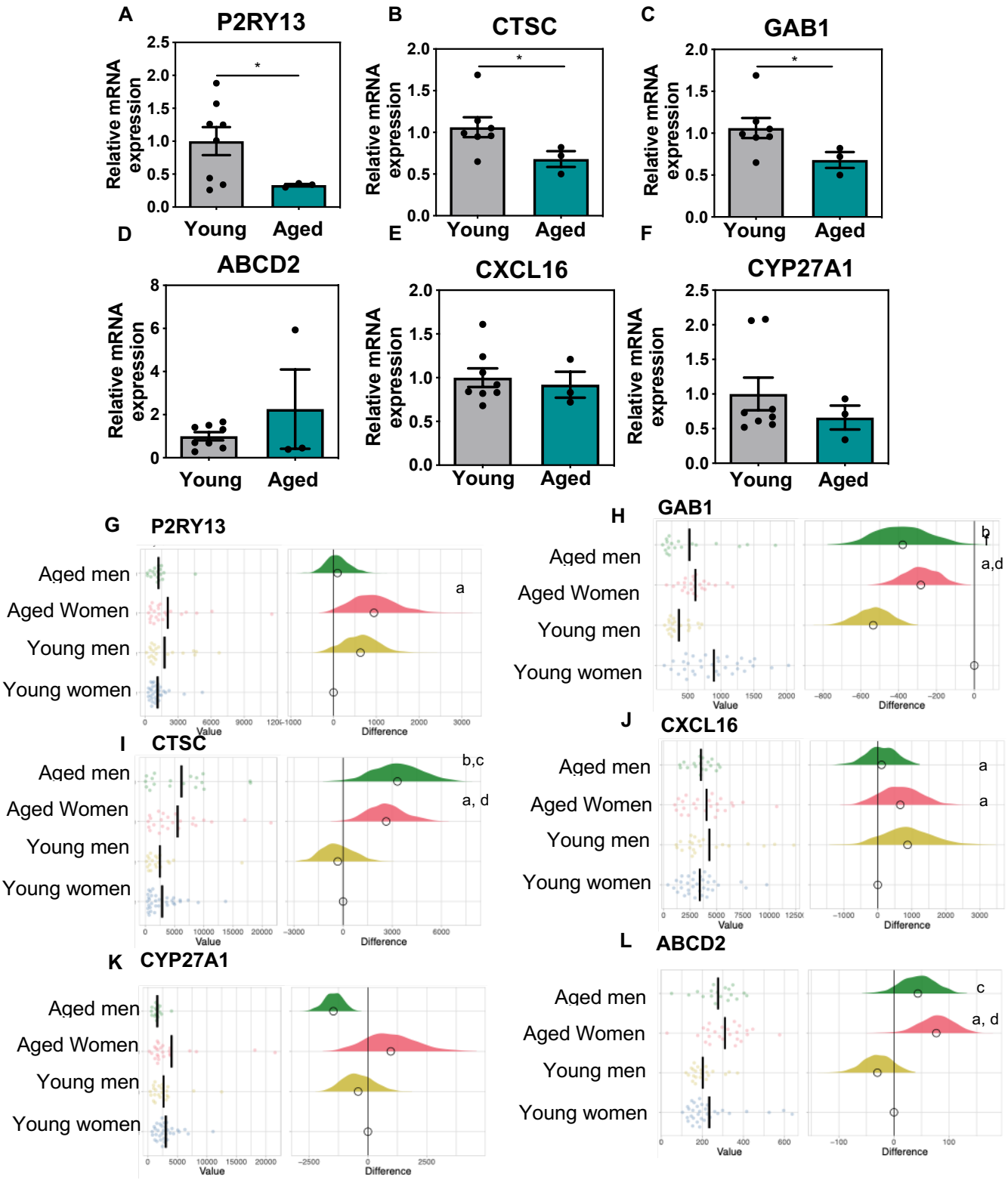

Fig 6.3 IRF8-regulated lipid-metabolic genes are differentially expressed in aged human monocytes.

(A) P2RY13, (B) CTSC, (C) GAB1, (D) ABCD2, (E) CXCL16 and (F) CYP27A1 mRNA expression determined by quantitative-PCR of healthy young and aged monocytes (n=7 young, n=3 aged). (G) P2RY13, (H) GAB1, (I) CTSC, (J) CXCL16, (K) CYP27A1, (L) ABCD2 gene expression, determined by microarray [231] in healthy young and aged PBMCs from men and women (n=33 young women, n=22 young men, n=24 aged women, n=18 aged men). Plots of difference data are presented as mean ± SEM (A-F) and mean (G-L), statistical analysis performed using unpaired students t-test (a= P ≤ 0.001 young women vs aged women, b= P ≤ 0.001 young women vs aged men, c= P ≤ 0.001 young men vs aged men, d= P ≤ 0.001 young men vs aged women, e= P ≤ 0.001 aged women vs aged men, f= P ≤ 0.001 young women vs young men).

6.5 Summary

As demonstrated in **Fig 6.4**, this chapter has established the following:

1. The gene expression of IRF8 is significantly reduced in aged human monocytes and monocyte subsets from healthy donors.
2. We have identified 70 IRF8-target genes that are differentially regulated with age and gender in PBMCs from healthy humans.
3. IRF8-regulated genes that are differentially expressed with age or gender in healthy PBMCs, are highly enriched in processes including 'Chemotaxis' and 'Inflammatory response'.
4. IRF8-target genes, that differ with age and gender in PBMCS and are enriched in 'Fat-cell differentiation' were also differentially regulated in healthy aged human monocytes.

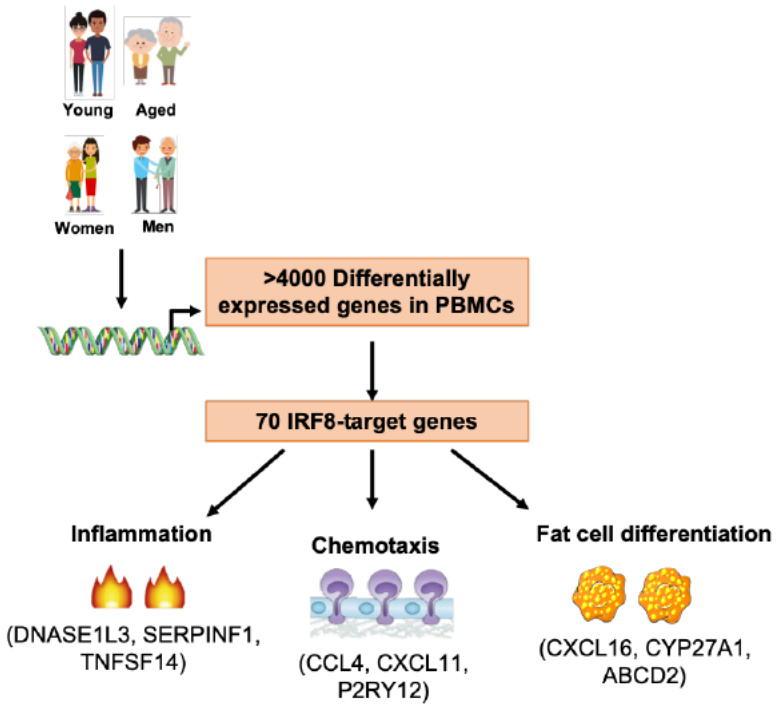

Fig 6.4 Summary diagram displaying the enriched processes in IRF8 target genes that are differentially regulated with age/or gender.

6.6 Discussion

Age-related disorders are becoming increasingly more prevalent, particularly as the aged population increases with improvements in healthcare and available medical treatments [202], [395]. Atherosclerosis is one such lipid-mediated inflammatory disorder that is highly prevalent amongst the aged population, specifically in individuals aged over 50 years [396]. Although young women are less likely to suffer from cardiovascular related diseases than men, due to the protective benefits of oestrogen, their risk increases with age [397]. Having identified an athero-protective role of myeloid-IRF8 reduction in mice (Chapter 3), we were intrigued to discover a significant reduction in the expression of IRF8 within aged monocytes and monocyte subsets. This complements studies from Stirewalt et al., 2009, whom display an age induced reduction of IRF8 within aged HSCs and T-cells.

6.6.1 Inflammatory and chemotaxis-related pathways are dysregulated within aged immune cells

Having identified a reduction in IRF8 in aged monocytes (**Fig 6.2 A**), we interrogated whether the regulation of genes regulated by IRF8, in M-IRF8KO^{LdlrKO} also differed with age and gender. Comparative analysis of IRF8-target genes with the age-related DEGs, identified in human PBMCs, led to the discovery of 70 DEGs that where associated with IRF8, age and gender. Pathway analysis identified 'Chemotaxis' as the most significantly regulated pathway, inferring possible age-induced differences in cell chemotaxis (CCR4, CXCL11, NR4A1) (**Fig 6.3**). Previous studies have shown defective neutrophil migration within aged mice challenged with Staphylococcus aureus infection, due to a

reduction in ICAM-1, owing to the defective resolution of inflammation phase [398]. This suggests, ageing impairs the migratory ability of neutrophils in response to infection, however, little evidence has been generated supporting defective age-induced migration of myeloid-cells.

Alongside ‘Chemotaxis’, ‘Inflammatory response’ was also amongst the most significantly enriched pathways. Age-related defective inflammatory response has been well studied amongst the aged population [399], [400]. Previous studies have demonstrated impaired production of TNFα in aged macrophages, impairing cutaneous T-cell entry in response to tuberculin purified protein [401]. In conjunction, Stout-Delgado et al., 2009, displayed aged plasmacytoid dendritic cells exhibit defective TLR9-induction of Type I IFNs in response to herpes simplex virus-2, that was concomitantly associated with impaired IRF7 upregulation [93]. Together, these studies highlight the dysregulated immune response to external stimuli, ultimately rendering the aged population at an increased risk of infection. Interestingly, Molony et al., 2017, were the first to identify the age-induced reduction of IRF8 was pivotal in defective type-I IFN production in monocytes [402]. Their studies investigating RIG-1 signalling in monocytes, in response to Influenza A virus concluded IRF8 expression was necessary to induce Type-I IFN production in monocytes [402]. Collectively, this highlights the crucial role of IRF8 in mediating immune responses within the aged population. Validation of IRF8 target genes identified that also differ with age and gender, would help identify possible biomarkers of ageing that may be used in future therapeutic diagnostics.

6.6.2 IRF8 regulates genes involved in lipid-mediated disorders that are differentially expressed with age and gender

Age-associated biomarkers of dysregulated lipid metabolism and lipid-mediated disorders are currently not well defined. Recent studies have uncovered an association between lipid-metabolism and chromatin remodelling, that may contribute to life longevity [403]. Plasma lipid and triglyceride protein complexes are known to increase with age, including free fatty acids and triglycerides [404]. Previous studies have displayed the fatty acid oxidation product, Acetyl-CoA, to impact on chromatin landscape. Histone acetyltransferases, including p300, are known to use Acetyl-CoA as a co-factor to add an acetyl group to the lysine on histones, thereby changing chromatin accessibility, impacting on gene transcription [405]. This implies altered plasma lipids may contribute to differential gene expression associated with ageing and age-related disorders, such as atherosclerosis [225], [396].

Diseases caused by the dysregulation of lipid metabolism, such as atherosclerosis, are more prevalent within the aged population [199], [396]. For this reason, our previous findings identifying a role for IRF8 in modulating genes crucial for lipid metabolism and atherosclerosis, prompted our investigation into the regulation of lipid-associated genes by age and gender. Although a limited number of differentially regulated genes where identified (**Fig 6.4**), possibly due to species variation of gene comparisons between human and mouse, we identified a series of genes that have been highly associated with cardiovascular disease, specifically atherosclerosis. The purinergic receptor, P2RY13, was significantly decreased by 60%, in aged monocytes (**Fig 6.4 A**) and this was also mirrored in aged female PBMCs, in comparison to the young equivalent (**Fig 6.4**

B). Interestingly, age-induced reduction of this receptor has been implicated in dysregulated neurogenesis within Alzheimer's disease that is thought to contribute to disease progression [406], [407]. Considering P2ry13 contributes to macrophage migration in a model of spinal cord injury [341], and reverse cholesterol transport in atherosclerosis [339], this raises the possibility that P2RY13 may also contribute to dysregulated leukocyte chemotaxis and reverse cholesterol transport within a high lipid environment of aged females.

GAB1, known for its role in growth receptor signalling, cell proliferation and survival, was also significantly reduced in aged monocytes [408], [409]. Interestingly, deficiency of GAB1 has been associated with increased atherosclerosis, mitochondrial damage and cardiomyocyte apoptosis which increases in an age-dependant manner [408], [410]. Therefore, implying age-dependant reduction of GAB1 in monocytes may contribute to the increased atherosclerosis often observed amongst the aged population. Aged PBMCs from males and females also show reduced Gab1 expression, however, the significant difference in GAB1 expression between young males and females is not replicated in aged males and females (**Fig 6.4 H**). This suggests GAB1 may also have a role in protecting young women against cardiovascular related disease.

Aged monocytes also display a significant reduction in CTSC expression, and a trend to decrease in CYP27A1. CTSC is known for its role in leukocyte activation, where, recent studies have demonstrated an athero-protective role when reduced in expression, via its modulation of macrophage polarization within the atherosclerotic plaque [411]. In contrast to aged monocytes, aged PBMCs in both males and females, display a significant increase in CTSC expression (**Fig**

6.4 I). This implies, CTSC expression maybe highly expressed in other cell types (T-, B-, NK-cells) other than monocytes, within PBMCs, owing to its substantial increase in expression, whilst also inferring a possible contribution in promoting the development of atherosclerosis in aged males and females. The cytochrome P450 enzyme, CYP27A1, however, is significantly reduced in aged male PBMCs only. CYP27A1 is well known for its role in the hydroxylation of cholesterol to form the oxysterol 27-hydroxycholesterol (27HC) that exhibits both athero-genic and athero-protective functions [69], [345]. 27HC activates the athero-protective nuclear liver-x-receptor (LXR), enabling promotion of cholesterol efflux by Abca1 and Abcg1 [69]. However, an abundance of 27HC *in vivo*, due to Cyp27a1 overexpression, promotes leukocyte chemotaxis, inflammation and reduces vascular repair ultimately contributing to an increase in atherosclerosis development [361], [412].

In contrast, the expression of the fatty acid transporter, ABCD2, or scavenger receptor, CXCL16, did not change in aged monocytes, however both their expression was significantly increased in aged PBMCs. ABCD2, is involved in the oxidation of monounsaturated fatty acids, where its deficiency is associated with hepatic steatosis and loss of glycaemic control [413]. On the other hand, CXCL16, is involved in macrophage cholesterol uptake, whereby increased expression has been implicated in promoting macrophage foam cell formation and atherosclerosis development [56]. Altogether this indicates, differential regulation of these genes may contribute to the increased prevalence of age-associated lipid-mediated disorders.

Collectively, we have identified a network of IRF8 target genes that are differentially regulated by age and gender in both human PBMCs and monocytes in young and aged individuals. Many IRF8-target genes are involved in processes, including chemotaxis and inflammation that are dysregulated within the aged population. Further experimental validation of these genes in human monocytes and their regulation by IRF8, would help identify a network of IRF8-regulated genes that may provide useful biomarkers in the onset of certain age-associated disorders.

Chapter 7: Discussion

7.1 Summary of findings

This thesis uncovers a novel role for myeloid-IRF8 reduction in retarding the development of atherosclerotic plaque development, when challenged with a high fat western diet.

Secondly, the data presented in this thesis highlights an IRF8 induced reprograming of the macrophage transcriptome, within a hyperlipidaemic environment. This ultimately resulted in the significant differential regulation of inflammatory, chemotaxis and lipid-mediated pathways. From this data, we postulated a potential mechanism by which myeloid-IRF8 reduction confers athero-protection, via its regulation of Fabp4 and Fabp5.

Thirdly, this study demonstrates a novel transcriptomic signature of IRF8-regulated IFN-inducible genes that are specific to myeloid cells from an hyperlipidaemic environment. Collectively, this data has identified novel IFNβ regulated process that are repressed by IRF8 (Cholesterol biosynthesis, transport and lipid metabolism) and induced by IRF8 (apoptosis and leukocyte migration) in BMDMs from an atherosclerotic environment.

Fourthly, this thesis has uncovered an association of differentially regulated IRF8 target genes in young and aged monocytes from a healthy population. Comparative analysis, against previously published results, highlighted novel genes and pathways previously shown to be regulated by IRF8, in western-diet fed mice, that have the potential to serve as IRF8-regulated biomarkers of healthy ageing.

The next section will discuss the value of investigating the role of myeloid-IRF8 reduction in atherosclerosis development and the interpretation of each principal finding. Consideration of alternative interpretations and limitations of the experiments within this present study will also be discussed.

7.2 Discussion

7.2.1 Myeloid-IRF8 reduction retards atherosclerotic plaque development

Atherosclerosis is a disorder that stems from the dysregulation of inflammation and lipid metabolism. Imbalances within cellular and systemic cholesterol homeostasis result in the retention of cholesterol rich lipoproteins within the artery wall. This predominantly occurs in regions of altered blood flow where the quiescent endothelium is disturbed. The sequestered lipoproteins undergo various modifications (enzymatic cleavage, oxidation), causing the lipoproteins to become pro-inflammatory triggering the activation and recruitment of monocytes and their differentiation into macrophages. Macrophages engulf the modified lipoproteins, forming cholesterol-laden foam cells. Defective clearance of macrophage foam cells contributes to plaque burden and severity whist increasing the production of pro-inflammatory cytokines that amplify the immune response. Macrophages, therefore, have a pivotal role in the pathogenesis of atherosclerosis.

IRF8 is a dual transcriptional activator and repressor of many processes that are crucial for the development and differentiation of myeloid-cells, in particular monocytes and macrophages [119], [125], [130]. However, current

understanding of the functional role of myeloid-IRF8 beyond myelopoiesis is limited. Previous work by Doring and Colleagues identify an atherogenic role for heamtopoetic-IRF8 deficiency. However, their primary focus involved the investigation of how dysregulated myelopoiesis, caused by IRF8 deficiency, impacts on atherosclerosis development without addressing the myeloid cell-specific role for IRF8 [175]. Considering macrophage-IRF8 has been previously shown to transcriptionally regulate IL-18bp and Arginase-1, both known to contribute to atherosclerosis [197], [233], our aim was to define the specific role of myeloid-IRF8 in the inflammatory, lipid-mediated disorder atherosclerosis.

The data generated within this thesis uncovers a novel role for myeloid-IRF8 reduction in retarding the development of atherosclerosis in M-IRF8KO^{LdlrKO} mice, when compared to WT^{LdlrKO} mice. Similarly, to Clement et al., 2018, we demonstrated M-IRF8KO^{LdlrKO} mice also develop fewer advanced stage plaques in comparison the WT^{LdlrKO} mice. However, myeloid-IRF8 reduction did not impact on the severity of advanced plaques generated, as demonstrated by the lack of difference observed in the formation of necrotic cores, fibrous cap area and diameter. Intriguingly, Clement et al., 2018 identified a similar plaque phenotype in CD11c-IRF8KO mice, with no differences observed in necrotic core or fibrotic collagen formation. Thus, suggesting IRF8- reduction in myeloid cells specifically result in a similar atherosclerotic plaque phenotype. In contrast, Doring et al., 2012, demonstrate IRF8-deficient macrophages display defective efferocytosis of apoptotic PMNs, contributing to their increased plaque necrotic cores. However, it must be noted that the increased plaque development was attributed to an expansion of PMNs due to the CML-like phenotype identified in the hematopoeitc-IRF8^{KO} mice. In contrary to Doring et al.,2012, M-IRF8KO^{LdlrKO} do

not develop a CML-like phenotype, demonstrated by the lack of difference in the number of circulating monocytes and neutrophils. Therefore, it is unlikely that the atherosclerotic plaques present within the WT^{LdlrKO} and M-$IRF8KO^{LdlrKO}$ mice display an abundance of apoptotic neutrophils of which macrophages are unable to effectively clear. This would, however, need to be confirmed by measuring the number of apoptotic cells, for example; via plaque TUNEL staining and performing an efferocytosis assay, for example where the number of fluorescently labelled cells efferocytosis by macrophages are counted [414]. This possibility is also supported by Clement and colleagues whom also demonstrate no difference in plaque neutrophils or necrotic cores within myeloid specific CD11c-IRF8KO mice. Collectively this raises the possibility that deletion of IRF8 within myeloid cells specifically is not sufficient to promote the development of advanced stage plaques, after 12 weeks of western diet.

To characterise the severity of advanced plaques generated, it would be beneficial to quantify collagen formation to identify for differences in plaque vulnerability. This could be achieved by, using Hoechst staining to measure the acellular region, and using oil-red-o to measure foam cell quantity. However, RNA-Seq gene expression studies from BMDMs of M-$IRF8KO^{LdlrKO}$ mice do not demonstrate a differential regulation of genes involved within the above processes, apart from lipid metabolism and possibly apoptosis. Thus implying, myeloid-IRF8 reduction does not differentially regulate genes crucial to many of the processes required for advanced plaque formation, and therefore resulting in minimal differences between the severity of advanced stage plaques developed in M-$IRF8KO^{LdlrKO}$ mice when compared to WT^{LdlrKO} mice.

7.2.2 Myeloid-IRF8 reduction promotes the formation of foamy macrophages that are less inflammatory

RNA-Seq analysis on the BMDMs of western diet fed mice, demonstrate IRF8 reduction transcriptionally reprograms macrophages. This transcriptional reprograming may contribute to the athero-protective phenotype of myeloid-IRF8 reduction. Pathway analysis of the differentially regulated IRF8 target genes in the BMDMs of western diet fed M-IRF8KO^{LdlrKO} mice highlight significant regulation of genes involved in inflammation and lipid-metabolism. Although, the role of IRF8 in mediating immune response to IFNγ-induced inflammation is well known [94], its transcriptional role in lipid-metabolism within a hyperlipidaemic environment is poorly understood. We demonstrate myeloid-IRF8 reduction negatively regulates pathways crucial for macrophage foam cell formation, including lipid transport (*Fabp3, Fabp4, Fabp5*) [307], cholesterol metabolism (*Ch25h, Cyp27a1*) [415] and reverse cholesterol transport (*P2ry12, P2ry13, P2ry14*) [337]. Although subsequent functional analysis demonstrated a lack of difference in the cholesterol ester content of acLDL challenged macrophages from M-IRF8KO^{LdlrKO} mice compared to controls. We intriguingly discovered myeloid-IRF8 reduction significantly increased macrophage foam cell formation in comparison to controls. M-IRF8KO^{LdlrKO} mice develop less atherosclerosis and display a reduction in inflammatory gene expression in their BMDMs. Previous studies have demonstrated foamy macrophages to develop a reduced inflammatory phenotype, due to LXR-mediated suppression of pro-inflammatory cytokines [79], [416]. Although we have not discovered IRF8-regulation of LXR target genes specifically involved in suppressing inflammation, for example, *Srebp2*, we identified a significant overlap of genes regulated by IRF8 and genes differentially expressed in foamy macrophages. Remarkably, many pro-

inflammatory IRF8 target genes where negatively expressed in IRF8-KO macrophages, whereas many IRF8 target genes involved in lipid metabolism within the foamy macrophages share a similar expression profile within IRF8KO^{LdlrKO} mice also. This is supported by our comparative data comparing the transcriptional regulation of IRF8KO^{LdlrKO} macrophages against inflammatory and lipid-related trem2hi aortic macrophages from western diet fed mice. IRF8KO^{LdlrKO} macrophages, importantly, display decreased expression of pro-inflammatory genes enriched within inflammatory aortic macrophages and an increased expression of genes enriched within lipid-associated trem2hi macrophages. However, additional studies quantifying the lipids within aortic macrophages, via oil-red-o staining would be required to verify *in vivo* differences in macrophage foam cell formation. Collectively this suggests, myeloid-IRF8 reduction promotes foam cell formation whilst maintaining an anti-inflammatory transcriptomic phenotype similar to that of aortic foamy macrophages (**Fig 7.1**).

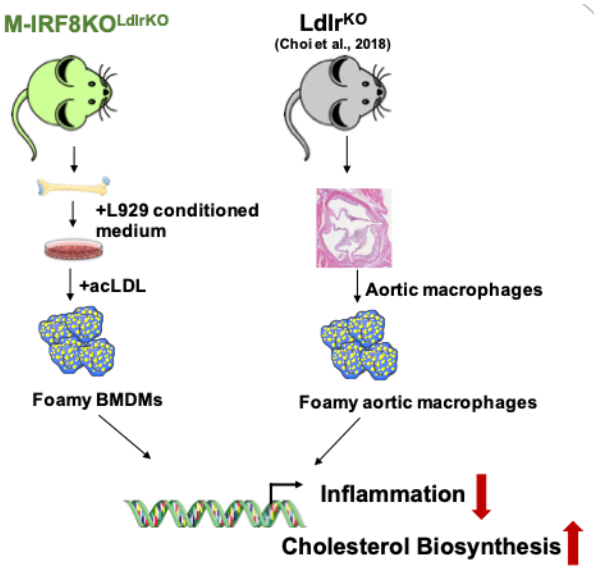

Fig 7.1 Schematic depicting transcriptional similarities between acLDL treated BMDMs from M-IRF8KOLdlrKO mice and foamy aortic macrophages from Choi et al.,2018.

7.2.3 Myeloid-IRF8 reduction negatively regulates macrophage migration

Leukocyte chemotaxis is a pivotal process in the development of atherosclerosis. It involves the adhesion and transmigration of cells, in particular monocytes, across the arterial membrane, aiding their entry into the lipid-enriched subendothelial space whereby monocytes differentiate into macrophages and subsequently become foam cells. Many studies blocking leukocyte chemotaxis, via inhibition of pro-migratory chemokines, Ccl2, Ccl5 Cx3cr1, abrogate atherosclerotic plaque formation [23], [417], [418]. This, therefore, demonstrates the importance of chemotaxis in atherosclerosis development. Surprisingly, we identified myeloid-IRF8 reduction negatively regulates genes involved in chemotaxis, ultimately resulting in the reduced migratory ability of IRF8KO^{LdlrKO} macrophages towards the chemoattractant MCP-1. Interestingly, we did not observe differences in the expression of well-known atherogenic, pro-chemotactic genes; Ccl2, Ccl5 and Cx3cr1. Instead, we identified significant IRF8 regulation of the purinergic receptors; P2ry12, Pry13 and P2ry14 whose role in leukocyte migration within atherosclerosis has not been well characterised. Interestingly, previous reports have uncovered an atherogenic phenotype of global P2ry12 and P2ry13 deficiency suggesting deficiency of purinergic receptors may contribute to atherosclerosis progression [419]. However, this was attributed to the inability of hepatic cells to effectively remove circulating cholesterol, via p2ry mediated holoparticle endocytosis resulting in significantly increased plasma cholesterol and subsequent plaque development. Although cell-specific deletion of P2ry12/13/14 has not been explored, to prevent hepatic-induced atherogenesis, previous studies exploring the global role of P2ry2 deficiency demonstrate a unique role in preventing ATP-

induced monocyte recruitment to atherosclerotic plaques [336]. Interestingly, this role in monocyte recruitment was further supported by recent studies demonstrating IRF8 regulation of P2x receptors was crucial for macrophage migration in a spinal cord injury [341]. Kobayakawa et al., 2019, demonstrate inhibition of IRF8 prevented macrophage migration via its regulation of purinergic receptors. This is one of the first studies to suggest that IRF8 regulates chemotaxis via purinergic receptors. Based on this exciting discovery, combined with our novel finding of the reduced migratory ability of IRF8KO^{LdlrKO} macrophages it is possible that myeloid-IRF8 reduction negatively regulates macrophage migration in a hyperlipidaemic environment due to its negative regulation of the purinergic receptors P2ry12/13/14. Additional investigation specifically inhibiting P2ry12/13 and P2ry14, using inhibitors or siRNA-mediated deletion, would clarify their role in macrophage migration within an hyperlipidaemic environment. Thus far this thesis has identified a novel functional role of myeloid-IRF8 reduction in negatively regulating macrophage migration.

7.2.4 IRF8 regulation of Fabp4 and Fabp5 modulates macrophage foam cell formation, cholesterol ester content and migration

The fatty acid binding proteins; Fabp3, Fabp4 and Fabp5, are involved in the transport of unsaturated and saturated fatty acids and have proven crucial in the maintenance of lipid-biosynthetic processes [350]. Previously, inhibition of Fabp4 and Fabp5 has been shown to abrogate atherosclerosis development via reduction of lipid accumulation and pro-inflammatory cytokine production [307], [420]. For this reason, we were intrigued when we identified a significant reduction of Fabp3, Fabp4 and Fabp5 gene expression in IRF8KO^{LdlrKO} macrophages.

To elucidate the role of the fatty acid binding proteins in response to myeloid-IRF8 reduction we measured macrophage foam cell formation, cholesterol ester content and migration in the presence of the Fabp4/5 inhibitor, BMS309403. In agreement with previous studies [307], [312], we identified a significant reduction in cholesterol ester and foam cell formation in WT^{LdlrKO} macrophages. However, no difference was observed in $IRF8KO^{LdlrKO}$ macrophages. This discovery suggests the athero-protective benefits of Fabp4 and Fabp5 are dependent on IRF8 expression. Previous studies demonstrate Fabp inhibition promotes ABCA1-induced cholesterol efflux, thereby reducing atherosclerotic plaque development [310]. Although we also saw a significant decreased in Abca1 gene expression within Fabp4/5 inhibitor treated WT^{LdlrKO} macrophages, further quantification of macrophage cholesterol efflux, by performing a cholesterol efflux assay, would help determine whether IRF8 regulation of Fabp also functionally impacts on cholesterol efflux.

Inhibition of Fabp4/5 has also been associated with reduced expression of the chemoattractant MCP-1 [307], although related differences in leukocyte chemotaxis in atherosclerosis have not been reported. Surprisingly, we demonstrated Fabp4/5 inhibition significantly reduces the migration of WT^{LdlrKO} macrophages towards MCP-1, without affecting $IRF8KO^{LdlrKO}$ macrophages. This supports the inhibitory effect of Fabp4/5 inhibition on macrophage migration is dependent on IRF8 expression.

Although Fabp4/5 inhibition is an attractive target for the prevention of atherosclerosis, many reports have highlighted adverse effects on aberrant

adipogenesis and severe hypoglycaemia in global Fabp4/5 deficiency. We have uncovered a novel myeloid-specific role of Fabp4/5 that is dependent on IRF8 that may prevent the previously identified adipocyte associated effects, due to the myeloid-specific reduction of the fatty acid binding proteins. Altogether this demonstrates, macrophage-IRF8 is a promising therapeutic target in the prevention of atherosclerosis development. By using small molecule siRNA-inhibitors encapsulated within lipid nanoparticles, it may be possible to reduce the expression of IRF8 and its target genes in myeloid cells specifically. Thus, reducing toxicity associated with global IRF8 and Fabp4/5 deficiency [421].

7.2.5 IRF8 reduction differentially regulates macrophage response to IFNβ

The interferon family constitute an array of widely expressed cytokines that form an integral part of the immune response to bacterial and viral infections. The IFN family constitutes two main classes of cytokines; Type I IFNs (α and β) and type II IFNs (γ) [134]. IFNγ has been highly associated with atherosclerosis, with many studies demonstrating the athero-protective benefits of IFNγ deletion [422], and athero-genic properties of exogenous IFNγ administration [423]. However, there is currently limited knowledge on the role of type I IFNs in atherosclerosis. Interestingly, a study by Goossens et al., 2010 was amongst the first to demonstrate myeloid-IFNβ signalling promotes atherosclerosis upon enhancement of macrophage recruitment [169]. This prompted our investigation into the role of myeloid-IRF8 in IFNβ signalling. RNA-Seq analysis on the IFNβ-treated BMDMs from IRF8KO^{LdlrKO} and WT^{LdlrKO} mice, revealed 373 significantly differentially regulated genes in response to IFNβ treatment. Pathway analysis demonstrated the differentially regulated genes, regulated by IFNβ stimulation,

were enriched in processes involving the anti-viral immune response and response to external natural stimulus. However, we intriguingly discovered a collection of IFNβ inducible genes that were positively regulated by IRF8 and involved in cholesterol biosynthesis and fatty acid metabolism. Previous studies have demonstrated differential type I IFN signalling transcriptionally reprograms lipid-biosynthetic processes via STAT2 [424] whilst promoting fatty acid oxidation allowing for activation of plasmacytoid dendritic cells [425]. These studies, however, have not eluded to the type of IFN responsible for the increase in type-I IFN induced lipid biosynthetic processes. In contrast, our data demonstrate IFNβ induces genes involved in lipid-biosynthetic processes in BMDMs from a hyperlipidaemic environment and their regulation is dependent on IRF8 expression.

Western diet-induced hypercholesteremia is known to induce chromatin remodelling of myeloid cells, resulting in epigenetic changes that alters myeloid cell response to a secondary stimuli [53], [378]. This phenomenon is termed innate 'trained' immunity [53], [378]. Previous studies have demonstrated monocytes from western diet fed mice display an enhanced inflammatory phenotype in comparison to chow fed mice. However, monocytes stimulated ex vivo with LPS or TLR2 displayed a stronger cytokine response than controls. This differential response was attributed to epigenetic remodelling due to changes in chromatin structure that were only present in western diet fed mice, as demonstrated by RNA-Seq and ATAQ-seq [378]. This raises the possibility that the hyperlipidaemic environment of western diet fed mice may transcriptionally alter the response of BMDMs to IFNβ, when stimulated ex vivo. Although we have not determined the IFNβ-induced IRF8 regulated differences in normal vs

western diet fed mice, we have uncovered previously unidentified genes enriched in processes including lipid metabolism and apoptosis that are dependent upon IRF8 expression when induced by IFNβ.

7.2.6 IRF8 and Ageing

Ageing is one of the most significant and prevalent risk factors in the development of disease, from cancer [229] to autoimmunity [226], neurodegeneration [407] to cardiovascular dysfunction [225]. One of the hallmarks of ageing is transcriptional dysregulation within immune cells, resulting in increased inflammation. As immune cells age, they undergo distinct epigenetic changes including reduced global closed heterochromatin and differences in DNA hypo- and hypermethylation [426]. Therefore, consequences of such epigenetic changes include changes in gene expression, resulting in aberrant transcriptional regulation of select processes in aged immune cells [427].

IRF8 is a transcriptional regulator of many processes that are differentially regulated in ageing, including; inflammation and lipid metabolism. Previous studies have identified reduced expression of IRF8 in hematopoietic stem cells and mature T-cells in humans [232]. Molony and colleagues have also acknowledged the importance of IRF8 expression in IFNβ response within aged monocytes, whereby diminished IRF8 resulted in a dysregulated IFNβ response [402]. Differences in the metabolism of lipids have also been shown to alter cell longevity, via chromatin remodelling [428]. This prompted our further investigation into how the newly identified IRF8 target genes in hyperlipidaemic mice, identified within this thesis, differ with age. Comparative analysis with the publicly available gene expression data from young and aged PBMCs from

ImmPort [231] uncovered a number of IRF8 target genes that were differentially regulated with age or gender (Chapter 6). Of the significant differentially regulated genes, 25% were involved in lipid-metabolic processes (*Cyp27a1, Gab1, Cxcl16, Ctsc, Abcd2* and *P2ry13*). Of these genes 6 also demonstrated gender specific differences (**Fig 6.4**). Although we were limited in aged samples and were therefore unable to investigate gender differences in young and aged monocytes, studies have demonstrated gender differences to have an impact on life span. Podolskiy and colleagues reported in cancers common to men and women, somatic DNA mutations where more prevalent amongst men than women. This suggests DNA damage occurs at different ages in both men and women [229]. Furthermore, studies have demonstrated gender-specific transcriptional differences in the brain resulting in differences in central nervous system associated mitochondrial metabolism and inflammation [228].

Collectively, these studies demonstrate sexual dimorphism impacts on the prevalence of age-associated diseases. Currently, we have identified a limited number of IRF8 target genes that differ with both age and gender in human PBMCs. However, it is possible that their differential regulation may contribute to the pathogenesis of certain age-associated diseases. To explore this concept in human monocytes, a powered study of at least an additional 9 subjects in each group would be required with additional validation of their regulation by IRF8, for example, by using siRNA targeted towards IRF8 *in vitro*. However, our current preliminary results suggest IRF8 may differentially regulate select genes involved in lipid metabolism that could serve as diagnostic biomarkers in the healthy aged population. Collectively, this data has the potential to be used as a pilot study that would be used to support a larger follow up investigation with 9 or more subjects.

7.3 Conclusion

Collectively, this thesis has uncovered a novel role for myeloid-IRF8 reduction in retarding the development of atherosclerosis. We have demonstrated IRF8 reduction transcriptionally reprogramed the macrophage transcriptome resulting in the differential regulation of many genes involved in inflammation, chemotaxis and lipid metabolism. Comparative analysis to published datasets have suggested macrophages from M-IRF8KO^{LdlrKO} mice transcriptionally resemble less-inflammatory, foamy aortic macrophages, from western diet fed mice. The data presented within this thesis suggests myeloid-IRF8 reduction may confer athero-protection upon decreasing the migratory ability of macrophages and reducing macrophage cholesterol ester content and foam cell formation via regulation of the fatty acid binding proteins; Fabp4 and Fabp5.

Furthermore, we have identified a novel signature of IRF8 regulated IFNβ inducible genes that are enriched in processes including lipid metabolism, inflammation and apoptosis within western diet fed BMDMs. Interestingly, many IRF8 regulated genes involved in lipid metabolism were also demonstrated to be differentially regulated with age in human monocytes, suggesting a potential IRF8-signature of lipid metabolic genes that differ with age.

In conclusion, this thesis identifies and reveals the impact of type I IFN signalling on myeloid-IRF8 regulated transcription in lipid metabolism. This thesis also highlights the reduction of myeloid-IRF8 regulated signalling pathways may serve as a potential therapeutic target in atherosclerosis.

References

[1] A. J. Lusis, “Atherosclerosis,” *Nature*, vol. 407, no. 6801, pp. 233–241, Sep. 2000.

[2] R. Lozano *et al.*, “Global and regional mortality from 235 causes of death for 20 age groups in 1990 and 2010: a systematic analysis for the Global Burden of Disease Study 2010.,” *Lancet (London, England)*, vol. 380, no. 9859, pp. 2095–128, Dec. 2012.

[3] J. P. Strong, G. T. Malcom, W. P. Newman 3rd, and M. C. Oalmann, “Early lesions of atherosclerosis in childhood and youth: natural history and risk factors,” *J Am Coll Nutr*, vol. 11 Suppl, pp. 51S-54S, 1992.

[4] P. Nigro, J. Abe, and B. C. Berk, “Flow Shear Stress and Atherosclerosis: A Matter of Site Specificity,” *Antioxid. Redox Signal.*, vol. 15, no. 5, pp. 1405–1414, Sep. 2011.

[5] I. Tabas, G. García-Cardeña, and G. K. Owens, “Recent insights into the cellular biology of atherosclerosis,” *Journal of Cell Biology*, vol. 209, no. 1. Rockefeller University Press, pp. 13–22, 13-Apr-2015.

[6] K.-A. Norton and A. S. Popel, “Effects of endothelial cell proliferation and migration rates in a computational model of sprouting angiogenesis,” *Sci. Rep.*, vol. 6, no. 1, p. 36992, Dec. 2016.

[7] Y. Huang *et al.*, “Normal glucose uptake in the brain and heart requires an endothelial cell-specific HIF-1α-dependent function,” *Proc. Natl. Acad. Sci. U. S. A.*, vol. 109, no. 43, pp. 17478–17483, Oct. 2012.

[8] C. B. and A. E. Delphine Moyon*, Luc Pardanaud*, Li Yuan, “Plasticity of endothelial cells during arterial-venous differentiation in the avian embryo,” 2001.

[9] L. Hajra, A. I. Evans, M. Chen, S. J. Hyduk, T. Collins, and M. I. Cybulsky,

"The NF-kappa B signal transduction pathway in aortic endothelial cells is primed for activation in regions predisposed to atherosclerotic lesion formation.," *Proc. Natl. Acad. Sci. U. S. A.*, vol. 97, no. 16, pp. 9052–7, Aug. 2000.

[10] N. E. Hastings, M. B. Simmers, O. G. McDonald, B. R. Wamhoff, and B. R. Blackman, "Atherosclerosis-prone hemodynamics differentially regulates endothelial and smooth muscle cell phenotypes and promotes pro-inflammatory priming," *Am. J. Physiol. Physiol.*, vol. 293, no. 6, pp. C1824–C1833, Dec. 2007.

[11] U. Förstermann *et al.*, "Nitric oxide synthase isozymes. Characterization, purification, molecular cloning, and functions.," *Hypertension*, vol. 23, no. 6_pt_2, pp. 1121–1131, Jun. 1994.

[12] M. Takahashi, U. Ikeda, J.-I. Masuyama, H. Funayama, S. Kano, and K. Shimada, "NITRIC OXIDE ATTENUATES ADHESION MOLECULE EXPRESSION IN HUMAN ENDOTHELIAL CELLS," *Cytokine*, vol. 8, no. 11, pp. 817–821, Nov. 1996.

[13] P. Ponnuswamy *et al.*, "eNOS protects from atherosclerosis despite relevant superoxide production by the enzyme in apoE mice.," *PLoS One*, vol. 7, no. 1, p. e30193, 2012.

[14] A. Hamik *et al.*, "Kruppel-like Factor 4 Regulates Endothelial Inflammation," *J. Biol. Chem.*, vol. 282, no. 18, pp. 13769–13779, May 2007.

[15] Z. Lin *et al.*, "Kruppel-Like Factor 2 (KLF2) Regulates Endothelial Thrombotic Function," *Circ. Res.*, vol. 96, no. 5, pp. e48-57, Mar. 2005.

[16] C. Delporte *et al.*, "Impact of myeloperoxidase-LDL interactions on enzyme activity and subsequent posttranslational oxidative modifications of apoB-100.," *J. Lipid Res.*, vol. 55, no. 4, pp. 747–57, Apr. 2014.

[17] J. M. Upston, J. Neuzil, and R. Stocker, “Oxidation of LDL by recombinant human 15-lipoxygenase: evidence for alpha-tocopherol-dependent oxidation of esterified core and surface lipids.,” *J. Lipid Res.*, vol. 37, no. 12, pp. 2650–61, Dec. 1996.

[18] T. Miyoshi *et al.*, “Deficiency of inducible NO synthase reduces advanced but not early atherosclerosis in apolipoprotein E-deficient mice,” *Life Sci.*, vol. 79, no. 6, pp. 525–531, Jul. 2006.

[19] M. Aviram, M. Rosenblat, A. Etzioni, and R. Levy, “Activation of NADPH oxidase required for macrophage-mediated oxidation of low-density lipoprotein.,” *Metabolism.*, vol. 45, no. 9, pp. 1069–79, Sep. 1996.

[20] G. Dai *et al.*, “Distinct endothelial phenotypes evoked by arterial waveforms derived from atherosclerosis-susceptible and -resistant regions of human vasculature.,” *Proc. Natl. Acad. Sci. U. S. A.*, vol. 101, no. 41, pp. 14871–6, Oct. 2004.

[21] F. K. Swirski *et al.*, “Ly-6Chi monocytes dominate hypercholesterolemia-associated monocytosis and give rise to macrophages in atheromata,” *J. Clin. Invest.*, vol. 117, no. 1, pp. 195–205, Jan. 2007.

[22] F. K. Swirski *et al.*, “Monocyte accumulation in mouse atherogenesis is progressive and proportional to extent of disease.,” *Proc. Natl. Acad. Sci. U. S. A.*, vol. 103, no. 27, pp. 10340–10345, Jul. 2006.

[23] C. Combadière *et al.*, “Combined inhibition of CCL2, CX3CR1, and CCR5 abrogates Ly6Chi and Ly6Clo monocytosis and almost abolishes atherosclerosis in hypercholesterolemic mice,” *Circulation*, vol. 117, no. 13, pp. 1649–1657, 2008.

[24] G. An *et al.*, “P-selectin glycoprotein ligand-1 is highly expressed on Ly-6Chi monocytes and a major determinant for Ly-6Chi monocyte recruitment

to sites of atherosclerosis in mice.," *Circulation*, vol. 117, no. 25, pp. 3227–3237, Jun. 2008.

[25] G. Chinetti-Gbaguidi, S. Colin, and B. Staels, "Macrophage subsets in atherosclerosis," *Nat. Rev. Cardiol.*, vol. 12, no. 1, pp. 10–17, Jan. 2015.

[26] F. De Paoli *et al.*, "Bone marrow-derived and peritoneal macrophages have different inflammatory response to oxLDL and M1/M2 marker expression - implications for atherosclerosis research," *Arterioscler. Thromb. Vasc. Biol.*, vol. 6, no. 4, pp. 29371–29374, Jun. 2015.

[27] V. Karuppagounder *et al.*, "Modulation of Macrophage Polarization and HMGB1-TLR2/TLR4 Cascade Plays a Crucial Role for Cardiac Remodeling in Senescence-Accelerated Prone Mice," *PLoS One*, vol. 11, no. 4, p. e0152922, Apr. 2016.

[28] B. Sun, B. B. Boyanovsky, M. A. Connelly, P. Shridas, D. R. van der Westhuyzen, and N. R. Webb, "Distinct mechanisms for OxLDL uptake and cellular trafficking by class B scavenger receptors CD36 and SR-BI," *J. Lipid Res.*, vol. 48, no. 12, pp. 2560–2570, Dec. 2007.

[29] D. E. Dove, Y. R. Su, L. L. Swift, M. F. Linton, and S. Fazio, "ACAT1 deficiency increases cholesterol synthesis in mouse peritoneal macrophages.," *Atherosclerosis*, vol. 186, no. 2, pp. 267–74, Jun. 2006.

[30] L. Yang *et al.*, "Enhancement of human ACAT1 gene expression to promote the macrophage-derived foam cell formation by dexamethasone," *Cell Res.*, vol. 14, no. 4, pp. 315–323, Aug. 2004.

[31] H. C. Stary *et al.*, "A definition of advanced types of atherosclerotic lesions and a histological classification of atherosclerosis: A report from the Committee on Vascular Lesions of the council on arteriosclerosis, American heart association," *Circulation*, vol. 92, no. 5. Lippincott Williams

& Wilkins, pp. 1355–1374, 01-Sep-1995.

[32] C. Niu *et al.*, “Macrophage Foam Cell-Derived Extracellular Vesicles Promote Vascular Smooth Muscle Cell Migration and Adhesion.,” *J. Am. Heart Assoc.*, vol. 5, no. 10, 2016.

[33] F. A. Yaghini *et al.*, “Angiotensin II-induced vascular smooth muscle cell migration and growth are mediated by cytochrome P450 1B1-dependent superoxide generation.,” *Hypertens. (Dallas, Tex. 1979)*, vol. 55, no. 6, pp. 1461–7, Jun. 2010.

[34] T. Zou, W. Yang, Z. Hou, and J. Yang, “Homocysteine enhances cell proliferation in vascular smooth muscle cells: role of p38 MAPK and p47phox,” *Acta Biochim. Biophys. Sin. (Shanghai).*, vol. 42, no. 12, pp. 908–915, Dec. 2010.

[35] D. Tayal, B. Goswami, B. Ch, ra Koner, and V. Mallika, “Role of homocysteine and lipoprotein (A) in atherosclerosis: An update,” *Biomed. Res.*, vol. 22, no. 4.

[36] U. Schönbeck, G. K. Sukhova, K. Shimizu, F. Mach, and P. Libby, “Inhibition of CD40 signaling limits evolution of established atherosclerosis in mice.,” *Proc. Natl. Acad. Sci. U. S. A.*, vol. 97, no. 13, pp. 7458–63, Jun. 2000.

[37] A. Schmidt, S. Lorkowski, D. Seidler, G. Breithardt, and E. Buddecke, “TGF-beta1 generates a specific multicomponent extracellular matrix in human coronary SMC,” *Eur. J. Clin. Invest.*, vol. 36, no. 7, pp. 473–482, Jul. 2006.

[38] D. E. Dove *et al.*, “ACAT1 deficiency disrupts cholesterol efflux and alters cellular morphology in macrophages,” *Arterioscler. Thromb. Vasc. Biol.*, vol. 25, no. 1, pp. 128–134, Jan. 2005.

[39] T. Devries-Seimon *et al.*, “Cholesterol-induced macrophage apoptosis requires ER stress pathways and engagement of the type A scavenger receptor.,” *J. Cell Biol.*, vol. 171, no. 1, pp. 61–73, Oct. 2005.

[40] J. Rothman and S. Munro, “The golgi apparatus: two organelles in tandem,” *Science (80-.).*, vol. 213, no. 4513, pp. 1212–1219, Sep. 1981.

[41] B. Feng *et al.*, “The endoplasmic reticulum is the site of cholesterol-induced cytotoxicity in macrophages,” *Nat. Cell Biol.*, vol. 5, no. 9, pp. 781–792, Sep. 2003.

[42] K. J. Travers, C. K. Patil, L. Wodicka, D. J. Lockhart, J. S. Weissman, and P. Walter, “Functional and genomic analyses reveal an essential coordination between the unfolded protein response and ER-associated degradation.,” *Cell*, vol. 101, no. 3, pp. 249–58, Apr. 2000.

[43] S. Oyadomari *et al.*, “Targeted disruption of the Chop gene delays endoplasmic reticulum stress-mediated diabetes.,” *J. Clin. Invest.*, vol. 109, no. 4, pp. 525–32, Feb. 2002.

[44] Y. Yuan, Q. Guo, Z. Ye, X. Pingping, N. Wang, and Z. Song, “Ischemic postconditioning protects brain from ischemia/reperfusion injury by attenuating endoplasmic reticulum stress-induced apoptosis through PI3K-Akt pathway,” *Brain Res.*, vol. 1367, pp. 85–93, 2011.

[45] B. Cai *et al.*, “MerTK receptor cleavage promotes plaque necrosis and defective resolution in atherosclerosis,” *J. Clin. Invest.*, vol. 127, no. 2, pp. 564–568, Feb. 2017.

[46] E. Thorp, D. Cui, D. M. Schrijvers, G. Kuriakose, and I. Tabas, “Mertk receptor mutation reduces efferocytosis efficiency and promotes apoptotic cell accumulation and plaque necrosis in atherosclerotic lesions of Apoe-/- mice,” *Arterioscler. Thromb. Vasc. Biol.*, vol. 28, no. 8, pp. 1421–1428, Aug.

2008.

[47] D. P. Faxon *et al.*, “Atherosclerotic Vascular Disease Conference: Writing Group III: pathophysiology.,” *Circulation*, vol. 109, no. 21, pp. 2617–25, Jun. 2004.

[48] K. J. Moore and I. Tabas, “Macrophages in the pathogenesis of atherosclerosis,” *Cell*, vol. 145, no. 3, pp. 341–355, 2011.

[49] F. Tacke *et al.*, “Monocyte subsets differentially employ CCR2, CCR5, and CX3CR1 to accumulate within atherosclerotic plaques,” *J. Clin. Invest.*, vol. 117, no. 1, pp. 185–194, Jan. 2007.

[50] F. Wang *et al.*, “Macrophage Foam Cell-Targeting Immunization Attenuates Atherosclerosis,” *Front. Immunol.*, vol. 9, p. 3127, Jan. 2019.

[51] M. Namiki *et al.*, “Local Overexpression of Monocyte Chemoattractant Protein-1 at Vessel Wall Induces Infiltration of Macrophages and Formation of Atherosclerotic Lesion,” *Arterioscler. Thromb. Vasc. Biol.*, vol. 22, no. 1, pp. 115–120, Jan. 2002.

[52] E. Trogan *et al.*, “Gene expression changes in foam cells and the role of chemokine receptor CCR7 during atherosclerosis regression in ApoE-deficient mice.”

[53] S. Bekkering, J. Quintin, L. A. B. Joosten, J. W. M. van der Meer, M. G. Netea, and N. P. Riksen, “Oxidized low-density lipoprotein induces long-term proinflammatory cytokine production and foam cell formation via epigenetic reprogramming of monocytes.,” *Arterioscler. Thromb. Vasc. Biol.*, vol. 34, no. 8, pp. 1731–8, Aug. 2014.

[54] H. Huang *et al.*, “Induction of inducible nitric oxide synthase (iNOS) expression by oxLDL inhibits macrophage derived foam cell migration,” *Atherosclerosis*, vol. 235, no. 1, pp. 213–222, Jul. 2014.

[55] C. R. Stewart *et al.*, “CD36 ligands promote sterile inflammation through assembly of a Toll-like receptor 4 and 6 heterodimer,” *Nat. Immunol.*, vol. 11, no. 2, pp. 155–161, Feb. 2010.

[56] A. M. Aslanian and I. F. Charo, “Targeted disruption of the scavenger receptor and chemokine CXCL16 accelerates atherosclerosis,” *Circulation*, vol. 114, no. 6, pp. 583–590, 2006.

[57] C. S. Robbins *et al.*, “Local proliferation dominates lesional macrophage accumulation in atherosclerosis,” *Nat. Med.*, vol. 19, no. 9, pp. 1166–1172, Sep. 2013.

[58] E. McNeill *et al.*, “Tracking monocyte recruitment and macrophage accumulation in atherosclerotic plaque progression using a novel hCD68GFP/ApoE -/- reporter mouse - Brief report,” *Arterioscler. Thromb. Vasc. Biol.*, vol. 37, no. 2, pp. 258–263, Feb. 2017.

[59] J. M. van Gils *et al.*, “The neuroimmune guidance cue netrin-1 promotes atherosclerosis by inhibiting the emigration of macrophages from plaques,” *Nat. Immunol.*, vol. 13, no. 2, pp. 136–143, Feb. 2012.

[60] A. Wanschel *et al.*, “Neuroimmune Guidance Cue Semaphorin 3E Is Expressed in Atherosclerotic Plaques and Regulates Macrophage Retention,” *Arterioscler. Thromb. Vasc. Biol.*, vol. 33, no. 5, pp. 886–893, May 2013.

[61] M. H. Aziz *et al.*, “The Upregulation of Integrin αDβ2 (CD11d/CD18) on Inflammatory Macrophages Promotes Macrophage Retention in Vascular Lesions and Development of Atherosclerosis.,” *J. Immunol.*, vol. 198, no. 12, pp. 4855–4867, Jun. 2017.

[62] P. F. Bradfield *et al.*, “Divergent JAM-C Expression Accelerates Monocyte-Derived Cell Exit from Atherosclerotic Plaques,” *PLoS One*, vol. 11, no. 7,

p. e0159679, Jul. 2016.

[63] M. Sekiya *et al.*, “Ablation of Neutral Cholesterol Ester Hydrolase 1 Accelerates Atherosclerosis,” *Cell Metab.*, vol. 10, no. 3, pp. 219–228, Sep. 2009.

[64] H. Okazaki *et al.*, “Identification of neutral cholesterol ester hydrolase, a key enzyme removing cholesterol from macrophages,” *J. Biol. Chem.*, vol. 283, no. 48, pp. 33357–33364, Nov. 2008.

[65] L. Yvan-Charvet *et al.*, “Combined deficiency of ABCA1 and ABCG1 promotes foam cell accumulation and accelerates atherosclerosis in mice,” *J. Clin. Invest.*, vol. 117, no. 12, pp. 3900–3908, Dec. 2007.

[66] X. Wang *et al.*, “macrophage ABCA1 and ABCG 1 but not SR-B1 promote macrophage reverse cholesterol transport in vivo,” *J. Clin. Invest.*, vol. 117, no. 8, pp. 2216–2224, 2007.

[67] C. Wu *et al.*, “Modulation of macrophage gene expression via LXRα serine 198 phosphorylation.,” *Mol. Cell. Biol.*, vol. 35, no. 11, pp. 2024–2034, 2015.

[68] P. S. Pannu, S. Allahverdian, and G. A. Francis, “Oxysterol generation and liver X receptor-dependent reverse cholesterol transport: Not all roads lead to Rome,” *Mol. Cell. Endocrinol.*, vol. 368, no. 1–2, pp. 99–107, 2013.

[69] M. Umetani *et al.*, “The cholesterol metabolite 27-hydroxycholesterol promotes atherosclerosis via proinflammatory processes mediated by estrogen receptor alpha,” *Cell Metab.*, vol. 20, no. 1, pp. 172–182, 2014.

[70] R. J. Aiello *et al.*, “Increased atherosclerosis in hyperlipidemic mice with inactivation of ABCA1 in macrophages,” *Arterioscler. Thromb. Vasc. Biol.*, vol. 22, no. 4, pp. 630–637, Apr. 2002.

[71] A. M. Allen and A. Graham, “Mitochondrial function is involved in regulation

of cholesterol efflux to apolipoprotein (apo)A-I from murine RAW 264.7 macrophages.," *Lipids Health Dis.*, vol. 11, p. 169, Dec. 2012.

[72] B. Feng, D. Zhang, G. Kuriakose, C. M. Devlin, M. Kockx, and I. Tabas, "Niemann-Pick C heterozygosity confers resistance to lesional necrosis and macrophage apoptosis in murine atherosclerosis," *Proc. Natl. Acad. Sci. U. S. A.*, vol. 100, no. 18, pp. 10423–10428, Sep. 2003.

[73] B. Feng *et al.*, "The endoplasmic reticulum is the site of cholesterol-induced cytotoxicity in macrophages," *Nat. Cell Biol.*, vol. 5, no. 9, pp. 781–792, Sep. 2003.

[74] E. Erbay *et al.*, "Reducing endoplasmic reticulum stress through a macrophage lipid chaperone alleviates atherosclerosis," *Nat. Med.*, vol. 15, no. 12, pp. 1383–1391, Dec. 2009.

[75] J. Nagenborg, P. Goossens, E. A. L. Biessen, and M. M. P. C. Donners, "Heterogeneity of atherosclerotic plaque macrophage origin, phenotype and functions: Implications for treatment," *Eur. J. Pharmacol.*, vol. 816, pp. 14–24, Dec. 2017.

[76] D. Gosselin *et al.*, "Environment Drives Selection and Function of Enhancers Controlling Tissue-Specific Macrophage Identities," *Cell*, vol. 159, no. 6, pp. 1327–1340, Dec. 2014.

[77] A. Erbilgin *et al.*, "Identification of CAD candidate genes in GWAS loci and their expression in vascular cells.," *J. Lipid Res.*, vol. 54, no. 7, pp. 1894–905, Jul. 2013.

[78] C. Cochain *et al.*, "Single-Cell RNA-Seq Reveals the Transcriptional Landscape and Heterogeneity of Aortic Macrophages in Murine Atherosclerosis," *Circ. Res.*, vol. 122, no. 12, pp. 1661–1674, Jun. 2018.

[79] K. Kim *et al.*, "Transcriptome Analysis Reveals Nonfoamy Rather Than

Foamy Plaque Macrophages Are Proinflammatory in Atherosclerotic Murine Models," *Circ. Res.*, vol. 123, no. 10, pp. 1127–1142, Oct. 2018.

[80] D. M. Fernandez *et al.*, "Single-cell immune landscape of human atherosclerotic plaques," *Nat. Med.*, pp. 1–13, Oct. 2019.

[81] J.-D. Lin *et al.*, "Single-cell analysis of fate-mapped macrophages reveals heterogeneity, including stem-like properties, during atherosclerosis progression and regression," *JCI Insight*, vol. 4, no. 4, Feb. 2019.

[82] J. Da Lin *et al.*, "Single-cell analysis of fate-mapped macrophages reveals heterogeneity, including stem-like properties, during atherosclerosis progression and regression," *JCI insight*, vol. 4, no. 4, Feb. 2019.

[83] L. Guo *et al.*, "CD163+ macrophages promote angiogenesis and vascular permeability accompanied by inflammation in atherosclerosis," *J. Clin. Invest.*, vol. 128, no. 3, pp. 1106–1124, Feb. 2018.

[84] J. T. Chai *et al.*, "Differential Gene Expression in Macrophages From Human Atherosclerotic Plaques Shows Convergence on Pathways Implicated by Genome-Wide Association Study Risk Variants," *Arterioscler. Thromb. Vasc. Biol.*, vol. 38, no. 11, pp. 2718–2730, Nov. 2018.

[85] G.-N. Zhao, D.-S. Jiang, and H. Li, "Interferon regulatory factors: at the crossroads of immunity, metabolism, and disease," *Biochim. Biophys. Acta - Mol. Basis Dis.*, vol. 1852, no. 2, pp. 365–378, 2015.

[86] A. Mancino *et al.*, "A dual cis-regulatory code links IRF8 to constitutive and inducible gene expression in macrophages," *Genes Dev.*, vol. 29, no. 4, pp. 394–408, 2015.

[87] A. Antonczyk *et al.*, "Direct Inhibition of IRF-Dependent Transcriptional Regulatory Mechanisms Associated With Disease," *Front. Immunol.*, vol.

10, p. 1176, May 2019.

[88] S. G. Remesh, V. Santosh, and C. R. Escalante, “Structural Studies of IRF4 Reveal a Flexible Autoinhibitory Region and a Compact Linker Domain,” *J. Biol. Chem.*, vol. 290, no. 46, pp. 27779–27790, Nov. 2015.

[89] H.-C. Chang Foreman, S. Van Scoy, T.-F. Cheng, and N. C. Reich, “Activation of Interferon Regulatory Factor 5 by Site Specific Phosphorylation,” *PLoS One*, vol. 7, no. 3, p. e33098, Mar. 2012.

[90] I. Marié, E. Smith, A. Prakash, and D. E. Levy, “Phosphorylation-Induced Dimerization of Interferon Regulatory Factor 7 Unmasks DNA Binding and a Bipartite Transactivation Domain,” *Mol. Cell. Biol.*, vol. 20, no. 23, p. 8803, 2000.

[91] H. M. Lazear *et al.*, “IRF-3, IRF-5, and IRF-7 Coordinately Regulate the Type I IFN Response in Myeloid Dendritic Cells Downstream of MAVS Signaling,” *PLoS Pathog.*, vol. 9, no. 1, p. e1003118, Jan. 2013.

[92] F. Steinhagen, L. G. Rodriguez, D. Tross, P. Tewary, C. Bode, and D. M. Klinman, “IRF5 and IRF8 modulate the CAL-1 human plasmacytoid dendritic cell line response following TLR9 ligation,” *Eur. J. Immunol.*, vol. 46, no. 3, pp. 647–655, 2016.

[93] H. W. Stout-Delgado, X. Yang, W. E. Walker, B. M. Tesar, and D. R. Goldstein, “Aging Impairs IFN Regulatory Factor 7 Up-Regulation in Plasmacytoid Dendritic Cells during TLR9 Activation,” *J. Immunol.*, vol. 181, no. 10, pp. 6747–6756, Nov. 2008.

[94] D. Langlais, L. B. Barreiro, and P. Gros, “The macrophage IRF8/IRF1 regulome is required for protection against infections and is associated with chronic inflammation,” *J. Exp. Med.*, p. jem.20151764, 2016.

[95] A. Antonczyk *et al.*, “Direct inhibition of IRF-dependent transcriptional

regulatory mechanisms associated with disease," *Front. Immunol.*, vol. 10, no. MAY, p. 1176, May 2019.

[96] H. Yamada, S. Mizuno, and I. Sugawara, "Interferon Regulatory Factor 1 in Mycobacterial Infection," *Microbiol. Immunol.*, vol. 46, no. 11, pp. 751–760, Nov. 2002.

[97] S. Lefebvre *et al.*, "A Specific Interferon (IFN)-stimulated Response Element of the Distal HLA-G Promoter Binds IFN-regulatory Factor 1 and Mediates Enhancement of This Nonclassical Class I Gene by IFN-β," *J. Biol. Chem.*, vol. 276, no. 9, pp. 6133–6139, Mar. 2001.

[98] R. Wessely *et al.*, "A central role of interferon regulatory factor-1 for the limitation of neointimal hyperplasia," *Hum. Mol. Genet.*, vol. 12, no. 2, pp. 177–187, Jan. 2003.

[99] K. Sikorski, J. Wesoly, and H. Bluyssen, "Data Mining of Atherosclerotic Plaque Transcriptomes Predicts STAT1-Dependent Inflammatory Signal Integration in Vascular Disease," *Int. J. Mol. Sci.*, vol. 15, no. 8, pp. 14313–14331, Aug. 2014.

[100] G. Ren, K. Cui, Z. Zhang, and K. Zhao, "Division of labor between IRF1 and IRF2 in regulating different stages of transcriptional activation in cellular antiviral activities," *Cell Biosci.*, vol. 5, no. 1, p. 17, Dec. 2015.

[101] P. D. DREW *et al.*, "NFκB and Interferon Regulatory Factor 1 Physically Interact and Synergistically Induce Major Histocompatibility Class I Gene Expression," *J. Interf. Cytokine Res.*, vol. 15, no. 12, pp. 1037–1045, Dec. 1995.

[102] J. Hiscott, "Triggering the innate antiviral response through IRF-3 activation.," *J. Biol. Chem.*, vol. 282, no. 21, pp. 15325–9, May 2007.

[103] H.-W. Chen, K. King, J. Tu, M. Sanchez, A. D. Luster, and S. Shresta, "The

roles of IRF-3 and IRF-7 in innate antiviral immunity against dengue virus.," *J. Immunol.*, vol. 191, no. 8, pp. 4194–201, Oct. 2013.

[104] A. A. Murphy, P. C. Rosato, Z. M. Parker, A. Khalenkov, and D. A. Leib, "Synergistic control of herpes simplex virus pathogenesis by IRF-3, and IRF-7 revealed through non-invasive bioluminescence imaging," *Virology*, vol. 444, no. 1–2, pp. 71–79, Sep. 2013.

[105] C. Schilte, M. R. Buckwalter, M. E. Laird, M. S. Diamond, O. Schwartz, and M. L. Albert, "Cutting Edge: Independent Roles for IRF-3 and IRF-7 in Hematopoietic and Nonhematopoietic Cells during Host Response to Chikungunya Infection," *J. Immunol.*, vol. 188, no. 7, pp. 2967–2971, Apr. 2012.

[106] L. Tang, B. Chen, B. Ma, and S. Nie, "Association between IRF5 polymorphisms and autoimmune diseases: a meta-analysis," *Genet. Mol. Res.*, vol. 13, no. 2, pp. 4473–4485, 2014.

[107] M. García-Bermúdez *et al.*, "Interferon regulatory factor 5 genetic variants are associated with cardiovascular disease in patients with rheumatoid arthritis," *Arthritis Res. Ther.*, vol. 16, no. 4, p. R146, Jul. 2014.

[108] S. Kondo *et al.*, "Mutations in IRF6 cause Van der Woude and popliteal pterygium syndromes," *Nat. Genet.*, vol. 32, no. 2, pp. 285–289, Oct. 2002.

[109] D. Ramnath *et al.*, "TLR3 drives IRF6-dependent IL-23p19 expression and p19/EBI3 heterodimer formation in keratinocytes," *Immunol. Cell Biol.*, vol. 93, no. 9, pp. 771–779, Oct. 2015.

[110] F. Moretti *et al.*, "A regulatory feedback loop involving p63 and IRF6 links the pathogenesis of 2 genetically different human ectodermal dysplasias," *J. Clin. Invest.*, vol. 120, no. 5, pp. 1570–1577, May 2010.

[111] K. Ochiai *et al.*, "Transcriptional Regulation of Germinal Center B and

Plasma Cell Fates by Dynamical Control of IRF4," *Immunity*, vol. 38, no. 5, pp. 918–929, May 2013.

[112] S. Ma, A. Turetsky, L. Trinh, and R. Lu, "IFN Regulatory Factor 4 and 8 Promote Ig Light Chain κ Locus Activation in Pre-B Cell Development," *J. Immunol.*, vol. 177, no. 11, pp. 7898–7904, Dec. 2006.

[113] D. L. Thibault *et al.*, "IRF9 and STAT1 are required for IgG autoantibody production and B cell expression of TLR7 in mice," *J. Clin. Invest.*, vol. 118, no. 4, pp. 1417–1426, Apr. 2008.

[114] T. Tamura, H. Yanai, D. Savitsky, and T. Taniguchi, "The IRF Family Transcription Factors in Immunity and Oncogenesis," *Annu. Rev. Immunol.*, vol. 26, no. 1, pp. 535–584, Apr. 2008.

[115] D. Kurotaki and T. Tamura, "Transcriptional and Epigenetic Regulation of Innate Immune Cell Development by the Transcription Factor, Interferon Regulatory Factor-8," *J. Interf. Cytokine Res.*, vol. 36, no. 7, pp. 433–441, 2016.

[116] D.-M. Shin, C.-H. Lee, and H. C. Morse, "IRF8 Governs Expression of Genes Involved in Innate and Adaptive Immunity in Human and Mouse Germinal Center B Cells," *PLoS One*, vol. 6, no. 11, p. e27384, 2011.

[117] B. Nelsen *et al.*, "Regulation of lymphoid-specific immunoglobulin μ heavy chain gene enhancer by ETS-domain proteins," *Science (80-.).*, vol. 261, no. 5117, pp. 82–86, Jul. 1993.

[118] E. Glasmacher *et al.*, "A genomic regulatory element that directs assembly and function of immune-specific AP-1 - IRF complexes," *Science (80-.).*, vol. 338, no. 6109, pp. 975–980, Nov. 2012.

[119] T. Tamura, D. Kurotaki, and S. ichi Koizumi, "Regulation of myelopoiesis by the transcription factor IRF8," *International Journal of Hematology*, vol.

101, no. 4. Springer Japan, pp. 342–351, 07-Apr-2015.

[120] C. Bovolenta *et al.*, “Molecular interactions between interferon consensus sequence binding protein and members of the interferon regulatory factor family.,” *Proc. Natl. Acad. Sci. U. S. A.*, vol. 91, no. 11, pp. 5046–50, May 1994.

[121] V. Bigley *et al.*, “Biallelic interferon regulatory factor 8 mutation: A complex immunodeficiency syndrome with dendritic cell deficiency, monocytopenia, and immune dysregulation,” *J. Allergy Clin. Immunol.*, vol. 141, no. 6, pp. 2234–2248, 2018.

[122] D. Sichien *et al.*, “IRF8 Transcription Factor Controls Survival and Function of Terminally Differentiated Conventional and Plasmacytoid Dendritic Cells, Respectively,” *Immunity*, vol. 45, no. 3, pp. 626–640, 2016.

[123] T. Holtschke *et al.*, “Immunodeficiency and chronic myelogenous leukemia-like syndrome in mice with a targeted mutation of the ICSBP gene,” 1996.

[124] H. Wang *et al.*, “A Reporter Mouse Reveals Lineage-Specific and Heterogeneous Expression of IRF8 during Lymphoid and Myeloid Cell Differentiation,” *J. Immunol.*, vol. 193, no. 4, pp. 1766–1777, Aug. 2014.

[125] D. Kurotaki *et al.*, “IRF8 inhibits C/EBPα activity to restrain mononuclear phagocyte progenitors from differentiating into neutrophils,” *Nat. Commun.*, vol. 5, p. 4978, 2014.

[126] D. Kurotaki *et al.*, “Transcription Factor IRF8 Governs Enhancer Landscape Dynamics in Mononuclear Phagocyte Progenitors,” *Cell Rep.*, vol. 22, no. 10, pp. 2628–2641, Mar. 2018.

[127] A. Yáñez and H. S. Goodridge, “Interferon regulatory factor 8 and the regulation of neutrophil, monocyte, and dendritic cell production,” *Current Opinion in Hematology*, vol. 23, no. 1. pp. 11–17, 2016.

[128] M. W. Feinberg *et al.*, “The Kruppel-like factor KLF4 is a critical regulator of monocyte differentiation.,” *EMBO J.*, vol. 26, no. 18, pp. 4138–48, Sep. 2007.

[129] D. Kurotaki *et al.*, “Essential role of the IRF8-KLF4 transcription factor cascade in murine monocyte differentiation.,” *Blood*, vol. 121, no. 10, pp. 1839–49, Mar. 2013.

[130] D. Kurotaki *et al.*, “Essential role of the IRF8-KLF4 transcription factor cascade in murine monocyte differentiation.,” *Blood*, vol. 121, no. 10, pp. 1839–49, Mar. 2013.

[131] U. Nagarajan, “Induction and Function of IFNβ During Viral and Bacterial Infection,” *Crit. Rev. Immunol.*, vol. 31, no. 6, pp. 459–474, 2011.

[132] K. Gibbert, J. Schlaak, D. Yang, and U. Dittmer, “IFN-α subtypes: distinct biological activities in anti-viral therapy,” *Br. J. Pharmacol.*, vol. 168, no. 5, pp. 1048–1058, Mar. 2013.

[133] V. Fensterl and G. C. Sen, “Interferons and viral infections,” *BioFactors*, vol. 35, no. 1, pp. 14–20, Jan. 2009.

[134] L. C. Platanias, “Mechanisms of type-I- and type-II-interferon-mediated signalling,” *Nat. Rev. Immunol.*, vol. 5, no. 5, pp. 375–386, May 2005.

[135] L. Sun, J. Wu, F. Du, X. Chen, and Z. J. Chen, “Cyclic GMP-AMP Synthase Is a Cytosolic DNA Sensor That Activates the Type I Interferon Pathway,” *Science (80-.).*, vol. 339, no. 6121, pp. 786–791, Feb. 2013.

[136] K. Honda *et al.*, “IRF-7 is the master regulator of type-I interferon-dependent immune responses,” *Nature*, vol. 434, no. 7034, pp. 772–777, Apr. 2005.

[137] H. Negishi, T. Taniguchi, and H. Yanai, “The Interferon (IFN) Class of Cytokines and the IFN Regulatory Factor (IRF) Transcription Factor

Family," *Cold Spring Harb. Perspect. Biol.*, vol. 10, no. 11, p. a028423, Nov. 2018.

[138] N. A. De Weerd *et al.*, "Structural basis of a unique interferon-β signaling axis mediated via the receptor IFNAR1," *Nat. Immunol.*, vol. 14, no. 9, pp. 901–907, Sep. 2013.

[139] T. H. Mogensen, "IRF and STAT Transcription Factors - From Basic Biology to Roles in Infection, Protective Immunity, and Primary Immunodeficiencies," *Front. Immunol.*, vol. 9, p. 3047, Jan. 2019.

[140] P. Tailor *et al.*, "The Feedback Phase of Type I Interferon Induction in Dendritic Cells Requires Interferon Regulatory Factor 8," *Immunity*, vol. 27, no. 2, pp. 228–239, Aug. 2007.

[141] P. Li *et al.*, "IRF8 and IRF3 cooperatively regulate rapid interferon-β induction in human blood monocytes," *Blood*, vol. 117, no. 10, pp. 2847–2854, Mar. 2011.

[142] F. Seif, M. Khoshmirsafa, H. Aazami, M. Mohsenzadegan, G. Sedighi, and M. Bahar, "The role of JAK-STAT signaling pathway and its regulators in the fate of T helper cells," *Cell Commun. Signal.*, vol. 15, no. 1, p. 23, Dec. 2017.

[143] C. M. Tato, G. A. Martins, F. A. High, C. B. DiCioccio, S. L. Reiner, and C. A. Hunter, "Cutting Edge: Innate Production of IFN-γ by NK Cells Is Independent of Epigenetic Modification of the IFN-γ Promoter," *J. Immunol.*, vol. 173, no. 3, pp. 1514–1517, Aug. 2004.

[144] A. Y. Mah and M. A. Cooper, "Metabolic regulation of natural killer cell IFN-γ production," *Crit. Rev. Immunol.*, vol. 36, no. 2, pp. 131–147, 2016.

[145] M. Kubin, M. Kamoun, and G. Trinchieri, "Interleukin 12 synergizes with B7/CD28 interaction in inducing efficient proliferation and cytokine

production of human T cells.," *J. Exp. Med.*, vol. 180, no. 1, pp. 211–22, Jul. 1994.

[146] M. Munder, M. Mallo, K. Eichmann, and M. Modolell, "Murine macrophages secrete interferon gamma upon combined stimulation with interleukin (IL)-12 and IL-18: A novel pathway of autocrine macrophage activation.," *J. Exp. Med.*, vol. 187, no. 12, pp. 2103–8, Jun. 1998.

[147] M. Nakahira *et al.*, "Synergy of IL-12 and IL-18 for IFN-gamma gene expression: IL-12-induced STAT4 contributes to IFN-gamma promoter activation by up-regulating the binding activity of IL-18-induced activator protein 1.," *J. Immunol.*, vol. 168, no. 3, pp. 1146–53, Feb. 2002.

[148] L. Darwich *et al.*, "Secretion of interferon-gamma by human macrophages demonstrated at the single-cell level after costimulation with interleukin (IL)-12 plus IL-18.," *Immunology*, vol. 126, no. 3, pp. 386–93, Mar. 2009.

[149] N. Nelson *et al.*, "Expression of IFN regulatory factor family proteins in lymphocytes: Induction of Stat-1 and IFN consensus sequence binding protein expression by T cell activation," *J. Immunol.*, vol. 156, no. 10, pp. 3711–3720, May 1996.

[150] Y. M. Kim, J. Y. Im, S. H. Han, H. S. Kang, and I. Choi, "IFN-gamma up-regulates IL-18 gene expression via IFN consensus sequence-binding protein and activator protein-1 elements in macrophages.," *J. Immunol.*, vol. 165, no. 6, pp. 3198–205, Sep. 2000.

[151] K. Y. Lee *et al.*, "Epigenetic disruption of interferon-γ response through silencing the tumor suppressor interferon regulatory factor 8 in nasopharyngeal, esophageal and multiple other carcinomas," *Oncogene*, vol. 27, no. 39, pp. 5267–5276, Sep. 2008.

[152] J. M. McGough *et al.*, "DNA methylation represses IFN-γ-induced and

signal transducer and activator of transcription 1-mediated IFN regulatory factor 8 activation in colon carcinoma cells," *Mol. Cancer Res.*, vol. 6, no. 12, pp. 1841–1851, Dec. 2008.

[153] T. Watanabe *et al.*, "The transcription factor IRF8 counteracts BCR-ABL to rescue dendritic cell development in chronic myelogenous leukemia," *Cancer Res.*, vol. 73, no. 22, pp. 6642–6653, Nov. 2013.

[154] J. B. Muhitch *et al.*, "Tumor-associated macrophage expression of interferon regulatory Factor-8 (IRF8) is a predictor of progression and patient survival in renal cell carcinoma," *J. Immunother. Cancer*, vol. 7, no. 1, p. 155, Dec. 2019.

[155] T. Kuwata *et al.*, "Gamma interferon triggers interaction between ICSBP (IRF-8) and TEL, recruiting the histone deacetylase HDAC3 to the interferon-responsive element.," *Mol. Cell. Biol.*, vol. 22, no. 21, pp. 7439–48, Nov. 2002.

[156] G. Tellides *et al.*, "Interferon-γ elicits arteriosclerosis in the absence of leukocytes," *Nature*, vol. 403, no. 6766, pp. 207–211, Jan. 2000.

[157] H. Ranjbaran *et al.*, "An inflammatory pathway of IFN-gamma production in coronary atherosclerosis.," *J. Immunol.*, vol. 178, no. 1, pp. 592–604, Jan. 2007.

[158] J. Zhang *et al.*, "Regulation of Endothelial Cell Adhesion Molecule Expression by Mast Cells, Macrophages, and Neutrophils," *PLoS One*, vol. 6, no. 1, p. e14525, Jan. 2011.

[159] K. Y. Stokes, E. C. Clanton, K. P. Clements, and D. N. Granger, "Role of Interferon-γ in Hypercholesterolemia-Induced Leukocyte–Endothelial Cell Adhesion," *Circulation*, vol. 107, no. 16, pp. 2140–2145, Apr. 2003.

[160] X.-Q. Wang, C. G. Panousis, M. L. Alfaro, G. F. Evans, and S. H.

Zuckerman, “Interferon-gamma-mediated downregulation of cholesterol efflux and ABC1 expression is by the Stat1 pathway.,” *Arterioscler. Thromb. Vasc. Biol.*, vol. 22, no. 5, pp. e5-9, May 2002.

[161] J. Li *et al.*, “Interferon-α priming promotes lipid uptake and macrophage-derived foam cell formation: A novel link between interferon-α and atherosclerosis in lupus,” *Arthritis Rheum.*, vol. 63, no. 2, pp. 492–502, Feb. 2011.

[162] C. G. Panousis and S. H. Zuckerman, “Regulation of cholesterol distribution in macrophage-derived foam cells by interferon-gamma.,” *J. Lipid Res.*, vol. 41, no. 1, pp. 75–83, Jan. 2000.

[163] A. B. Reiss *et al.*, “Immune complexes and IFN-gamma decrease cholesterol 27-hydroxylase in human arterial endothelium and macrophages.,” *J. Lipid Res.*, vol. 42, no. 11, pp. 1913–22, Nov. 2001.

[164] Y. Inagaki, S. Yamagishi, S. Amano, T. Okamoto, K. Koga, and Z. Makita, “Interferon-gamma-induced apoptosis and activation of THP-1 macrophages.,” *Life Sci.*, vol. 71, no. 21, pp. 2499–508, Oct. 2002.

[165] N. Caraccio *et al.*, “Effect of Type I Interferon(s) on Cell Viability and Apoptosis in Primary Human Thyrocyte Cultures,” *Thyroid*, vol. 19, no. 2, pp. 149–155, Feb. 2009.

[166] I. Tabas, “Macrophage death and defective inflammation resolution in atherosclerosis.,” *Nat. Rev. Immunol.*, vol. 10, no. 1, pp. 36–46, Jan. 2010.

[167] S.-H. Juang *et al.*, “IFN-β Induces Caspase-Mediated Apoptosis by Disrupting Mitochondria in Human Advanced Stage Colon Cancer Cell Lines,” *J. Interf. Cytokine Res.*, vol. 24, no. 4, pp. 231–243, Apr. 2004.

[168] S. H. Schirmer *et al.*, “Blocking Interferon β Stimulates Vascular Smooth Muscle Cell Proliferation and Arteriogenesis,” *J. Biol. Chem.*, vol. 285, no.

45, pp. 34677–34685, Nov. 2010.

[169] P. Goossens *et al.*, “Myeloid type I interferon signaling promotes atherosclerosis by stimulating macrophage recruitment to lesions,” *Cell Metab.*, vol. 12, no. 2, pp. 142–153, Aug. 2010.

[170] P. Y. Lee *et al.*, “Type I interferon modulates monocyte recruitment and maturation in chronic inflammation,” *Am. J. Pathol.*, vol. 175, no. 5, pp. 2023–2033, Nov. 2009.

[171] Y. Delneste *et al.*, “Interferon-γ switches monocyte differentiation from dendritic cells to macrophages,” *Blood*, vol. 101, no. 1, pp. 143–150, Jan. 2003.

[172] M. C. S. Boshuizen *et al.*, “Interferon-β promotes macrophage foam cell formation by altering both cholesterol influx and efflux mechanisms,” *Cytokine*, vol. 77, pp. 220–226, Jan. 2016.

[173] J. Schönheit *et al.*, “PU.1 Level-Directed Chromatin Structure Remodeling at the Irf8 Gene Drives Dendritic Cell Commitment,” *Cell Rep.*, vol. 3, no. 5, pp. 1617–1628, 2013.

[174] N. Li *et al.*, “IRF8 inhibits C/EBPα activity to restrain mononuclear phagocyte progenitors from differentiating into neutrophils,” *Nat. Commun.*, vol. 1861, no. 6, pp. 245–258, 2006.

[175] Y. Döring *et al.*, “Hematopoietic interferon regulatory factor 8-deficiency accelerates atherosclerosis in mice.,” *Arterioscler. Thromb. Vasc. Biol.*, vol. 32, no. 7, pp. 1613–1623, 2012.

[176] H. Yang and S. Chen, “The effect of interleukin-10 on apoptosis in macrophages stimulated by oxLDL,” *Eur. J. Pharmacol.*, vol. 657, no. 1–3, pp. 126–130, Apr. 2011.

[177] M. Clément *et al.*, “Deletion of IRF8 (Interferon Regulatory Factor 8)-

dependent dendritic cells abrogates proatherogenic adaptive immunity," *Circ. Res.*, vol. 122, no. 6, pp. 813–820, Mar. 2018.

[178] J. W. Hodge *et al.*, "Enhanced Activation of T Cells by Dendritic Cells Engineered to Hyperexpress a Triad of Costimulatory Molecules," *JNCI J. Natl. Cancer Inst.*, vol. 92, no. 15, pp. 1228–1239, Aug. 2000.

[179] D. Leonard *et al.*, "Coronary heart disease in systemic lupus erythematosus is associated with interferon regulatory factor-8 gene variants," *Circ. Cardiovasc. Genet.*, vol. 6, no. 3, pp. 255–263, 2013.

[180] S. Manzi *et al.*, "Age-specific Incidence Rates of Myocardial Infarction and Angina in Women with Systemic Lupus Erythematosus: Comparison with the Framingham Study," *Am. J. Epidemiol.*, vol. 145, no. 5, pp. 408–415, Mar. 1997.

[181] S. Rajagopalan *et al.*, "Endothelial cell apoptosis in systemic lupus erythematosus: a common pathway for abnormal vascular function and thrombosis propensity," *Blood*, vol. 103, no. 10, pp. 3677–3683, May 2004.

[182] P. Y. Lee *et al.*, "Type I interferon as a novel risk factor for endothelial progenitor cell depletion and endothelial dysfunction in systemic lupus erythematosus," *Arthritis Rheum.*, vol. 56, no. 11, pp. 3759–3769, Nov. 2007.

[183] E. F. Borba, E. Bonfá, C. G. C. Vinagre, J. A. F. Ramires, and R. C. Maranhão, "Chylomicron metabolism is markedly altered in systemic lupus erythematosus," *Arthritis Rheum.*, vol. 43, no. 5, pp. 1033–1040, May 2000.

[184] M. J. Kaplan and J. E. Salmon, "How does interferon-α insult the vasculature? Let me count the ways," *Arthritis and Rheumatism*, vol. 63, no. 2. NIH Public Access, pp. 334–336, Feb-2011.

[185] D. Leonard *et al.*, "Coronary heart disease in systemic lupus erythematosus

is associated with interferon regulatory factor-8 gene variants," *Circ. Cardiovasc. Genet.*, vol. 6, no. 3, pp. 255–263, Jun. 2013.

[186] T. (Dazhong) Huang, J. Behary, and A. Zekry, "Non-alcoholic fatty liver disease (NAFLD): a review of epidemiology, risk factors, diagnosis and management," *Intern. Med. J.*, p. imj.14709, Nov. 2019.

[187] E. Gaudio, V. Nobili, A. Franchitto, P. Onori, and G. Carpino, "Nonalcoholic fatty liver disease and atherosclerosis," *Intern. Emerg. Med.*, vol. 7, no. SUPPL. 3, pp. 297–305, 2012.

[188] V. W.-S. Wong *et al.*, "Coronary artery disease and cardiovascular outcomes in patients with non-alcoholic fatty liver disease," *Gut*, vol. 60, no. 12, pp. 1721–1727, Dec. 2011.

[189] J. L. Mellinger *et al.*, "Hepatic steatosis and cardiovascular disease outcomes: An analysis of the Framingham Heart Study," *J. Hepatol.*, vol. 63, no. 2, pp. 470–476, Aug. 2015.

[190] N. Becares *et al.*, "Impaired LXRα Phosphorylation Attenuates Progression of Fatty Liver Disease," *Cell Rep.*, vol. 26, no. 4, 2019.

[191] J. Tong *et al.*, "Hepatic Interferon Regulatory Factor 6 Alleviates Liver Steatosis and Metabolic Disorder by Transcriptionally Suppressing Peroxisome Proliferator-Activated Receptor γ in Mice," *Hepatology*, vol. 69, no. 6, p. hep.30559, Apr. 2019.

[192] F. Alzaid *et al.*, "IRF5 governs liver macrophage activation that promotes hepatic fibrosis in mice and humans," *JCI Insight*, vol. 1, no. 20, Dec. 2016.

[193] X.-A. Wang *et al.*, "Interferon regulatory factor 9 protects against hepatic insulin resistance and steatosis in male mice," *Hepatology*, vol. 58, no. 2, pp. 603–616, Aug. 2013.

[194] J. Tong *et al.*, "Hepatic Interferon Regulatory Factor 6 Alleviates Liver

Steatosis and Metabolic Disorder by Transcriptionally Suppressing Peroxisome Proliferator-Activated Receptor γ in Mice," *Hepatology*, vol. 69, no. 6, p. hep.30559, Apr. 2019.

[195] A. Montagner *et al.*, "Liver PPARα is crucial for whole-body fatty acid homeostasis and is protective against NAFLD.," *Gut*, vol. 65, no. 7, pp. 1202–14, Jul. 2016.

[196] F. Alzaid *et al.*, "IRF5 governs liver macrophage activation that promotes hepatic fibrosis in mice and humans," *Ref. Inf. JCI Insight*, vol. 1, no. 20, p. 88689, 2016.

[197] B. Pourcet *et al.*, "The nuclear receptor LXR modulates interleukin-18 levels in macrophages through multiple mechanisms.," *Sci. Rep.*, vol. 6, p. 25481, 2016.

[198] V. Kontis, J. E. Bennett, C. D. Mathers, G. Li, K. Foreman, and M. Ezzati, "Future life expectancy in 35 industrialised countries: projections with a Bayesian model ensemble," *Lancet*, vol. 389, no. 10076, pp. 1323–1335, Apr. 2017.

[199] T. Head, S. Daunert, and P. J. Goldschmidt-Clermont, "The Aging Risk and Atherosclerosis: A Fresh Look at Arterial Homeostasis.," *Front. Genet.*, vol. 8, p. 216, 2017.

[200] X. Xia, Q. Jiang, J. McDermott, and J.-D. J. Han, "Aging and Alzheimer's disease: Comparison and associations from molecular to system level," *Aging Cell*, vol. 17, no. 5, p. e12802, Oct. 2018.

[201] C. S. Cătană, A. G. Atanasov, and I. Berindan-Neagoe, "Natural products with anti-aging potential: Affected targets and molecular mechanisms," *Biotechnology Advances*, vol. 36, no. 6. Elsevier, pp. 1649–1656, 01-Nov-2018.

[202] C. López-Otín, M. A. Blasco, L. Partridge, M. Serrano, and G. Kroemer, “The hallmarks of aging,” *Cell*, vol. 153, no. 6. Elsevier, p. 1194, 06-Jun-2013.

[203] F. Erdel, K. Kratz, S. Willcox, J. D. Griffith, E. C. Greene, and T. de Lange, “Telomere Recognition and Assembly Mechanism of Mammalian Shelterin.,” *Cell Rep.*, vol. 18, no. 1, pp. 41–53, 2017.

[204] L. Li, S. Lejnine, V. Makarov, and J. P. Langmore, “In vitro and in vivo reconstitution and stability of vertebrate chromosome ends,” *Nucleic Acids Res.*, vol. 26, no. 12, pp. 2908–2908, Jun. 1998.

[205] F. d’Adda di Fagagna *et al.*, “A DNA damage checkpoint response in telomere-initiated senescence,” *Nature*, vol. 426, no. 6963, pp. 194–198, Nov. 2003.

[206] J. Liu, L. Wang, Z. Wang, and J.-P. Liu, “Roles of Telomere Biology in Cell Senescence, Replicative and Chronological Ageing.,” *Cells*, vol. 8, no. 1, 2019.

[207] C. Sidler, R. Wóycicki, Y. Ilnytskyy, G. Metz, I. Kovalchuk, and O. Kovalchuk, “Immunosenescence is associated with altered gene expression and epigenetic regulation in primary and secondary immune organs,” *Front. Genet.*, vol. 4, p. 211, 2013.

[208] D. Glass *et al.*, “Gene expression changes with age in skin, adipose tissue, blood and brain,” *Genome Biol.*, vol. 14, no. 7, p. R75, Jul. 2013.

[209] Y. Sun, N. Miao, and T. Sun, “Detect accessible chromatin using ATAC-sequencing, from principle to applications.,” *Hereditas*, vol. 156, p. 29, 2019.

[210] S. Venkatesh and J. L. Workman, “Histone exchange, chromatin structure and the regulation of transcription,” *Nat. Rev. Mol. Cell Biol.*, vol. 16, no. 3,

pp. 178–189, Mar. 2015.

[211] R. Bahar *et al.*, “Increased cell-to-cell variation in gene expression in ageing mouse heart,” *Nature*, vol. 441, no. 7096, pp. 1011–1014, Jun. 2006.

[212] K. Voutetakis, A. Chatziioannou, E. S. Gonos, and I. P. Trougakos, “Comparative meta-analysis of transcriptomics data during cellular senescence and in vivo tissue ageing,” *Oxid. Med. Cell. Longev.*, vol. 2015, p. 732914, 2015.

[213] J. P. de Magalhães, J. Curado, and G. M. Church, “Meta-analysis of age-related gene expression profiles identifies common signatures of aging,” *Bioinformatics*, vol. 25, no. 7, pp. 875–881, Apr. 2009.

[214] S. Fujii, K. Liu, C. Smith, A. J. Bonito, and R. M. Steinman, “The Linkage of Innate to Adaptive Immunity via Maturing Dendritic Cells In Vivo Requires CD40 Ligation in Addition to Antigen Presentation and CD80/86 Costimulation,” *J. Exp. Med.*, vol. 199, no. 12, pp. 1607–1618, Jun. 2004.

[215] J. Ye *et al.*, “Tumor-derived γδ regulatory T cells suppress innate and adaptive immunity through the induction of immunosenescence.,” *J. Immunol.*, vol. 190, no. 5, pp. 2403–14, Mar. 2013.

[216] S. Della Bella *et al.*, “Peripheral blood dendritic cells and monocytes are differently regulated in the elderly,” *Clin. Immunol.*, vol. 122, no. 2, pp. 220–228, Feb. 2007.

[217] F. Rahmatpanah, S. Agrawal, V. M. Scarfone, S. Kapadia, D. Mercola, and A. Agrawal, “Transcriptional Profiling of Age-Associated Gene Expression Changes in Human Circulatory CD1c+ Myeloid Dendritic Cell Subset,” *Journals Gerontol. Ser. A*, vol. 74, no. 1, pp. 9–15, Jan. 2019.

[218] L. C. Greaves *et al.*, “Clonal Expansion of Early to Mid-Life Mitochondrial

DNA Point Mutations Drives Mitochondrial Dysfunction during Human Ageing," *PLoS Genet.*, vol. 10, no. 9, p. e1004620, Sep. 2014.

[219] O. Hashizume *et al.*, "Epigenetic regulation of the nuclear-coded GCAT and SHMT2 genes confers human age-associated mitochondrial respiration defects," *Sci. Rep.*, vol. 5, no. 1, p. 10434, Sep. 2015.

[220] A. Hiona *et al.*, "Mitochondrial DNA Mutations Induce Mitochondrial Dysfunction, Apoptosis and Sarcopenia in Skeletal Muscle of Mitochondrial DNA Mutator Mice," *PLoS One*, vol. 5, no. 7, p. e11468, Jul. 2010.

[221] S. Seidler, H. W. Zimmermann, M. Bartneck, C. Trautwein, and F. Tacke, "Age-dependent alterations of monocyte subsets and monocyte-related chemokine pathways in healthy adults," *BMC Immunol.*, vol. 11, no. 1, p. 30, Jun. 2010.

[222] J. Nyugen, S. Agrawal, S. Gollapudi, and S. Gupta, "Impaired Functions of Peripheral Blood Monocyte Subpopulations in Aged Humans," *J. Clin. Immunol.*, vol. 30, no. 6, pp. 806–813, Nov. 2010.

[223] A. Merino, P. Buendia, A. Martin-Malo, P. Aljama, R. Ramirez, and J. Carracedo, "Senescent CD14 + CD16 + Monocytes Exhibit Proinflammatory and Proatherosclerotic Activity," *J. Immunol.*, vol. 186, no. 3, pp. 1809–1815, Feb. 2011.

[224] B. D. Pence and J. R. Yarbro, "Aging impairs mitochondrial respiratory capacity in classical monocytes," *Exp. Gerontol.*, vol. 108, pp. 112–117, Jul. 2018.

[225] W. Du *et al.*, "Age-associated vascular inflammation promotes monocytosis during atherogenesis.," *Aging Cell*, vol. 15, no. 4, pp. 766–77, 2016.

[226] A. C. Hearps *et al.*, "Aging is associated with chronic innate immune activation and dysregulation of monocyte phenotype and function," *Aging*

Cell, vol. 11, no. 5, pp. 867–875, Oct. 2012.

[227] C. R. Beam, C. Kaneshiro, J. Y. Jang, C. A. Reynolds, N. L. Pedersen, and M. Gatz, "Differences Between Women and Men in Incidence Rates of Dementia and Alzheimer's Disease.," *J. Alzheimers. Dis.*, vol. 64, no. 4, pp. 1077–1083, 2018.

[228] N. C. Berchtold *et al.*, "Gene expression changes in the course of normal brain aging are sexually dimorphic," *Proc. Natl. Acad. Sci. U. S. A.*, vol. 105, no. 40, pp. 15605–15610, Oct. 2008.

[229] D. I. Podolskiy, A. V Lobanov, G. V Kryukov, and V. N. Gladyshev, "Analysis of cancer genomes reveals basic features of human aging and its role in cancer development," *Nat. Commun.*, vol. 7, p. 12157, 2016.

[230] A. Bouman, M. Schipper, M. J. Heineman, and M. M. Faas, "Gender Difference in the Non-Specific and Specific Immune Response in Humans," *Am. J. Reprod. Immunol.*, vol. 52, no. 1, pp. 19–26, Jul. 2004.

[231] K. A. Zalocusky *et al.*, "The 10,000 Immunomes Project: Building a Resource for Human Immunology," *Cell Rep.*, vol. 25, no. 2, pp. 513-522.e3, Oct. 2018.

[232] D. L. Stirewalt *et al.*, "Decreased IRF8 expression found in aging hematopoietic progenitor/stem cells," *Leukemia*, vol. 23, no. 2. NIH Public Access, pp. 391–393, Feb-2009.

[233] B. Pourcet *et al.*, "LXRa regulates macrophage arginase 1 through PU.1 and interferon regulatory factor 8," *Circ. Res.*, vol. 109, no. 5, pp. 492–501, 2011.

[234] M. C. Gage *et al.*, "Endothelium-specific insulin resistance leads to accelerated atherosclerosis in areas with disturbed flow patterns: A role for reactive oxygen species," *Atherosclerosis*, vol. 230, no. 1, pp. 131–139,

Sep. 2013.

[235] A. N. Seneviratne *et al.*, “Interferon Regulatory Factor 5 Controls Necrotic Core Formation in Atherosclerotic Lesions by Impairing Efferocytosis,” *Circulation*, vol. 136, no. 12, pp. 1140–1154, Sep. 2017.

[236] W. Newman, R. O. Duda, and P. E. Hart, “Use of the Hough Transformation To Detect Lines and Curves in Pictures.”

[237] I. Pineda-Torra, M. Gage, A. de Juan, and O. M. Pello, “Isolation, Culture, and Polarization of Murine Bone Marrow-Derived and Peritoneal Macrophages.,” *Methods Mol. Biol.*, vol. 1339, pp. 101–9, 2015.

[238] X. Zhang, R. Goncalves, and D. M. Mosser, “The isolation and characterization of murine macrophages.,” *Curr. Protoc. Immunol.*, vol. Chapter 14, p. Unit 14.1, Nov. 2008.

[239] M. Haeussler *et al.*, “The UCSC Genome Browser database: 2019 update,” *Nucleic Acids Res.*, vol. 47, no. D1, pp. D853–D858, Jan. 2019.

[240] A. Untergasser *et al.*, “Primer3—new capabilities and interfaces,” *Nucleic Acids Res.*, vol. 40, no. 15, pp. e115–e115, Aug. 2012.

[241] K. Korthauer *et al.*, “A practical guide to methods controlling false discoveries in computational biology.”

[242] Y. Zhou *et al.*, “Metascape provides a biologist-oriented resource for the analysis of systems-level datasets,” *Nat. Commun.*, vol. 10, no. 1, p. 1523, Dec. 2019.

[243] M. Griesemer, J. A. Kimbrel, C. E. Zhou, A. Navid, and P. D’haeseleer, “Combining multiple functional annotation tools increases coverage of metabolic annotation,” *BMC Genomics*, vol. 19, no. 1, p. 948, Dec. 2018.

[244] S. Chowdhury and R. R. Sarkar, “Comparison of human cell signaling pathway databases—evolution, drawbacks and challenges,” *Database*,

vol. 2015, Jan. 2015.

[245] M. Scheller *et al.*, “Altered development and cytokine responses of myeloid progenitors in the absence of transcription factor, interferon consensus sequence binding protein,” *Blood*, vol. 94, no. 11, pp. 3764–3771, 1999.

[246] N. M. Adams *et al.*, “Transcription Factor IRF8 Orchestrates the Adaptive Natural Killer Cell Response Optimal NK cell proliferation & viral control Article Transcription Factor IRF8 Orchestrates the Adaptive Natural Killer Cell Response,” *Immunity*, vol. 48, pp. 1172–1182, 2018.

[247] S. B. Joseph *et al.*, “Synthetic LXR ligand inhibits the development of atherosclerosis in mice,” *Proc. Natl. Acad. Sci.*, vol. 99, no. 11, pp. 7604–7609, 2002.

[248] 3 and Peter Tontonoz Michelle N. Bradley,1 Cynthia Hong,1 Mingyi Chen,1 Sean B. Joseph,1 Damien C. Wilpitz,1 Xuping Wang,2 Aldons J. Lusis,2 Allan Collins,3 Willa A. Hseuh,3 Jon L. Collins,4 Rajendra K. Tangirala, “Ligand activation of LXR beta reverses atherosclerosis and cellular cholesterol overload in mice lacking LXR alpha and apoE.”

[249] M. S. Kappus *et al.*, “Activation of Liver X Receptor Decreases Atherosclerosis in Ldlr−/− mice in the Absence of ABCA1 and ABCG1 in Myeloid Cells,” *Arterioscler. Thromb. Vasc. Biol.*, vol. 34, no. 001140, pp. 1–5, Feb. 2014.

[250] R. C. Stone *et al.*, “Interferon regulatory factor 5 activation in monocytes of systemic lupus erythematosus patients is triggered by circulating autoantigens independent of type I interferons,” *Arthritis Rheum.*, vol. 64, no. 3, pp. 788–798, Mar. 2012.

[251] B. Baharvand-Ahmadi, K. Sharifi, and M. Namdari, “Prevalence of non-alcoholic fatty liver disease in patients with coronary artery disease.,” *ARYA*

Atheroscler., vol. 12, no. 4, pp. 201–205, Jul. 2016.

[252] K. Wójcik-Cichy, E. Koślińska-Berkan, and A. Piekarska, “The influence of NAFLD on the risk of atherosclerosis and cardiovascular diseases.,” *Clin. Exp. Hepatol.*, vol. 4, no. 1, pp. 1–6, Mar. 2018.

[253] J. Feng, H. Wang, D.-M. Shin, M. Masiuk, C.-F. Qi, and H. C. Morse, “IFN regulatory factor 8 restricts the size of the marginal zone and follicular B cell pools,” *J. Immunol.*, vol. 186, no. 3, pp. 1458–1466, Feb. 2011.

[254] A. V Paschall *et al.*, “IFN regulatory factor 8 represses GM-CSF expression in T cells to affect myeloid cell lineage differentiation.,” *J. Immunol.*, vol. 194, no. 5, pp. 2369–79, 2015.

[255] R. K. Tangirala, E. M. Rubin, and W. Palinski, “Quantitation of atherosclerosis in murine models: correlation between lesions in the aortic origin and in the entire aorta, and differences in the extent of lesions between sexes in LDL receptor-deficient and apolipoprotein E-deficient mice.,” *J. Lipid Res.*, vol. 36, no. 11, pp. 2320–8, 1995.

[256] Y. Nakashima, A. S. Plump, E. W. Raines, J. L. Breslow, and R. Ross, “ApoE-deficient mice develop lesions of all phases of atherosclerosis throughout the arterial tree.,” *Arterioscler. Thromb. a J. Vasc. Biol.*, vol. 14, no. 1, pp. 133–40, Jan. 1994.

[257] P. A. VanderLaan, C. A. Reardon, and G. S. Getz, “Site Specificity of Atherosclerosis: Site-Selective Responses to Atherosclerotic Modulators,” *Arterioscler. Thromb. Vasc. Biol.*, vol. 24, no. 1, pp. 12–22, 2004.

[258] X. Zhao *et al.*, “Discriminating carotid atherosclerotic lesion severity by luminal stenosis and plaque burden: a comparison utilizing high-resolution magnetic resonance imaging at 3.0 Tesla.,” *Stroke*, vol. 42, no. 2, pp. 347–53, Feb. 2011.

[259] A. Daugherty *et al.*, “Recommendation on Design, Execution, and Reporting of Animal Atherosclerosis Studies A Scientific Statement From the American Heart Association AHA Scientific Statement,” *Arter. Thromb Vasc Biol*, vol. 37, pp. 131–157, 2017.

[260] Z.-Y. Li, S. P. S. Howarth, T. Tang, and J. H. Gillard, “How Critical Is Fibrous Cap Thickness to Carotid Plaque Stability?,” *Stroke*, vol. 37, no. 5, pp. 1195–1199, May 2006.

[261] R. Virmani, F. D. Kolodgie, A. P. Burke, A. Farb, and S. M. Schwartz, “Lessons From Sudden Coronary Death,” *Arterioscler. Thromb. Vasc. Biol.*, vol. 20, no. 5, pp. 1262–1275, May 2000.

[262] R. Virmani *et al.*, “Atherosclerotic Plaque Progression and Vulnerability to Rupture,” *Arterioscler. Thromb. Vasc. Biol.*, vol. 25, no. 10, pp. 2054–2061, Oct. 2005.

[263] M. H. M. Barros, F. Hauck, J. H. Dreyer, B. Kempkes, and G. Niedobitek, “Macrophage polarisation: an immunohistochemical approach for identifying M1 and M2 macrophages.,” *PLoS One*, vol. 8, no. 11, p. e80908, 2013.

[264] P. Menon and E. A. Fisher, “Immunostaining of Macrophages, Endothelial Cells, and Smooth Muscle Cells in the Atherosclerotic Mouse Aorta.,” *Methods Mol. Biol.*, vol. 1339, pp. 131–48, 2015.

[265] M. Scheller, J. Schönheit, K. Zimmermann, U. Leser, F. Rosenbauer, and A. Leutz, “Cross talk between Wnt/β-catenin and Irf8 in leukemia progression and drug resistance.,” *J. Exp. Med.*, vol. 210, no. 11, pp. 2239–56, Oct. 2013.

[266] A. L. Shaffer *et al.*, “IRF4 addiction in multiple myeloma.,” *Nature*, vol. 454, no. 7201, pp. 226–31, Jul. 2008.

[267] S. Gargiulo *et al.*, “Evaluation of growth patterns and body composition in C57Bl/6J mice using dual energy X-ray absorptiometry.,” *Biomed Res. Int.*, vol. 2014, p. 253067, 2014.

[268] N. J. G. Smith *et al.*, “A comparison of dietary and caloric restriction models on body composition, physical performance, and metabolic health in young mice,” *Nutrients*, vol. 11, no. 2, 2019.

[269] J. D. Waight *et al.*, “Myeloid-derived suppressor cell development is regulated by a STAT/IRF-8 axis,” *J. Clin. Invest.*, vol. 123, no. 10, pp. 4464–4478, Oct. 2013.

[270] E. Saito *et al.*, “Down-regulation of Irf8 by Lyz2-cre/loxP accelerates osteoclast differentiation in vitro.,” *Cytotechnology*, 2016.

[271] J. Han *et al.*, “Nonalcoholic fatty liver disease represents a greater metabolic burden in patients with atherosclerosis,” *Medicine (Baltimore).*, vol. 98, no. 11, p. e14896, Mar. 2019.

[272] J.-F. Marquis *et al.*, “Interferon Regulatory Factor 8 Regulates Pathways for Antigen Presentation in Myeloid Cells and during Tuberculosis,” *PLoS Genet.*, vol. 7, no. 6, p. e1002097, Jun. 2011.

[273] Y. Ma *et al.*, “Hyperlipidemia and atherosclerotic lesion development in Ldlr-deficient mice on a long-term high-fat diet.,” *PLoS One*, vol. 7, no. 4, p. e35835, 2012.

[274] X. Zhao *et al.*, “Discriminating carotid atherosclerotic lesion severity by luminal stenosis and plaque burden: a comparison utilizing high-resolution magnetic resonance imaging at 3.0 Tesla.,” *Stroke*, vol. 42, no. 2, pp. 347–53, Feb. 2011.

[275] S.-M. Zhang *et al.*, “Interferon regulatory factor 8 modulates phenotypic switching of smooth muscle cells by regulating the activity of myocardin.,”

Mol. Cell. Biol., vol. 34, no. 3, pp. 400–14, 2014.

[276] P.-W. Fok, “Growth of necrotic cores in atherosclerotic plaque.”

[277] A. Fernández-Ortiz *et al.*, “Characterization of the relative thrombogenicity of atherosclerotic plaque components: Implications for consequences of plaque rupture,” *J. Am. Coll. Cardiol.*, vol. 23, no. 7, pp. 1562–1569, Jun. 1994.

[278] M. Ackers-Johnson *et al.*, “Myocardin Regulates Vascular Smooth Muscle Cell Inflammatory Activation and Disease,” *Arterioscler. Thromb. Vasc. Biol.*, vol. 35, no. 4, pp. 817–828, Apr. 2015.

[279] J. Albarrán-Juárez, H. Kaur, M. Grimm, S. Offermanns, and N. Wettschureck, “Lineage tracing of cells involved in atherosclerosis.,” *Atherosclerosis*, vol. 251, pp. 445–453, Aug. 2016.

[280] X.-A. Wang *et al.*, “Interferon regulatory factor 9 protects against hepatic insulin resistance and steatosis in male mice,” *Hepatology*, vol. 58, no. 2, pp. 603–616, Aug. 2013.

[281] E. L. Gautier *et al.*, “Systemic analysis of PPARγ in mouse macrophage populations reveals marked diversity in expression with critical roles in resolution of inflammation and airway immunity.,” *J. Immunol.*, vol. 189, no. 5, pp. 2614–24, Sep. 2012.

[282] J. R. Clapper *et al.*, “Diet-induced mouse model of fatty liver disease and nonalcoholic steatohepatitis reflecting clinical disease progression and methods of assessment,” *Am. J. Physiol. Liver Physiol.*, vol. 305, no. 7, pp. G483–G495, Oct. 2013.

[283] N. Dror *et al.*, “Identification of IRF-8 and IRF-1 target genes in activated macrophages,” *Mol. Immunol.*, vol. 44, no. 4, pp. 338–346, Jan. 2007.

[284] A. Yáñez, M. Y. Ng, N. Hassanzadeh-Kiabi, and H. S. Goodridge, “IRF8

acts in lineage-committed rather than oligopotent progenitors to control neutrophil vs monocyte production," *Blood*, vol. 125, no. 9, pp. 1452–1459, 2015.

[285] K. Turcotte, S. Gauthier, A. Tuite, A. Mullick, D. Malo, and P. Gros, "A mutation in the Icsbp1 gene causes susceptibility to infection and a chronic myeloid leukemia-like syndrome in BXH-2 mice," *J. Exp. Med.*, vol. 201, no. 6, pp. 881–890, Mar. 2005.

[286] K. M. Patel *et al.*, "Macrophage sortilin promotes LDL uptake, foam cell formation, and atherosclerosis," *Circ. Res.*, vol. 116, no. 5, pp. 789–796, Feb. 2015.

[287] A. Duco Steven Koenis, L. Medzikovic, P. Bas van Loenen, W. Zwart, E. Kalkhoven, and C. Jacoba de Vries, "Nuclear Receptor Nur77 Limits the Macrophage Inflammatory Response through Transcriptional Reprogramming of Mitochondrial Metabolism Data Resources GSE102394," 2018.

[288] Y.-W. Hu *et al.*, "Nur77 Decreases Atherosclerosis Progression in apoE−/− Mice Fed a High-Fat/High-Cholesterol Diet," *PLoS One*, vol. 9, no. 1, p. e87313, Jan. 2014.

[289] S. L. Hyzy, R. Olivares-Navarrete, Z. Schwartz, and B. D. Boyan, "BMP2 induces osteoblast apoptosis in a maturation state and noggin-dependent manner," *J. Cell. Biochem.*, vol. 113, no. 10, pp. 3236–3245, Oct. 2012.

[290] J. Yang *et al.*, "Cutting edge: IRF8 regulates Bax transcription in vivo in primary myeloid cells," *J Immunol*, vol. 187, no. 9, pp. 4426–4430, 2011.

[291] J. Lascorz, K. Hemminki, and A. Försti, "Systematic enrichment analysis of gene expression profiling studies identifies consensus pathways implicated in colorectal cancer development.," *J. Carcinog.*, vol. 10, p. 7, Mar. 2011.

[292] V. Szentes, M. Gazdag, I. Szokodi, and C. A. Dézsi, “The Role of CXCR3 and Associated Chemokines in the Development of Atherosclerosis and During Myocardial Infarction.,” *Front. Immunol.*, vol. 9, p. 1932, 2018.

[293] D. Segers *et al.*, “Atherosclerotic Plaque Stability Is Affected by the Chemokine CXCL10 in Both Mice and Humans,” *Int. J. Inflam.*, vol. 2011, pp. 1–9, 2011.

[294] Q. N. Dinh *et al.*, “Advanced atherosclerosis is associated with inflammation, vascular dysfunction and oxidative stress, but not hypertension,” *Pharmacol. Res.*, vol. 116, pp. 70–76, Feb. 2017.

[295] L. Honold and M. Nahrendorf, “Resident and Monocyte-Derived Macrophages in Cardiovascular Disease.,” *Circ. Res.*, vol. 122, no. 1, pp. 113–127, 2018.

[296] M. P. Creyghton *et al.*, “Histone H3K27ac separates active from poised enhancers and predicts developmental state,” *Proc. Natl. Acad. Sci.*, vol. 107, no. 50, pp. 21931–21936, Dec. 2010.

[297] C. A. Bursill, R. P. Choudhury, Z. Ali, D. R. Greaves, and K. M. Channon, “Broad-Spectrum CC-Chemokine Blockade by Gene Transfer Inhibits Macrophage Recruitment and Atherosclerotic Plaque Formation in Apolipoprotein E–Knockout Mice,” *Circulation*, vol. 110, no. 16, pp. 2460–2466, Oct. 2004.

[298] J. Gosling *et al.*, “MCP-1 deficiency reduces susceptibility to atherosclerosis in mice that overexpress human apolipoprotein B,” *J. Clin. Invest.*, vol. 103, no. 6, pp. 773–778, Mar. 1999.

[299] L. Yvan-Charvet, N. Wang, and A. R. Tall, “Role of HDL, ABCA1, and ABCG1 transporters in cholesterol efflux and immune responses,” *Arterioscler Thromb Vasc Biol*, vol. 30, no. 2. NIH

Public Access, pp. 139–143, Feb-2010.

[300] D. Li *et al.*, “Roles of Purinergic Receptor P2Y, G Protein–Coupled 12 in the Development of Atherosclerosis in Apolipoprotein E–Deficient Mice,” *Arterioscler. Thromb. Vasc. Biol.*, vol. 32, no. 8, pp. e81-9, Aug. 2012.

[301] P.-J. D. F. Guns, J. Hendrickx, T. Van Assche, P. Fransen, and H. Bult, “P2Y receptors and atherosclerosis in apolipoprotein E-deficient mice.,” *Br. J. Pharmacol.*, vol. 159, no. 2, pp. 326–36, Jan. 2010.

[302] Y. Isobe *et al.*, “Comprehensive analysis of the mouse cytochrome P450 family responsible for omega-3 epoxidation of eicosapentaenoic acid,” *Sci. Rep.*, vol. 8, no. 1, p. 7954, Dec. 2018.

[303] Y. Liu *et al.*, “25-Hydroxycholesterol activates the expression of cholesterol 25-hydroxylase in an LXR-dependent mechanism.”

[304] S. Holm *et al.*, “Fatty acid binding protein 4 is associated with carotid atherosclerosis and outcome in patients with acute ischemic stroke,” *PLoS One*, vol. 6, no. 12, p. e28785, Dec. 2011.

[305] M. Furuhashi *et al.*, “Serum FABP5 concentration is a potential biomarker for residual risk of atherosclerosis in relation to cholesterol efflux from macrophages,” *Sci. Rep.*, vol. 7, no. 1, p. 217, Dec. 2017.

[306] M. Miyazaki *et al.*, “Stearoyl-CoA Desaturase 1 Gene Expression Is Necessary for Fructose-mediated Induction of Lipogenic Gene Expression by Sterol Regulatory Element-binding Protein-1c-dependent and -independent Mechanisms,” *J. Biol. Chem.*, vol. 279, no. 24, pp. 25164–25171, Jun. 2004.

[307] H. Pei *et al.*, “Therapeutic potential of a synthetic FABP4 inhibitor 8g on atherosclerosis in ApoE-deficient mice: The inhibition of lipid accumulation and inflammation,” *RSC Adv.*, vol. 6, no. 58, pp. 52518–52527, May 2016.

[308] M. Roden, “Blocking Fatty Acids’ Mystery Tour: A Therapy for Metabolic Syndrome?,” *Cell Metabolism*, vol. 6, no. 2. Elsevier, pp. 89–91, 08-Aug-2007.

[309] Y. Lin *et al.*, “Practical assessment of the quantification of atherosclerotic lesions in apoE-/- mice,” *Mol. Med. Rep.*, vol. 12, no. 4, pp. 5298–5306, Oct. 2015.

[310] L. Makowski, K. C. Brittingham, J. M. Reynolds, J. Suttles, and G. S. Hotamisligil, “The fatty acid-binding protein, aP2, coordinates macrophage cholesterol trafficking and inflammatory activity: Macrophage expression of aP2 impacts peroxisome proliferator-activated receptor γ and IκB kinase activities,” *J. Biol. Chem.*, vol. 280, no. 13, pp. 12888–12895, Apr. 2005.

[311] L. Makowski *et al.*, “Lack of macrophage fatty-acid-binding protein aP2 protects mice deficient in apolipoprotein E against atherosclerosis.,” *Nat. Med.*, vol. 7, no. 6, pp. 699–705, 2001.

[312] A. Bosquet *et al.*, “FABP4 inhibitor BMS309403 decreases saturated-fatty-acid-induced endoplasmic reticulum stress-associated inflammation in skeletal muscle by reducing p38 MAPK activation,” *Biochim. Biophys. Acta - Mol. Cell Biol. Lipids*, vol. 1863, no. 6, pp. 604–613, Jun. 2018.

[313] M. L. E. MacDonald *et al.*, “Despite antiatherogenic metabolic characteristics, SCD1-deficient mice have increased inflammation and atherosclerosis.,” *Arterioscler. Thromb. Vasc. Biol.*, vol. 29, no. 3, pp. 341–7, Mar. 2009.

[314] M. Lukasova, C. Malaval, A. Gille, J. Kero, and S. Offermanns, “Nicotinic acid inhibits progression of atherosclerosis in mice through its receptor GPR109A expressed by immune cells,” *J. Clin. Invest.*, vol. 121, no. 3, pp. 1163–1173, Mar. 2011.

[315] C.-Y. Ku, Y.-H. Liu, H.-Y. Lin, S.-C. Lu, and J.-Y. Lin, “Liver fatty acid-binding protein (L-FABP) promotes cellular angiogenesis and migration in hepatocellular carcinoma,” *Oncotarget*, vol. 7, no. 14, pp. 18229–46, Apr. 2016.

[316] R. Tripathi, P. Sharma, P. Chakraborty, and P. K. Varadwaj, “Next-generation sequencing revolution through big data analytics,” *Front. Life Sci.*, vol. 9, no. 2, pp. 119–149, Apr. 2016.

[317] L. N. Rao, T. Ponnusamy, S. Philip, R. Mukhopadhyay, V. V. Kakkar, and L. Mundkur, “Hypercholesterolemia Induced Immune Response and Inflammation on Progression of Atherosclerosis in Apob tm2Sgy Ldlr tm1Her/J Mice,” *Lipids*, vol. 50, no. 8, pp. 785–797, Aug. 2015.

[318] I. Tabas and K. E. Bornfeldt, “Macrophage Phenotype and Function in Different Stages of Atherosclerosis,” *Circ. Res.*, vol. 118, no. 4, pp. 653–667, 2016.

[319] G. Chinetti-Gbaguidi, S. Colin, and B. Staels, “Macrophage subsets in atherosclerosis,” *Nat. Rev. Cardiol*, vol. 12, no. 10, 2015.

[320] H. Hetterich *et al.*, “AHA classification of coronary and carotid atherosclerotic plaques by grating-based phase-contrast computed tomography Computed tomography gb-PCCT Grating-based phase-contrast computed tomography HE Hematoxylin-Eosin IVUS Intravascular ultrasound KIT Karlsruhe Institute of Technology MRI Magnetic resonance imaging NPV Negative predictive value OCT Optical coherence tomography PPV Positive predictive value,” *Eur Radiol*, vol. 26, pp. 3223–3233, 2016.

[321] A. Gisterå and G. K. Hansson, “The immunology of atherosclerosis,” *Nat. Rev. Nephrol.*, vol. 13, no. 6, pp. 368–380, 2017.

[322] I. G. Gomez *et al.*, “Metalloproteinase-mediated Shedding of Integrin β2 promotes macrophage efflux from inflammatory sites.,” *J. Biol. Chem.*, vol. 287, no. 7, pp. 4581–9, Feb. 2012.

[323] L. S. Bisgaard *et al.*, “Bone marrow-derived and peritoneal macrophages have different inflammatory response to oxLDL and M1/M2 marker expression – implications for atherosclerosis research,” *Sci. Rep.*, vol. 6, no. 1, p. 35234, Dec. 2016.

[324] X. Luo *et al.*, “The tumor suppressor interferon regulatory factor 8 inhibits β-catenin signaling in breast cancers, but is frequently silenced by promoter methylation.,” *Oncotarget*, vol. 8, no. 30, pp. 48875–48888, Jul. 2017.

[325] M. Tshuikina, H. Jernberg-Wiklund, K. Nilsson, and F. Öberg, “Epigenetic silencing of the interferon regulatory factor ICSBP/IRF8 in human multiple myeloma,” *Exp. Hematol.*, vol. 36, no. 12, pp. 1673-1681.e1, Dec. 2008.

[326] T. Tamura, P. Thotakura, T. S. Tanaka, M. S. H. Ko, and K. Ozato, “Identification of target genes and a unique cis element regulated by IRF-8 in developing macrophages,” *Blood*, vol. 106, no. 6, pp. 1938–1947, 2005.

[327] E. A. Heller *et al.*, “Chemokine CXCL10 Promotes Atherogenesis by Modulating the Local Balance of Effector and Regulatory T Cells,” *Circulation*, vol. 113, no. 19, pp. 2301–2312, May 2006.

[328] D. Segers *et al.*, “Atherosclerotic Plaque Stability Is Affected by the Chemokine CXCL10 in Both Mice and Humans,” *Int. J. Inflam.*, vol. 2011, pp. 1–9, 2011.

[329] J. Pan *et al.*, “AIM2 accelerates the atherosclerotic plaque progressions in ApoE−/− mice,” *Biochem. Biophys. Res. Commun.*, vol. 498, no. 3, pp. 487–494, Apr. 2018.

[330] B. Mallavia *et al.*, “Gene Deficiency in Activating Fcγ Receptors Influences

the Macrophage Phenotypic Balance and Reduces Atherosclerosis in Mice," *PLoS One*, vol. 8, no. 6, p. e66754, Jun. 2013.

[331] K. Turcotte *et al.*, "Genetic control of myeloproliferation in BXH-2 mice," 2004.

[332] J. Aliberti *et al.*, "Essential role for ICSBP in the in vivo development of murine CD8alpha + dendritic cells.," *Blood*, vol. 101, no. 1, pp. 305–10, Jan. 2003.

[333] D. A. Jaitin *et al.*, "Lipid-Associated Macrophages Control Metabolic Homeostasis in a Trem2-Dependent Manner," *Cell*, vol. 178, no. 3, pp. 686-698.e14, Jul. 2019.

[334] S. C. A. de Jager *et al.*, "Leukocyte-Specific CCL3 Deficiency Inhibits Atherosclerotic Lesion Development by Affecting Neutrophil Accumulation," *Arterioscler. Thromb. Vasc. Biol.*, vol. 33, no. 3, pp. e75-83, Mar. 2013.

[335] C. Zollbrecht *et al.*, "Expression pattern in human macrophages dependent on 9p21.3 coronary artery disease risk locus," *Atherosclerosis*, vol. 227, no. 2, pp. 244–249, 2013.

[336] P. Stachon *et al.*, "Extracellular ATP Induces Vascular Inflammation and Atherosclerosis via P2Y 2 in Mice," *Arterioscler. Thromb. Vasc. Biol.*, p. ATVBAHA.115.307397, 2016.

[337] L. Lichtenstein *et al.*, "Increased atherosclerosis in P2Y13/apolipoprotein E double-knockout mice: contribution of P2Y13 to reverse cholesterol transport," *Cardiovasc. Res.*, vol. 106, no. 2, pp. 314–323, May 2015.

[338] D. Ferrari, L. Vitiello, M. Idzko, and A. la Sala, "Purinergic signaling in atherosclerosis," *Trends Mol. Med.*, vol. 21, no. 3, pp. 184–192, 2015.

[339] M. Goffinet *et al.*, "P2Y13 Receptor Regulates HDL Metabolism and

Atherosclerosis In Vivo," *PLoS One*, vol. 9, no. 4, p. e95807, Apr. 2014.

[340] L. Lichtenstein *et al.*, "Lack of P2Y13 in mice fed a high cholesterol diet results in decreased hepatic cholesterol content, biliary lipid secretion and reverse cholesterol transport," *Nutr. Metab. (Lond).*, vol. 10, no. 1, p. 67, Nov. 2013.

[341] K. Kobayakawa *et al.*, "Macrophage centripetal migration drives spontaneous healing process after spinal cord injury," *Sci. Adv.*, vol. 5, no. 5, p. eaav5086, May 2019.

[342] K. A. Jacobson, A. A. Ivanov, S. de Castro, T. K. Harden, and H. Ko, "Development of selective agonists and antagonists of P2Y receptors.," *Purinergic Signal.*, vol. 5, no. 1, pp. 75–89, Mar. 2009.

[343] A. D. Michelson, "P2Y12 antagonism: promises and challenges.," *Arterioscler. Thromb. Vasc. Biol.*, vol. 28, no. 3, pp. s33-8, Mar. 2008.

[344] G. S. Ferreira *et al.*, "Aerobic Exercise Training Selectively Changes Oxysterol Levels and Metabolism Reducing Cholesterol Accumulation in the Aorta of Dyslipidemic Mice.," *Front. Physiol.*, vol. 8, p. 644, 2017.

[345] M. Umetani *et al.*, "27-Hydroxycholesterol is an endogenous SERM that inhibits the cardiovascular effects of estrogen.," *Nat. Med.*, vol. 13, no. 10, pp. 1185–1192, 2007.

[346] D. R. Bauman, A. D. Bitmansour, J. G. McDonald, B. M. Thompson, G. Liang, and D. W. Russell, "25-Hydroxycholesterol secreted by macrophages in response to Toll-like receptor activation suppresses immunoglobulin A production.," *Proc. Natl. Acad. Sci. U. S. A.*, vol. 106, no. 39, pp. 16764–9, Sep. 2009.

[347] L. O. Martinez, C. Cabou, V. Pons, and C. Malaval, "P2Y receptors in atherosclerosis: from lipid metabolism to vascular functions," *Wiley*

Interdiscip. Rev. Membr. Transp. Signal., vol. 1, no. 6, pp. 743–754, Nov. 2012.

[348] W. Sun *et al.*, “Legumain suppresses OxLDL-induced macrophage apoptosis through enhancement of the autophagy pathway,” *Gene*, vol. 652, pp. 16–24, Apr. 2018.

[349] P. J. Barter, H. B. Brewer, M. J. Chapman, C. H. Hennekens, D. J. Rader, and A. R. Tall, “Cholesteryl ester transfer protein: A novel target for raising HDL and inhibiting atherosclerosis,” *Arteriosclerosis, Thrombosis, and Vascular Biology*, vol. 23, no. 2. pp. 160–167, 01-Feb-2003.

[350] M. Furuhashi and G. S. Hotamisligil, “Fatty acid-binding proteins: Role in metabolic diseases and potential as drug targets,” *Nature Reviews Drug Discovery*, vol. 7, no. 6. NIH Public Access, pp. 489–503, Jun-2008.

[351] M. Furuhashi *et al.*, “Treatment of diabetes and atherosclerosis by inhibiting fatty-acid-binding protein aP2.,” *Nature*, vol. 447, no. 7147, pp. 959–65, Jun. 2007.

[352] Y. Nakayama *et al.*, “Role of PKR and Type I IFNs in Viral Control during Primary and Secondary Infection,” *PLoS Pathog.*, vol. 6, no. 6, p. e1000966, Jun. 2010.

[353] G. E. Price, A. Gaszewska-Mastarlarz, and D. Moskophidis, “The role of alpha/beta and gamma interferons in development of immunity to influenza A virus in mice.,” *J. Virol.*, vol. 74, no. 9, pp. 3996–4003, May 2000.

[354] M. A. Samuel and M. S. Diamond, “Alpha/Beta Interferon Protects against Lethal West Nile Virus Infection by Restricting Cellular Tropism and Enhancing Neuronal Survival,” *J. Virol.*, vol. 79, no. 21, pp. 13350–13361, Nov. 2005.

[355] S. G. Thacker *et al.*, “Type I interferons modulate vascular function, repair,

thrombosis, and plaque progression in murine models of lupus and atherosclerosis," *Arthritis Rheum.*, vol. 64, no. 9, pp. 2975–2985, Sep. 2012.

[356] Y. Mitani *et al.*, "Cross talk of the interferon-alpha/beta signalling complex with gp130 for effective interleukin-6 signalling.," *Genes Cells*, vol. 6, no. 7, pp. 631–40, Jul. 2001.

[357] A. Takaoka *et al.*, "Cross Talk Between Interferon-gamma and -alpha /beta Signaling Components in Caveolar Membrane Domains," *Science (80-.).*, vol. 288, no. 5475, pp. 2357–2360, Jun. 2000.

[358] T. Haupl *et al.*, "The type 1 interferon signature: facts, fads and fallacies," *Ann. Rheum. Dis.*, vol. 70, no. Suppl 2, pp. A24–A24, Mar. 2011.

[359] A. Piaszyk-Borychowska *et al.*, "Signal integration of IFN-I and IFN-II with TLR4 involves sequential recruitment of STAT1-Complexes and NFκB to enhance pro-inflammatory transcription," *Front. Immunol.*, vol. 10, no. JUN, p. 1253, Jun. 2019.

[360] Á. Baldán *et al.*, "Impaired development of atherosclerosis in hyperlipidemic Ldlr-/- and ApoE-/- mice transplanted with Abcg1-/- bone marrow," *Arterioscler. Thromb. Vasc. Biol.*, vol. 26, no. 10, pp. 2301–2307, Oct. 2006.

[361] L. Zurkinden *et al.*, "Effect of Cyp27A1 gene dosage on atherosclerosis development in ApoE-knockout mice," *FASEB J.*, vol. 28, no. 3, pp. 1198–1209, 2014.

[362] L. Gonzalez and B. L. Trigatti, "Macrophage Apoptosis and Necrotic Core Development in Atherosclerosis: A Rapidly Advancing Field with Clinical Relevance to Imaging and Therapy," *Can. J. Cardiol.*, vol. 33, no. 3, pp. 303–312, Mar. 2017.

[363] Y. Döring *et al.*, “Vascular CXCR4 Limits Atherosclerosis by Maintaining Arterial Integrity,” *Circulation*, vol. 136, no. 4, pp. 388–403, Jul. 2017.

[364] M. J. Butcher, B. N. Gjurich, T. Phillips, and E. V Galkina, “The IL-17A/IL-17RA axis plays a proatherogenic role via the regulation of aortic myeloid cell recruitment.,” *Circ. Res.*, vol. 110, no. 5, pp. 675–87, Mar. 2012.

[365] L. Icardi *et al.*, “The Sin3a repressor complex is a master regulator of STAT transcriptional activity,” *Proc. Natl. Acad. Sci.*, vol. 109, no. 30, pp. 12058–12063, Jul. 2012.

[366] S. Nozell, T. Laver, K. Patel, and E. N. Benveniste, “Mechanism of IFN-beta-mediated inhibition of IL-8 gene expression in astroglioma cells.,” *J. Immunol.*, vol. 177, no. 2, pp. 822–830, Jul. 2006.

[367] A. Abbas *et al.*, “The ABC transporters in lipid flux and atherosclerosis,” *Prog. Lipid Res.*, vol. 50, no. 6, pp. 673–685, 2015.

[368] L. M. Pennell and E. N. Fish, “Interferon-β regulates dendritic cell activation and migration in experimental autoimmune encephalomyelitis,” *Immunology*, vol. 152, no. 3, pp. 439–450, Nov. 2017.

[369] F. Herschke *et al.*, “Cell-cell fusion induced by measles virus amplifies the type I interferon response.,” *J. Virol.*, vol. 81, no. 23, pp. 12859–71, Dec. 2007.

[370] L. Chen *et al.*, “Monocytic cell junction proteins serve important roles in atherosclerosis via the endoglin pathway,” *Mol. Med. Rep.*, vol. 16, no. 5, pp. 6750–6756, May 2017.

[371] A. Mendoza-Naranjo *et al.*, “Functional Gap Junctions Accumulate at the Immunological Synapse and Contribute to T Cell Activation,” *J. Immunol.*, vol. 187, no. 6, pp. 3121–3132, Sep. 2011.

[372] A. Sancho, I. Vandersmissen, S. Craps, A. Luttun, and J. Groll, “A new

strategy to measure intercellular adhesion forces in mature cell-cell contacts," *Sci. Rep.*, vol. 7, no. 1, p. 46152, May 2017.

[373] S. M. Pokharel, N. K. Shil, and S. Bose, "Autophagy, TGF-β, and SMAD-2/3 Signaling Regulates Interferon-β Response in Respiratory Syncytial Virus Infected Macrophages," *Front. Cell. Infect. Microbiol.*, vol. 6, p. 174, Dec. 2016.

[374] J. Li *et al.*, "Interferon-α priming promotes lipid uptake and macrophage-derived foam cell formation: A novel link between interferon-α and atherosclerosis in lupus," *Arthritis Rheum.*, vol. 63, no. 2, pp. 492–502, Feb. 2011.

[375] P. L. S. M. Gordts *et al.*, "Reducing Macrophage Proteoglycan Sulfation Increases Atherosclerosis and Obesity through Enhanced Type I Interferon Signaling," *Cell Metab.*, vol. 20, pp. 813–826, 2014.

[376] K. Kyrylkova, S. Kyryachenko, M. Leid, and C. Kioussi, "Detection of Apoptosis by TUNEL Assay," in *Methods in molecular biology (Clifton, N.J.)*, vol. 887, 2012, pp. 41–47.

[377] D. Yang *et al.*, "IFN regulatory factor 8 mediates apoptosis in nonhemopoietic tumor cells via regulation of Fas expression.," *J. Immunol.*, vol. 179, no. 7, pp. 4775–82, Oct. 2007.

[378] A. Christ *et al.*, "Western Diet Triggers NLRP3-Dependent Innate Immune Reprogramming," *Cell*, vol. 172, no. 1–2, pp. 162-175.e14, Jan. 2018.

[379] P. J. Park, "ChIP–seq: advantages and challenges of a maturing technology," *Nat. Rev. Genet.*, vol. 10, no. 10, pp. 669–680, Oct. 2009.

[380] J. Barlic, W. Zhu, and P. M. Murphy, "Atherogenic lipids induce high-density lipoprotein uptake and cholesterol efflux in human macrophages by up-regulating transmembrane chemokine CXCL16 without engaging CXCL16-

dependent cell adhesion.," *J. Immunol.*, vol. 182, no. 12, pp. 7928–7936, Jun. 2009.

[381] E. J. Gaynor, S. E. Geoghegan, and D. O'Neill, "Ageism in stroke rehabilitation studies," *Age Ageing*, vol. 43, no. 3, pp. 429–431, May 2014.

[382] C. R. Kleiveland, "Peripheral Blood Mononuclear Cells," in *The Impact of Food Bioactives on Health*, Cham: Springer International Publishing, 2015, pp. 161–167.

[383] G. D. Thomas *et al.*, "Human Blood Monocyte Subsets: A New Gating Strategy Defned Using Cell Surface Markers Identifed by Mass Cytometry," *Arterioscler. Thromb. Vasc. Biol.*, vol. 37, no. 8, pp. 1548–1558, Aug. 2017.

[384] A. A. Patel *et al.*, "The fate and lifespan of human monocyte subsets in steady state and systemic inflammation," *J. Exp. Med.*, vol. 214, no. 7, pp. 1913–1923, Jul. 2017.

[385] C. Farina, D. Theil, B. Semlinger, R. Hohlfeld, and E. Meinl, "Distinct responses of monocytes to Toll-like receptor ligands and inflammatory cytokines," *Int. Immunol.*, vol. 16, no. 6, pp. 799–809, Apr. 2004.

[386] W. A. Nockher and J. E. Scherberich, "Expanded CD14+ CD16+ monocyte subpopulation in patients with acute and chronic infections undergoing hemodialysis.," *Infect. Immun.*, vol. 66, no. 6, pp. 2782–90, Jun. 1998.

[387] C. F. Hodkinson *et al.*, "Whole Blood Analysis of Phagocytosis, Apoptosis, Cytokine Production, and Leukocyte Subsets in Healthy Older Men and Women: The ZENITH Study," *Journals Gerontol. Ser. A Biol. Sci. Med. Sci.*, vol. 61, no. 9, pp. 907–917, Sep. 2006.

[388] I. Heimbeck *et al.*, "Standardized single-platform assay for human monocyte subpopulations: Lower CD14+CD16++ monocytes in females," *Cytom. Part A*, vol. 77A, no. 9, pp. 823–830, Sep. 2010.

[389] S. Lively and L. C. Schlichter, “Microglia Responses to Pro-inflammatory Stimuli (LPS, IFNγ+TNFα) and Reprogramming by Resolving Cytokines (IL-4, IL-10).,” *Front. Cell. Neurosci.*, vol. 12, p. 215, 2018.

[390] A. Ngkelo, K. Meja, M. Yeadon, I. Adcock, and P. A. Kirkham, “LPS induced inflammatory responses in human peripheral blood mononuclear cells is mediated through NOX4 and Gi-alpha dependent PI-3kinase signalling,” *J. Inflamm.*, vol. 9, no. 1, p. 1, Jan. 2012.

[391] M. W. Wichmann, D. Inthorn, H.-J. Andress, and F. W. Schildberg, “Incidence and mortality of severe sepsis in surgical intensive care patients: The influence of patient gender on disease process and outcome,” *Intensive Care Med.*, vol. 26, no. 2, pp. 167–172, Mar. 2000.

[392] T. Fülöp, A. Larbi, and G. Pawelec, “Human T Cell Aging and the Impact of Persistent Viral Infections,” *Front. Immunol.*, vol. 4, p. 271, Sep. 2013.

[393] K. Higuchi *et al.*, “Endothelial Gab1 deletion accelerates angiotensin II-dependent vascular inflammation and atherosclerosis in apolipoprotein E knockout mice.,” *Circ. J.*, vol. 76, no. 8, pp. 2031–40, 2012.

[394] V. Herías *et al.*, “Leukocyte Cathepsin C Deficiency Attenuates Atherosclerotic Lesion Progression by Selective Tuning of Innate and Adaptive Immune Responses,” *Arterioscler. Thromb. Vasc. Biol.*, vol. 35, no. 1, pp. 79–86, Jan. 2015.

[395] S. Ponnappan and U. Ponnappan, “Aging and immune function: Molecular mechanisms to interventions,” *Antioxidants and Redox Signaling*, vol. 14, no. 8. Mary Ann Liebert, Inc., pp. 1551–1585, 15-Apr-2011.

[396] L. Zhang *et al.*, “Aging-related atherosclerosis is exacerbated by arterial expression of tumor necrosis factor receptor-1: evidence from mouse models and human association studies,” *Hum. Mol. Genet.*, vol. 19, no. 14,

pp. 2754–2766, Jul. 2010.

[397] D. Fairweather, “Sex differences in inflammation during atherosclerosis,” *Clinical Medicine Insights: Cardiology*, vol. 8, no. Suppl. 3. SAGE Publications, pp. 49–59, 2015.

[398] A. L. Brubaker, J. L. Rendon, L. Ramirez, M. A. Choudhry, and E. J. Kovacs, “Reduced Neutrophil Chemotaxis and Infiltration Contributes to Delayed Resolution of Cutaneous Wound Infection with Advanced Age,” *J. Immunol.*, vol. 190, no. 4, pp. 1746–1757, Feb. 2013.

[399] C. Franceschi and J. Campisi, “Chronic Inflammation (Inflammaging) and Its Potential Contribution to Age-Associated Diseases,” *Journals Gerontol. Ser. A Biol. Sci. Med. Sci.*, vol. 69, no. Suppl 1, pp. S4–S9, Jun. 2014.

[400] L. Ferrucci and E. Fabbri, “Inflammageing: chronic inflammation in ageing, cardiovascular disease, and frailty.,” *Nat. Rev. Cardiol.*, vol. 15, no. 9, pp. 505–522, 2018.

[401] E. Agius *et al.*, “Decreased TNF-alpha synthesis by macrophages restricts cutaneous immunosurveillance by memory CD4+ T cells during aging.,” *J. Exp. Med.*, vol. 206, no. 9, pp. 1929–1940, Aug. 2009.

[402] R. D. Molony, J. T. Nguyen, Y. Kong, R. R. Montgomery, A. C. Shaw, and A. Iwasaki, “Aging impairs both primary and secondary RIG-I signaling for interferon induction in human monocytes,” *Sci. Signal.*, vol. 10, no. 509, p. eaan2392, Dec. 2017.

[403] K. Papsdorf and A. Brunet, “Linking Lipid Metabolism to Chromatin Regulation in Aging.,” *Trends Cell Biol.*, vol. 29, no. 2, pp. 97–116, Feb. 2019.

[404] N. Kawanishi *et al.*, “Effects of aging on serum levels of lipid molecular species as determined by lipidomics analysis in Japanese men and

women," *Lipids Health Dis.*, vol. 17, no. 1, p. 135, Dec. 2018.

[405] K. E. Wellen, G. Hatzivassiliou, U. M. Sachdeva, T. V Bui, J. R. Cross, and C. B. Thompson, "ATP-citrate lyase links cellular metabolism to histone acetylation.," *Science*, vol. 324, no. 5930, pp. 1076–80, May 2009.

[406] J. Stefani *et al.*, "Disruption of the Microglial ADP Receptor P2Y13 Enhances Adult Hippocampal Neurogenesis.," *Front. Cell. Neurosci.*, vol. 12, p. 134, 2018.

[407] L. W. Bonham, D. W. Sirkis, and J. S. Yokoyama, "The Transcriptional Landscape of Microglial Genes in Aging and Neurodegenerative Disease," *Front. Immunol.*, vol. 10, p. 1170, Jun. 2019.

[408] K. Higuchi *et al.*, "Endothelial Gab1 deletion accelerates angiotensin II-dependent vascular inflammation and atherosclerosis in apolipoprotein E knockout mice.," *Circ. J.*, vol. 76, no. 8, pp. 2031–40, 2012.

[409] K. Mood, C. Saucier, Y.-S. Bong, H.-S. Lee, M. Park, and I. O. Daar, "Gab1 Is Required for Cell Cycle Transition, Cell Proliferation, and Transformation Induced by an Oncogenic Met Receptor," *Mol. Biol. Cell*, vol. 17, no. 9, p. 3717, 2006.

[410] J. Zhao *et al.*, "Cardiac Gab1 deletion leads to dilated cardiomyopathy associated with mitochondrial damage and cardiomyocyte apoptosis," *Cell Death Differ.*, vol. 23, no. 4, pp. 695–706, Apr. 2016.

[411] M. Herías *et al.*, "Leukocyte Cathepsin C deficiency attenuates atherosclerotic lesion progression by selective tuning of innate and adaptive immune responses," *Arterioscler. Thromb. Vasc. Biol.*, vol. 35, no. 1, p. 79, 2015.

[412] X. Fu *et al.*, "27-Hydroxycholesterol Is an Endogenous Ligand for Liver X Receptor in Cholesterol-loaded Cells," *J. Biol. Chem.*, vol. 276, no. 42, pp.

38378–38387, Oct. 2001.

[413] J. Liu *et al.*, “The absence of ABCD2 sensitizes mice to disruptions in lipid metabolism by dietary erucic acid.,” *J. Lipid Res.*, vol. 53, no. 6, pp. 1071–9, Jun. 2012.

[414] M. C. Gage, “Measuring Apoptotic Cell Engulfment (Efferocytosis) Efficiency,” Humana Press, New York, NY, 2019, pp. 143–152.

[415] G. Escher, Z. Krozowski, K. D. Croft, and D. Sviridov, “Expression of sterol 27-hydroxylase (CYP27A1) enhances cholesterol efflux,” *J. Biol. Chem.*, vol. 278, no. 13, pp. 11015–11019, 2003.

[416] N. J. Spann *et al.*, “Regulated Accumulation of Desmosterol Integrates Macrophage Lipid Metabolism and Inflammatory Responses,” *Cell*, vol. 151, no. 1, pp. 138–152, Sep. 2012.

[417] N. R. Veillard *et al.*, “Antagonism of RANTES Receptors Reduces Atherosclerotic Plaque Formation in Mice,” *Circ. Res.*, vol. 94, no. 2, pp. 253–261, Feb. 2004.

[418] D. Teupser, S. Pavlides, M. Tan, J.-C. Gutierrez-Ramos, R. Kolbeck, and J. L. Breslow, “Major reduction of atherosclerosis in fractalkine (CX3CL1)-deficient mice is at the brachiocephalic artery, not the aortic root.,” *Proc. Natl. Acad. Sci. U. S. A.*, vol. 101, no. 51, pp. 17795–800, Dec. 2004.

[419] L. Lichtenstein *et al.*, “Increased atherosclerosis in P2Y<inf>13</inf>/apolipoprotein e double-knockout mice: Contribution of P2Y<inf>13</inf> to reverse cholesterol transport,” *Cardiovasc. Res.*, vol. 106, no. 2, pp. 314–323, 2015.

[420] L. Makowski *et al.*, “Lack of macrophage fatty-acid-binding protein aP2 protects mice deficient in apolipoprotein E against atherosclerosis,” *Nat. Med.*, vol. 7, no. 6, pp. 699–705, Jun. 2001.

[421] Y. Uemura, T. Naoi, Y. Kanai, and K. Kobayashi, “The efficiency of lipid nanoparticles with an original cationic lipid as a siRNA delivery system for macrophages and dendritic cells,” *Pharm. Dev. Technol.*, vol. 24, no. 3, pp. 263–268, Mar. 2019.

[422] C. Buono, C. E. Come, G. Stavrakis, G. F. Maguire, P. W. Connelly, and A. H. Lichtman, “Influence of Interferon-γ on the Extent and Phenotype of Diet-Induced Atherosclerosis in the LDLR-Deficient Mouse,” *Arterioscler. Thromb. Vasc. Biol.*, vol. 23, no. 3, pp. 454–460, Mar. 2003.

[423] S. C. Whitman, P. Ravisankar, H. Elam, and A. Daugherty, “Exogenous interferon-gamma enhances atherosclerosis in apolipoprotein E-/- mice.,” *Am. J. Pathol.*, vol. 157, no. 6, pp. 1819–24, Dec. 2000.

[424] Autumn Gabrielle *et al.*, *Rapid transcriptional reprogramming of the lipid biosynthesis genes in response to type I interferon*, vol. 196, no. 1 Supplement. Williams & Wilkins, 2016.

[425] D. Wu *et al.*, “Type 1 Interferons Induce Changes in Core Metabolism that Are Critical for Immune Function.,” *Immunity*, vol. 44, no. 6, pp. 1325–36, 2016.

[426] Z. Hu *et al.*, “Nucleosome loss leads to global transcriptional up-regulation and genomic instability during yeast aging,” *Genes Dev.*, vol. 28, no. 4, pp. 396–408, Feb. 2014.

[427] A. E. Kane and D. A. Sinclair, “Epigenetic changes during aging and their reprogramming potential,” *Critical Reviews in Biochemistry and Molecular Biology*, vol. 54, no. 1. Taylor & Francis, pp. 61–83, 02-Jan-2019.

[428] K. Papsdorf and A. Brunet, “Linking Lipid Metabolism to Chromatin Regulation in Aging,” *Trends in Cell Biology*, vol. 29, no. 2. Elsevier Current Trends, pp. 97–116, 01-Feb-2019.

Appendix 1

Western blot scans

Fig S1.1 IRF8 western blot.
Cell lysates from WT^{LdlrKO} and M-$IRF8KO^{LdlrKO}$ were subjected to immunoprecipitation using an anti-IRF8 antibody, expected band size 48kDa.

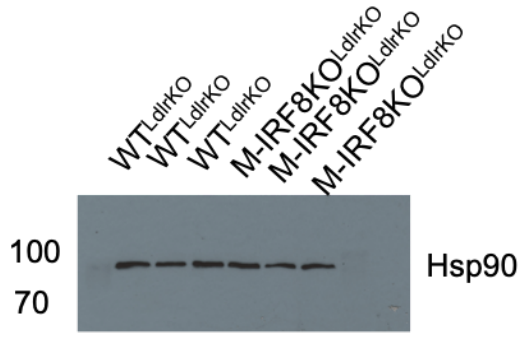

Fig S1.2 Hsp90 western blot.
Cell lysates from WT^{LdlrKO} and M-$IRF8KO^{LdlrKO}$ were subjected to immunoprecipitation using an anti-Hsp90 antibody, expected band size 90kDa.